Memoria de Tesis Doctoral

NEUTRINO WINDOWS TO THE ORIGIN OF MATTER

SALVADOR ROSAURO-ALCARAZ

Dirigida por el Dr. Enrique Fernández-Martínez

Departamento de Física Teórica
Instituto de Física Teórica UAM/CSIC

Madrid, Junio de 2021

PUBLICATIONS

This thesis is based upon the following works:

[1] M. Blennow, E. Fernandez-Martinez, A. Olivares-Del Campo, S. Pascoli, S. Rosauro-Alcaraz, and A. V. Titov. «Neutrino Portals to Dark Matter.» In: *Eur. Phys. J. C* 79.7 (2019), p. 555. DOI: 10.1140/epjc/s10052-019-7060-5. arXiv: 1903.00006 [hep-ph].

[2] M. Blennow, E. Fernandez-Martinez, T. Ota, and S. Rosauro-Alcaraz. «Physics potential of the ESSνSB.» In: *Eur. Phys. J. C* 80.3 (2020), p. 190. DOI: 10.1140/epjc/s10052-020-7761-9. arXiv: 1912.04309 [hep-ph].

[3] E. Fernández-Martínez, J. López-Pavón, T. Ota, and S. Rosauro-Alcaraz. «ν electroweak baryogenesis.» In: *JHEP* 10 (2020), p. 063. DOI: 10.1007/JHEP10(2020)063. arXiv: 2007.11008 [hep-ph].

[4] Enrique Fernandez-Martinez, Mathias Pierre, Emanuelle Pinsard, and Salvador Rosauro-Alcaraz. «Inverse Seesaw, dark matter and the Hubble tension.» In: (June 2021). arXiv: 2106.05298 [hep-ph].

Other works done during the thesis, but not included here are:

[1] L. Merlo and S. Rosauro-Alcaraz. «Predictive Leptogenesis from Minimal Lepton Flavour Violation.» In: *JHEP* 07 (2018), p. 036. DOI: 10.1007/JHEP07(2018)036. arXiv: 1801.03937 [hep-ph].

[2] Monojit Ghosh, Tommy Ohlsson, and Salvador Rosauro-Alcaraz. «Sensitivity to light sterile neutrinos at ESSnuSB.» In: *JHEP* 03 (2020), p. 026. DOI: 10.1007/JHEP03(2020)026. arXiv: 1912.10010 [hep-ph].

[3] Samuel J. Witte, Salvador Rosauro-Alcaraz, Samuel D. McDermott, and Vivian Poulin. «Dark photon dark matter in the presence of inhomogeneous structure.» In: *JHEP* 06 (2020), p. 132. DOI: 10.1007/JHEP06(2020)132. arXiv: 2003.13698 [astro-ph.CO].

[4] B. Abi et al. «Prospects for beyond the Standard Model physics searches at the Deep Underground Neutrino Experiment.» In: *Eur. Phys. J. C* 81.4 (2021), p. 322. DOI: 10.1140/epjc/s10052-021-09007-w. arXiv: 2008.12769 [hep-ex].

[5] Guillermo Fernandez-Moroni, Pedro A. N. Machado, Ivan Martinez-Soler, Yuber F. Perez-Gonzalez, Dario Rodrigues, and Salvador Rosauro-Alcaraz. «The physics potential of a reactor neutrino experiment with Skipper CCDs: Measuring the weak mixing angle.» In: *JHEP* 03 (2021), p. 186. DOI: 10.1007/JHEP03(2021)186. arXiv: 2009.10741 [hep-ph].

[6] Pilar Coloma, Jacobo López-Pavón, Salvador Rosauro-Alcaraz, and Salvador Urrea. «New physics from oscillations at the DUNE near detector, and the role of systematic uncertainties.» In: (May 2021). arXiv: 2105.11466 [hep-ph].

CONTENTS

Neutrino windows to the origin of matter

Salvador Rosauro Alcaraz

Junio de 2021

Abstract

The Standard Model of particle Physics (SM) is a quantum field theory based on the $SU(3)_c \times SU(2)_L \times U(1)_Y$ gauge group, which has so far precisely described strong and electroweak interactions between elementary particles.

We know, however, that the SM cannot be the end of the story, as it is not able to give a consistent description of gravity. Thus, the SM has to be the low energy version of a more complete theory. Besides, there are other questions, both experimental and theoretical ones, which the SM cannot answer that call for the existence of Physics beyond the Standard Model (BSM).

On the experimental side, the observation of non-baryonic particle dark matter (DM) in the Universe through its gravitational effects call for an extension of the SM to include such new states. Additionally, through Big Bang nucleosynthesis (BBN) and CMB observations, we know that there is an imbalance between matter and antimatter. However, even though the SM has all the necessary ingredients to explain such an asymmetry, it was shown that it cannot generate the observed imbalance between baryons and antibaryons, such that BSM Physics is also necessary to explain this fact. Moreover, we have overwhelming evidence for BSM Physics from the observation of the neutrino oscillation phenomenon. This is arguably the clearest signal for BSM Physics from laboratory experiments. Thus, the neutrino sector seems a particularly greenfield area of investigation in order to find new Physics and to relating different open problems of the SM.

This thesis focuses on the study of a future neutrino super beam to study neutrino oscillations and probe for the still unknown parameters characterizing the neutrino sector, such as CP violation, and the neutrino mass ordering. Secondly, we study the possibility that the DM is primarily interacting with neutrinos through the neutrino portal, and that therefore large neutrino detectors acting as observatories might be our best probe to explore the dark sector. Later on we will consider the possibility that a keV neutrino arising from the neutrino mass mechanism could be itself the DM. In the third part we will study the possible relation between the neutrino mass mechanism and the matter-antimatter asymmetry.

Resumen

El Modelo Estándar de física de partículas (ME) es una teoría cuántica de campos basada en el grupo gauge $SU(3)_c \times SU(2)_L \times U(1)_Y$, que ha descrito hasta ahora las interacciones fuertes y electroébiles entre partículas elementales con gran precisión.

Sabemos, sin embargo, que el ME no puede ser el final de la historia, ya que no es capaz de describir consistentemente la gravedad. Por tanto, el ME debe ser una versión a bajas energías de una teoría más completa. Además, hay otras preguntas, tanto experimentales como teóricas, que el ME no puede responder y que reclaman la existencia de física más allá del Modelo Estándar (BSM por sus siglas en inglés).

Experimentalmente, la observación de materia oscura no bariónica (MO) en el Universo a través de sus efectos gravitacionales necesita la extensión del ME para incluir tales estados. Además, través de Big Bang nucleosíntesis (BBN) y observaciones del CMB, sabemos que hay un desequilibrio entre materia y antimateria. Sin embargo, aunque el ME tiene todos los ingredientes necesarios para explicar esta asimetría, se demostró que no puede generar este desequilibrio entre bariones y antibariones, por lo que necesitamos física BSM para explicar este hecho. Así mismo, tenemos evidencia incontestable de la existencia de física BSM por la observación del fenómeno de oscilaciones de neutrinos. Esta es probablemente la señal más clara de física BSM procedente de experimentos en laboratorio. Por tanto, el sector de los neutrinos parece un campo particularmente próspero que investigar para encontrar nueva física y relacionar diferentes problemas abiertos del ME.

Esta tesis se enfoca en el estudio de un futuro súper haz de neutrinos para estudiar oscilaciones y investigar los parámetros característicos del sector de los neutrinos aun desconocidos, como violación de CP, y el orden de las masas de los neutrinos. En segundo lugar, estudiamos la posibilidad de que la MO interaccione principalmente con los neutrinos a través del portal de neutrinos, y que por tanto grandes detectores de neutrinos actuando como observatorios puedan ser nuestra mejor baza para explorar el sector oscuro. Posteriormente consideraremos la posibilidad de que un neutrino de masa del orden del keV generado por el mecanismo de masas de neutrinos puede ser en sí mismo la MO. En la tercera parte estudiaremos la posible relación entre el mecanismo de masas de neutrinos y la asimetría materia-antimateria.

MOTIVACIÓN Y OBJETIVOS

El Modelo Estándar de física de partículas (ME) es una teoría cuántica de campos basada en el grupo gauge $SU(3)_c \times SU(2)_L \times U(1)_Y$, que ha descrito hasta ahora las interacciones fuertes y electroébiles entre partículas elementales con gran precisión.

Sabemos, sin embargo, que el ME no puede ser el final de la historia, ya que no es capaz de describir consistentemente la gravedad. Por tanto, el ME debe ser una versión a bajas energías de una teoría más completa. Además, hay otras preguntas, tanto experimentales como teóricas, que el ME no puede responder y que reclaman la existencia de física más allá del Modelo Estándar (BSM por sus siglas en inglés).

Experimentalmente, la observación de materia oscura no bariónica (MO) en el Universo a través de sus efectos gravitacionales, por ejemplo, en las curvas de rotación de las galaxias o sus huellas en el fondo cósmico de microondas (CMB por sus siglas en inglés), necesita la extensión del ME para incluir tales estados. Esta componente conforma alrededor del $\sim 25\%$ del Universo que observamos hoy en día.

Uno podría pensar que tenemos una gran comprensión del 5% del resto de la energía del Universo, correspondiente a su contenido bariónico, dado nuestro gran éxito en testar el ME y confirmar sus predicciones con extraordinaria precisión. Esto no podría estar más lejos de la realidad. Efectivamente, a través de Big Bang nucleosíntesis (BBN) y observaciones del CMB, sabemos que hay un desequilibrio entre materia y antimateria. Sin embargo, aunque el ME tiene todos los ingredientes necesarios para explicar esta asimetría, se demostró que no puede generar este desequilibrio entre bariones y antibariones, por lo que necesitamos física BSM para explicar este hecho.

Además, tenemos evidencia incontestable de la existencia de física BSM por la observación del fenómeno de oscilaciones de neutrinos. Resultados de oscilaciones de neutrinos están correctamente descritos por masas no nulas de los neutrinos, lo cual está en contra de los neutrinos sin masa en el ME. Esta es probablemente la señal más clara de física BSM procedente de experimentos en laboratorio. Además, la existencia de neutrinos masivos introduce otras preguntas en el sector de los neutrinos, como saber si los neutrinos son Dirac o Majorana, impulsando grandes esfuerzos experimentales.

Desde un pusto de vista teórico, hay varias preguntas que el ME no puede responder, más allá de la inclusión de gravedad en la teoría. Por un lado tenemos el "problema de CP fuerte". El término $\theta G_{\mu\nu}\tilde{G}^{\mu\nu}$, donde $G_{\mu\nu}$ es el tensor campo de $SU(3)_c$ y θ es una constante adinesional, puede estar presente a nivel árbol en el lagrangiano del ME

y romper CP en las interacciones fuertes. Sin embargo, por medidas del momento eléctrico dipolar del neutrón, sabemos que $\theta \lesssim 10^{-10}$. Resolver el problema de CP fuerte correspondería a entender por qué θ es tan pequeño, por ejemplo, a través de una simetría.

Segundo, la masa del bosón de Higgs se ha medido alrededor de la escala electrodébil (ED). Sin embargo, a diferencia de las masas de los fermiones y los bosones gauge, la masa del escalar no está protegida por ninguna simetría, de manera que si la nueva física (NF) está a una escala Λ_{NF}, la masa del Higgs recibiría correcciones de orden Λ_{NF}^2. Por lo tanto, si el ME describe las interacciones entre partículas hasta la escala de Planck, tendríamos una contribución a la masa del Higgs de orden M_{Pl}^2, y por tanto el valor observado de la masa sería consecuencia de un ajuste extremadamente fino entre diferentes contribuciones. Este es el conocido como "problema de la jerarquía" y apunta hacia la existencia de NF no lejos de la escala ED para evitar el ajuste fino tanto como sea posible.

Además, el Universo se está acelerando, lo que significa que hay una contribución a su densidad de energía, conocida como energía oscura, que es constante. Esta es la llamada constante cosmológica, Λ, que podría explicarse a través de la energía del vacío del ME. Sin embargo, una estimación de esta contribución difiere por más de 50 órdenes de magnitud del valor medido de Λ, representanto otro problema de ajuste fino del ME.

Finalmente, el ME es incapaz de explicar por qué hay tres copias o familias de fermiones, solo diferenciados por sus masas, que abarcan unos seis órdenes de magnitud. Esto se conoce como el "problema del sabor", y empeora con la inclusión de masas de neutrinos para explicar las oscilaciones de neutrinos. Efectivamente, en este caso las diferencias de masas abarcan hasta 12 órdenes de magnitud. Además, el patrón de mezcla observado en el sector de los quarks es sorprendentemente diferente al del sector leptónico. Atacar el problema del sabor generalmente se basa en algún argumento de simetría para explicar las masas y mezclas de los fermiones observadas.

El sector de los neutrinos parece un campo particularmente próspero que investigar para encontrar NF y relacionar diferentes problemas abiertos del ME. El estudio de las oscilaciones de neutrinos ya nos ha llevado a la necesidad de incluir nuevos estados para generar masas de neutrinos ligeras. Sin embargo, sigue habiendo algunas incógnitas como el tamaño de la violación de CP en el sector de los leptones, un ingrediente neceaario para explicar la asimetría bariónica y que es muy pequeño en el sector de los quarks, o el orden de los neutrinos, que implicaría diferentes expectativas en la búsqueda del decaimiento doble beta sin neutrinos ($0\nu2\beta$), demostrando la naturaleza Majorana de los neutrinos.

Si el mecanismo responsable de las masas de los neutrinos ligeros introduce nuevos estados alrededor del keV, representaría un buen

candidato a MO. Por otro lado, los neutrinos podrían conectar el ME con otros sectores oscuros. En algunos escenarios, los nuevos estados necesarios para explicar masas de neutrinos son singletes del ME de tal manera que puede ser un portal entre el ME y MO. Además, los estados más pesados que pueden explicar la pequeñez de las masas de los neutrinos podrían ayudar también en la generación de la asimetría bariónica en el Universo temprano.

Por tanto, comprender completamente el sector de los neutrinos es una pieza fundamental para entender el problema del sabor, dado que los neutrinos representan una gran proporción del puzle, a través de la precisa determinación de los parámetros de mezcla leptónicos, el origen de la MO en el Universo o la generación de la asimetría bariónica.

La primera parte de esta tesis se enfoca en el estudio de un futuro súper haz de neutrinos para estudiar oscilaciones y investigar los parámetros característicos del sector de los neutrinos aun desconocidos, como violación de CP, y el orden de las masas de los neutrinos. En segundo lugar, estudiamos la posibilidad de que la MO interaccione principalmente con los neutrinos a través del portal de neutrinos, y que por tanto grandes detectores de neutrinos actuando como observatorios puedan ser nuestra mejor baza para explorar el sector oscuro. Posteriormente consideraremos la posibilidad de que un neutrino de masa del orden del keV generado por el mecanismo de masas de neutrinos puede ser en sí mismo la MO. En la tercera parte estudiaremos la posible relación entre el mecanismo de masas de neutrinos y la asimetría materia-antimateria.

OVERVIEW AND GOALS

The Standard Model of particle Physics (SM) is a quantum field theory based on the $SU(3)_c \times SU(2)_L \times U(1)_Y$ gauge group, which has so far precisely described strong and electroweak interactions between elementary particles.

We know, however, that the SM cannot be the end of the story, as it is not able to give a consistent description of gravity. Thus, the SM has to be the low energy version of a more complete theory. Besides, there are other questions, both experimental and theoretical ones, which the SM cannot answer that call for the existence of Physics beyond the Standard Model (BSM).

On the experimental side, the observation of non-baryonic particle dark matter (DM) in the Universe through its gravitational effects, for example, in the rotation curves of galaxies or its imprint in the cosmic microwave background (CMB), call for an extension of the SM to include such new states. This component makes up about $\sim 25\%$ of the Universe we observe today.

One could be led to think that we have a strong understanding of 5% of the energy budget of the Universe, corresponding to its baryonic content, given our great success in testing the SM and confirming its predictions with outstanding accuracy. This could not be further from true. Indeed, through Big Bang nucleosynthesis (BBN) and CMB observations, we know that there is an imbalance between matter and antimatter. However, even though the SM has all the necessary ingredients to explain such an asymmetry, it was shown that it cannot generate the observed imbalance between baryons and antibaryons, such that BSM Physics is also necessary to explain this fact.

Moreover, we have overwhelming evidence for BSM Physics from the observation of the neutrino oscillation phenomenon. Neutrino oscillation results are nowadays well described by non-zero neutrino masses, which is at odds with massless neutrinos in the SM. This is arguably the clearest signal for BSM Physics from laboratory experiments. Additionally, the existence of non-zero light neutrino masses opens other questions in the neutrino sector, such as whether neutrinos are Dirac or Majorana particles, pushing great experimental efforts.

From a theoretical perspective, there are several questions the SM cannot address, apart from the inclusion of gravity in the theory. On the one hand, we have the "strong CP problem". The term $\theta G_{\mu\nu}\tilde{G}^{\mu\nu}$, where $G_{\mu\nu}$ is the $SU(3)_c$ field strength tensor and θ is a dimensionless constant, can be present in the SM lagrangian at tree level and break CP in strong interactions. However, from measurements of the

neutron electric dipole moment, we know that $\theta \lesssim 10^{-10}$. Solving the strong CP problem amounts to understanding why θ is so small, for example, through a symmetry argument.

Second, the Higgs boson mass has been measured to be around the electroweak scale. Nonetheless, unlike fermion and gauge boson masses, the scalar mass is not protected by any symmetry, such that if the New Physics (NP) is at a scale Λ_{NP}, the Higgs mass would receive corrections of order Λ_{NP}^2. Thus, if the SM described particle interactions up to the Planck scale, we would have a contribution to the Higgs mass of order M_{Pl}^2, and thus the observed value of the scalar mass would be the consequence of an extreme fine tuning between the different contributions. This is the so-called "hierarchy problem" and it points to the existence of NP not far from the EW scale to avoid fine tuning as much as possible.

Moreover, the Universe is accelerating, which means that there is a contribution to its energy density, dubbed as dark energy, which is constant. This is the so-called cosmological constant, Λ, which could in principle be explained through the vacuum energy of the SM. However, an estimation of such a contribution differs by more than 50 orders of magnitude from the measured value for Λ, representing another fine tuning problem of the SM.

Finally, the SM fails to explain why there are three copies or families of fermions, just differing by their masses, which span about six orders of magnitude. This is known as the "flavour problem", and is worsened with the inclusion of light neutrino masses to explain neutrino oscillations. Indeed, in this case the mass difference could span up to 12 orders of magnitude. Furthermore, the flavour mixing pattern observed in the quark sector is strikingly different from the one in the lepton sector. Tackling the flavour problem generally relies on some symmetry argument to explain the observed fermion masses and mixings.

The neutrino sector seems a particularly greenfield area of investigation in order to find NP and to relating different open problems of the SM. The study of neutrino oscillations has already led us to the necessity to include new states in order to generate light neutrino masses. However, there are still some unknowns such as the size of CP violation in the lepton sector, a necessary ingredient to explain the baryon asymmetry and which is too small in the quark sector, or the neutrino ordering, which would imply different expectations in the search for neutrinoless double beta decay ($0\nu2\beta$) decay, signaling the Majorana nature of neutrinos.

If the mechanism responsible for light neutrino masses introduces new states around the keV scale, it would represent a good DM candidate. On the other hand, neutrinos could connect the SM and other dark sectors. Indeed, in some scenarios, the new states needed to explain neutrino masses are SM singlets such that they can become a

portal between the SM and DM. Moreover, heavier states which could explain the smallness of light neutrino masses might also help in the generation of the baryon asymmetry in the Early Universe.

Therefore, fully understanding the neutrino sector is key to understanding the flavour problem, given that neutrinos represent a large portion of the puzzle, through the precise determination of the leptonic mixing parameters, the origin of the DM in the Universe or the generation of the baryon asymmetry.

The first part of this thesis focuses on the study of a future neutrino super beam to study neutrino oscillations and probe for the still unknown parameters characterizing the neutrino sector, such as CP violation, and the neutrino mass ordering. Secondly, we study the possibility that the DM is primarily interacting with neutrinos through the neutrino portal, and that therefore large neutrino detectors acting as observatories might be our best probe to explore the dark sector. Later on we will consider the possibility that a keV neutrino arising from the neutrino mass mechanism could be itself the DM. In the third part we will study the possible relation between the neutrino mass mechanism and the matter-antimatter asymmetry.

Part I

NEUTRINO PHYSICS

1

INTRODUCTION

1.1 NEUTRINOS IN THE STANDARD MODEL

The existence of neutrinos was first proposed by Pauli in 1930 in order to fulfill energy-momentum conservation in β decays. Although their interactions were well described by Fermi's description of weak interactions, it was not until 1956 when Cowan and Reines experimentally proved the existence of neutrinos taking advantage from the copious production of neutrinos in a nuclear reactor.

Today, neutrinos are described by the Standard Model (SM) of particle physics [1–10], which is a quantum field theory based on the gauge group $SU(3)_c \times SU(2)_L \times U(1)_Y$, where c, L and Y denote colour, left-handed chirality and hypercharge, respectively. The particle content of the SM consists of three copies or families of fermions which have the same gauge interactions and only differ by their mass. Each family can be divided into quarks, particles which are charged under $SU(3)c$, and leptons, singlets of $SU(3)_c$. The fermionic particle content of the SM and their charges are summarised in Tab. 1.1, where the subindexes α and $L(R)$ correspond to the flavour and left(right)-handed chirality, respectively.

In addition, the SM contains a scalar H, the higgs doublet, which is a singlet under $SU(3)_c$, a doublet of $SU(2)_L$ and has hypercharge $Y = 1/2$. Upon spontaneous symmetry breaking (SSB), the higgs

	$SU(3)_c$	$SU(2)_L$	$U(1)_Y$
$Q_{\alpha L} = (u_{\alpha L},\ d_{\alpha L})^T$	3	2	1/6
$u_{\alpha R}$	3	1	2/3
$d_{\alpha R}$	3	1	-1/3
$L_{\alpha L} = (\nu_{\alpha L},\ l_{\alpha L})^T$	1	2	-1/2
$l_{\alpha R}$	1	1	-1

Table 1.1: Gauge charges of the SM fermions. The subindex α denotes the family, being $\alpha = e,\ \mu,\ \tau$ for leptons, and $u,\ c,\ t$ or $d,\ s,\ b$ for up and down-type quarks, respectively.

field acquires a vacuum expectation value (vev), v_H, which generates quark and charged lepton masses, as well as the masses for the W and Z bosons. Thus, at low energies $SU(2)_L \times U(1)_Y$ is spontaneously broken to $U(1)_{EM}$. The electric charge, Q, of the SM particles is given by the relation $Q = T_3 + Y$, where T_3 is the third component of the weak isospin. Notice that given the particle content and their charges, neutrinos are massless particles in the SM due to gauge and Lorentz invariance.

Each of the neutrino flavours are defined so that the charge current (CC) interactions with the W bosons and the charged lepton mass eigenstates are diagonal. The CC lagrangian reads as

$$\mathcal{L}_{CC} \supset -\frac{g}{\sqrt{2}} \sum_{\alpha=e,\mu,\tau} \bar{l}_{\alpha L} \gamma^\mu P_L \nu_{\alpha L} W^+_\mu + h.c., \tag{1.1}$$

where g is the $SU(2)_L$ coupling constant. Additionally, neutrinos have neutral current (NC) interactions with the Z boson

$$\mathcal{L}_{NC} \supset -\frac{g}{2\cos\theta_W} \sum_{\alpha=e,\mu,\tau} \bar{\nu}_{\alpha L} \gamma^\mu P_L \nu_{\alpha L} Z_\mu + h.c., \tag{1.2}$$

where θ_W is the weak mixing angle given by $\sin^2\theta_W = 1 - m_W^2/m_Z^2$. At low energies, we can integrate out the W and Z bosons to obtain effective four-fermion interactions, of the form

$$\mathcal{L}^{eff}_{CC} \supset -2\sqrt{2} G_F \sum_{\alpha,\beta=e,\mu,\tau} \left(\bar{\nu}_{\alpha L} \gamma^\mu P_L l_{\alpha L}\right) \left(\bar{l}_{\beta L} \gamma^\mu P_L \nu_{\beta L}\right), \tag{1.3}$$

where $G_F \equiv \sqrt{2} g^2/(8 m_W^2)$ is the Fermi constant, and similarly with the NC interaction lagrangian. Thus, we find that Fermi theory of weak interactions is just the low-energy manifestation of the electroweak theory.

1.2 EVIDENCE FOR NEUTRINO MASSES

On general grounds, if neutrinos are massive particles, the flavour and mass eigenstates will generally not coincide and will be related by

$$\nu_{\alpha L} = \sum_i^n (V_\nu)_{\alpha i} \nu_{iL}, \tag{1.4}$$

where V_ν is a unitary matrix which diagonalizes the neutrino mass matrix and ν_i are the mass eigenstates. In the following we will assume $n = 3$, but notice that this does not need to be the case. A similar relation can be found for the charged lepton mass matrix, with another rotation V_l. The only physical quantity appears in the CC interaction lagrangian from Eq. 1.1 and is the combination $U = V_l^\dagger V_\nu$, which is known as the Pontecorvo-Maki-Nakagawa-Sakata (PMNS) mixing matrix [11–15], and is equivalent to the CKM matrix for the

quark sector. Working in the basis where the flavour and mass eigenstates for the charged leptons coincide, we then have

$$\nu_{\alpha L} = \sum_{i}^{3} U_{\alpha i} \nu_{i,L}. \tag{1.5}$$

The mixing matrix U can be parametrised by three mixing angles, and, depending on whether neutrinos are Dirac or Majorana particles, by one or three CP violating phases, respectively, such that

$$U = \mathcal{R}(\theta_{23}, 0)\mathcal{R}(\theta_{13}, \delta)\mathcal{R}(\theta_{12}, 0)P_M, \tag{1.6}$$

where $\mathcal{R}(\theta_{ij}, \delta)$ is a rotation matrix in the ij-plane with complex phase δ and the matrix $P_M = diag\left(1, e^{i\alpha_1/2}, e^{i\alpha_2/2}\right)$ is only present in the case neutrinos are Majorana particles.

There are different ways to probe for neutrino masses. They can be divided into direct searches, which directly probe the absolute neutrino mass, or indirect ones, which study processes that can only take place if neutrino masses are non-zero.

1.2.1 *Kinematic searches for neutrino masses*

These searches probe directly the absolute neutrino mass by studying the kinematics of different particle decays. The processes are allowed already in the SM with massless neutrinos, but its rate can be computed as a function of the neutrino mass and thus, precisely measuring it, can allow to measure a combination of neutrino masses. So far, no positive signal of non-zero neutrino masses has been found, and thus only upper bounds on a given combination of neutrino masses are available. The most significant one comes from the KATRIN experiment [16] which studies the endpoint of the tritium β-decay spectrum to determine the effective electron neutrino mass, given by

$$m^2_{\nu_e} = \sum_{i}^{3} |U_{ei}|^2 m^2_{\nu_i}. \tag{1.7}$$

The reason why KATRIN uses tritium β-decay is because it has one of the lowest known Q values[1] of ~ 18 keV, and the experimental sensitivity increases with the ratio m_{ν_α}/Q, with α denoting the neutrino flavour in the final state. The latest bound from KATRIN sets the first-ever bound on m_{ν_e} below the eV scale. In particular, it was found that $m_{\nu_e} < 0.8$ eV at 90% CL. Similarly, bounds on the $\nu_{\mu(\tau)}$ mass can be obtained studying pion (tau) decay, but the constraints are much weaker.

1 The Q value is the difference between the total energy in the initial and final states of the decay not taking into account the neutrino mass.

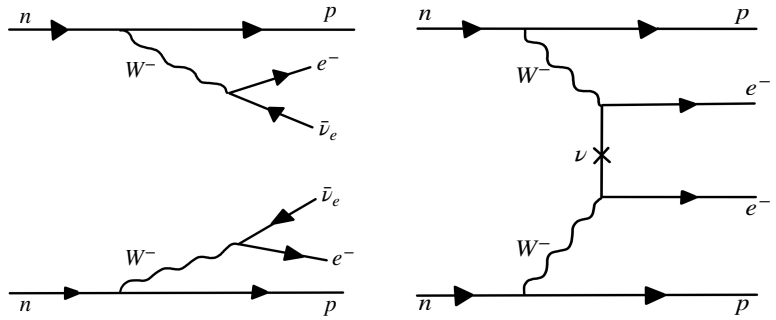

Figure 1.1: Feynman diagrams for the double β-decay process (left panel) and for neutrinoless double β-decay (right panel) where no neutrinos are present in the final state.

1.2.2 *Neutrinoless double beta decay*

Some nuclei with mass and atomic numbers (A, Z), respectively, can undergo double beta decay into another nuclei with $(A, Z+2)$, emitting a pair of electrons and electron antineutrinos. The Feynman diagram for such a process is depicted in the left panel of Fig. 1.1, where two neutrons, n, decay into a proton, p, an electron, e, and an electron antineutrino, $\bar{\nu}_e$, each.

On the other hand, if neutrinos were to be Majorana particles, lepton number would be broken, and then the process on the right panel of Fig. 1.1 would also be possible. In this case, there would be no antineutrinos in the final state, only the two electrons. This process is known as neutrinoless double beta ($0\nu2\beta$) decay, and is not possible in the SM. It can be shown that, if $0\nu2\beta$ decay takes place, at least one of the neutrinos is necessarily of Majorana nature. This is known as the "Black Box" theorem [17–22].

There has been a great experimental effort to look for this rare process using different nuclei and technologies, but we still lack a positive signal, such that some bounds have been placed on the effective neutrino Majorana mass, $m_{\beta\beta}$, which is given by

$$m_{\beta\beta} = \left| \sum_i^3 U_{ei}^2 m_{\nu_i} \right|, \tag{1.8}$$

where we have assumed that any new Physics responsible for the Majorana nature of neutrinos is heavy enough to be neglected in the process. Notice that the elements U_{ei} are in general complex and depend on the Majorana phases α_1 and α_2, such that cancellations could eventually appear making $m_{\beta\beta}$ very small. This can be seen in Fig. 1.2, taken from Ref. [23], for normal hierarchy (NH) shown as a red band. In fact, $m_{\beta\beta}$ in Fig. 1.2 is represented as bands because the Majorana phases are completely unkown, such that for a given m_{lightest} the Majorana phases can take any value between $[0,\ 2\pi)$.

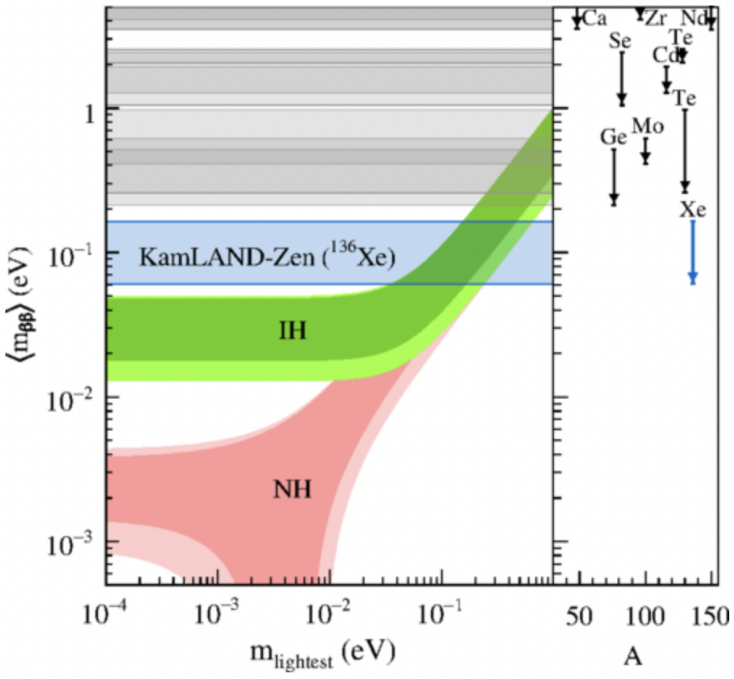

Figure 1.2: Effective Majorana neutrino mass as a function of the lightest neutrino mass, m_{lightest}, which corresponds to ν_1 for normal hierarchy and to ν_3 for inverted hierarchy. In the right part of the plot we have the different nuclei used in the different searches as a function of their mass number. Taken from Ref. [23].

Experimental searches put bounds on the half life-time of the given isotope, $T^{0\nu}_{1/2}$, but in order to translate it into a bound on $m_{\beta\beta}$ one needs to take into account the nuclear matrix element for the transition, $M^{0\nu}$, which has large uncertainties. Therefore, as $(T^{0\nu}_{1/2})^{-1} \propto |M^{0\nu}|^2 m^2_{\beta\beta}$ [24], the final bound on $m_{\beta\beta}$ is given as a range taking into account these uncertainties, as can be seen in Table 1.2 and Fig. 1.2.

1.2.3 *Cosmological bounds*

Massive neutrinos can have an impact in the evolution of the Universe. Indeed, if neutrinos are massive particles, they tend to suppress the matter power spectrum at small scales by erasing small

Experiment	$T^{0\nu}_{1/2}$ ($\times 10^{25}$ years)	$m_{\beta\beta}$ (eV)
GERDA [25]	> 8.0	$< 0.12 - 0.26$
CUORE [26]	> 1.5	$< 0.11 - 0.52$
KamLAND-Zen [23]	> 10.7	$< 0.061 - 0.165$

Table 1.2: $T^{0\nu}_{1/2}$ and $m_{\beta\beta}$ constraints at 90% CL from some of the most important experimental searches, taken from Ref. [27].

structures because of their large free-streaming distances [28]. Thus, combining cosmological and astrophysical observations can place an upper bound on the sum of light neutrino masses, which is nowadays[2] around [29]

$$\sum_i m_{\nu_i} < 0.2 \text{ eV at } 95\% \text{ CL}, \tag{1.9}$$

using the *Planck* 2015 [30] and baryon accoustic osccilations (BAO) [31–33] datasets.

1.2.4 *Neutrino oscillations*

The existence of light neutrino masses and mixings is well established nowadays thanks to the observation of neutrino oscillations. This was one of the first experimental evidence for the existence of physics beyond the SM (BSM), given that neutrinos are exactly massless in the SM.

1.2.4.1 *Experimental roadmap towards neutrino oscillations*

The first experiment detecting neutrino flavour change was the Homestake experiment [34] studying neutrinos from the Sun. They found a smaller number of ν_e detected through CC interactions compared to the expectation from simulations relying on solar models, which indicated that either solar models were incomplete or some aspect in neutrino physics was not understood. Indeed, if neutrinos oscillate, then it is only natural that the number of ν_e-events detected through CC interactions is smaller than what is expected in the absence of oscillations.

Subsequent experiments, the so-called "gallium" experiments [35–39], together with water cherenkov detectors like Kamiokande and later Super-Kamiokande (SK) [40], confirmed the depletion of electron neutrino events from the Sun and that it actually depended on the energy of the incoming neutrinos. Finally, the SNO Collaboration [41–44] used heavy water and its capabilities to measure events through both CC and NC interactions, as well as ν_e elastic scattering, to settle the solar neutrino problem. Even if neutrinos oscillated or underwent flavour change, NC interactions are insensitive to the particular neutrino flavour, such that a measurement of the solar neutrino flux through NC interactions should be in agreement with the expected flux from simulations in the absence of oscillations, as was indeed the case.

2 Assuming a minimal ΛCDM model. There are degeneracies and correlations with other parameters, such as the number of relativistic degrees of freedom, N_{eff}, such that the bounds can change depending on the assumptions and on the particular cosmological model used.

Apart from studying solar neutrinos, SK was also able to study the atmospheric neutrino flux arising from cosmic rays entering the atmosphere. Atmospheric neutrinos are made up of ν_μ neutrinos coming from pion and muon decay and ν_es from muon decay, in a ratio $N_{\nu_\mu}/N_{\nu_e} \sim 2$, and have energies at the GeV scale spanning several orders of magnitude. SK observed as well a depletion of the measured number of events with respect to simulations assuming no oscillations which depended on the zenith angle of the incoming neutrino [45] and on their energy.

There are other neutrino sources that can be studied, namely reactor neutrinos and accelerator neutrinos. The advantage of experiments studying these kind of sources is that the neutrino flux is better understood and under control. Particularly important experiments in this category are the KamLAND experiment [46], which studied reactor neutrinos at a baseline such that it could provide a complementary determination of the so-called "solar" oscillation parameters and accelerator neutrino experiments such as MINOS [47] and K2K [48] which confirmed the ν_μ disappearance observed in SK. Finally, after the efforts of Double-Chooz [49], RENO [50] and Daya-Bay [51] used reactor experiments to determine the value of the so-called "reactor" mixing angle, θ_{13}, which was believed at the time to be zero or very small based on theoretical bias.

These experimental results, with the exception of some anomalous results, are well described by the PMNS mixing matrix from Eq. (1.6) and can typically be understood in the context of 2-flavour oscillations, which we introduce in the following.

1.2.4.2 *Vacuum oscillations*

The oscillation probability in vacuum for an initial neutrino produced in a given weak process, $|\nu_\alpha\rangle$, to be detected as another given flavour eigenstate, $|\nu_\beta\rangle$, can be heuristically obtained using quantum mechanical arguments. A given flavour state is a superposition of mass eigenstates

$$|\nu_\alpha\rangle = \sum_i^3 U^*_{\alpha i}|\nu_i\rangle, \tag{1.10}$$

which have an energy $E = \sqrt{m_i^2 + p_i^2}$. The propagation states are the $|\nu_i\rangle$, such that we have

$$|\nu_\alpha(t)\rangle = \sum_i^3 U^*_{\alpha i} e^{iEt}|\nu_i\rangle, \tag{1.11}$$

at any given time t. Given that neutrinos are very light, we can assume they are relativistic, such that $p_i \sim E$ and $t \sim L$, with L the

distance between the source and the detector points. Performing an expansion we have

$$|\nu_\alpha(t)\rangle \simeq \sum_i^3 U_{\alpha i}^* e^{iEt} e^{i\frac{m_i^2 L}{2E}} |\nu_i\rangle. \tag{1.12}$$

The final probability in vacuum is thus given by

$$P(\nu_\alpha \to \nu_\beta) = |\langle \nu_\beta | \nu_\alpha(t)\rangle|^2. \tag{1.13}$$

Using the same arguments for the oscillation probability for an antineutrino, one just needs to change $U^* \to U$, such that the oscillation probability in vacuum for neutrinos and antineutrinos is

$$\begin{aligned} P(\overset{(-)}{\nu}_\alpha \to \overset{(-)}{\nu}_\beta) = \delta_{\alpha\beta} - 4\sum_{i>j} Re\left[U_{\alpha i}^* U_{\beta i} U_{\alpha j} U_{\beta j}^*\right] \sin^2\left(\frac{\Delta m_{ij}^2 L}{4E}\right) \\ \pm 2\sum_{i>j} Im\left[U_{\alpha i}^* U_{\beta i} U_{\alpha j} U_{\beta j}^*\right] \sin\left(\frac{\Delta m_{ij}^2 L}{4E}\right), \end{aligned} \tag{1.14}$$

where we have defined the mass-squared difference, $\Delta m_{ij}^2 \equiv m_i^2 - m_j^2$.

It is useful to study the 2-neutrino oscillation case, which is actually applicable in most experimental searches. In this case, there is only one effective mixing angle, θ_{eff}, and one mass-squared difference, Δm^2. The appearance probability is given by

$$P(\nu_\alpha \to \nu_\beta) = \sin^2 2\theta_{eff} \sin^2\left(\frac{\Delta m^2 L}{4E}\right), \tag{1.15}$$

while the disappearance is just $P(\nu_\alpha \to \nu_\alpha) = 1 - P(\nu_\alpha \to \nu_\beta)$. In this context, in order to measure both Δm^2 and θ_{eff} we need to perform an experiment whose $L/E \sim \Delta m^2$, such that oscillations are observed at the detector. The amplitude of the oscillation will be controlled by $\sin^2 2\theta_{eff}$.

1.2.4.3 *Matter oscillations*

When propagating through a medium like the Earth or the Sun, neutrinos can potentially interact with the electrons, protons and neutrons through elastic coherent interactions, such that their propagation is different than in vacuum [52]. In particular, for a medium of unpolarized non-relativistic particles the so-called matter potential would be given by $A_{CC} \simeq \sqrt{2} G_F n_e$ for CC interaction of ν_e with electrons in the media, where n_e is the density of electrons, while for NC interactions any SM neutrino can have an interaction and it would be $A_{NC} \simeq G_F n_n / \sqrt{2}$, where n_n is the neutron density. For antineutrinos we would have $A_i \to -A_i$.

It is useful to work in the two-flavour approximation, as it already shows all the interesting physical effects. In this case, neutrino oscillations in vacuum can be described by just one mass-squared difference,

Δm^2, and a single mixing angle, θ, such that the full hamiltonian in flavour space with matter effects would be

$$\mathcal{H}_M = \frac{1}{4E}\begin{pmatrix} -\Delta m^2 \cos 2\theta & \Delta m^2 \sin 2\theta \\ \Delta m^2 \sin 2\theta & \Delta m^2 \cos 2\theta \end{pmatrix} + \begin{pmatrix} A_{CC} - A_{NC} & 0 \\ 0 & -A_{NC} \end{pmatrix}, \tag{1.16}$$

where the first part corresponds to vacuum oscillations and the second to matter effects. We can add an overall quantity, $A_{NC} - A_{CC}/2$, proportional to the identity, such that the oscillation probability remains invariant. Thus, one needs to solve the following equation to obtain the oscillation probability

$$i\frac{d}{dt}\begin{pmatrix} \nu_e \\ \nu_\mu \end{pmatrix} = \begin{pmatrix} -\frac{\Delta m^2}{4E}\cos 2\theta + \frac{A_{CC}}{2} & \frac{\Delta m^2}{4E}\sin 2\theta \\ \frac{\Delta m^2}{4E}\sin 2\theta & \frac{\Delta m^2}{4E}\cos 2\theta - \frac{A_{CC}}{2} \end{pmatrix}\begin{pmatrix} \nu_e \\ \nu_\mu \end{pmatrix}. \tag{1.17}$$

The rotation diagonalizing the hamiltonian from Eq. (1.17) and the eigenvalues are different from the vacuum ones. In particular we will have an effective mass-squared difference, $\Delta\tilde{m}^2$, and mixing angle, $\tilde{\theta}$, given by

$$\begin{aligned} \Delta\tilde{m}^2 &= \Delta m^2 \sqrt{\sin^2 2\theta + \left(\frac{2A_{CC}E}{\Delta m^2} - \cos^2 2\theta\right)^2}, \\ \tan 2\tilde{\theta} &= \frac{\tan 2\theta}{\frac{2A_{CC}E}{\Delta m^2 \cos 2\theta} - 1}. \end{aligned} \tag{1.18}$$

From the expression of the effective mixing angle in Eq. (1.18) we can already observe a completely different feature of oscillations in matter with respect to the vacuum ones. Even for small mixing angles in vacuum, and depending on the sign of Δm^2, for the proper environment we can have $\tan 2\tilde{\theta} \to \infty$, such that $\tilde{\theta} = \pi/4$ and we have maximal mixing. This is known as the Mikheyev-Smirnov-Wolfenstein effect [52, 53]. Thus, matter effects are sensitive to the ordering, i.e., the sign of Δm^2.

1.2.4.4 *Status of neutrino oscillations*

After the discovery of a non-zero θ_{13} [50, 54–57] the emerging picture from the last decades of neutrino oscillation searches consolidates a structure for the PMNS matrix describing lepton flavour mixing strikingly different from its CKM counterpart in the quark sector. This makes the SM flavour puzzle, the question of why fermion masses span over six orders of magnitude and the mixing for quarks and leptons is so different, even more intriguing. Far from the hierarchical structure described through the tiny mixing angles of the CKM, large mixing angles characterize the lepton mixing, as can be seen from the latest determination of oscillation parameters in Tab. 1.3, taken from Ref. [58] for normal ordering (NO) and inverted ordering

	Best fit point $\pm 1\sigma$	
	Normal Ordering	Inverted Ordering
$\sin^2\theta_{12}$	$0.304^{+0.012}_{-0.012}$	$0.304^{+0.013}_{-0.012}$
$\sin^2\theta_{23}$	$0.573^{+0.016}_{-0.020}$	$0.575^{+0.016}_{-0.019}$
$\sin^2\theta_{13}$	$0.02219^{+0.00062}_{-0.00063}$	$0.02238^{+0.00063}_{-0.00062}$
$\delta(^\circ)$	197^{+27}_{-24}	282^{+26}_{-30}
$\frac{\Delta m^2_{21}}{10^{-5}\ \mathrm{eV}^2}$	$7.42^{+0.21}_{-0.20}$	$7.42^{+0.21}_{-0.20}$
$\frac{\Delta m^2_{3l}}{10^{-3}\ \mathrm{eV}^2}$	$+2.517^{+0.026}_{-0.028}$	$-2.498^{+0.028}_{-0.028}$

Table 1.3: Three neutrino oscillation parameters from a global fit [58]. The best fit corresponds to NO for which $\Delta m^2_{3l} \equiv \Delta m^2_{31}$, while for IO we have $\Delta m^2_{3l} \equiv \Delta m^2_{32}$.

(IO), depending on the sign of Δm^2_{3l}. The "atmospheric" mixing angle θ_{23} is presently compatible with maximal mixing as well as with a large but non-maximal value in either the first or the second octant [58]. Similarly, the "solar" mixing angle θ_{12} is around 33° and only $\theta_{13} \sim 8 - 9^\circ$ is relatively small and its value is still comparable in magnitude to the Cabibbo angle, the largest in the CKM. The large mixing opens the window to the present and next generation of neutrino oscillation experiments to tackle new questions that could provide answers to fundamental open problems.

The discovery of the violation of the particle-antiparticle symmetry in the lepton sector would be extremely suggestive, given that CP violation is a necessary ingredient to explain the matter over antimatter excess to which we owe our existence and that the CKM contribution has been shown to be insufficient [59, 60] for this purpose. Although present experiments such as T2K [61, 62] and NOνA [63] provided some initial hints on the potentially CP violating phase δ, they have diluted with the latest results [58] such that more precise experiments are needed to discover CP violation. Similarly, neutrino oscillation experiments already show some preference for normal ordering with respect to inverted ordering. This parameter is a fundamental input to combine with the searches for the neutrinoless double beta decay process in order to probe the Majorana nature of neutrinos. Finally, present experiments as well as their successors T2HK [64] and DUNE [65] will also provide even more precise measurements of the oscillation parameters that could hold the key to discriminate among different flavour models addressing the flavour puzzle.

2

THE QUEST FOR CP VIOLATION

2.1 THE ESS NEUTRINO SUPER-BEAM

The European Spallation Source (ESS) at Lund provides an opportunity to build a new-generation, long-baseline neutrino oscillation experiment with an unprecedented neutrino luminosity through an upgrade of the ESS Linac [66]. Its 2.5 GeV protons would lead to a rather low energy neutrino flux, between 200 and 600 MeV. This energy range is very well suited for a water Cerenkov detector of the MEMPHYS type [67, 68]. In Ref. [66] a greenfield study optimizing the physics reach to leptonic CP violation was performed for this ESS neutrino Super-Beam facility (ESSnuSB). Interestingly, the outcome of this optimization, as well as follow-up studies [69–71], was that the best baseline at which to study the neutrino beam from the ESS facility at a MEMPHYS-type detector would be between 400 and 600 km. Two candidate mines that could host the detector were identified: Garpenberg at 540 km and Zinkgruvan at 360 km from the ESS site. This choice makes the ESSnuSB design unique, as the neutrino flux observed by the detector mainly corresponds to the second maximum of the $\nu_\mu \to \nu_e$ oscillation probability, with a marginal contribution of events at the first oscillation peak.

For the value of $\theta_{13} = 8.6^\circ$ currently preferred [72] by Daya Bay [73] and RENO [74], the "atmospheric" term of the $\nu_\mu \to \nu_e$ oscillation probability [75], which is governed by oscillations driven by the large frequency Δm^2_{31} and with an amplitude $\sin^2 2\theta_{13}$, dominates over the sub-leading "solar" term driven by Δm^2_{21} with amplitude $\sin^2 2\theta_{12}$ at the first oscillation maximum. Thus, the interference between the two, which is the only term dependent on the yet unknown CP violating phase δ, will also be a sub-leading contribution to the full oscillation probability at the first peak and potentially hidden by systematic uncertainties. Conversely, at the second oscillation maximum the slower "solar" oscillation has had more time to develop and thus the CP violating interference term can give a significant contribution to the oscillation probability, thus increasing the sensitivity to CP violation [76].

The price to pay in order to observe the oscillation probability at its second maximum is high. Despite this being the optimal choice

to maximize the dependence of the oscillation probability on the leptonic CP violating phase, the ratio of the oscillation baseline to the neutrino energy (L/E) needs to be a factor 3 larger compared to the first maximum. This implies roughly an order of magnitude less statistics than if the experiment had been designed at the first peak. Indeed, the neutrino flux decreases with L^{-2} from the beam divergence and the neutrino cross section and beam collimation increase with the neutrino energy. Despite the unprecedented neutrino luminosity from the upgraded ESS linac and the megaton-class MEMPHYS detector, only around 100 signal events for each beam polarity would be accumulated after 10 years data taking (2 years in neutrinos and 8 years in antineutrinos) at the 540 km Garpenberg baseline (see Fig. 7 of Ref. [66]). Conversely, the 360 km Zinkgruvan baseline has a 2.25 times larger neutrino flux. However, the neutrino spectrum for this baseline is rather centered at the first oscillation minimum while the first and second peaks are sampled by the high and low energy tails respectively. Overall this gives similar statistics at the second oscillation maximum when compared to the Garpenberg option, but also some additional statistics at the first peak and in between.

For the ESSnuSB the increased dependence on the CP violating phase of the probability is well worth the loss of precious neutrino events at the second maximum. Indeed, it could provide unprecedented discovery potential to leptonic CP violation or the most precise measurement of the corresponding phase after discovery, which could be instrumental in tackling the flavour puzzle. Moreover, as pointed out in Ref. [76] and as we will elaborate in later sections, this choice also makes the physics reach much more resilient against unexpected sources of systematic errors, since the signal, while small, has a leading dependence on the unknown parameters. Conversely, statistics will be the bottleneck of the ESSnuSB physics reach and thus longer periods of data taking would greatly increase its capabilities.

On the other hand, other potential oscillation searches, different from the CP violation search, will be negatively impacted by the choice of the second oscillation maximum baseline. In particular the sensitivity to the octant of θ_{23} is severely reduced by this choice. Indeed, this measurement mainly relies on the "atmospheric" term of the oscillation probability, which is leading at the first maximum instead, together with θ_{13} information from reactor measurements and Δm^2_{31} and $\sin^2 2\theta_{23}$ from ν_μ disappearance. Similarly the ν_μ disappearance data and hence the precise determination of Δm^2_{31} and $\sin^2 2\theta_{23}$ are negatively affected by the choice of the second oscillation maximum. The lack of knowledge on the octant of θ_{23} can lead to "octant degeneracies" [77] that in turn somewhat limit the CP discovery potential of the ESSnuSB [78]. The sensitivity to the mass ordering is also limited at the ESSnuSB given the small matter effects from the low energy and short baseline. However, since these matter effects

are small, the resulting "sign degeneracies" [79] do not compromise the sensitivity to δ of the facility [66, 78].

A very effective and convenient way of increasing both the octant and mass ordering sensitivity of a neutrino Super Beam experiment is to combine the signal from the neutrino beam with the huge atmospheric neutrino sample that can be collected at such a detector [80, 81]. In the case of the ESSnuSB this combination is particularly synergistic. Indeed, the atmospheric neutrino sample can provide not only significantly increased sensitivity to the octant and the mass ordering to solve parametric degeneracies, but also improved precision to Δm^2_{31} and $\sin^2 2\theta_{23}$ which is otherwise one of the main drawbacks of the setup.

In this work we will combine the observation of the ESSnuSB flux tuned for the second maximum of the ν_e appearance probability with the complementary atmospheric neutrino data, more strongly dominated by the first maximum and ν_μ disappearance, and characterized by stronger matter effects. We will explore how the physics reach of the facility improves when beam data is considered together with the atmospheric neutrino sample and then review the optimization of the ESSnuSB facility using both data sets. Finally, we will discuss which sources of systematic errors among the ones considered impact the final sensitivity more significantly.

This paper is organized as follows. In Section 2.2 we discuss the peculiarities of the neutrino oscillation probability and the appearance of parametric degeneracies when observing at the second oscillation maximum. In Section 2.3 we describe the experimental setup considered and the details of the numerical simulations performed. Section 2.4 describes the results of the simulations and in Section 6.6 we present our conclusions and summarize our work.

2.2 MEASUREMENTS AT THE SECOND OSCILLATION PEAK

The determination of the oscillation parameters at beam experiments is, in general, hindered by the appearance of degenerate solutions, cf. e.g., Refs. [82–86]. These degeneracies have been extensively studied for the experimental setups of T2HK [87–92] and DUNE [65, 87, 91, 93–104] (and also their combination [105, 106]). As stated in Section 2.1, the L/E range which the ESSnuSB focuses on is different from those of other forthcoming experiments,[1] Therefore, here we will discuss the peculiarities of ESSnuSB and the differences from other experiments in the determination of the oscillation parameters

1 The MOMENT proposal [107–110] with $L = 150$ km can access to the oscillation probability with similar L/E to the ESSnuSB. The T2HKK proposal [111–121], in which the first and the second oscillation maxima are measured with two detectors located at different sites, would also cover the similar L/E range to the ESSnuSB.

before presenting our numerical results. The ν_e appearance oscillation probability in matter is given by [75] (see also [122–124]):

$$\begin{aligned} P(\overset{(-)}{\nu}_\mu \to \overset{(-)}{\nu}_e) = s^2_{23} \sin^2 2\theta_{13} \left(\frac{\Delta_{31}}{\tilde{B}_\mp}\right)^2 \sin^2\left(\frac{\tilde{B}_\mp L}{2}\right) \\ + c^2_{23} \sin^2 2\theta_{12} \left(\frac{\Delta_{21}}{A}\right)^2 \sin^2\left(\frac{A_{CC} L}{2}\right) \\ + \tilde{J} \frac{\Delta_{21}}{A_{CC}} \frac{\Delta_{31}}{\tilde{B}_\mp} \sin\left(\frac{A_{CC} L}{2}\right) \sin\left(\frac{\tilde{B}_\mp L}{2}\right) \cos\left(\pm\delta - \frac{\Delta_{31} L}{2}\right), \end{aligned} \tag{2.1}$$

where $\Delta_{ij} \equiv \Delta m^2_{ij}/2E$, $\tilde{J} = c_{13} \sin 2\theta_{12} \sin 2\theta_{23} \sin 2\theta_{13}$, and $\tilde{B}_\mp \equiv |A_{CC} \mp \Delta_{31}|$. In this expression the only dependence in the CP violating phase δ appears in the last term, which is the interference between the "atmospheric" oscillation in the first term and the "solar" in the second. Since $\sin 2\theta_{13} \sim 0.3$ while $\Delta_{21} L \sim 0.05$ at the first oscillation peak, the "atmospheric" term tends to dominate the oscillation probability and the interesting CP interference is only subleading. Conversely, at the second oscillation maximum $\Delta_{21} L \sim 0.1$ so that the dependence on δ of the oscillation probability is much higher which allows to improve the sensitivity to this parameter [76]. This can be seen in Fig. 2.1 where the change in the probability upon changing the values of δ is much more significant at the second peak maximum compared to the first.

In Eq. (2.1) the leading dependence on the mass ordering comes from the "atmospheric" term, as it goes as the inverse of the square of $\tilde{B}_\mp$. For $E \sim |\Delta m^2_{31}|/(2A_{CC})$ there will be a resonance which will produce an enhancement in neutrinos against antineutrinos or viceversa depending on the mass ordering. For a typical average matter density of 3.0 g/cm^3 one finds that the approximate energy for this resonance to happen is $E \sim \mathcal{O}(\text{GeV})$. Given that the peak of the flux for ESSnuSB happens at $E \sim \mathcal{O}(100)$ MeV (see Fig. 2.1), the importance of the matter effects and hence of the sensitivity to the mass ordering for this facility is not expected to be significant.

The bi-probability plots [79] shown in Fig. 2.2 help to illustrate the degeneracy problem at the ESSnuSB experiment. Here all oscillation parameters other than δ, the octant of θ_{23}, and the sign of Δm^2_{31} are fixed at the current best fit values [72], and the matter density along the neutrino baseline is assumed to be constant with an average density of 3.0 g/cm^3. The baseline length L and the neutrino energies E are set to $L = 540$ km (ESS-Garpenberg) and $E = \{280, 380, 480\}$ MeV. The ellipses show the variation of the appearance probabilities for the neutrino and antineutrino channels from changes in δ. The four ellipses in each plot correspond to the different choices of the octant of θ_{23} and the mass ordering. When the ellipses overlap sharing the same region in the $P(\nu_\mu \to \nu_e)$-$P(\bar{\nu}_\mu \to \bar{\nu}_e)$ plane, the same oscillation probabilities can be obtained by changing δ, the octant of θ_{23} and/or the mass ordering, implying the existence of degenerate solutions.

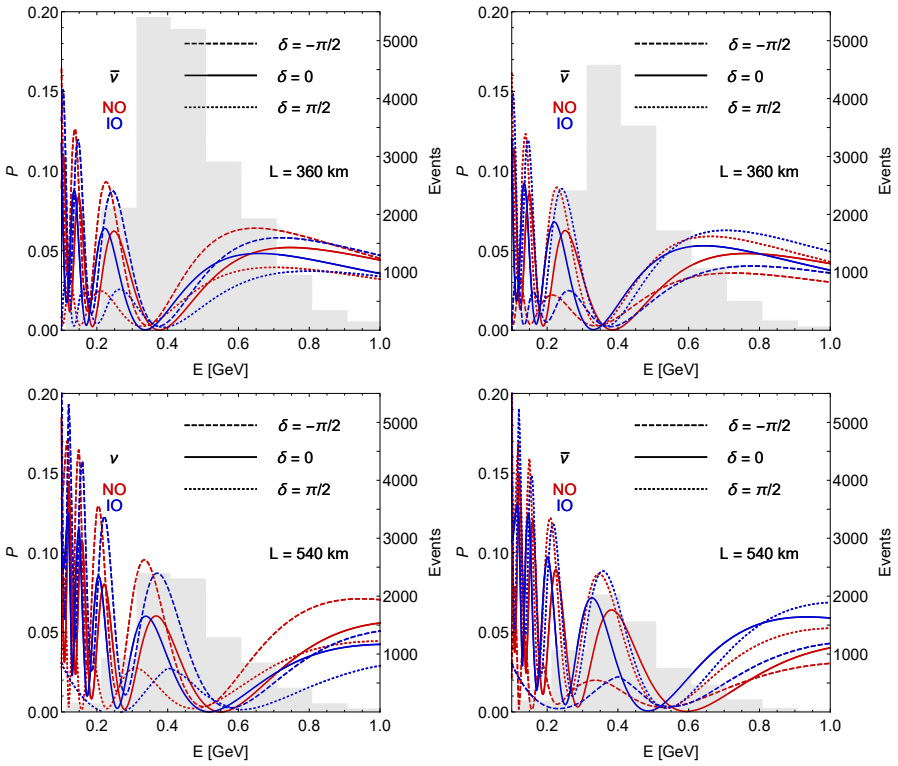

Figure 2.1: Oscillation probabilities for the Zinkgruvan (upper panels) and Garpenberg (lower panels) baselines as a function of the energy for neutrinos (left panels) and antineutrinos (right panels). The red (blue) lines are for normal (inverted) ordering and three different values of $\delta = -\pi/2$, 0 and $\pi/2$ are represented by the dashed, solid and dotted lines respectively. The grey histograms show the number of events that would be obtained in each energy bin for a 2/8 time splitting between neutrino/antineutrino mode if the oscillation probability was 1. Thus, they serve as a guide of what energies of the oscillation probability would be well-sampled by the ESSnuSB setup.

Let us first focus on the middle plot with $E = 380$ MeV where the oscillation probabilities are close to the second maximum, $|\Delta_{31}|/2 \sim 3\pi/2$. The centres of the ellipses are located on the CP conserving line $P(\nu_\mu \to \nu_e) = P(\bar{\nu}_\mu \to \bar{\nu}_e)$, which reflects the fact that the matter effect, which could induce an explicit difference between the neutrino and antineutrino oscillation probabilities unrelated to the intrinsic CP violation from δ, is irrelevant for this energy and baseline. The major axes of the ellipses extend widely along the diagonal line orthogonal to the CP conserving line. This means that the CP violating term proportional to $\sin\delta$ in Eq.(2.1) is very relevant in the oscillation probability for this energy and baseline, leading to the improved CP sensitivity at the second oscillation peak.

The "fake" CP violation effect due to the matter effect separates the two ellipses with opposite mass ordering at the first oscillation maximum, where T2HK focuses on, causing the δ-sign(Δm^2_{31}) degeneracy in the CP violation search, cf. the right most plot in Fig. 2.3. Conversely, the CP violation search at the second oscillation maximum is not noticeably affected by the matter effect [78, 125]. Changing the value of θ_{23}, the ellipses almost keep the same shape and move in parallel along the CP conserving line, which causes the δ-θ_{23} degeneracy [84, 85].

The vertices of the ellipses are located at $\delta = \{\pi/2, -\pi/2\}$, where the oscillation probabilities do not change much with a change of δ. As a consequence, the precision in the determination of δ becomes worse close to the oscillation maxima [126]. In other words, since the two points with δ and $\pi - \delta$ on an ellipse are close to each other around $\delta = \{\pi/2, -\pi/2\}$, it is hard to separate them [126]. Although at the probability level from Fig. 2.2 the expectation would be that this quasi-degeneracy effect occurs similarly at $\delta = \pi/2$ and $\delta = -\pi/2$, the numerical simulations we will report in Section 2.4 show that the ESSnuSB suffers this effect more severely at $\delta = -\pi/2$ than at $\delta = \pi/2$. This is due to the significant difference in event rates between these two points. Indeed, for $\delta = -\pi/2$, the oscillation probability for neutrinos is enhanced while the antineutrino one is suppressed. Since both the flux and the cross section are also smaller for antineutrinos, this strongly penalizes the measurement at $\delta = -\pi/2$ since the antineutrino sample is essentially lost given that the event rate at the second oscillation peak is already necessarily small. On the other hand, at $\delta = \pi/2$, the oscillation probability for neutrinos is suppressed, but the larger cross section and flux compensate for it and prevents such a big loss of sensitivity.

In the energy region that the ESSnuSB focuses on, the oscillation phase changes rapidly. As a consequence, the shape and location of the ellipses changes very significantly even within the same energy bin. In Fig. 2.2, we also show the bi-probability plots with E =280 and 480 MeV where the oscillation probabilities are approaching the min-

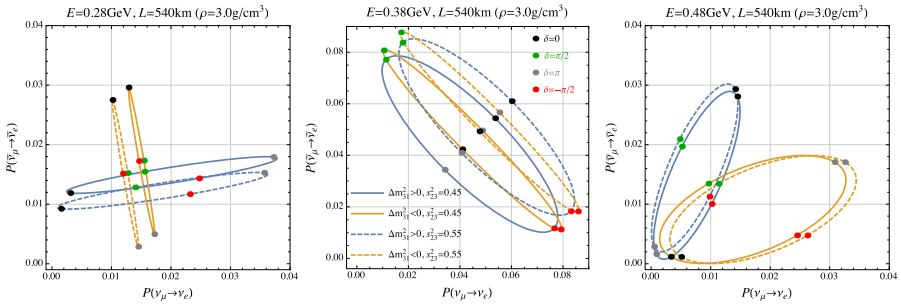

Figure 2.2: Bi-probability plots for the ESS-Garpenberg setup $L = 540$ km. Three plots for three different neutrino energies: $E = \{280, 380, 480\}$ MeV from left to right. The four ellipses in each plot for the different choices of $(s^2_{23} \equiv \sin^2\theta_{23}, \text{sign}[\Delta m^2_{31}])$: blue solid for $(0.45, +)$, orange solid for $(0.45, -)$, blue dashed for $(0.55, +)$, and orange dashed for $(0.55, -)$. The energies $E = 380$ MeV and $E = 480$ MeV correspond to the vicinity of the second oscillation maximum and the first oscillation minimum.

ima, which are also well-covered by the ESSnuSB flux. The ellipses are not distributed symmetrically to the CP conserving line, which means that, contrary to the second peak, matter effects do have some impact on the oscillation probabilities. However, this impact is still subleading, given the rather low energy, and does not shift the energies where the extrema are located, cf. Fig. 2.1. As a result, the two ellipses for the different mass hierarchies are not separated in the entire energy region.

The drastic shape change of the ellipses when varying the energy is largely due to the ratio of the $\sin\delta$ and the $\cos\delta$ terms in the oscillation probability, see Eq. (2.1). The $\sin\delta$ term is most significant close to the oscillation peak with $|\Delta m^2_{31}|L/(4E) \simeq 3\pi/2$ for $E \simeq 380$ MeV. As the probabilities depart from the maximum, the major axes of the ellipses start following along the direction of the CP conserving line, which means that the $\cos\delta$ term increases in importance as we approach the minima with $|\Delta m^2_{31}|L/(4E) \simeq \pi$ (right panel of Fig. 2.2) or $|\Delta m^2_{31}|L/(4E) \simeq 2\pi$ (left panel). In the left and the right plots, the ellipses with different mass orderings intersect each other at points with different values of δ at different energies. Therefore, in principle, with precise enough measurements at various energies, one could determine the value of δ and the sign of Δm^2_{31} separately. However, the oscillations are too fast for the ~ 100 MeV resolution achievable at these energies with a water Cerenkov detector to resolve and also the event rate at the second maximum is not large enough to perform a very fine binning. Thus, it is not possible to track the rapid oscillations in Fig. 2.1, although some mild sensitivity to the mass ordering can be achievable.

A large overlap between the two ellipses with different mass orderings and different octants at the oscillation maximum (middle panel

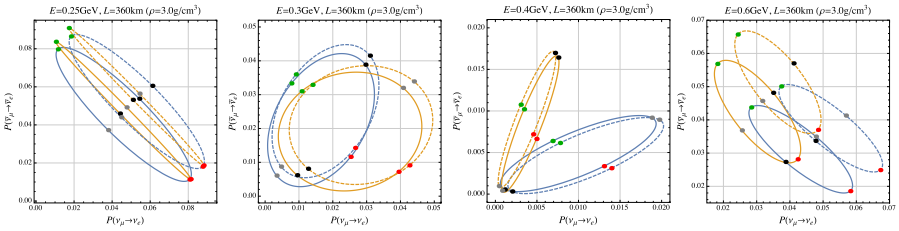

Figure 2.3: Bi-probability plots for $L = 360$ km (ESS-Zinkgruvan). In this energy range $E = 250 - 600$ MeV, the oscillation probabilities experience the second maximum, the first minimum, and the first maximum.

in Fig. 2.2), where most of the statistics is concentrated, suggests that the mass ordering sensitivity at the beam experiment is affected by the octant degeneracy.

The ellipses for different octants barely separate in the entire energy region, which implies a rather poor sensitivity to θ_{23} in the appearance channel leading to octant degeneracies that can spoil both the determination of δ and of the mass ordering at the ESSnuSB. Conversely, for experiments focusing on the first maxium the two ellipses for different octants are more separated [78], cf. the right panel in Fig. 2.3. Therefore, we will explore the impact of the addition of the atmospheric neutrino data collected at the far detector of the ESSnuSB to the beam data since atmospheric neutrinos can provide both sensitivity to the θ_{23} octant and the mass ordering helping to lift parametric degeneracies [80, 81].

The mass ordering sensitivity from an observation of atmospheric neutrinos comes from the oscillation signals driven by Δm^2_{31} and the matter effect (first term in Eq. (2.1)) and therefore, it does not depend on the value of δ. On the other hand, the sensitivity is better for θ_{23} in the second octant than the first octant, since the term is proportional to $\sin^2\theta_{23}$ [127].

If the shorter baseline $L = 360$ km (ESS-Zinkgruvan) is instead considered, the neutrino flux at the high energy tail up to $E \sim 600$ MeV covers the first oscillation maximum. This situation corresponds to the bi-probability ellipses presented in the right panel of Fig. 2.3, which show the same shape and position characteristic of other experiments located at the first oscillation maximum such as T2HK. The matter effect is not significant enough to completely separate the two mass orderings. In the relevant energy range (200-600 MeV), the oscillation probabilities go from the first maximum (right panel) to the first minimum (middle panels) and to the second maximum (left panel). The leftmost panel with $E = 250$ MeV, where the second oscillation peak would be located, looks very similar to that with $E = 380$ MeV in the case of $L = 540$ km. The ellipses for the different mass orderings are separated more clearly in the case of $L = 360$ km than $L = 540$ km in a large energy region, which leads to a slightly better

sensitivity to the mass ordering even though the baseline is shorter. From the information at the first oscillation maximum, the ESSnuSB with $L = 360$ km also has better sensitivity to θ_{23} than the $L = 540$ km option, so that it is expected that the longer baseline option will benefit more from the addition of the atmospheric neutrino data, which helps to determine θ_{23} and its octant.

2.3 SIMULATION AND EXPERIMENTAL DETAILS

The simulation of the ESSnuSB data has been performed with the GLoBES software [128, 129]. We have assumed that the neutrino beam will shine on a near and a far detector to reduce the systematic uncertainties [66]. The far detector is a 1 Mt MEMPHYS-like water Cerenkov detector [68], while the near detector has been assumed to be identical to the far detector in terms of efficiencies and background rejection capabilities with a fiducial mass of 0.1 kt. The response of the detectors has been implemented through migration matrices, both for the signal efficiency and the background rejection from Ref. [68].

A beam power of 5 MW with 2.5 GeV protons and an exposure of 1.7×10^7 operating seconds per year has been assumed [66]. The fluxes have been simulated explicitly at 1 km for the near detector [130], accounting for possible geometrical effects since the source cannot be considered point-like, as well as for 100 km (and consequently rescaled) for the longer baselines considered for the far detector [66]. The event rate peaks around $\mathcal{O}(100)$ MeV energies (see Fig.2.1), so the dominant contribution to the cross section will be in the quasi-elastic regime (QE). For the cross section we use the results from the Genie [131] tune G18_10a_00_000.

We have assumed a total running time of 10 years. Nonetheless, we will also study the dependence of the physics reach on the relative running time spent in positive and negative focusing in order to optimize it for the measurement of CP violation. Likewise, although the preferred location of the far detector for the ESSnuSB is the Garpenberg mine at 540 km [66], different baselines, with emphasis in the alternative Zinkgruvan option at 360 km, will be studied to address the optimal choice. Finally, we will also study how the CP discovery potential depends on the total exposure.

Throughout all the simulations we adopt the same treatment of the systematic errors from Table 2.1 as in Ref. [87]. Unless otherwise specified, we will assume the "Optimistic" systematics from the first "Opt." column in Table 2.1 although we will also show how the results are affected when the more conservative ones in the second column "Cons." are considered instead. All systematics have been introduced as nuisance parameters and the results presented have been obtained minimizing the χ^2 over all of them. The systematic uncer-

Systematic uncertainty	Optimistic	Conservative
Fiducial volume ND	0.2%	0.5%
Fiducial volume FD	1%	2.5%
Flux error ν	5%	7.5%
Flux error $\bar{\nu}$	10%	15%
NC background	5%	7.5%
Cross section $\times$ eff. QE	10%	15%
Ratio $\nu_e/\nu_m u$ QE	3.5%	11%

Table 2.1: Systematic uncertainties for a super beam as described in Ref. [87] for two different scenarios, the "Optimistic" one and the "Conservative" scenario where systematics are larger.

tainties associated to fluxes and cross sections have been assumed to be fully correlated between near and far detector and uncorrelated between neutrino and antineutrino components and different flavours. The uncertainties on the fiducial volumes of the near and far detectors were not assumed to be correlated. Additionally, to account for the uncertainty in the cross section between the near and far detector, arising from the different flavour composition of the beam (mainly ν_μ in the near site and ν_e for the signal in the far detector), a completely uncorrelated systematic is included for their ratio (last row of Table 2.1). Therefore, the χ^2 will be given by

$$\chi^2 = \min_{n_{s_i}} \left(\hat{\chi}^2_{FD}[n_{s_C}] + \hat{\chi}^2_{ND}[n_{s_C}, n_{s_U}] + \frac{n^2_{s_C}}{\sigma^2_{n_{s_C}}} + \frac{n^2_{s_U}}{\sigma^2_{n_{s_U}}} \right), \tag{2.2}$$

where $\hat{\chi}^2_{FD}$ ($\hat{\chi}^2_{ND}$) corresponds to the far (near) detector and n_{s_C} (n_{s_U}) are the correlated (uncorrelated) systematic uncertainties.

We have added to the resulting χ^2 a gaussian prior with the central values and 1σ errors from Ref. [72] for "solar" and "reactor" parameters. For the "atmospheric" parameters we set a prior on $\sin^2 2\theta_{23}$ and $|\Delta m^2_{31}|$ given that the octant for θ_{23} and the mass ordering are still unknown. Since the determination of these two parameters comes primarily from atmospherics, when adding this sample to the beam data no prior has been added on θ_{23} and Δm^2_{31}.

The simulation of the atmospheric neutrino sample in MEMPHYS is the one used in the analysis from Ref. [81] where the neutrino fluxes at Gran Sasso from Honda calculations [132] were used. This is a conservative estimate as fluxes become larger at higher geomagnetic latitudes such as Garpenberg or Zinkgruvan. In the simulation the events are separated between fully and partially contained events in the detector and stopping from through-going muon events. The neutral current contamination in each bin was included assuming the same ratio as Super-Kamiokande between neutral-current and

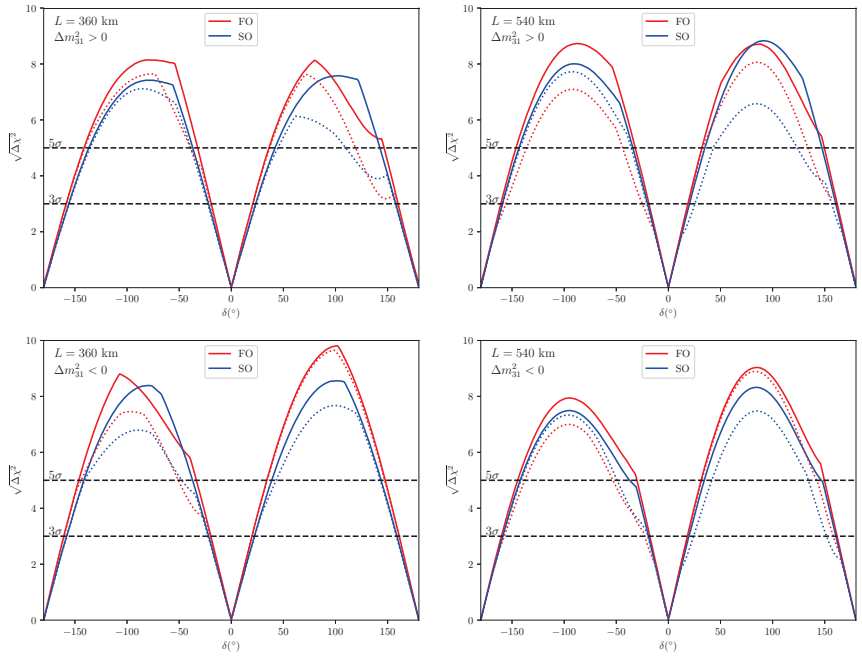

Figure 2.4: Significance with which CP conserving values of δ can be excluded for the Zinkgruvan 360 km (left panels) and Garpenberg 540 km (right panels) options. The upper (lower) plots are for normal (inverted) mass ordering while the red (blue) curves correspond to θ_{23} in the first (second) octant. The dashed lines correspond to the beam data only, while the continuous lines correspond to the results studying events from the beam and from atmospheric neutrinos. The running time splitting has been assumed to be t_ν=$t_{\bar{\nu}} = 5$ years.

unoscillated charged-current events [133]. For further details on the atmospheric sample see [81].

2.4 RESULTS

In Fig. 2.4 we show the impact on the CP discovery potential of the ESSnuSB before (dashed lines) and after (solid lines) the inclusion of the atmospheric sample for the Zinkgruvan (360 km) and Garpenberg (540 km) options in the left and right panels, respectively. The plots represent the $\sqrt{\Delta\chi^2}$ with which CP conserving values of $\delta = 0$ or π can be disfavoured as a function of the true value of δ. We take the minimum of $\Delta\chi^2$ between $\delta = 0$ and π. The $\sqrt{\Delta\chi^2}$ can be interpreted as the significance for exclusion of CP-conserving values (and hence evidence for CP violation) as long as the assumptions behind Wilks' theorem hold [134]. Deviations from these assumptions can be sizable for presently running experiments, but are expected to be smaller for next generation facilities [135].

Even though the sensitivity of the atmospheric neutrino dataset to δ is almost negligible, the improvement of the ESSnuSB physics reach

upon its inclusion is quite remarkable. The improvement is generally larger for the longer 540 km baseline than for the Zinkgruvan 360 km option. This is in line with the expectations discussed in Section 2.2 of the atmospheric sample being more complementary to the beam information at the longer baseline. Indeed, at the second oscillation maximum the ν_μ disappearance oscillation is not sampled as efficiently as at the first peak and this deteriorates the determination of the atmospheric oscillation parameters θ_{23} and Δm^2_{31}, which play an important role in the measurement of δ. Conversely, the 360 km baseline has higher statistics and some events also cover the first oscillation maximum such that the atmospheric oscillation information is less complementary and the gain upon its inclusion is less noticeable. From these results we can conclude that the ESSnuSB setup combined with the atmospheric neutrino sample would be able to rule out CP-conserving values of δ for $\sim 60\%$ ($\sim 55\%$) of the possible values of δ at the 5σ level regardless of the octant and the mass ordering when observing at the 540 km (360 km) baseline.

Figure 2.4 also shows that the gain in CP discovery potential is much more pronounced in some particular regions of the parameter space, especially for $\delta < 0$ and θ_{23} in the first octant or $\delta > 0$ and the second octant. In these examples the dotted curves for beam only often show a kink that reduces the slope and the values of δ for which CP violation could be discovered with high significance. Conversely, the corresponding solid curves with atmospheric data either do not display the kink or develop it at higher significance so that the resulting CP-discovery potential is much larger. These kinks occur due to the presence of an unresolved octant degeneracy at a CP-conserving value of δ that prevents drawing conclusions regarding CP violation. When atmospheric data is added, the sensitivity to the octant improves and these degeneracies are either lifted or only show up at much higher significance.

This situation is illustrated in Fig. 2.5, where the allowed regions at the $\Delta\chi^2 = 25$ level are shown in the δ-$\sin^2\theta_{23}$ plane. The left (right) panels assume the true values $\delta = -40^\circ$ ($\delta = 150^\circ$), $\sin^2 2\theta_{23} = 0.418$ ($\sin^2 2\theta_{23} = 0.582$) and normal ordering. As can be seen, when only the beam information is taken into account (blue curves), an octant degeneracy that spreads the allowed region towards CP conserving values appears. Conversely, the atmospheric data on their own (red curves) have no capability to determine δ at all, but can instead rule out the wrong octant of θ_{23}. Thus, the combination of the two data sets (black curves) very significantly improves the CP discovery potential of the facility in these areas of parameter space. The dotted lines correspond to "sign" degeneracies with the opposite mass ordering to the one chosen as true value. In the right panel this degeneracy is also solved with atmospheric data while for the values of δ and θ_{23} chosen in the left panel a small sign degeneracy remains be-

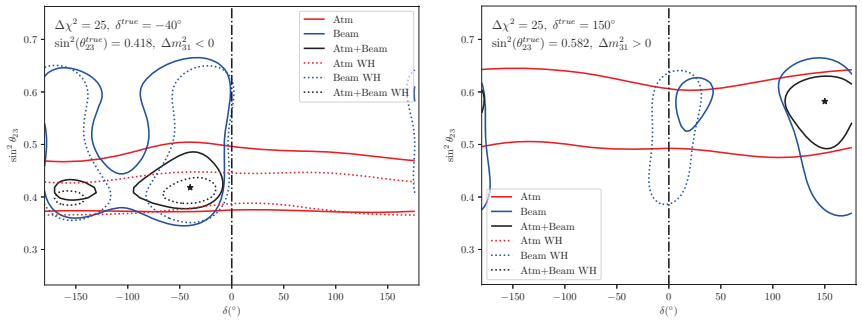

Figure 2.5: Allowed regions at $\Delta\chi^2 = 25$ for different assumed values of $\sin^2\theta_{23}$ and δ represented by the star for a 540 km baseline (Garpenberg location). The red curves correspond to the atmospheric dataset alone, the blue to the beam-only information and the black curves to the combination of both. Dotted regions are allowed with the wrong mass ordering. The running time splitting has been assumed to be t_ν=$t_{\bar{\nu}} = 5$ years.

tween the 4 and 5σ level. Notice that an "intrinsic degeneracy" [82] at $\delta \simeq \pi - \delta_{true}$ also shows up at the 5σ level when only the beam information is taken into account. As for the "sign" degeneracy, the atmospheric neutrino data is enough to lift it for the parameters chosen in the right panel while a small remnant is present in the left. In any case, both the "intrinsic" and the "sign" degeneracies appear at $\delta \simeq \pi - \delta_{true}$, given the comparatively small matter effects for the setup, and their allowed regions are smaller or comparable to that of the true solution so that only the "octant"degeneracy plays a significant role in reducing the CP-discovery potential when atmospheric data is not exploited to lift it.

In Fig. 2.6 we show how the significance with which the ESSnuSB would be able to disfavour the wrong octant of θ_{23} as a function of the true value of θ_{23} (blue lines). As already anticipated in Section 2.2, this capability improves dramatically upon the inclusion of the atmospheric neutrino sample (red lines) and thus the potentially dangerous "octant" degeneracies are lifted. The curves are almost identical for both mass orderings and for the Zinkgruvan and Garpenberg baselines.

The significance with which the ESSnuSB would be able to disfavour the wrong mass ordering is shown in Fig. 2.7, where dotted (solid) lines correspond to beam only data (beam and atmospheric data). The left (right) panels correspond to the 360 km (540 km) baseline and upper (lower) panels are for the scenario in which the true ordering is normal (inverted). As can be seen the ESSnuSB beam data allows to disfavour the wrong mass ordering at around the 3σ (2σ) level for the 360 km (540 km) baseline for any value of δ and the octant. When the atmospheric data is added, the sensitivity to the wrong ordering is boosted to the 4-5σ level or even higher

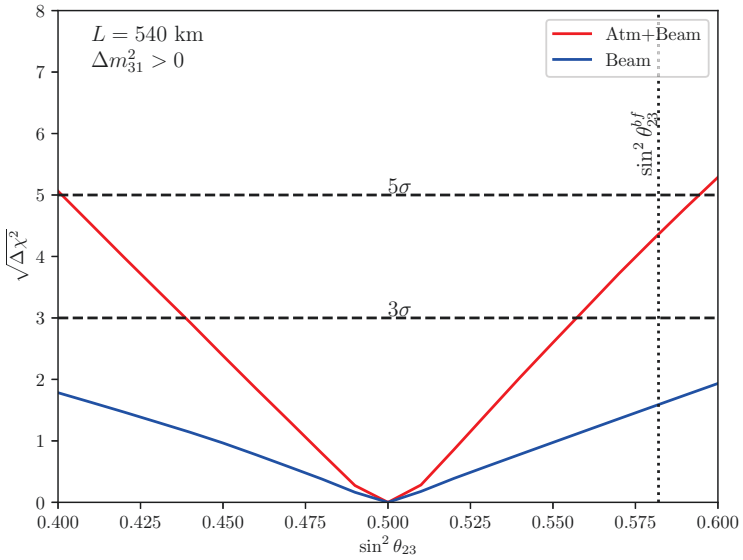

Figure 2.6: Significance with which the wrong octant would be disfavoured as a function of the actual value of θ_{23} with beam-only information (blue lines) and including also the atmospheric dataset (red lines) for the baseline to Garpenberg ($L = 540$ km) and normal mass ordering. The running time splitting has been assumed to be t_ν=$t_{\bar{\nu}} = 5$ years. The results for the Zinkgruvan site ($L = 360$ km) and for inverted ordering are very similar. The vertical line represents the present best fit for θ_{23} from [72].

for the particular case of normal ordering and second octant of θ_{23} ($\sin^2\theta_{23} = 0.582$ from Ref. [72]) for which the signal in atmospheric neutrinos is enhanced, as expected from Eq.(2.1). For normal ordering (upper panels) the inclusion of the atmospheric neutrino data also change the shape of the curve, in particular a larger increase in the significance is seen around $\delta = 0$ than for other values. This is due to the solution of the octant degeneracy since, as can be seen in the middle panel of Fig. 2.2 or the first panel of Fig. 2.3, for $\delta = 0$ and normal ordering the ellipse with opposite octant and ordering has a significant overlap.

In Fig. 2.8 we analyze the precision with which the ESSnuSB experiment would be able to measure the CP violating phase δ. In this figure we assumed the currently preferred option of normal ordering and second octant of θ_{23}. In the upper panels we show the improvement in the 1σ allowed region with which δ would be constrained by adding the atmospheric neutrino sample (solid lines) to the beam information alone (dotted lines). As can be seen, both for the 360 km (left panel) and 540 km baseline (right panel), the precision with which δ could be determined has a very pronounced shape. For CP violating values of δ around $\pm 90^\circ$, the 1σ uncertainty in the measurement peaks leading to the poorest precision, while for δ around 0 or 180° the most precise measurements would be achieved.

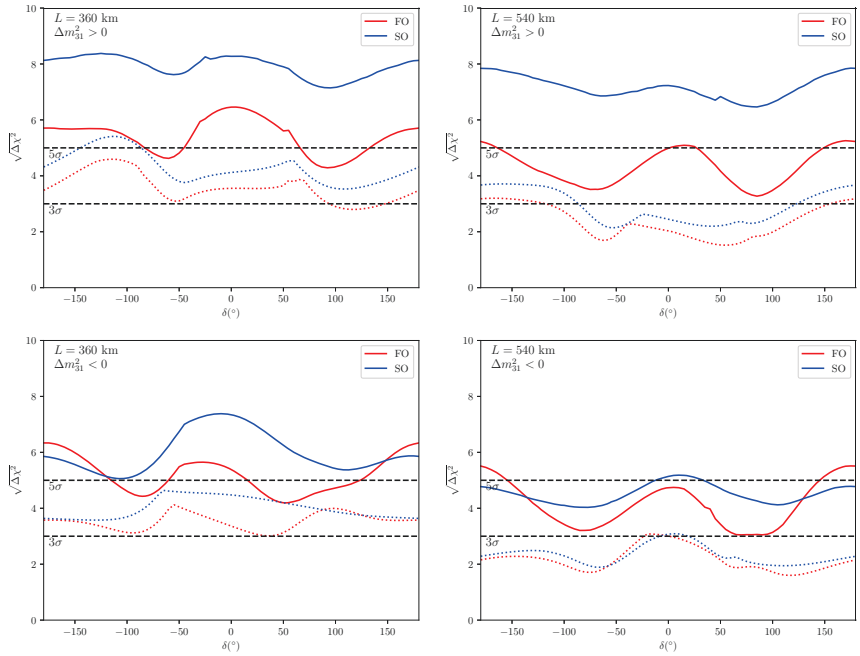

Figure 2.7: Significance with which the wrong mass ordering would be disfavoured for θ_{23} in the first octant (red lines) or second octant (blue lines) and the true mass ordering being normal (upper plots) or inverted (lower plots). Dashed lines correspond to the beam only data while solid lines correspond to the addition of the atmospheric sample. The left panels correspond to the baseline to Zinkgruvan while the right ones to the location of the Garpenberg mine. The running time has been assumed to be t_ν=$t_{\bar{\nu}} = 5$ years.

As discussed in Ref. [126], this structure follows from the dependence of the oscillation probability on δ shown in Eq.(2.1). At an oscillation peak $|\Delta m^2_{31}|L/(4E) = (2n-1)\pi/2$ and thus mainly $\sin\delta$ is probed. Since the derivative of $\sin\delta$ vanishes at $\delta = \pm 90^\circ$, the precision with which δ can be determined is worst close to these values. In order to constrain δ around $\delta = \pm 90^\circ$, measurements away from the oscillation maxima to determine $\cos\delta$ would instead be necessary. These off-peak measurements are easier at the Zinkgruvan 360 km baseline since the statistics is higher and also the beam is not exactly centered at the maximum, while they are very challenging at Garpenberg since very few events away from the oscillation peak are expected. This explains why the reconstructed sensitivities around $\delta = \pm 90^\circ$ are much worse in the right panel compared to the left. Moreover, the double-peak structure that can be seen for $\delta = -90^\circ$ for 540 km corresponds to the "intrinsic" degeneracies depicted in Fig. 2.5 that merge into one bigger allowed region. Since, as seen in Fig. 2.5, the addition of atmospheric data can lift these degeneracies, in the solid lines where this information was included the difference between the two baselines is significantly reduced.

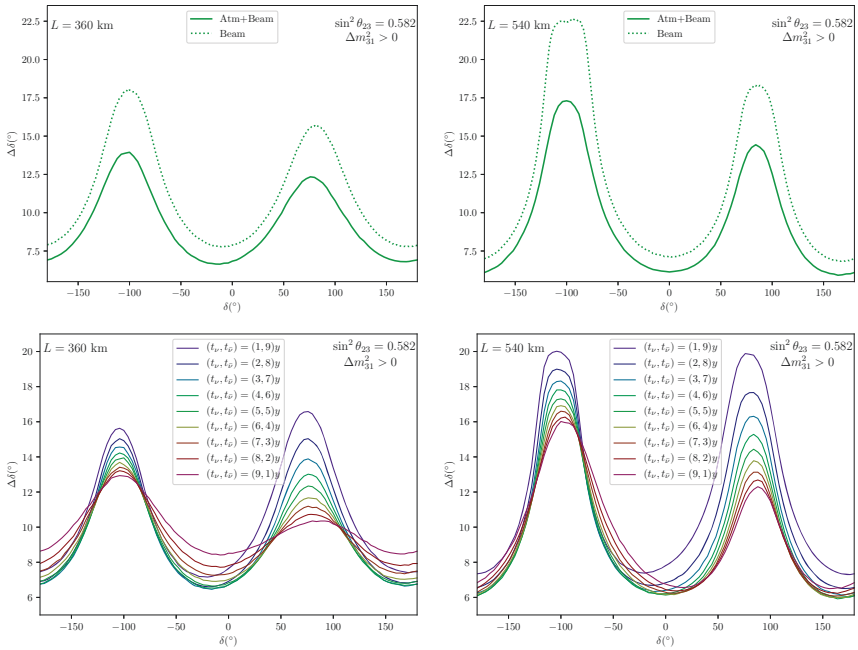

Figure 2.8: Precision (spread of the 1σ allowed region) on the determination of δ for the baseline to Zinkgruvan $L = 360$ km (left panels) and Garpenberg $L = 540$ km (right panels) for the current best-fit parameters [72]. In the upper panels we show the comparison between the precision obtained with (solid lines) and without (dashed lines) the atmospheric sample for a running time of 5 years in each focusing. In the lower plots we show the dependence of the precision on the relative running time in each mode, where t_ν ($t_{\bar\nu}$) corresponds to the time the experiment would run in neutrino (antineutrino) mode, combining atmospheric and beam datasets.

Conversely, for $\delta = 0$ or 180° the measurement on peak is what allows to determine δ and, since this is better covered at the longer 540 km baseline, the precision is slightly better there. This fact also translates into the better CP-discovery potential observed for the 540 km baseline in Fig. 2.4. Since the error in δ is smaller around CP-conserving values, the 540 km option could get closer to these values but still allow to claim the discovery of CP violation with high significance.

In the lower panels of Fig. 2.8, the impact of changing the relative running times in positive focusing (neutrino mode) and negative focusing (antineutrino mode) is shown. Since off-peak measurements are required for $\delta = \pm 90^\circ$, statistics are crucial and easier to accumulate in neutrino mode, since fluxes and cross sections are larger, and thus the best precision would be obtained by devoting longer periods of data taking to positive focusing. Conversely, around $\delta = 0$ or 180° the complementarity between the neutrino and antineutrino samples pays off and more even splits of the running time provide better sensitivity.

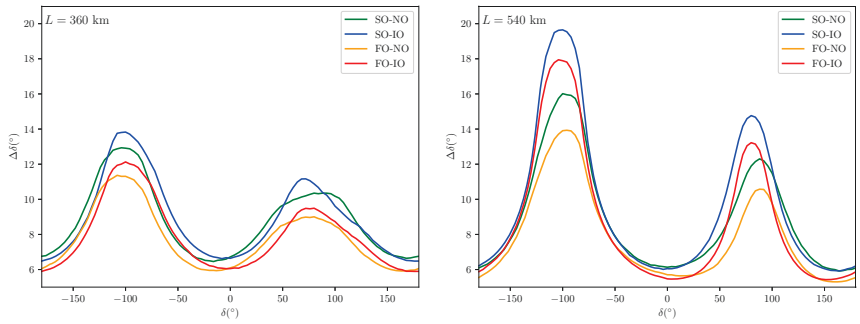

Figure 2.9: Precision on the measurement of δ for a total running time of 10 years when the relative running time in neutrino and antineutrino modes is optimized for each value of δ. This corresponds to running similar times in neutrino and antineutrino modes around $\delta = 0, 180^\circ$ and maximizing the neutrino runs around $\delta = \pm 90^\circ$.

Since the ESSnuSB would be a next-generation facility, its measurement strategy can profit from the previous hints by preceding oscillation experiments and adapt the splitting between neutrino and antineutrino modes depending on what value of δ data point to. If such a strategy is followed and the best splitting between neutrino and antineutrino modes is adopted for each value of δ, the precision presented in Fig. 2.9 would be obtained. If the mass ordering is confirmed to be normal and θ_{23} lies in the second octant as present data prefer, the precision with which the ESSnuSB facility would determine δ ranges from 16° (13°) for $\delta \sim -90^\circ$ to 6° (7°) for $\delta \sim 0$ or $\delta \sim 180^\circ$ for 540 km (360 km).

From Figs. 2.4 and 2.9 one can conclude that if the experiments preceding the ESSnuSB do not find any evidence for CP violation, the best option would be the 540 km baseline and a more or less even split of the neutrino and antineutrino running times. Indeed, this choice would minimize the errors with which δ would be determined around CP-conserving values and allow to increase the CP-discovery potential. On the other hand, if the previous set of experiments determine δ to be close to maximally CP violating, then the best scenario for the ESSnuSB would be the shorter 360 km baseline and increased neutrino run time to determine δ with the best precision possible.

In Fig. 2.10 we show the impact of individual systematic uncertainties on the fraction of values of δ for which CP violation could be discovered ($\Delta\chi^2 \geq 25$). The sources of uncertainty considered, summarized in Table 2.1, are the flux uncertainties for the signal ($\delta\phi_S$) and background ($\delta\phi_B$), the cross section systematic ($\delta\sigma$), the neutral current background (δNC_B), and the uncertainty on the ratio of the electron and muon flavour neutrino cross section ($\delta\sigma_e/\sigma_\mu$). The plot shows that the systematic uncertainties that most significantly affect the performance of the ESSnuSB are the ones related to the back-

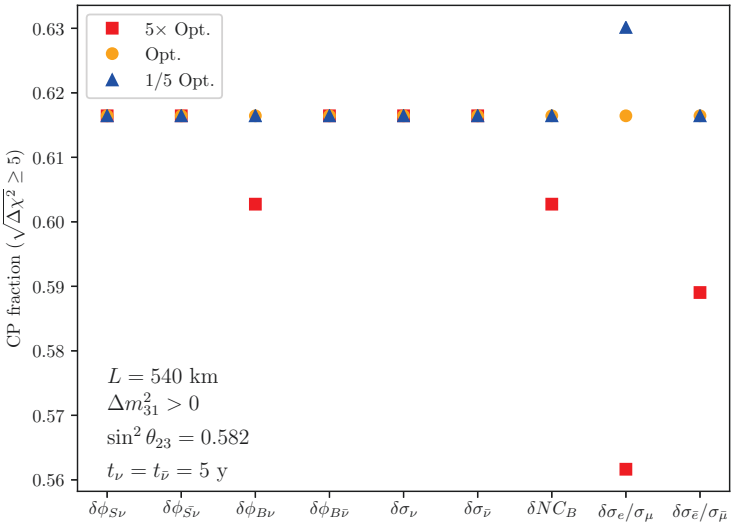

Figure 2.10: Impact of different sources of systematic errors on the fraction of values of δ for which a $\Delta\chi^2 > 25$ exclusion of CP conservation would be possible at the Garpenberg mine. The orange circles correspond to the CP fraction with the "Optimistic" systematics from Table 2.1, red squares correspond to assuming that particular uncertainty to be 5 times larger and blue triangles to reducing the uncertainty by a factor of 5.

ground components of the beam, since for these the determination at the near detector is more challenging. Namely, $\delta\phi_B$, δNC_B as well as $\delta\sigma_e/\sigma_\mu$ since the only ν_e present at the near detector that would allow to fix this parameter are those from the intrinsic background contamination of the beam. Among these, the strongest impact on the sensitivity is due to the cross section ratio since, not only it is difficult to constrain, but it is also most relevant to the signal at the far detector, which consists of ν_e. Indeed, reducing or increasing this particular source of systematic error has the biggest impact on the physics reach. The impact is in any event limited, since the main bottleneck to the performance when observing at the second oscillation peak is statistics. In particular, a reduction of this systematic by a factor of 5 improves the CP fraction by $\sim 2\%$ (no impact for $\bar{\nu}$) while the same factor in the opposite direction worsens the sensitivity by $\sim 9\%$ ($\sim 4\%$).

The importance of these systematic errors in the physics reach is crucially dependent on the baseline of the experiment. In the left panel of Fig. 2.11 we show the fraction of all the possible values of δ for which it would be possible to rule out $\delta = 0$ or $\delta = 180^\circ$ with a $\Delta\chi^2 = 25$ or higher significance. The upper blue line is for the more optimistic systematics from Table 2.1 and the lower red one for the more conservative values. As can be seen, the fraction of values of δ at which a 5σ discovery would be possible, peaks between 400 km and 700 km in both cases. But this peak is much more pronounced

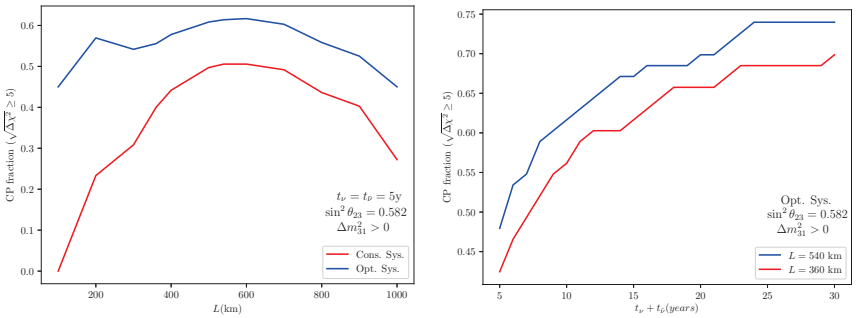

Figure 2.11: Fraction of values of δ for which CP violation could be discovered above 5σ for different baselines to the far detector (left panel) for the two different sets of systematics from Table 2.1. In the right panel we show the CP fraction for the Garpenberg ($L = 540$ km) and Zinkgruvan ($L = 360$ km) mines, assuming the current best fit values for the oscillation parameters and the "Optimistic" systematics for increasing total exposure.

when the more conservative values are assumed for the systematic uncertainties. Indeed, for larger values of the systematics, the shorter baselines are strongly penalized since the dependence of the oscillation probability is subleading around the first peak and easily hidden by the systematics. Conversely, if very small systematic errors can be achieved, then the main limiting factor would be statistics and shorter baselines would perform better. Thus, by measuring at the second oscillation maximum the ESSnuSB setup becomes much more resilient to sources of systematic errors unaccounted for than when observing only at the first peak.

In the right panel of Fig. 2.11 we show how the fraction of values of δ for which CP violation would be discovered at the 5σ level by the ESSnuSB beam and atmospheric data increases with the exposure. As expected from an observation at the second oscillation peak, statistics is the main factor controlling the final reach of the experiment. Indeed, for 5 years data taking the CP fraction is around 46%, by 10 years it increases to 62% and reaches 70% for 20 years of exposure. The slope only flattens significantly after 25 years.

2.5 CONCLUSIONS

In this paper we have performed an exhaustive analysis of the physics reach of the ESSnuSB facility exploring its capability to determine all the presently unknown neutrino oscillation parameters such as the mass ordering and the octant of θ_{23} but with a focus on the discovery of leptonic CP violation and a precision measurement of δ, which are the main declared goals of the experiment. For the first time we combined the atmospheric neutrino sample that would also be observed at the facility with the beam information and studied

the complementarity between the two data sets. We studied how the physics reach of the facility could be optimized by exploring different baselines and focusing on the two candidate sites of Zinkgruvan at 360 km and Garpenberg at 540 km. We have also explored how the time split between neutrino and antineutrino modes can be exploited to improve the physics reach.

We conclude that the inclusion of the atmospheric data set can significantly increase the ESSnuSB physics reach. Due to the peculiarities of observing the oscillation probability at the second oscillation maximum we find that this combination is particularly synergistic. The atmospheric neutrino sample not only significantly increases the sensitivity to the mass ordering, like for other similar facilities [80, 81], but it is also very effective in improving the constraints on Δm^2_{31} and θ_{23} and its octant. These measurements are especially challenging for the beam alone when sitting at the second maximum, given the low statistics, particularly in antineutrinos and in the ν_μ disappearance channel. However, the determination of δ can be affected by correlations with θ_{23} [85] and degeneracies with the wrong octant and thus the atmospheric information is also crucial to increase the CP discovery potential of the ESSnuSB indirectly. We find this complementarity is somewhat more pronounced for the longer 540 km baseline since there the flux is more centered at the second oscillation peak and the statistics are smaller so it benefits more from the information gained from the atmospheric neutrino data.

Regarding the optimal baseline, we find the choice is rather dependent of the actual value of δ. For $\delta \sim \pm 90^\circ$ a precise measurement needs events away from the oscillation maximum. In this sense the shorter 360 km baseline is better since the statistics for off-peak events are higher and this leads to a more precise measurement. Conversely, if δ is close to CP conserving values and the previous set of measurements have not been able to claim the discovery of CP violation, the longer 540 km baseline would allow to cover a larger part of the parameter space. Indeed, after 10 years of data taking, the fraction of values of δ for which a 5σ discovery would be possible is 56% for Zinkgruvan and 62% for Garpenberg.

As for the splitting of the data taking time between neutrino and antineutrino modes, the optimal strategy also depends on the value of δ. This fact could be exploited since previous and present data at the time of the measurement should already show a strong preference for some part of the parameter space. Thus, the running strategy can be adapted to the situation optimizing the precision with which this measurement can be performed. In particular we find again that given the need of going beyond measurements at the peak for $\delta \sim \pm 90^\circ$, statistics is much more relevant and maximizing the time in neutrino mode translates to the best precision for these values. Conversely, close to CP-conserving values of δ, the information

from events on-peak is most relevant and the complementarity between neutrino and antineutrino modes pays off so that a more even split of the running time would provide the best precision.

Finally we explored the possible bottlenecks for the physics reach of the facility exploring how it is affected by varying the values of the different systematic errors considered as well as the total exposure. As expected, the choice of observing the oscillation probability at its second maximum significantly reduces the impact of the systematic errors. We find that around the first oscillation peak the fraction of values of δ for which a 5σ discovery is possible is reduced by more than a factor 2 when considering the more conservative values of Table 2.1. On the other hand, at the second peak the reduction is only by a factor around 1.2. Among the different sources of systematic uncertainties considered, the most important is the possible difference in the ratio of the electron to muon neutrino cross sections. This uncertainty is difficult to constrain from near detector information since the flux is mainly composed of ν_μ, but the far detector signal consists of ν_e. Conversely, the observation at the second maximum considerably reduces the number of events and statistics play a much more relevant role. At the longer 540 km baseline, the fraction of values of δ allowing for a discovery would go from 47% to 62% and 70% for data taking periods of 5, 10, and 20 years, respectively.

3

GENERATING NEUTRINO MASSES

3.1 WEINBERG OPERATOR

As already mentioned in Section 1.1, neutrinos are exactly massless in the SM. Given the experimental observation of neutrino oscillations, it is clear that we need to include BSM physics in order to explain this phenomenon. As a starting point, we can use the powerful tool of effective field theories (EFT) in order to generate neutrino masses just with the SM field content and effective operators of dimension $d > 4$.

It can be shown that there is only one $d = 5$ operator that can be constructed with the SM field content respecting gauge invariance, namely the Weinberg operator, given by [136]

$$\mathcal{L} \supset -\frac{1}{2}\frac{\kappa}{\Lambda}\left(\bar{L}_L^c \tilde{H}^*\right)\left(\tilde{H}^\dagger L_L\right) + h.c., \tag{3.1}$$

where $\tilde{H} \equiv i\sigma_2 H^*$ and the superscript c denotes charge conjugation, such that $\psi^c \equiv C\bar{\psi}^T$; Λ is a new physics scale and κ a dimensionless coupling. Interestingly, after SSB, the consequence of the Weinberg operator is to generate a Majorana mass term for neutrinos given by

$$m_\nu = \kappa\frac{v_H^2}{2\Lambda}, \tag{3.2}$$

where $v_H \sim 246$ GeV is the Higgs vev. For neutrino masses around 0.1 eV, and assuming $\kappa \sim 1$, it is easy to find that the new physics scale should be $\Lambda \sim \mathcal{O}(10^{14})$ GeV, near the grand unification (GUT) scale. Note however that the assumption that $\kappa \sim 1$ does not need to hold and therefore the BSM physics scale could span several orders of magnitude.

Another consequence of the Weinberg operator generating light neutrino masses is that they are Majorana particles, as the term from Eq. (3.1) breaks lepton number (L) by $\Delta L = 2$.

The power of the EFT approach is that, many BSM models generating Majorana masses for neutrinos will reduce to the Weinberg operator once we integrate out the new heavy degrees of freedom[1].

1 Exceptions to this can be found, where neutrino masses are generated from $d = 7$ or higher-dimensional operators [137].

Following a bottom-up approach, we can now discuss renormalizable models generating the operator in Eq. (3.1), in particular the celebrated Seesaw mechanism for neutrino masses.

3.2 THE SEESAW MECHANISM

The most minimal extension we can make to the SM in order to generate light neutrino masses is the inclusion of right-handed neutrinos, so that we write a Yukawa term in the same fashion we do for the other SM fermions:

$$\mathcal{L} \supset -\bar{L}_L \tilde{H} Y_\nu N_R + h.c., \tag{3.3}$$

where N_R are the right-handed (RH) neutrino fields and Y_ν is a $3 \times n$ complex Yukawa matrix with n the number of RH neutrinos introduced. Notice however that in order to respect gauge invariance, the N_R are SM singlets, such that a Majorana mass term for these fields can be written at the lagrangian level, making the full mass term for the neutrinos read as

$$\mathcal{L}_{mass} = -\bar{L}_L \tilde{H} Y_\nu N_R - \frac{1}{2} \bar{N}_R^c M N_R + h.c., \tag{3.4}$$

where M is a Majorana mass whose scale is completely free. After SSB the Higgs develops a vev, we find the following Majorana mass matrix for the field $n_L \equiv \begin{pmatrix} \nu_L & N_R^c \end{pmatrix}$:

$$\mathcal{M}_\nu = \begin{pmatrix} 0 & m_D \\ m_D^T & M \end{pmatrix}, \tag{3.5}$$

where $m_D \equiv v_H Y_\nu / \sqrt{2}$. Now if there is a large hierarchy between M and m_D, such that $M \gg m_D$, it is straightforward to block diagonalize $\mathcal{M}_\nu$ and find, in the basis where M is real and diagonal

$$m_\nu \sim -m_D M^{-1} m_D^T, \quad m_{heavy} \sim M. \tag{3.6}$$

It is clear that light neutrino masses are tiny because of the large hierarchy of scales between the EW scale and the Majorana mass scale M. In particular, for $Y_\nu \sim \mathcal{O}(1)$ and $m_\nu \sim 0.1$ eV, M sits at the GUT scale, just as anticipated when studying neutrino masses in the EFT context with the Weinberg operator from Eq. (3.1). This is the well known Type-I Seesaw Mechanism [138–141], which is able to explain the lightness of neutrino masses through a hierarchy of scales, while keeping natural $\mathcal{O}(1)$ Yukawa couplings for the neutrinos. However, the mixing between the active and heavy states is given by $\tan\theta \sim m_D M^{-1}$, being very strongly suppressed by the Majorana mass, making this scenario very difficult to test experimentally. Other examples of models which generate the Weinberg operator from Eq. (3.1) after integrating out the heavy fields are the Type-II [142, 143] and Type-III [144] Seesaw mechanisms, which introduce an $SU(2)_L$ scalar or fermion triplet, respectively.

3.3 LOW-SCALE SEESAW MECHANISMS

Although the Type-I Seesaw introduced in Section 3.2 successfully explains the lightness of neutrino masses, and potentially also the origin of the matter-antimatter asymmetry in the Universe [145], it also worsens the Higgs hierarchy problem [146, 147] and is experimentally out-of-reach given the high scale for the heavy neutrinos. Notice that, for the small active-heavy mixing expected in the Type-I Seesaw, we can rewrite m_ν from Eq. (3.6) as

$$m_\nu \sim -\theta m_D^T, \tag{3.7}$$

such that if we have $Y_\nu \sim \mathcal{O}(1)$ and m_D is at the EW scale, θ needs to be suppressed at the level of $\theta \sim 10^{-13}$ in order to explain light neutrino masses.

Another possibility could be, instead of explaining neutrino masses through a hierarchy of scales, to explain it through a symmetry which protects neutrino masses and make them naturally small. This is the case in the so-called low-scale Seesaw scenarios such as the inverse or the linear Seesaws [148–151], in which an approximate lepton number symmetry [152–154] protects light neutrino masses. As an illustrative example, we can study the case of the inverse Seesaw, but most of the results in the following will apply as well to any low-scale scenario in which active-heavy mixing can be large.

In the inverse Seesaw scenario [151] we introduce to the SM particle content n Dirac singlet neutrinos, N, such that we can write the following mass term

$$\mathcal{L}_{mass} \supset -\bar{L}_L \tilde{H} N_R - \bar{N}_L M_N N_R - \frac{1}{2}\bar{N}_L^c \mu N_L + h.c., \tag{3.8}$$

where M_N is a Dirac mass and μ is a Majorana mass for N_L, which is small given that we are assuming an approximate lepton number symmetry. In particular, if we assign lepton number $+1$ to L_L, N_L and N_R, it is clear that μ "softly" breaks it by $\Delta L = 2$. Notice that we could write a Majorana mass for N_R as well, but it would only contribute at the loop level to light neutrino masses. After SSB, the Higgs develops a vev and, arranging the fields as $\begin{pmatrix} \nu_L & N_L & N_R^c \end{pmatrix}$, we find the following mass matrix for neutrinos

$$\mathcal{M}_\nu = \begin{pmatrix} 0 & 0 & m_D^T \\ 0 & \mu & M_N^T \\ m_D & M_N & 0 \end{pmatrix}. \tag{3.9}$$

Assuming that $M_N \gg m_D \gg \mu$, we find that light neutrino masses are given by

$$m_\nu \sim m_D M_N^{-1} \mu \left(M_N^T\right)^{-1} m_D^T = \theta \mu \theta^T, \tag{3.10}$$

where in the last step we have made used of the definition of $\theta \equiv m_D M_N^{-1}$ as the ratio between the Dirac mass generated from the Higgs and the heavy singlet neutrino mass. It is thus clear from Eq. (3.10) that, for an L-breaking term $\mu \sim \mathcal{O}(\text{keV})$, light neutrino masses can be explained with $\theta \sim 10^{-2}$. Moreover, in the limit where L is conserved, $\mu \to 0$, the active-heavy mixing can still be sizeable, even though light neutrinos are exactly massless in that limit.

It is clear from this example why low-scale realizations of the Seesaw are very appealing from a phenomenological point of view. Light neutrino masses can be naturally explained through an approximate symmetry, allowing to have large active-heavy mixing θ, although it is nonetheless constrained by precision EW and flavour observables [155]. Additionally, the new heavy states, which form pseudo-Dirac pairs with a small mass splitting $\Delta M \sim \mu$, can live at the EW scale or even below, in reach for present and future collider experiments [156–158] to be found. Given the rich phenomenology of low-scale Seesaws, we will be working in the context of these scenarios in the following in order to address other open question of the SM.

Part II

DARK MATTER

4

INTRODUCTION

The evidence for the existence of dark matter (DM) is overwhelming, supported by many astrophysical and cosmological observations. It makes up around 26% of the Universe energy density, being about 5 times more abundant than baryonic matter, and given that the SM does not have any viable candidate for DM, it constitutes one of the most clear experimental hints for the existence of BSM Physics. In the following, we will introduce some of the evidence for DM and the properties inferred from them.

4.1 EVIDENCE FOR DARK MATTER

Astrophysical and cosmological observations have provided evidence for the existence of vast amounts of a new type of matter in the Universe that does not emit or absorb light, thus dubbed as dark matter. Although there are some modifications of Newtonian dynamics, the so-called MOND theories, which could account for some of the observations, these have proved insufficient when both astrophysical and cosmological probes are taken into account simultaneously.

The first evidence for DM came from the observations of the Coma cluster by Fritz Zwicky [159] in 1933. From the peculiar motion of objects in the Coma cluster, the total mass of the cluster could be inferred, which did not agree with the expectation from the luminous objects observed. Thus, some kind of non-luminous matter should be introduced in order to account for the difference in mass.

Later on, in the 70s, the idea of some kind of non-luminous matter took strength with the observation of the rotation curves of spiral galaxies by Vera Rubin and others [160, 161]. Indeed, naively applying Gauss law to a spiral galaxy leads to the following relation between the velocity of bounded objects to the galaxy and their distance to the galactic centre:

$$v = \sqrt{\frac{GM(r)}{r}}, \tag{4.1}$$

where G is Newton's constant and $M(r)$ is the mass contained inside the radius r. In the outskirts of the galaxy, where M does not increase considerably, we would expect a behaviour like $v \sim r^{-1/2}$. Instead,

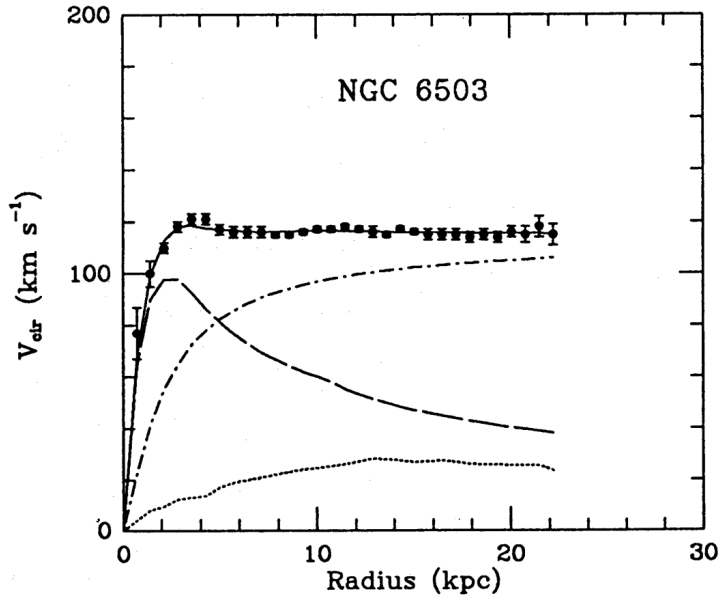

Figure 4.1: Rotation curve of the spiral galaxy NGC 6503, showing a flat behaviour for radius larger than about 3 kpc, taken from Ref. [162]. The dots correspond to the measurements, while the different curves correspond to the contribution from luminous matter (dashed line) and DM (dash-dotted line).

what was found was that v remains constant, such that $M(r) \propto r$ in Eq. (4.1). This is shown in Fig. 4.1 taken from Ref. [162].

Another strong indication for DM is the paradigmatic example of the Bullet Cluster, a dynamical system which underwent a collision, as observed by the Chandra X-ray satellite. Nonetheless, most of the matter inferred from weak-lensing analyses is displaced from the visible components. The accepted interpretation is that the dark matter components of the clusters crossed without interacting significantly [163, 164].

On cosmological scales, we have the exquisite measurements from the cosmic microwave background (CMB) performed by WMAP [165] and later improved by Planck [166]. Indeed, in the ΛCDM model for cosmology, DM is the seeder of the structure we observe in our Universe, playing a fundamental role in structure formation. Without the DM component of the Universe, we could not reconcile the level of anisotropies observed at the epoch of the CMB, at the level of $\delta T/T \sim 10^{-5}$, with the large scale structure observed today. Combining all these measurements, the best determination for the energy density of DM in the Universe is [166]

$$\Omega_{DM} h^2 = 0.1198 \pm 0.0012, \tag{4.2}$$

to be compared with the much smaller baryonic component, $\Omega_b h^2 = 0.02233 \pm 0.00015$.

4.2 DARK MATTER PROPERTIES

From several observations and also null results in experiments, we can infer some of the DM properties.

- Non-baryonic: the results inferred from the CMB and Big Bang Nucleosynthesis (BBN) suggest that only about 5% of the total energy budget of the Universe is made out of baryonic matter. Thus, we must conclude that DM is non-baryonic.
- Neutral: DM particles should be neutral or at most milicharged. Otherwise they would scatter light and thus not be dark. Several probes place bounds on the DM electric charge, from CMB measurementes, which would be affected if DM particles could scatter off electrons and protons at recombination, to the non-observation of DM in direct detection experiments.
- Non-relativistic: numerical simulations of structure formation in the Early Universe show that DM needs to be non-relativistic (cold) at the epoch of structure formation, in order for it to seed the large scale structure (LSS) observed. However, simulations with cold DM lead to too much substructure in DM halos which have not yet been observed. These results may be accommodated with warm DM, i.e. DM only slightly relativistic such that it would erase the smallest substructures in better agreement with observations. On the other hand, properly taking into account the baryon interactions could also explain the discrepancy, as well as some degree of self-interactions giving rise to DM scatterings.
- Long-lived: DM is a long-lived (if not stable) particle, whose lifetime should be larger than the age of the Universe. This is clear from its footprint in the CMB anisotropies, its fundamental role in structure formation and its observation from the gravitational effects on galaxies and clusters nowadays.
- Collisionless: dynamical systems, such as the Bullet Cluster, set an upper bound to the self-interactions of DM particles, at the level of $\sigma/m < 1.25\ \mathrm{cm}^2/\mathrm{g}$. Nonetheless, some level of self-interactions could help reconciling the amount of substructure observed and the one resulting from simulations, as already described.

4.3 DARK MATTER PRODUCTION THROUGH FREEZE-OUT

In this section we present the generalities of arguably the most simple DM production mechanism, the freeze-out of a massive non-relativistic species, largely based on Ref. [167].

Let us assume that DM has some interaction with SM particles strong enough so that processes that create and destroy DM, such as 2 to 2 processes like DM DM $\leftrightarrow$ SM SM are in thermal equilibrium in the primeval plasma. The equation governing the DM number density is

$$\frac{dn}{dt} + 3Hn = -\langle\sigma v\rangle \left(n^2 - n_{eq}^2\right), \tag{4.3}$$

where n is the DM number density, H is the Hubble expansion rate, $\langle\sigma v\rangle$ is the thermally averaged cross section and n_{eq} is the equilibrium density. We can rewrite Eq. (4.3) in terms of the yield, defined as $Y \equiv n/s$, which is a constant over the expansion of the Universe if there are no interactions. Exchanging also the dependence on the temperature by $x \equiv m/T$, we arrive at

$$\frac{x}{Y_{eq}}\frac{dY}{dx} = -\frac{\Gamma}{H}\left[\left(\frac{Y}{Y_{eq}}\right)^2 - 1\right], \tag{4.4}$$

where it is clear that when annihilations are not effective, with $\Gamma \equiv n\langle\sigma v\rangle \ll H$, they freeze-out and the DM yield remains constant. In the non-relativistic regime we are interested in, namely $x \gg 3$, the equilibrium yield is given by

$$Y_{eq} = \frac{45}{2\pi^4}\left(\frac{\pi}{8}\right)^{1/2}\frac{g}{g_{*S}}x^{3/2}e^{-x}, \tag{4.5}$$

with g the species internal degrees of freedom and g_{*S} the entropy relativistic degrees of freedom given by

$$g_{*S} = \sum_{i=\text{bosons}} g_i\left(\frac{T_i}{T}\right)^3 + \frac{7}{8}\sum_{i=\text{fermions}} g_i\left(\frac{T_i}{T}\right)^3. \tag{4.6}$$

It is useful to consider the approximation of instantaneous freeze-out in order to understand the basics of the mechanism. In this case, when annihilations are no longer effective, at $x = x_f$, DM will instantaneously decouple from the plasma. Rewriting Eq. (4.4) in terms of $\Delta \equiv Y - Y_{eq}$ and assuming an s-wave annihilation cross section such that $\langle\sigma v\rangle \sim \sigma_0$, we find

$$\frac{d\Delta}{dx} = -\frac{dY_{eq}}{dx} - \lambda x^{-2}\Delta(\Delta + 2Y_{eq}), \tag{4.7}$$

where $\lambda \simeq 0.026 m_{DM} M_{Pl}\sigma_0$ with m_{DM} the DM mass and we are assuming a radiation dominated Universe with $g_{*S} \sim 100$. For $1 < x \ll x_f$, Y closely tracks the equilibrium yield, such that $\Delta, d\Delta/dx \sim 0$, and we get, at x_f,

$$\Delta_f \sim \frac{x_f^2}{2\lambda}, \tag{4.8}$$

where we have used $dY_{eq}/dx \sim -Y_{eq}$ around x_f. Now for $x \gg x_f$, Y_{eq} is negligible, such that we need to solve

$$\frac{d\Delta}{dx} \sim -\lambda x^{-2}\Delta^2, \tag{4.9}$$

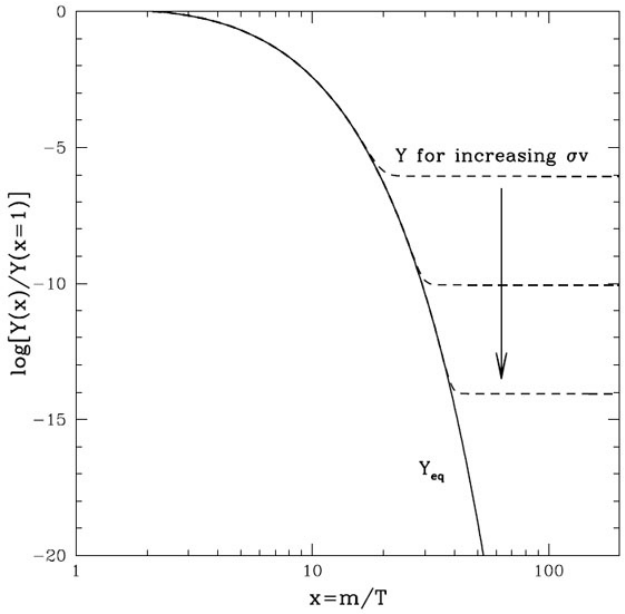

Figure 4.2: Freeze-out of a massive particle species in the Early Universe. The dashed lines correspond to the actual yield for different annihilation cross sections while the solid line corresponds to the equilibrium density. This figure was taken from Ref. [167].

between $x = x_f$ and $x \to \infty$. The yield today, Y_∞, is then

$$Y_\infty \sim \frac{x_f^2}{\lambda(2 + x_f)}, \tag{4.10}$$

and the relic density would be given by

$$\Omega_{DM} h^2 = \frac{m_{DM} Y_\infty s_0 h^2}{\rho_c}, \tag{4.11}$$

where s_0 is the entropy density today and ρ_c the critical density. It can be shown that, very generally, $x_f \sim 15 - 20$ [167], such that substituting numerical factors in Eq. (4.11), we get $\Omega_{DM} h^2 \sim 10^{-10} \sigma_0^{-1}$ GeV^{-2}, from which it is clear that the smaller the annihilation cross section is, the greater the final relic density becomes, as can be seen in Fig. 4.2. In order to recover the observed relic density, we find an annihilation cross section of DM with SM particles of the order of $\sigma_0 \sim 10^{-11}$ GeV^{-2}, which is the size one would expect for a typical weak-interaction process, with $\langle \sigma v \rangle \sim G_F^2 m_{DM}^2$, for a DM particle around the GeV scale. This is the so-called "WIMP miracle", as it was found that, on very general grounds, we could explain the DM in the Universe with an interaction whose strength is similar to that of weak interactions in the SM, and it has driven most of the experimental expectations in the DM community for the past 20 years.

Indeed, if there is a dominant interaction between DM and some SM species responsible for its production through freeze-out, then it

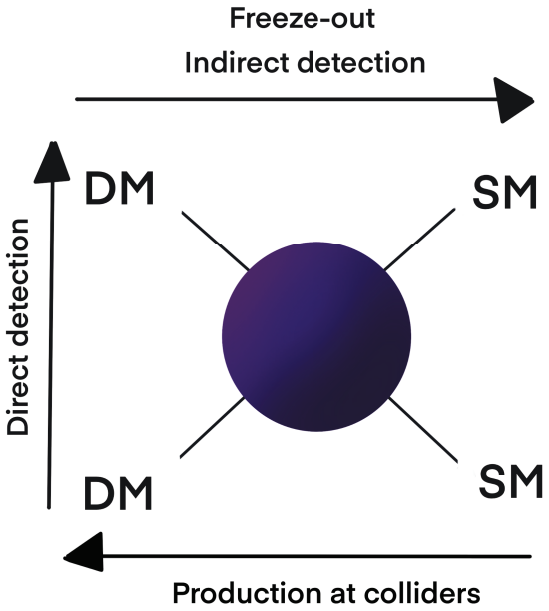

Figure 4.3: Depiction of the different processes involved in the production through freeze-out, direct and indirect detection experiments, and the DM production at colliders.

can potentially be found through this same interaction in experimental searches. In Fig. 4.3 a sketch of the different possibilities and the particular process being probed are shown, following the different arrows.

Direct detection experiments take advantage of the presence of DM in the galactic halo which can elastically scatter off nuclei or electrons in a terrestrial detector. In Fig. 4.4 a summary of the main direct detection experiment results is shown together with some prospects for future searches. In these experiments, the maximum recoil energy for the test particle expected is

$$E_R^{max} \sim 2\frac{m_{DM}^2 m}{(m_{DM}+m)^2} v_{DM}^2, \tag{4.12}$$

where v_{DM} is the DM velocity today, which is $v_{DM} \sim 10^{-3}$, and m is the mass of the test particle, either nucleons or electrons in most direct detection experiments. From these expression it is clear why most of the direct detection experiment results are on the DM-nucleon cross section, as protons and nucleons are more massive than electrons and therefore the recoil energy larger, being more easily probed experimentally. However, given the null results of direct detection experiments, a great effort has also been done to probe the DM interactions with electrons, as in the case of the Xenon1T experiment [168]. In-

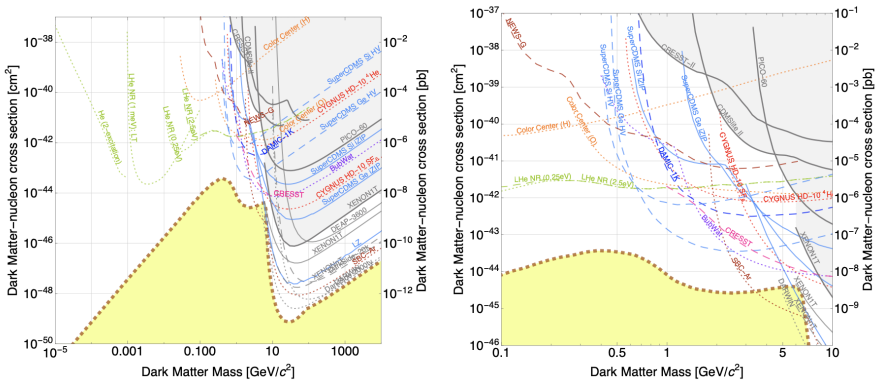

Figure 4.4: Summary plot with the most relevant direct detection results at 90% C.L. taken from Ref. [169]. The yellow region corresponds to the so-called neutrino floor from different neutrino sources. The right panel shows the same bounds and prospects zooming in the range of DM masses.

deed, if the DM mass were not to be at the $\mathcal{O}(\text{GeV})$ scale but rather below, the recoil energy for nucleons would be suppressed by the ratio $m_{DM}/m_{\text{nucleon}}$ and thus it would be much more difficult to search for, so that studying electron recoils for lighter DM masses is better.

On the other hand, the same process responsible for the DM production through freeze-out, its annihilation into SM particles, can happen today in high DM-density regions of the Universe such as the galactic centre or dwarf spheroidal galaxies producing a large flux of energetic particles, including gamma rays, cosmic rays [170] and neutrino. In particular gamma ray searches are very useful as these particles are not deflected by magnetic fields and attenuate very little over galactic distances. Nonetheless, apart from the annihilation cross section, we need some astrophysical input for these searches, encoded in the so-called J-factor

$$J \equiv \int_{\Delta\Omega} \int_{los} \rho_{DM}^2 dl d\Omega, \tag{4.13}$$

where ρ_{DM} is the DM density distribution, and the integral is over a solid angle, $\Delta\Omega$, and along the line-of-sight, "los". Thus, a particular profile for the DM distribution needs to be assumed for these indirect searches, which is typically the Navarro-Frenk-White (NFW) profile [171]. The most stringent constraints on DM annihilation to SM particles come from the Fermi-LAT telescope [172], shown in Fig. 4.5. Bounds to other annihilation channels such as $\tau^+\tau^-$ have also been obtained by using measurements of dwarf galaxies and not finding any positive signal of DM annihilation. There is, however, an excess in the signal when looking for DM in the galactic centre, but given the large astrophysical backgrounds in this region of the galaxy, we still lack a conclusive insight about the origin of this excess.

Finally, colliders like the Large Hadron Collider (LHC) can also look for DM. Indeed, from Fig. 4.5 we could have two SM particles

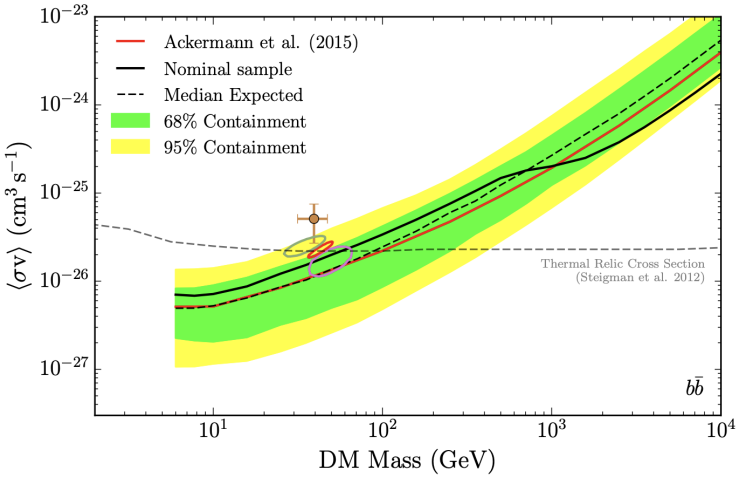

Figure 4.5: Upper bound on the annihilation cross section of DM into a pair of b quark-antiquark. The dashed gray line corresponds to the target thermal relic cross section needed to produce DM through freeze-out. Taken from Ref. [172].

interacting and producing DM in the detector, which would eventually escape. In this case DM could be searched for through missing energy or studying displaced vertices [173].

5

NEUTRINO PORTALS TO DARK MATTER

5.1 WHERE COULD DARK MATTER BE HIDING?

The unknown origin of neutrino masses and mixing together with the existence of the DM component of the Universe constitute our most significant experimental evidence for physics beyond the SM and therefore the best windows to explore new physics. Neutrinos and DM also share an elusive nature with very weak interactions with the other SM particles. Indeed, neutrinos only participate in the weak interactions of the SM while all direct and indirect searches for DM interactions with the SM, other than gravity, are so far negative or inconclusive. A tantalising avenue of investigation is the possibility of a stronger connection between these two sectors. In this case, the best way to probe DM would be through the neutrino sector.

Several works have investigated the phenomenology of a dominant interaction between the neutrino and DM sectors and the possibility to probe DM through neutrinos both via its cosmological implications [174–187] as well as through indirect searches [187–191]. In the presence of this interaction, DM would no longer be collisionless, but able to scatter with neutrinos in the Early Universe, affecting matter density fluctuations. Moreover, the power spectrum would show a suppression at small scales [182, 183, 187] or even an oscillatory pattern [176–178, 181]. Indirect detection searches for DM annihilating to neutrinos in the galactic centre have also been performed at neutrino detectors and used to constrain neutrino-DM interactions [187–189]. The propagation of neutrinos through DM halos could be modified as well, leading to dips in supernova neutrino spectra due to resonant interactions with DM [192, 193], or affect the spectrum or isotropy of the high energy cosmic neutrinos observed by IceCube [194–196].

However, it is not straightforward to envision a scenario in which the neutrino-DM interactions dominate the DM phenomenology. Indeed, gauge invariance dictates that the interactions of the LH SM neutrinos with DM will be equal to those of their charged lepton counterparts in the $SU(2)_L$ doublets. In this case, the best windows to DM would instead be the charged leptons rather than the more elusive neutrinos.

In the following, we will investigate some gauge-invariant SM extensions that lead to sizeable neutrino-DM interactions, exploring if neutrino probes could dominate our sensitivity to the dark sector. This is actually a rather natural possibility. In fact, if DM does not participate in any of the SM gauge interactions, the natural expectation is that the strongest connection to DM will be via singlets of the SM gauge group. Indeed, if non-singlet fields were involved instead, the dimensionality of the operators linking the two sectors would have to increase in order to comply with gauge invariance. This reasoning leads to the three well-known SM portals to the dark sector: the "gauge boson portal" [197], the "Higgs portal" [198], and the "neutrino portal" [190, 199, 200]. The neutrino portal includes the addition of RH neutrinos N_R, which makes this option particularly appealing in connection to the evidence of neutrino masses and mixing from neutrino oscillations.

Since the neutrino portal relies on the mixing between N_R and the light SM neutrinos to connect the neutrino and DM sectors, this mixing needs to be sizeable. As already mentioned in Chapter 3, in models with an approximate lepton number (L) symmetry such as the linear [149, 150] or inverse [151] Seesaw mechanisms, neutrino masses are suppressed by the small L-breaking parameters while light neutrino mixing with N_R is unsuppressed. In the present study, we will assume relatively large mixing angles noting that they can be compatible with neutrino masses, but we will not specify a concrete neutrino mass generation mechanism, since these small lepton number violating parameters, and hence light neutrino masses, will have no significant impact on the phenomenology related to DM.

We will consider fermionic DM and, more specifically, Dirac DM, which has the richest phenomenology when interacting with SM neutrinos. Indeed, the dominant term in the annihilation cross section to neutrinos is not velocity suppressed, and DM annihilations therefore lead to interesting signatures in indirect searches. Alternative scenarios with a Majorana, scalar, or vector DM candidate will lead to a velocity-dependent annihilation cross section to neutrinos [187]. While such possibilities are viable, they are difficult to probe experimentally at neutrino detectors. This is due to the fact that the DM velocity in the halo today is $v_{\text{halo}} = 10^{-3}c$ [201], which significantly reduces the annihilation rate to neutrinos.

In Section 5.2, we summarise relevant experimental searches for DM and constraints coming from cosmology. In Section 5.3, we consider the simplest gauge-invariant scenario, in which DM is coupled directly to the full SM lepton doublet. In this case, as expected, the charged lepton probes tend to dominate the constraints on the DM parameter space. Further, in Section 5.4, we introduce the neutrino portal involving one new Dirac sterile neutrino N, which will communicate with the dark sector. We present two realisations of the

neutrino portal, for scalar [202–205] and vector [206] interactions between the DM and N in Sections 5.5 and 5.6, respectively. For both of them, we investigate the parameter space, demonstrating that current and future neutrino experiments have the dominant role in constraining it.

5.2 CONSTRAINTS ON INTERACTIONS OF DM WITH SM PARTICLES

In the next sections, we will explore the parameter space of different possible gauge-invariant ways to realise interactions of neutrinos with DM. For each realisation, we will investigate whether it is possible for these neutrino-DM interactions to play a dominant role in the DM phenomenology. In particular, we will address whether or not the DM relic abundance can be achieved via the neutrino-DM interactions and/or if indirect DM searches via its annihilation into neutrinos (probed at neutrino detectors) can be the dominant test of the model parameter space. We will use the observables presented in this section to place constraints on the parameter space of each scenario.

5.2.1 *Indirect detection searches for DM annihilation to neutrinos*

DM annihilating in high density regions such as the Milky Way can generate a significant monochromatic flux of neutrinos with energy $E_\nu = m_\chi$, where m_χ is the DM mass. This flux is proportional to the integral of the DM density squared along the line of sight and can be searched for in neutrino detectors such as Super-Kamiokande (SK) [40] or Borexino [207].

Several analyses that use neutrino detectors to probe the DM parameter space have been performed in the literature [187–189, 191, 208–211]. For small DM masses in the range $2 - 17$ MeV, we can exploit the upper bound on the monochromatic antineutrino flux set by Borexino [212] and convert it to a conservative upper bound of $\langle \sigma v_r \rangle \lesssim 10^{-22} - 10^{-20}$ cm^3/s on the thermally averaged annihilation cross section σ multiplied by the relative velocity v_r of DM particles, as discussed in Ref. [187]. Likewise, between 10 and 200 MeV, SK can place an upper bound of $\langle \sigma v_r \rangle \lesssim 10^{-25} - 10^{-23}$ cm^3/s (depending on the DM mass) [187]. For DM with a mass between 1 GeV and 10 TeV annihilating in the galactic centre, the SK collaboration has performed a dedicated analysis and set an upper bound of $\langle \sigma v_r \rangle \sim 10^{-24} - 10^{-22}$ cm^3/s [209]. We will also consider the general upper bound on $\langle \sigma v_r \rangle$ derived in Ref. [188] by calculating the cosmic diffuse neutrino signal from DM annihilations in all halos in the Universe and comparing it to the measured atmospheric neutrino background by Fréjus [213], AMANDA [214], and SK. This bound

applies to m_χ in the range between 100 MeV and 100 TeV and excludes $\langle \sigma v_r \rangle \gtrsim 10^{-23} - 10^{-21}$ cm^3/s (depending on m_χ). As argued in Ref. [188], this bound could be improved by one or even two orders of magnitude with dedicated analyses by existing neutrino experiments such as SK.

The next generation experiment Hyper-Kamiokande (HK) [92] will be sensitive to approximately one order of magnitude smaller cross sections in this mass range. Indeed, with a 187 kton fiducial mass and an exposure time of 10 years, HK could probe the parameter space almost down to the relic density cross section ($\langle \sigma v_r \rangle = 3 \times 10^{-26}$ cm^3/s [215]). Possible improvements such as additional mass from a second tank together with Gd doping for background reduction would allow to probe beyond this value [210]. Similarly, the ESSνSB project [66] envisions a 500 kton fiducial water detector, MEMPHYS [67], that would have slightly better sensitivity than HK from the additional fiducial mass. Similarly, future DM and neutrino detectors such as DARWIN [216] and DUNE [65] will be able to further constrain the DM annihilation cross section to neutrinos. DARWIN will set stronger bounds for DM masses between 100 MeV and 1 GeV [217], while DUNE will be able to exclude thermal DM masses between 25 and 100 MeV [211].

Competitive constraints from DM annihilations in the Sun to neutrinos, or other SM particles that decay to neutrinos, have also been derived by neutrino detectors such as SK [218] and IceCube [219]. These exploit the higher DM concentration expected in the solar interior since it could capture DM particles from the halo via scatterings. In all the realisations under study we explore the connection between the DM and neutrino sectors with very suppressed interactions with the rest of the SM, in particular with quarks. Thus, in these scenarios, the Sun does not accrete DM particles effectively and the constraints from these searches do not apply.

5.2.2 *Indirect detection searches for DM annihilation to charged leptons*

DM interactions with charged leptons will always be present either at tree level, if DM couples to the full doublet, or at loop level in the neutrino portal scenarios. Therefore, we will take into account indirect detection searches for DM annihilations to charged leptons from the Fermi satellite [220], as well as from their imprint in the cosmic microwave background (CMB) as observed by Planck [166, 221].

5.2.3 *Direct detection searches*

DM will not couple directly to the quarks in any of the scenarios that we will discuss. Nevertheless, such couplings will arise at

loop level in a similar way to the DM-charged lepton interactions. As we will see, bounds from direct detection experiments, such as XENON1T [222], are so stringent that they will still constrain the parameter space for large DM masses. Recently, direct detection of sub-GeV DM via scattering off electrons has gained significant attention [169, 223–225]. We have also considered this process and found it to be sub-leading with respect to other relevant constraints.

5.2.4 *Constraints from cosmology*

If DM remains in thermal equilibrium with neutrinos during Big Bang nucleosynthesis (BBN), it can spoil its predictions [226, 227]. Similarly, the effective number of neutrinos, as constrained by CMB measurements, would be affected if DM remained in equilibrium after neutrinos decoupled from the photon plasma [228–230]. Thus, to avoid these two effects, we will not consider DM masses $m_\chi < 10$ MeV. Moreover, neutrino-DM interactions can also have an effect in the formation of large scale structures (LSS) since, as DM particles scatter off neutrinos, they diffuse out and erase small scale perturbations. This effect leads to a suppression of the amount of small scale structures today. By comparing LSS predictions to observations, one can set an upper bound on the strength of the elastic scattering between DM and neutrinos [181, 231]. Nevertheless, for the models we are presenting in this work, the mixing between the sterile and SM neutrino suppresses the neutrino-DM elastic scattering and, consequently, its effect on LSS constrains regions of the parameter space already ruled out by CMB and BBN constraints [187].

5.3 COUPLING TO THE FULL LEPTON DOUBLET

In this section, we will study the simplest scenario, in which the neutrino-DM interaction arises from a direct coupling to the full SM $SU(2)$ lepton doublet. In order to avoid specifying the nature of the mediator, we will adopt an effective field theory approach, simply adding a $d = 6$, 4-fermion interaction.

5.3.1 *Model*

Since the 4-fermion operator needs to involve two LH SM lepton doublets $L_\alpha = (\nu_{\alpha L}, \ell_{\alpha L})^T$, $\alpha = e, \mu, \tau$, its Lorentz structure is fixed to be $\overline{L_\alpha}\gamma^\mu L_\alpha$. For definiteness we will assume a vector structure for the DM part. An axial coupling would instead lead to a velocity-suppressed DM annihilation cross section to neutrinos for both DM relic abundance and indirect searches. The cross section for DM annihilation to charged leptons would however have an additional term only suppressed by the lepton mass, and thus, it would tend to dom-

inate over the annihilation cross section to neutrinos. Therefore, we will not consider this option in what follows.

The Lagrangian describing the neutrino-DM interaction is thus given by

$$\mathcal{L} = \mathcal{L}_{\rm SM} + \overline{\chi}\left(i\partial\!\!\!/ - m_\chi\right)\chi + \frac{c_\alpha}{\Lambda^2}\overline{\chi}\gamma_\mu\chi\overline{L_\alpha}\gamma^\mu L_\alpha, \tag{5.1}$$

where χ is a Dirac fermion DM particle, and flavour diagonal couplings c_α/Λ^2 between DM and the lepton doublets have been assumed in order to avoid new sources of flavour violation. For the effective description to be consistent we will require that $\Lambda^2/c_\alpha \gg m_\chi^2$. The simplest UV completion which leads to the $d = 6$ operator in Eq. (5.1) is via the exchange of a new heavy vector boson that couples both to χ and L_α.

The Lagrangian in Eq. (5.1) implies that, in this naive gauge-invariant scenario, the coupling between the SM neutrinos and DM will be accompanied by a DM-charged lepton coupling of the same strength. Therefore, the strongest constraints on this model will typically come from indirect searches for DM annihilations to charged leptons. The DM relic abundance will also be set by its annihilation into leptons, either neutrinos or charged leptons, with the annihilation cross section given by

$$\langle\sigma v_r\rangle \approx \frac{c_\alpha^2 m_\chi^2}{2\pi\Lambda^4}\left(1 - \frac{m_\alpha^2}{4m_\chi^2}\right)\sqrt{1 - \frac{m_\alpha^2}{m_\chi^2}}, \tag{5.2}$$

where m_α is the lepton mass for the different α flavour.

5.3.2 *Results*

In Fig. 5.1, we show regions in the parameter space of the DM mass m_χ and the new physics scale Λ excluded by different experiments. The blue line corresponds to the correct DM relic density $\Omega_{\rm DM}h^2 = 0.1193 \pm 0.0009$ [166] obtained through the thermal freeze-out mechanism. This line has been computed with `micrOMEGAs` [232]. In the upper hatched region, the DM-lepton interaction would be too weak, leading to overclosure of the Universe ($\Omega_{\rm DM}h^2 > 0.12$). In the region below the blue line, the relic density is smaller than the observed DM abundance. If there are additional production mechanisms contributing to the DM density, this region is also viable.

The constraints from indirect DM searches outlined in Section 5.2 are shown as different shaded regions. The light green (Planck [166, 221]) and orange (Fermi satellite [220]) regions correspond to the bounds from DM annihilation to charged leptons described in Section 5.2.2. The remaining shaded regions correspond to the constraints from DM annihilation to neutrinos as searched for in neutrino detectors and summarised in Section 5.2.1. In the upper-left panel of Fig. 5.1, we show in different colours the bounds coming from different neutrino experiments. The SK analyses [187, 209] are

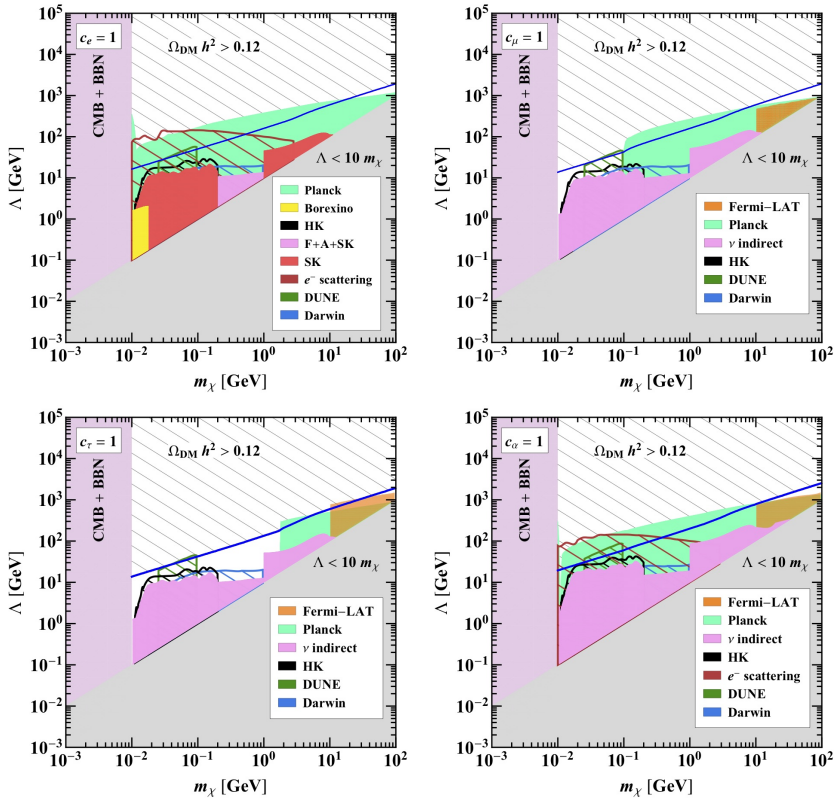

Figure 5.1: Constraints on the DM mass m_χ and the new physics scale Λ. The upper and bottom-left panels correspond to couplings to only one of the lepton doublets (electron, muon, or tau), while the bottom-right panel corresponds to all three couplings being of equal strength. Along the blue line we recover the correct DM relic abundance from thermal freeze-out. The coloured shaded regions are excluded by different experiments, while the hatched areas correspond to prospective sensitivities of future experiments. The lower bound $m_\chi \gtrsim 10$ MeV is set by observations of the CMB and BBN. See text for further details.

shown in red while the Borexino bounds [212] are displayed in yellow. The pink colour corresponds to the bounds from [208] obtained by combining the atmospheric neutrino data.[1] The dark red hatched region corresponds to prospective sensitivity of experiments on DM-electron scattering [224], while the blue, black, and green hatched regions correspond to prospects from different neutrino experiments as described in Section 5.2.1. In the following panels and in the rest of the paper we show all present indirect detection constraints from neutrino experiments in pink colour.

As can be seen in Fig. 5.1, the strongest constraints come from DM annihilation to charged leptons as probed by Fermi-LAT [220] for $\chi\overline{\chi} \to \tau^+\tau^-$, $\mu^+\mu^-$ and from Planck [166, 221] for $\chi\overline{\chi} \to \ell^+\ell^-$, $\ell = e, \mu, \tau$. The latter are in agreement with the results of Ref. [233], where, in particular, the dimension 6 operator given in Eq. (5.1) has been analysed. Indirect searches at neutrino detectors will always play a sub-leading role as long as annihilation to charged leptons is possible. Indeed, present constraints from DM annihilation to charged leptons are strong enough to rule out the entire allowed region of the parameter space that could lead to the correct DM relic density as long as the coupling to electrons is sizeable. However, if DM dominantly couples to the heavier lepton generations, allowed windows open up for $m_\chi < m_\mu$ (m_τ) (see the upper-right and bottom-left panels of Fig. 5.1). In this case, the DM relic density would be set by its annihilation to neutrinos, and the most relevant present constraints come from the results of SK and Borexino. The prospects for HK and DUNE would be very promising in these scenarios, allowing to probe most of the parameter space up to and beyond where the relic density is entirely explained by freeze-out based on neutrino interactions.

Regarding the constraints that could be set by the DM effects in the spectrum or isotropy of high energy cosmic neutrinos as observed by IceCube [194], these would lie in the region of the parameter space already excluded by the number of relativistic degrees of freedom in the early Universe [228–230].

From Fig. 5.1 it is clear that, as long as light DM couples to the electron doublet, this option for a neutrino-DM coupling is mostly ruled out by DM-electron interactions. However, if the DM coupling to L_e is negligible and DM dominantly couples to L_μ and/or L_τ, the viable part of parameter space with $m_\chi < m_\mu$ (m_τ) can be probed by the neutrino experiments.

5.4 COUPLING VIA THE NEUTRINO PORTAL

Given the results of the previous section, we will now explore whether the neutrino portal option is able to lead to a rich neutrino-

1 "F+A+SK" in the corresponding legend stands for Fréjus + AMANDA + SK.

DM phenomenology without being in conflict with indirect searches involving charged leptons. The first necessary ingredient is to have sizeable mixing between the SM neutrinos and the new sterile neutrinos that will mediate the DM interaction. Therefore, the sterile-light neutrino mixing should not scale with the light neutrino masses, unlike in the canonical Seesaw mechanism. Therefore, we will instead attribute the smallness of neutrino masses to an approximate lepton number (or $B - L$) symmetry rather than to a hierarchy of scales between the Dirac and Majorana masses. The new singlets will thus form pseudo-Dirac pairs since lepton number violation will necessarily be very small to account for the lightness of SM neutrinos. This is the case for instance in the popular "inverse" [151] and "linear" [149, 150] Seesaw mechanisms based on such a symmetry.

As a simplifying assumption we will here consider the addition of only one (pseudo-)Dirac sterile neutrino that will serve as portal between the SM neutrinos and DM. Neglecting this small lepton number violation, the couplings between the SM and the new Dirac singlet neutrino are given by

$$\mathcal{L} = \mathcal{L}_{\text{SM}} + \overline{N}\left(i\partial\!\!\!/ - m_N\right) N - \lambda_\alpha \overline{L_\alpha} \tilde{H} N_R, \tag{5.3}$$

where N is the Dirac sterile neutrino and $\tilde{H} = i\sigma_2 H^*$, with H being the Higgs doublet.

Electroweak symmetry breaking gives rise to the neutrino Dirac mass term

$$\left(\overline{\nu_{\alpha L}},\, \overline{N_L}\right) M_\nu N_R + \text{h.c.}\,, \tag{5.4}$$

where $M_\nu = (\lambda_\alpha v,\, m_N)^T$ is the neutrino mass matrix and $v = \langle H^0 \rangle = 174$ GeV is the Higgs vacuum expectation value (vev). Diagonalising $M_\nu M_\nu^\dagger$ with a 4×4 unitary matrix U,

$$U^\dagger M_\nu M_\nu^\dagger U = \text{diag}\left(m_1^2, m_2^2, m_3^2, m_4^2\right), \tag{5.5}$$

we find the mass of the heavy neutrino to be

$$m_4 = \sqrt{m_N^2 + \sum_\alpha |\lambda_\alpha|^2 v^2}\,. \tag{5.6}$$

As expected, the lepton number symmetry forbids light neutrino masses. In order to account for neutrino masses, small breaking of this symmetry via terms such as $\mu\, \overline{N_L} N_L^c$ (inverse Seesaw), or $\lambda'_\alpha \overline{L_\alpha} \tilde{H} N_L^c$ (linear Seesaw) can be added. Since these small parameters would have negligible impact in the phenomenology of neutrino-DM interactions, we will not consider them in what follows.

The neutrino mixing matrix U, which relates LH flavour neutrino fields and the neutrino fields with definite masses as

$$\begin{pmatrix} \nu_{\alpha L} \\ N_L \end{pmatrix} = U \begin{pmatrix} \nu_{iL} \\ \nu_{4L} \end{pmatrix}, \quad \alpha = e, \mu, \tau, \quad i = 1, 2, 3, \tag{5.7}$$

has the form

$$U = \begin{pmatrix} U_{\alpha i} & U_{\alpha 4} \\ U_{si} & U_{s4} \end{pmatrix}. \tag{5.8}$$

The upper-left 3×3 block $U_{\alpha i}$ would correspond to the Pontecorvo–Maki–Nakagawa–Sakata (PMNS) matrix once the small lepton number-breaking terms that induce neutrino masses are taken into account. Note that this matrix, being a 3×3 sub-block of a larger unitary matrix will, in general, not be unitary. The upper-right 3×1 block $U_{\alpha 4}$ describes the mixing between the active flavour neutrinos and the LH component of the heavy neutrino with mass m_4. The last row of the matrix U specifies the admixture of each ν_{jL}, $j = 1, 2, 3, 4$, in the LH sterile neutrino N_L. As we will see in what follows, the DM-related phenomenology is driven by the mixing of active-heavy mixing matrix elements $U_{\alpha 4}$. We will use the unitarity deviations of the PMNS matrix to constrain these mixings [155]. The mixing elements of interest are given by

$$U_{\alpha 4} = \frac{\theta_\alpha}{\sqrt{1 + \sum_\alpha |\theta_\alpha|^2}},\ U_{s4} = \frac{1}{\sqrt{1 + \sum_\alpha |\theta_\alpha|^2}},\ \sum_{i=1}^{3} |U_{si}|^2 = \sum_{\alpha=e}^{\tau} |U_{\alpha 4}|^2, \tag{5.9}$$

with $\theta_\alpha = \lambda_\alpha v / m_N$. Note that, even though the SM neutrino masses have been neglected, the mixing with the extra singlet neutrino that will act as portal can still be sizeable. For definiteness we will fix the mixing to the different flavours to their 1σ limit from Ref. [155], namely:

$$|\theta_e| = 0.031, \quad |\theta_\mu| = 0.011, \quad |\theta_\tau| = 0.044. \tag{5.10}$$

In the following sections, we will explore two possible ways in which these Dirac neutrinos could couple to the dark sector and become portals between it and the SM neutrinos.

5.5 NEUTRINO PORTAL WITH A SCALAR MEDIATOR

In this first example, we will assume that DM is composed of a new fermion, singlet under the SM gauge group, and that a new scalar mediates the Dirac neutrino-DM interactions.

5.5.1 *Model*

The Lagrangian of the model we will consider is given by

$$\begin{aligned} \mathcal{L} =& \mathcal{L}_{\text{SM}} + \overline{\chi}\left(i\partial\!\!\!/ - m_\chi\right)\chi + \overline{N}\left(i\partial\!\!\!/ - m_N\right)N + \partial_\mu S^* \partial^\mu S \\ & - \left[\lambda_\alpha \overline{L_\alpha} \tilde{H} N_R + \overline{\chi}\left(y_L N_L + y_R N_R\right) S + \text{h.c.}\right] \\ & - \mu_S^2 |S|^2 - \lambda_S |S|^4 - \lambda_{SH} |S|^2 H^\dagger H, \end{aligned} \tag{5.11}$$

where χ is a Dirac fermion DM candidate and S is a complex scalar. The fields χ and S form the dark sector of the model (they are SM

singlets), while N serves as a mediator between the dark sector and SM. The Lagrangian in Eq. (5.11) respects a global $U(1)_L$ lepton number symmetry under which L_α, N, and S^* have the same charge and which protects the SM neutrino masses. Moreover, the Lagrangian respects a global $U(1)_D$ dark symmetry, under which χ and S have equal charges. This preserved symmetry ensures the stability of χ, if $m_\chi < m_S$, where $m_S^2 = \mu_S^2 + \lambda_{SH} v^2$ is the mass squared of the scalar S. For $m_\chi > m_S$, the roles of χ and S would change, and S would be a DM candidate. While this possibility is perfectly viable, it is more difficult to probe at neutrino detectors, as the DM annihilation cross section to neutrinos is velocity-suppressed. In what follows we assume that $m_\chi < m_S$ and focus on fermionic DM.

This model was previously considered in Refs. [203, 205]. However, we will go beyond these works by performing a comprehensive analysis of the sensitivity of neutrino experiments to the parameter space of this model.

We will limit ourselves to the case in which DM is lighter than the heavy neutrino,[2] i.e., $m_\chi < m_4$. This is the so-called direct annihilation regime [234], since DM annihilates through the mediator directly to SM particles. As intended, the only channel for DM annihilation at tree level is the one into light neutrinos. This process occurs via a diagram involving a t-channel exchange of the scalar mediator S. In the opposite regime, which is usually referred to as secluded [234], DM annihilates to heavy neutrinos, which subsequently decay. The phenomenology of this regime has been studied in Refs. [235–238].

Neglecting velocity-suppressed terms, we find the following thermally averaged cross section for DM annihilation to neutrinos:

$$\begin{aligned} \langle \sigma v_r \rangle &\approx \frac{y_L^4}{32\pi} \left(\sum_{i=1}^{3} |U_{si}|^2 \right)^2 \frac{m_\chi^2}{\left(m_\chi^2 + m_S^2\right)^2} \\ &\approx \frac{y_L^4}{32\pi} \left(\sum_{\alpha=e,\mu,\tau} |\theta_\alpha|^2 \right)^2 \frac{m_\chi^2}{\left(m_\chi^2 + m_S^2\right)^2} \,. \end{aligned} \tag{5.12}$$

The product $y_L \sqrt{\sum_\alpha |\theta_\alpha|^2}$ controls $\langle \sigma v_r \rangle$ and, in order to allow for sufficient annihilation to reproduce the observed relic density, it cannot be too small. The value of the coupling y_L is limited by the requirement of perturbativity. We will restrict ourselves to $y_L < 4\pi$. Since the coupling y_R does not enter Eq. (5.12), and thus, does not affect the tree-level neutrino-DM interactions, in what follows we set it to zero for simplicity. Regarding the mixing parameters θ_α, the bounds on them depend on the mass of the heavy neutrino. For definiteness we will assume that the heavy neutrino has a mass above the electroweak scale. At this scale the bounds on heavy neutrino mixing derived

2 Otherwise the $\chi\overline{\chi} \to \nu_i \overline{\nu_4}$ or $\chi\overline{\chi} \to \nu_4 \overline{\nu_4}$ channels would dominate the annihilation cross section and only sub-dominant DM interactions with the 3 light SM neutrinos ν_i would be allowed.

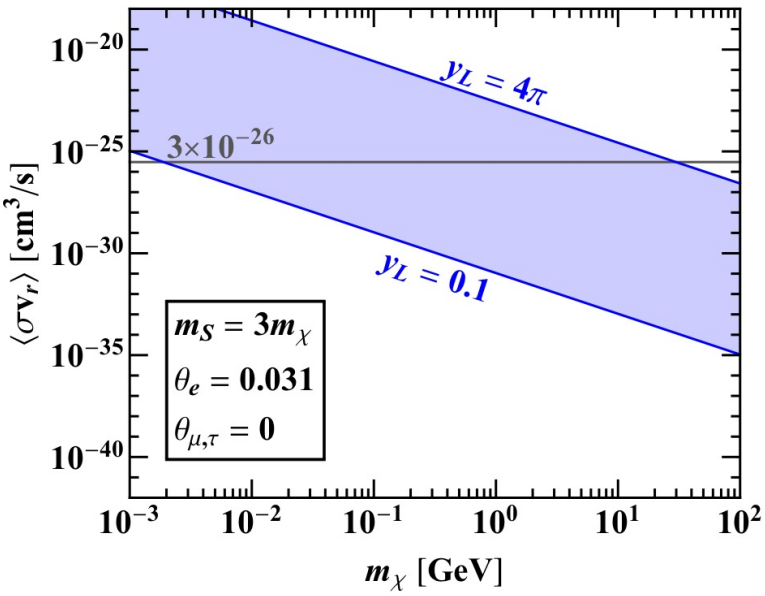

Figure 5.2: Thermally averaged annihilation cross section multiplied by the relative velocity for $\chi\overline{\chi} \to \nu\overline{\nu}$. We have fixed $m_S = 3m_\chi$, $\theta_e = 0.031$, $\theta_\mu = \theta_\tau = 0$, and varied y_L between 0.1 and 4π.

in the global analysis of flavour and electroweak precision data performed in Ref. [155] apply. If smaller masses were instead considered, more stringent constraints from collider and beam-dump searches and, eventually, production in meson and beta decays could potentially apply [157] (see discussion in Section 5.6.3). In any case, all the observables relevant to DM phenomenology have a sub-leading dependence on m_4. We also consider the case where the coupling $\lambda_{SH} = 0$, ensuring the neutrino portal regime. In Refs. [203, 205], the radiative generation of the $|S|^2 H^\dagger H$ operator was considered and its effects on m_S as well as on the invisible width of the Higgs boson were found to be negligible.

In Fig. 5.2, we show the region of the parameter for which the correct thermal relic abundance is obtained. This region spans DM masses up to 100 GeV for $|\theta_e| = 0.031$, $\theta_\mu = \theta_\tau = 0$, and y_L between 0.1 and 4π while keeping $m_S = 3m_\chi$ as a benchmark.

Annihilation of DM into charged lepton-antilepton pairs $\ell^+\ell^-$ ($\ell = e, \mu, \tau$), proceeds via the one-loop diagrams[3] shown in Fig. 5.3 (in unitary gauge).

The dominant contribution comes from the first and second diagrams, while the contribution from the last diagram is suppressed by

3 The Feynman diagrams in this article are produced with the `TikZ-Feynman` package [239].

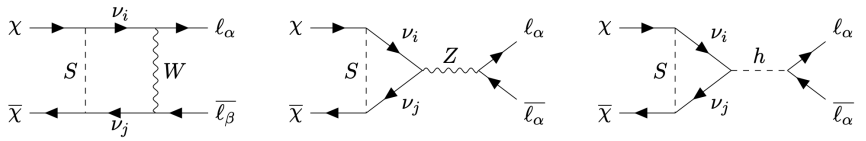

Figure 5.3: One-loop diagrams (in unitary gauge) contributing to annihilation of DM into charged lepton-antilepton pairs $\ell_\alpha\overline{\ell_\beta}$, $\alpha, \beta = e, \mu, \tau$. The indices i and j run from 1 to 4.

the small Yukawa couplings of the charged leptons. The first diagram leads to the following effective operator:

$$\mathcal{L} \supset -a_{SW}\frac{g^2}{m_W^2}\overline{\chi}\gamma^\mu P_R\chi\,\overline{\ell_\alpha}\gamma_\mu P_L\ell_\beta\,, \tag{5.13}$$

where g is the weak coupling constant. Neglecting external momenta, the effective coupling a_{SW} is given by

$$a_{SW} = |U_{s4}|^2 U_{\alpha 4}U^*_{\beta 4}\frac{y_L^2}{(4\pi)^2}G\left(\frac{m_S^2}{m_4^2}\right), \tag{5.14}$$

where the loop function $G(x)$ reads

$$G(x) = \frac{x - 1 - \log x}{4\Big(1 - x\Big)^2}\,. \tag{5.15}$$

The second diagram in Fig. 5.3 leads to the following effective interaction of DM with the Z boson:

$$\mathcal{L} \supset -a_Z\frac{g}{\cos\theta_W}\overline{\chi}\gamma^\mu P_R\chi Z_\mu\,, \tag{5.16}$$

where θ_W is the Weinberg angle and a_Z is the effective coupling, which in the limit of zero external momenta is given by

$$a_Z = |U_{s4}|^2\left(1 - |U_{s4}|^2\right)\frac{y_L^2}{(4\pi)^2}G\left(\frac{m_S^2}{m_4^2}\right)\,. \tag{5.17}$$

These contributions have been also computed using a combination of packages: `FeynRules` [240, 241] to produce a model file, `FeynArts` [242] for generating the diagrams and `FormCalc` [243] for computing their numerical contributions. For numerical evaluation of the Passarino-Veltman functions we have used `LoopTools` [243]. We have also considered the limit of zero external momenta, which effectively corresponds to the limit of small DM and charged lepton masses, and confronted the analytical results obtained in this approximation using the package `ANT` [244] with the `LoopTools` results. For DM masses between 1 MeV and 100 GeV that we are interested in, the approximation works very well. The availability of analytical expressions allows for an easier exploration of the parameter space.

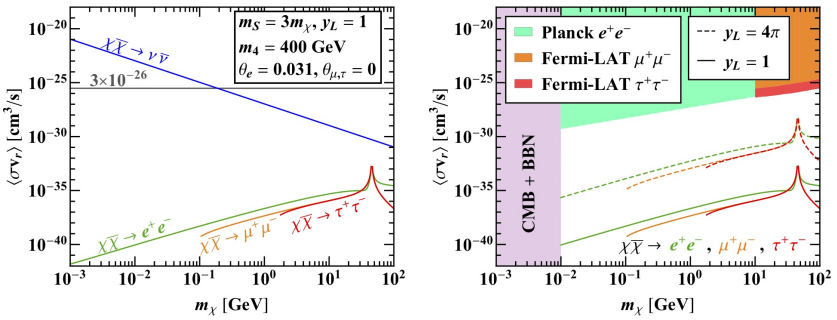

Figure 5.4: Thermally averaged annihilation cross section multiplied by the relative velocity for DM annihilation into e^+e^-, $\mu^+\mu^-$, and $\tau^+\tau^-$. We have fixed $m_S = 3m_\chi$, $m_4 = 400$ GeV, $y_L = 1$, $\theta_e = 0.031$, and $\theta_{\mu,\tau} = 0$. The *left* panel provides comparison with $\langle\sigma v_r\rangle$ for DM annihilation into neutrinos assuming the same set of model parameters. The *right* panel displays the indirect detection constraints coming from Planck and Fermi-LAT. The lower bound $m_\chi \gtrsim 10$ MeV is set by observations of the CMB and BBN. See text for further details.

In Fig. 5.4, we present the cross sections for annihilation of DM into e^+e^-, $\mu^+\mu^-$, and $\tau^+\tau^-$ for benchmark values of the model parameters. We fix $m_S = 3m_\chi$, $m_4 = 400$ GeV, $y_L = 1$, $\theta_e = 0.031$, and $\theta_{\mu,\tau} = 0$. As can be seen from the left panel, the annihilation cross sections to charged leptons are several orders of magnitude smaller than the cross section for DM annihilation into neutrinos. The difference in the cross sections becomes smaller when the DM mass approaches $m_Z/2$, and the cross sections for $\chi\bar{\chi} \to \ell^+\ell^-$ exhibit a resonant behaviour due to the second diagram in Fig. 5.3. In the right panel, we show the indirect detection constraints from Planck [166, 221] and Fermi-LAT [220]. Note that those constraints assume a 100% annihilation rate into a single SM channel. Even for $y_L = 4\pi$ the resulting annihilation cross sections into charged leptons are well below the experimental constraints. Thus, the considered realisation of the neutrino portal does provide an example of a gauge-invariant model in which the neutrino-DM interactions dominate DM phenomenology.

At one-loop level DM also interacts with quarks via diagrams involving Z and h, which are analogous to those in Fig. 5.3. The corresponding effective DM-nucleon spin-independent scattering cross section reads [205]

$$\sigma_n = \frac{\mu_n^2}{\pi} \frac{\left(Z f_p + (A - Z) f_n\right)^2}{A^2}, \tag{5.18}$$

where μ_n is the reduced mass of the nucleon, A is the total number of nucleons in a nuclei, Z is the number of protons,

$$f_p = \left(4\sin^2\theta_W - 1\right) \frac{G_F a_Z}{\sqrt{2}}, \quad f_n = \frac{G_F a_Z}{\sqrt{2}}, \tag{5.19}$$

with a_Z given in Eq. (5.17), and G_F being the Fermi constant. The radiative coupling of DM to the Higgs, $\overline{\chi}\chi h$, would also give a contribution to direct detection searches. This contribution is however suppressed by the small quark Yukawa couplings. Direct detection of a SM singlet fermion DM candidate at one loop has been recently studied in detail in [245]. Moreover, an interesting example, which also provides radiative generation of neutrino masses, has been presented in [246].

The most stringent constraint on DM-nucleon spin-independent cross section for $m_\chi \gtrsim 10$ GeV comes from XENON1T [222]. As we will see in the next subsection, this constraint is strong enough to probe the loop-suppressed scattering process if the value of the coupling y_L is sufficiently large. We have also considered DM scattering off electrons and found that the corresponding cross section is much smaller than the projected sensitivities of silicon, germanium, and xenon experiments derived in Ref. [224]. Thus, DM-electron scattering cannot provide an additional probe of the considered neutrino portal model.

5.5.2 *Results*

In this subsection, we explore the parameter space to find regions that satisfy all direct and indirect detection constraints and in which the DM phenomenology could be dominated by its interactions with SM neutrinos. We show our results in the m_χ-m_S plane to determine the masses of the DM and the dark scalar that are presently allowed and could lead to the correct relic abundance (see Fig. 5.5).

In Fig. 5.5 the triangular region $m_S < m_\chi$ is forbidden by DM stability. Along the blue line(s) computed with `micrOMEGAs`,[4] the DM relic density matches the observed value $\Omega_{\rm DM}h^2 = 0.1193 \pm 0.0009$ [166]. Above this line (the upper hatched region), the DM relic density is bigger than the measured value, i.e., DM overcloses the Universe. Below this line, the relic abundance would be smaller than the observed value. However, if there is an additional production mechanism, the relic abundance could also be compatible with this region.

As can be seen in the figure indirect searches for annihilation to neutrinos, together with direct detection bounds by XENON1T for large DM masses, are the only probes that are presently constraining the allowed parameter space. The prospects to explore the remaining allowed regions through annihilation to neutrinos are very promising. In particular DUNE would be able to detect the neutrino signal in the range $25 - 100$ MeV if the DM abundance is entirely due to this process.

4 We have implemented the effective DM couplings to the Z boson and to the charged leptons via exchange of the W boson (see Fig. 5.3) to the `FeynRules` model file.

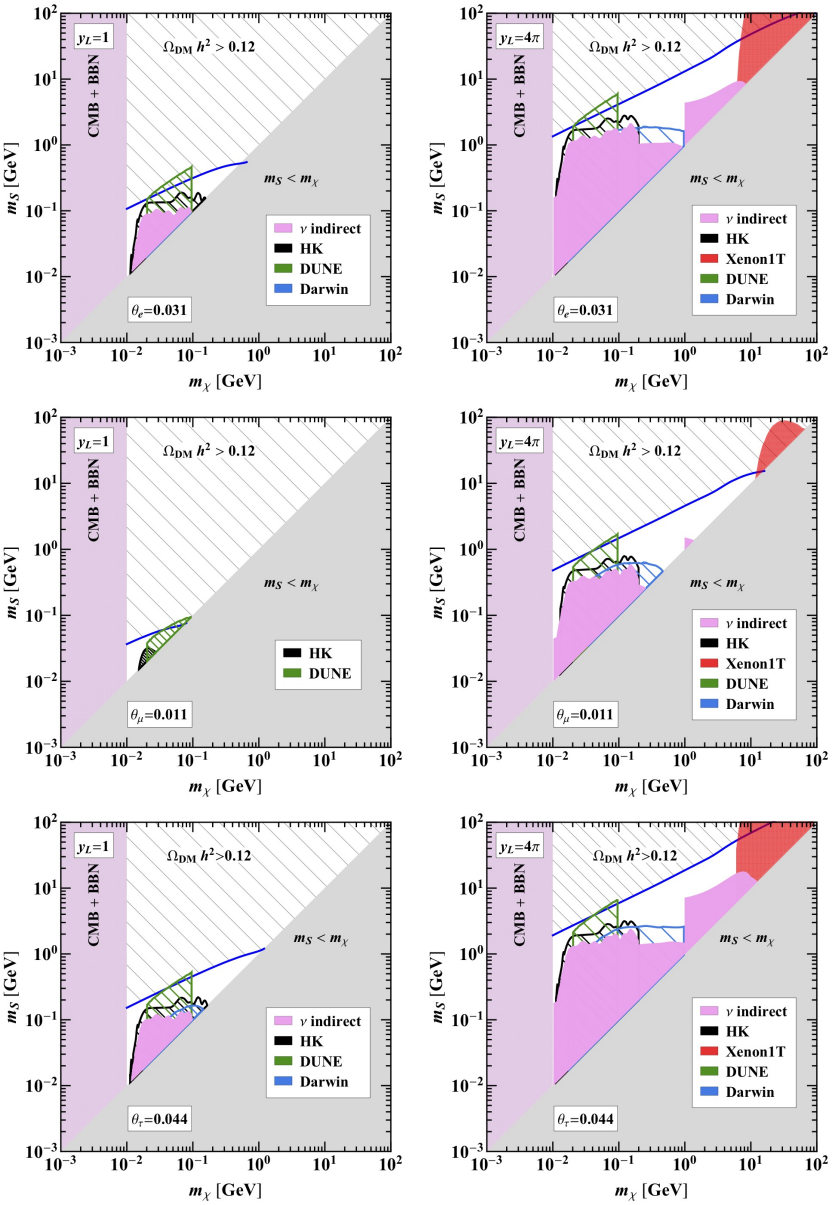

Figure 5.5: Constraints on the DM mass m_χ and the dark scalar mass m_S. We have fixed $\theta_e = 0.031$, $\theta_{\mu,\tau} = 0$; $\theta_\mu = 0.011$, $\theta_{e,\tau} = 0$; and $\theta_\tau = 0.044$, $\theta_{e,\mu} = 0$ (from top to bottom), considering $y_L = 1$ and 4π. Along the blue line the DM relic density matches the observed value. The coloured shaded regions are excluded by different experiments, while the hatched areas correspond to prospective sensitivities of future experiments. The lower bound $m_\chi \gtrsim 10$ MeV is set by observations of the CMB and BBN. See text for further details.

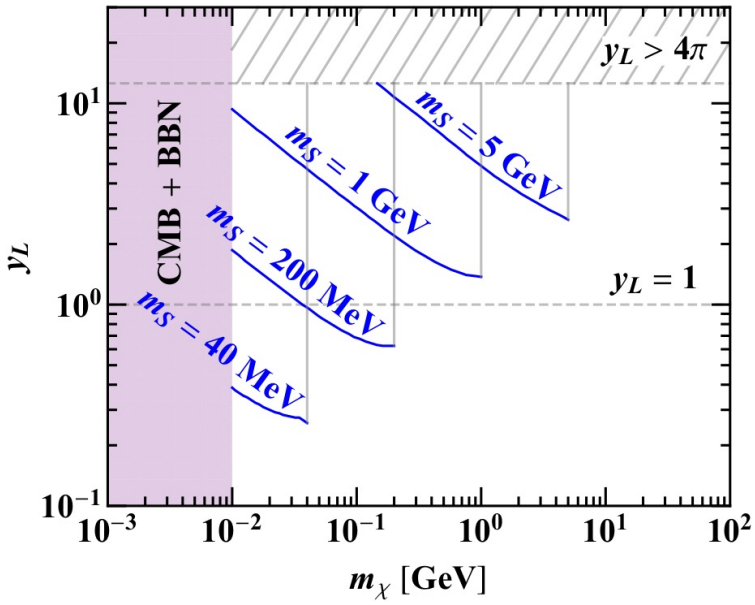

Figure 5.6: Values of the DM mass m_χ and the coupling y_L required to reproduce the observed relic abundance. We have fixed $m_S = 0.04$, 0.2, 1, and 5 GeV, and have considered the representative case of $\theta_e = 0.031$, while keeping $\theta_{\mu,\tau} = 0$. Along (above) the blue lines the DM relic density matches (is less than) the observed value. The lower bound $m_\chi \gtrsim 10$ MeV is set by observations of the CMB and BBN.

In Fig. 5.6, we fix m_S to several representative values, namely $m_S = 0.04$, 0.2, 1, and 5 GeV, and show the lines corresponding to the correct relic abundance in the m_χ-y_L plane. These results have been obtained with `micrOMEGAs`. Small values of y_L are ruled out since they do not lead to efficient DM annihilation. As can be seen, a lighter dark scalar allows for smaller values of y_L. For $m_S \gtrsim 500$ MeV, the values of $y_L \gtrsim 1$ are required to yield the observed relic density.

Overall, the cosmologically allowed parameter space of the model is already constrained by the current neutrino detectors as well as XENON1T.[5] Moreover, the next generation of neutrino experiments, in particular DUNE, will be able to probe thermal MeV fermion DM in the considered scenario.

5.6 NEUTRINO PORTAL WITH A VECTOR MEDIATOR

In this second example, we will again assume that DM is composed of a new Dirac fermion, this time coupled to a new massive vector

5 For $m_\chi > 5$ GeV, DARWIN will have a better sensitivity to spin-independent DM-nucleon cross section than that of XENON1T [216]. However, for $y_L = 4\pi$, these masses are already ruled by XENON1T, while for $y_L = 1$, they are not allowed by the relic abundance constraint.

boson. The Dirac singlet neutrino will also interact with this boson so as to provide the neutrino-DM interaction.

5.6.1 *Model*

The Lagrangian of the model is given by

$$\begin{aligned}\mathcal{L} =& \mathcal{L}_{\rm SM} + \overline{\chi}\left(i\partial\!\!\!/ - m_\chi\right)\chi + \overline{N}\left(i\partial\!\!\!/ - m_N\right)N \\ &+ \left[g'\overline{\chi_R}\gamma^\mu\chi_R Z'_\mu + g'\overline{N_L}\gamma^\mu N_L Z'_\mu - \lambda_\alpha\overline{L_\alpha}\tilde{H}N_R + \text{h.c.}\right] \\ &- \frac{1}{4}Z'_{\mu\nu}Z'^{\mu\nu} + \frac{1}{2}m^2_{Z'}Z'_\mu Z'^\mu\,,\end{aligned} \tag{5.20}$$

where χ is a Dirac fermion DM candidate, Z' is a new vector boson mediating the interaction between neutrinos and DM, and N is the Dirac sterile neutrino connecting the dark and visible sectors through its mixing with the active neutrinos. This Lagrangian could for instance describe a new $U(1)'$ gauge symmetry spontaneously broken by the vev of a scalar SM singlet charged under it, that would induce masses for the Z' as well as for the heavy neutrino N and the DM. The particular mechanism is not relevant for the rest of the discussion and will not be elaborated further. We will also assume there is an additional conserved charge (e.g., a $\mathbb{Z}_2$ symmetry) not shared between the neutrino and the DM that prevents their mixing. Note that in order to keep the Lagrangian in Eq. (5.20) anomaly free without introducing new fields, the simplest option is to couple the LH part of the Dirac sterile neutrino and the RH part of the DM to the new gauge boson with the same coupling g'.

As in the previous scenario, we will assume that the DM mass $m_\chi < m_4$ so that the dominant DM annihilation channel is to the three light SM neutrinos. This is a tree-level process and its cross section is given by

$$\begin{aligned}\langle\sigma v_r\rangle &\approx \frac{g'^4}{8\pi}\left(\sum_{i=1}^{3}|U_{si}|^2\right)^2\frac{m_\chi^2}{(4m_\chi^2 - m_{Z'}^2)^2} \\ &\approx \frac{g'^4}{8\pi}\left(\sum_{\alpha=e,\mu,\tau}|\theta_\alpha|^2\right)^2\frac{m_\chi^2}{(4m_\chi^2 - m_{Z'}^2)^2}\,.\end{aligned} \tag{5.21}$$

Note however that, for $m_{Z'} \lesssim m_\chi$, the tree-level DM annihilation to a pair of Z' bosons is allowed. When this channel is open, it will dominate over the direct annihilation into neutrinos, since the latter is suppressed by neutrino mixing. This is the so-called secluded annihilation regime [234], which we do not consider in the present study.

In this scenario, as can be seen from Fig. 5.7, the correct relic abundance can be obtained purely from annihilation to the SM neutrinos for values of the new gauge coupling g' between 0.1 and 4π, and DM masses in the $0.01 - 100$ GeV range. In this figure, we have fixed $m_{Z'} = 3m_\chi$, $|\theta_e| = 0.031$, and $\theta_\mu = \theta_\tau = 0$ as benchmark values.

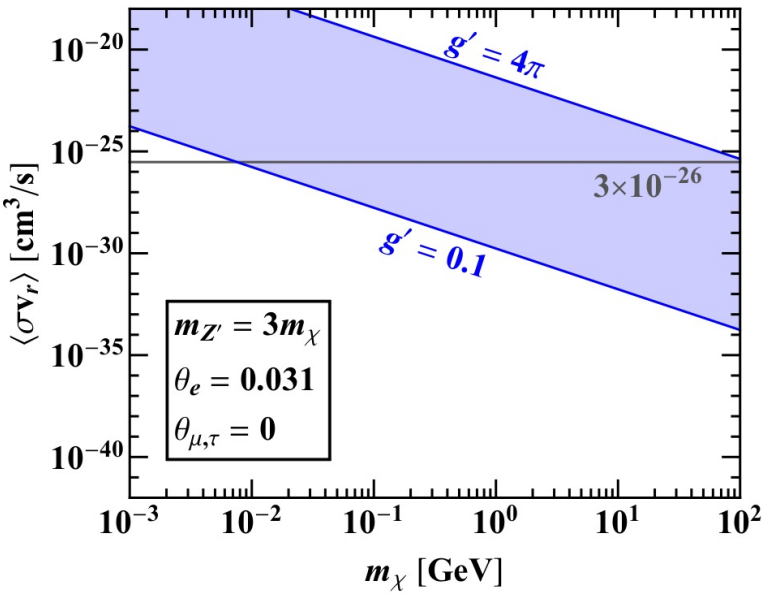

Figure 5.7: Thermally averaged annihilation cross section multiplied by the relative velocity for $\chi\overline{\chi} \to \nu\overline{\nu}$. We have fixed $m_{Z'} = 3m_\chi$, $\theta_e = 0.031$, $\theta_\mu = \theta_\tau = 0$, and varied g' between 0.1 and 4π.

A direct coupling between the Z' boson and the charged leptons will also be induced through the loop diagrams in Fig. 5.8. Neglecting external momenta for the charged leptons, the effective vertex from the first loop diagram is given by

$$\mathcal{L} \supset -a_W g' \overline{\ell_\alpha} \gamma^\mu P_L \ell_\beta Z'_\mu \,, \tag{5.22}$$

where

$$a_W = |U_{s4}|^2 U_{\alpha 4} U^*_{\beta 4} \frac{g^2}{(4\pi)^2} \frac{m_4^2}{2m_W^2} \,. \tag{5.23}$$

5.6.2 *Mixing with the Z boson*

Since the neutrino mass eigenstates have components that couple both to the Z and the Z', mixing between the two gauge bosons will be induced at loop level [197] through the second diagram in Fig. 5.8. The kinetic and mass mixings are described by the effective Lagrangian

$$\mathcal{L}_{Z'Z} = -\frac{\sin\epsilon}{2} Z'_{\mu\nu} Z^{\mu\nu} + \delta m^2 Z'_\mu Z^\mu \,. \tag{5.24}$$

Notice that these two terms could be present already at the Lagrangian level after gauge symmetry breaking. These would represent additional free parameters of the Lagrangian. However, these parameters do not contribute to the neutrino portal of interest here. Conversely, the neutrino mixing required for the neutrino portal does induce the

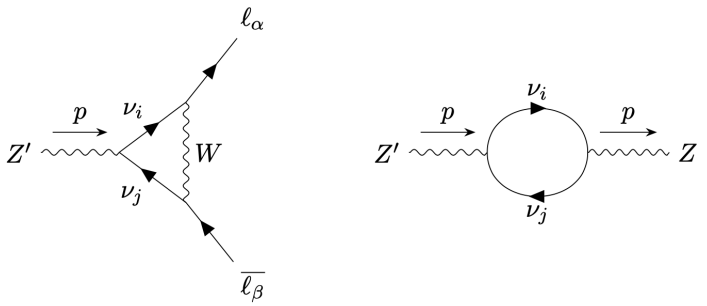

Figure 5.8: One-loop diagrams contributing to the coupling of the Z' boson to charged leptons (*left*) and to kinetic and mass mixing between the Z' and Z bosons (*right*).

Z-Z' mixing at the loop level. Barring fine-tuned cancellations between the allowed free parameters at the Lagrangian level and the loop-induced contributions from neutrino mixing, the minimum contribution present in our set-up will be the latter. We will therefore set the tree-level parameters to zero and require that the loop-induced contributions are below the present experimental constraints on Z-Z' mixing. We find the following results for the mixing parameters:

$$\delta m^2 = \frac{2}{(4\pi)^2} g' \frac{g}{\cos\theta_W} |U_{s4}|^2 \left(1 - |U_{s4}|^2\right) m_4^2 \, f_1, \tag{5.25}$$

$$\sin\epsilon = \frac{2}{(4\pi)^2} g' \frac{g}{\cos\theta_W} |U_{s4}|^2 \left(1 - |U_{s4}|^2\right) f_2, \tag{5.26}$$

where f_1 and f_2 are functions of $x \equiv m_4^2/p^2$, namely,

$$f_1(x) = \frac{1}{12}\Bigg\{4x^2\left(1-x^{-1}\right)^3 \coth^{-1}(1-2x) + 2x - x^{-1}\log(x) - 2\sqrt{x\left(4-x^{-1}\right)^3}\arctan\left(\left(4x-1\right)^{-1/2}\right)\Bigg\}, \tag{5.27}$$

$$f_2(x) = -\frac{x^2}{6}\Bigg\{4\left(2x-3+x^{-2}\right)\coth^{-1}(1-2x) + 4 + x^{-2}\log(x) - 2\sqrt{x^{-1}(4-x^{-1})}\left(2+x^{-1}\right)\arctan\left((4x-1)^{-1/2}\right)\Bigg\}. \tag{5.28}$$

For the purposes of this work $p^2 \sim m_\chi^2$, and thus, f_1 and f_2 will only depend on the ratio of the masses of the heavy neutrino and the DM particle. Following Ref. [247], we first diagonalise the kinetic term through a non-unitary transformation and then perform a rotation to diagonalise the mass term. The mass eigenstates Z_1 and Z_2 have masses given by

$$m_{Z_{1,2}}^2 = \frac{\sec^2\epsilon}{2}\left(m_Z^2 + m_{Z'}^2 - 2\delta m^2 \sin\epsilon \mp \Delta\right), \tag{5.29}$$

where

$$\Delta = \text{sgn}\left(m_{Z'}^2 - m_Z^2\left(1-2\sin^2\epsilon\right) - 2\delta m^2 \sin\epsilon\right) \times \sqrt{m_Z^4 + m_{Z'}^4 + 4\delta m^4 - 4\left(m_Z^2 + m_{Z'}^2\right)\delta m^2 \sin\epsilon - 2m_Z^2 m_{Z'}^2\left(1-2\sin^2\epsilon\right)} \tag{5.30}$$

From Eq. (5.29), one can easily verify that in the limit of small mass and kinetic mixing, i.e., $\delta m^2 \to 0$ and $\sin\epsilon \to 0$, the masses $m_{Z_1} \to m_Z$ and $m_{Z_2} \to m_{Z'}$. After the full diagonalisation, we can write the Z and Z' in terms of the mass eigenstates Z_1 and Z_2 as follows:

$$Z_\mu = \left(\cos\xi - \tan\epsilon\sin\xi\right) Z_{1\mu} - \left(\sin\xi + \tan\epsilon\cos\xi\right) Z_{2\mu}, \tag{5.31}$$

$$Z'_\mu = \sec\epsilon\left(\sin\xi\, Z_{1\mu} + \cos\xi\, Z_{2\mu}\right), \tag{5.32}$$

where ξ is the angle related to the mass diagonalisation, which is defined through

$$\tan(2\xi) = \frac{2\cos\epsilon\left(m_Z^2\sin\epsilon - \delta m^2\right)}{m_{Z'}^2 - m_Z^2\left(1-2\sin^2\epsilon\right) - 2\delta m^2\sin\epsilon}. \tag{5.33}$$

The two angles ξ and ϵ will control the phenomenology associated to the Z-Z' mixing and consequently, the possible Z' couplings to fermions.

The loop-induced kinetic mixing parameter ϵ depends solely on the ratio $x \approx m_4^2/m_\chi^2$, providing the coupling g' and the element U_{s4} of the neutrino mixing matrix are fixed (see Eqs. (5.26) and (5.28)), and increases with it. Fixing $|\theta_e| = 0.031$ and $\theta_{\mu,\tau} = 0$, we find that for $x = 4$, which is the lowest value preventing the $\chi\overline{\chi} \to \nu_i\overline{\nu_4}$, $i = 1,2,3$, channels, and $g' = 1$ (4π), the mixing parameter $|\sin\epsilon|$ is of order of 10^{-6} (10^{-5}). For values of x as large as 10^4 and $g' = 1$ (4π), the value of $|\sin\epsilon|$ does not exceed approximately 10^{-5} (10^{-4}).

Generally, these values can be probed in beam dump and fixed target experiments searching for visible decay products (electrons and muons) of the Z_2 boson with mass between approximately 1 MeV and 1 GeV (see, e.g., [248, 249]). However, in the considered model the Z_2 decays mostly invisibly, either to a pair of the SM neutrinos or, if it is heavy enough, to a pair of DM particles, while its decays to charged leptons are suppressed. Thus, the bounds from fixed target experiments will not apply in this case. The supernova constraints cover nearly the same Z_2 masses, but a different range of $\epsilon \sim 10^{-10} - 10^{-7}$ [248], which thus are also avoided. For larger Z_2 masses, up to 100 GeV, collider experiments place the best constraints on $\epsilon \sim 10^{-4} - 10^{-3}$ (see, e.g., Ref. [249]). There exist also collider searchers for Z_2 decaying invisibly, which constrain $\epsilon \lesssim 10^{-3}$ for $m_{Z_2} < 8$ GeV [250]. These collider constraints are above the values of the loop-induced kinetic mixing parameter in our model. Finally, the much weaker constraint from the invisible Z_1 width, $\epsilon \lesssim 0.03$ [251], is also evaded.

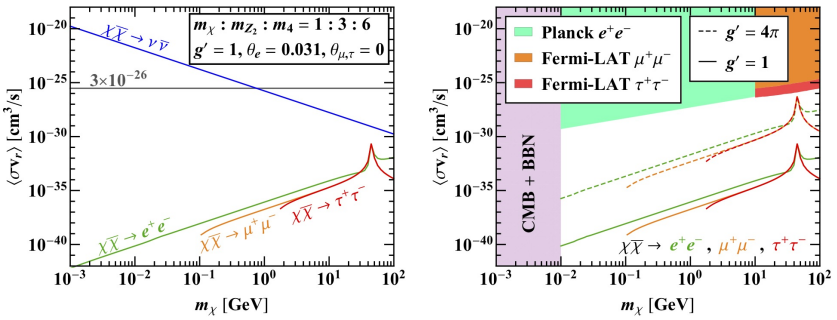

Figure 5.9: Thermally averaged annihilation cross section multiplied by the relative velocity for DM annihilation into e^+e^-, $\mu^+\mu^-$, and $\tau^+\tau^-$. We have fixed $m_\chi : m_{Z_2} : m_4 = 1 : 3 : 6$, $g' = 1$, $\theta_e = 0.031$, and $\theta_{\mu,\tau} = 0$. The *left* panel provides comparison with $\langle\sigma v_r\rangle$ for DM annihilation into neutrinos assuming the same set of model parameters. The *right* panel displays the indirect detection constraints coming from Planck and Fermi-LAT. The lower bound $m_\chi \gtrsim 10$ MeV is set by observations of the CMB and BBN. See text for further details.

Together with the first diagram in Fig. 5.8, the size of ξ and ϵ will determine how relevant the DM annihilation to a pair of charged leptons is. We find that the tree-level annihilation to neutrinos dominates over that to charged leptons. In Fig. 5.9, we show a particular example of this behaviour for $m_4 = 2m_{Z_2}$, $m_{Z_2} = 3m_\chi$, $g' = 1$, $|\theta_e| = 0.031$, and $\theta_\mu = \theta_\tau = 0$. It is clear from this figure that the annihilation to charged leptons is unconstrained by current experimental searches. Note that the Planck and Fermi-LAT constraints shown in the right panel of Fig. 5.9 assume a 100% annihilation rate into a single SM channel.

5.6.3 *Results*

The allowed region of the parameter space in the m_χ-m_{Z_2} plane that satisfy cosmological, indirect and direct detection constraints for this model are presented in Fig. 5.10 for $g' = 1$ and 4π, setting $\theta_\alpha \neq 0$ one at a time and keeping two other mixing angles fixed to zero. For definiteness, in the figure we set $m_4 = 2m_{Z_2}$. Notice that this choice is not relevant for the interaction between the SM neutrinos and DM and only plays a role in the loop-induced processes that are sub-dominant. Nevertheless, if the Z_2 originates from a new $U(1)'$ gauge group, its mass m_{Z_2}, as well as that of the Dirac neutrino m_4, are generated after the breaking of the symmetry. Thus, the natural expectation is that m_4 is not much heavier than m_{Z_2} as long as the new gauge coupling g' is $\mathcal{O}(1)$. Hence, unlike for the scalar example, it is not appropriate to set m_4 to a value above the electroweak scale while exploring (sub-)GeV Z_2 boson masses.

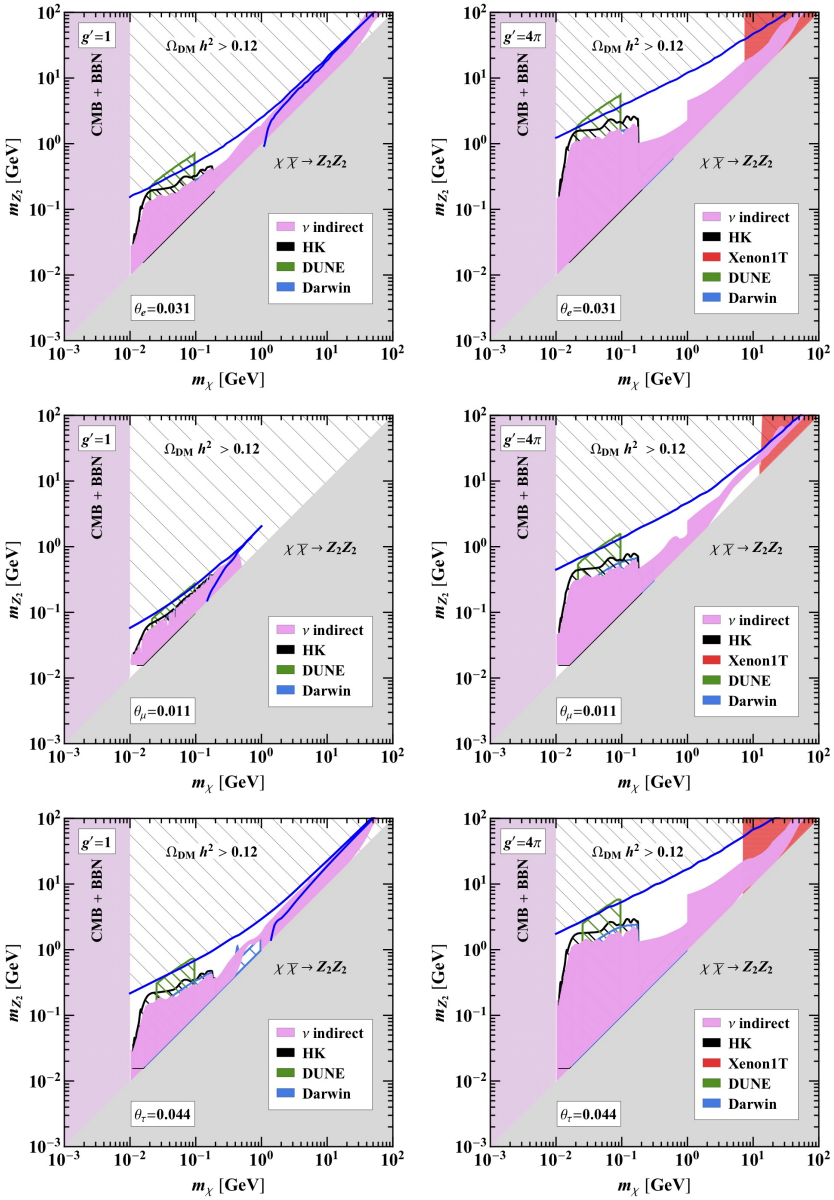

Figure 5.10: Constraints on the DM mass m_χ and m_{Z_2}. Along the blue lines, computed with `micrOMEGAs`, the DM relic density matches the observed value. The coloured shaded regions are excluded by different experiments. The lower bound $m_\chi \gtrsim 10$ MeV is set by observations of the CMB and BBN. See text for further details.

Below the electroweak scale constraints on the neutrino mixing parameters θ_α are *a priori* much more stringent [157]. However, in the model under investigation the heavy neutrino decays mostly invisibly to either a SM neutrino and the Z_2 (if $m_4 > m_{Z_2}$), or a SM neutrino and a pair of the DM particles (if $m_4 < m_{Z_2}$), assuming $g' \gtrsim 1$. This implies that the existing collider and beam dump constraints[6] should be rescaled with the corresponding branching ratios and become even weaker than the non-unitarity constraints imposed previously for the scalar realisation. The bounds from peak searches in leptonic decays of pions and kaons will however apply, since they rely entirely on the kinematics of a two-body decay. Thus, the non-unitarity constraints actually dominate down to $m_4 \approx m_K \approx 0.5$ GeV, where m_K is the kaon mass. In the region $m_4 \sim 0.01 - 0.4$ GeV, the bounds on U_{e4} and $U_{\mu 4}$ from peak searches are very stringent. We do not display them explicitly in Fig. 5.10, because they are m_4-dependent, while all the constraints shown in the figures have an extremely sub-leading dependence on m_4, as outlined above. Thus, Fig. 5.10 is to be interpreted as generally valid for any neutrino mass $m_4 > m_K$.

The blue line was calculated with `micrOMEGAs` and represents the DM and vector boson masses that will produce the correct relic abundance in a thermal scenario, while the masses in the upper hatched area would generate too much DM. A key difference with respect to the previous model is that here the DM annihilation cross section to neutrinos proceeds via an s-channel and thus is enhanced for $m_{Z_2} \sim 2m_\chi$, as can be seen from Eq. (5.21). This explains the second branch of the blue line below the resonant condition in the panels with $g' = 1$. A line where the relic abundance can be obtained below $m_{Z_2} = 2m_\chi$ also occurs for $g' = 4\pi$ but, since the cross section is larger, the relic abundance is achieved for $m_\chi > 100$ GeV, which is ruled out by XENON1T. This resonant effect also explains the shape of the indirect detection constraints which follow the same trend.

Similar to the previous model in Section 5.5, the direct detection constraints from XENON1T become relevant at large DM masses for $g' = 4\pi$. However, even for values of the gauge coupling this large, we have checked that direct detection constraints from the elastic DM scattering off electrons are negligible.

The complementarity between cosmological observables, DM, and neutrino experiments allows us to set very strong bounds on the DM and Z_2 masses for this particular realisation, ruling out significant portions of the parameter space. There are still allowed regions for larger values of the gauge coupling consistent with a thermal DM candidate that yields the observed DM relic abundance. However, future neutrino experiments such as DUNE will be able to probe down

6 If the heavy neutrino decays before reaching the detector, the constraints from beam dump experiments will not apply at all.

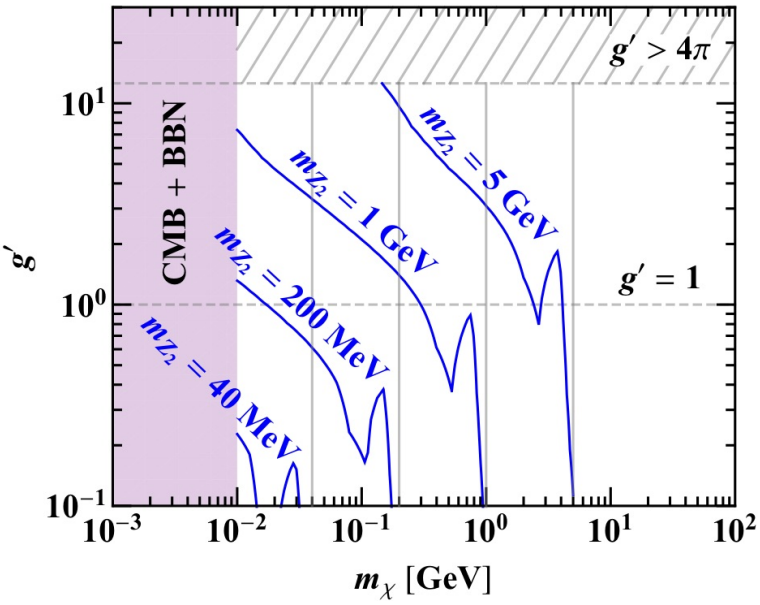

Figure 5.11: Values of the DM mass m_χ and the coupling g' required to reproduce the observed relic abundance. We have fixed $m_{Z_2} =$ 0.04, 0.2, 1, and 5 GeV, and have considered the representative case of $\theta_e = 0.031$, while keeping $\theta_{\mu,\tau} = 0$. Along (above) the blue lines the DM relic density matches (is less than) the observed value. We do not consider $m_\chi > m_{Z_2}$ to ensure the neutrino portal regime. The lower bound $m_\chi \gtrsim 10$ MeV is set by observations of the CMB and BBN.

to the value for which the correct relic abundance is obtained in some parts of the parameter space.

It is worth noticing that the sensitivity of present and future neutrino detectors to DM annihilations into neutrinos is largely independent of the flavour to which the sterile neutrino dominantly couples. Indeed, regardless of the original flavour composition produced by the DM annihilations, neutrino oscillations will tend to populate all flavours with similar fractions when the flux arrives to the detector. The main differences between the three rows in Fig. 5.10 are due to the different magnitude of the mixing allowed to the different flavours, with more stringent constraints applying for the mixing with muon neutrinos.

Finally, in Fig. 5.11, we fix m_{Z_2} to several values, namely, $m_{Z_2} = 0.04$, 0.2, 1, and 5 GeV, and show the lines corresponding to the correct relic abundance in the m_χ-g' plane. These results were obtained using `micrOMEGAs`. Small values of g' are ruled out except for DM masses in the proximity of the resonance, i.e., when $m_\chi \approx m_{Z_2}/2$. As can be seen from this figure, a lighter dark vector boson allows for smaller values of g'. For $m_{Z_2} \gtrsim 1$ GeV, values of $g' \gtrsim 1$ are required to yield the observed relic density, except for the resonance region. The dip

towards $m_\chi \approx m_{Z_2}$ corresponds to opening of new DM annihilation channels at tree level.

5.7 CONCLUSIONS

Despite the tremendous improvement over the last years in the sensitivity of direct, indirect and collider searches for dark matter, its discovery still eludes us. An interesting possibility is that its interactions with SM particles happen dominantly with the neutrino sector. This option would not only explain our failure to detect any DM interactions (except gravitational) so far, it would also connect our two present experimental signals of physics beyond the SM. Indeed, a rich phenomenology that would stem from the connection of these two sectors has been explored and discussed in the literature. $SU(2)$ gauge invariance would naively dictate that neutrinos share all their interactions with their charged lepton counterparts, which are much easier to detect. We have therefore explored whether a dominant neutrino-DM interaction is allowed in simple gauge-invariant models without conflicting with searches through charged leptons.

We first explored the simplest scenario, in which DM couples to the full lepton doublet. We verified that, as long as the DM is heavier than the charged lepton(s) it couples to, the bounds from DM annihilation to charged leptons preclude neutrino-DM couplings sizeable enough to be probed, even ruling out all of the parameter space that would not lead to overclosure of the Universe. Alternatively, if DM couples to τ (μ) and is lighter than the charged lepton, its phenomenology is dominated by the interaction with neutrinos. This region is constrained by present neutrino detectors and will be fully probed for certain DM masses by future experiments.

We have then explored the option of the neutrino portal to DM and showed, as an example, two specific realisations with scalar and vector couplings, respectively. In the neutrino portal DM couples directly to new heavy neutrinos. Indeed, their singlet nature makes them natural candidates to probe the dark sector since they are allowed to interact with it via relevant or marginal operators. These right-handed neutrinos are also a natural addition to the SM particle content so as to account for the evidence for neutrino masses and mixings. The mixing between the SM neutrinos and the new singlets will induce neutrino-DM interactions at tree level, but DM-charged lepton couplings only at loop level.

In the two realisations explored we find that it is indeed possible for neutrino detectors to place the most stringent and competitive bounds through searches for DM annihilations to neutrinos. Present searches at Super-Kamiokande, Fréjus, or Borexino are ruling out large areas of the parameter space. Interestingly, future projects such as Hyper-Kamiokande, MEMPHYS, DARWIN, or DUNE will be able

to probe the cross section very close and beyond the value required to explain the DM abundance solely by annihilation to SM neutrinos. These new searches will effectively cover most of the parameter space, probing if the right-handed singlet fermions that can explain the origin of neutrino masses also represent our best window to the discovery of the dark matter sector.

6

KEV DARK MATTER AND THE HUBBLE TENSION

6.1 INTRODUCTION

A significant and intriguing tension between local, late-time determinations of the Hubble rate and its preferred value when measured from early Universe probes persists. Analyses from type-Ia supernovae and strong lensing consistently favor values of H_0 significantly larger than those determined from the CMB and baryon acoustic oscillations data. A tension at the level of $4-6\,\sigma$ [252, 253], depending on the specific assumptions, exists between the Planck value from the CMB spectrum [166] and the one obtained by the SH_0ES collaboration [254] from supernovae measurements. Among the many different solutions proposed [255], those that also address another open problem are particularly appealing. For instance, the authors of Refs. [256, 257] have proposed that a light Majoron contributing to $\Delta N_{\rm eff}$ and decaying to neutrinos after BBN may alleviate the discrepant determinations of H_0. This scenario would thus link the solution to the Hubble tension to the origin of neutrino masses and mixings.

Indeed, neutrino masses and mixings as required by the observation of the neutrino oscillation phenomenon, can be naturally accounted for through the Weinberg operator [136]. This operator violates L by two units. Thus, if this breaking is dynamical, the Majoron, the Goldstone boson associated to the spontaneous symmetry breaking of Lepton number, would be intimately linked to the origin of neutrino masses and mixings.

In this work we investigate a dynamical origin for the small Lepton number breaking of the inverse Seesaw scenario. Several constructions based on dynamical Lepton number breaking have been explored in the past [258–268]. We consider a Seesaw-like mechanism in the scalar sector so that a small vacuum expectation value is naturally induced for the scalar with Lepton number two [260]. Thus, neutrino masses will be proportional to this small parameter. The dynamical symmetry breaking will also imply the presence of a Majoron with the potential of alleviating the Hubble tension.

Furthermore, inverse Seesaw realizations may also lead to sterile neutrinos at the few keV scale which are good DM candidates [269–

271]. While production via mixing [272] is ruled out[1] by the stringent constraints from searches of X-ray lines [276], the correct DM relic abundance could be achieved from the decay of heavier states instead [269–271, 277–281]. After investigating this possibility, we find that the couplings of the scalars to neutrinos can lead to both the correct DM relic abundance through freeze-in via decays and the necessary Majoron population so as to alleviate the Hubble tension.

In Section 6.2 we introduce the particle content and Lagrangian of the inverse Seesaw model with dynamical breaking of L considered. In Section 6.3 we discuss the dark matter production mechanism as well as its phenomenology and constraints in the parameter space. In Section 6.4 we analyze the conditions under which also the Hubble tension can be alleviated as proposed in Refs. [256, 257]. Finally, in Section 6.5 we discuss and summarize the allowed regions of the parameter space..

6.2 THE MODEL

The simplest extension of the SM particle content to account for the neutrino masses and mixing evidence is the addition of fermion singlets, i.e. right-handed neutrinos. Furthermore, if a large Majorana mass is also included for the right-handed neutrinos, the smallness of neutrino masses is naturally explained through the hierarchy between this mass and the electroweak scale via the celebrated canonical type-I Seesaw [138–141]. Conversely, a Majorana mass significantly above the electroweak scale destabilizes the Higgs mass, worsening the electroweak hierarchy problem [146, 147] and greatly hinders the testability of the mechanism.

It is therefore appealing to consider low-scale alternatives to the canonical Seesaw mechanism. This option was investigated in Refs. [152–154, 282] showing that the smallness of neutrino masses can also be naturally explained by an approximate Lepton number symmetry. Two types of fermion singlets may be included according to their L assignment. The first option is Dirac pairs with $L = 1$ for which, in the limit of exact L, only the right-handed component may have a Yukawa coupling to the active SM neutrinos. The second option is Majorana sterile neutrinos with $L = 0$ which, for exact L symmetry, do not couple to any other fermion. At this level, three neutrinos remain massless. When the L symmetry is slightly broken, small neutrino masses can be induced, the Dirac neutrinos may split into pseudo-Dirac pairs, and additional suppressed couplings are allowed.

Following this principle, we extend the SM particle content with Dirac pairs with their corresponding right and left-handed components N_R and N_L. At least two of these pairs are required to reproduce the correct neutrino masses and mixings (in this case with the

1 Except in the presence of a sizable Lepton number asymmetry [273–275].

lightest neutrino massless). We also consider one Majorana sterile neutrino n_L. The L violation that will induce the standard neutrino masses will be dynamical and originated through two scalars ϕ_1 and ϕ_2. All the new states are singlets of the SM gauge group and their Lepton number charge assignment L is given in Table 6.1.

State	N_R	N_L	n_L	ϕ_1	ϕ_2
L	1	1	0	1	2

Table 6.1: New fermions and scalars with their charge under Lepton number. $\phi_{1,2}$ are SM singlet scalars while N_R is right-handed and N_L and n_L are left-handed SM singlet fermions.

According to this assignment the Lagrangian of the model can be parametrized as:

$$\begin{aligned}\mathcal{L} \supset & -\overline{L}_L\tilde{H}Y_\nu N_R - \overline{N}_L M N_R - \frac{1}{2}\overline{N}_L\phi_2 Y_{LL} N_L^c - \frac{1}{2}\overline{N_R^c}\phi_2 Y_{RR} N_R \\ & - \frac{1}{2}\overline{n}_L\mu_{ss} n_L^c - \overline{N}_L\phi_1 Y_{Ls} n_L^c - \overline{N_R^c}\phi_1^\dagger Y_{Rs} n_L^c + \text{h.c.} + V(\phi_1,\phi_2,H),\end{aligned} \tag{6.2.1}$$

where L_L are the SM lepton doublets and H the Higgs doublet.

6.2.1 *Scalar potential*

Since we want to explore a dynamical breaking of L, we also consider a Seesaw-like mechanism in the scalar sector to avoid hierarchy problems and account for the smallness of the L-violating vev in a technically natural way. To this end, we mimic the type-II Seesaw [142, 143, 283, 284] and assume that the vev of ϕ_2 will be induced by that of ϕ_1 as in Ref. [260]. In particular, the scalar potential is given by

$$\begin{aligned}V = & \frac{m_H^2}{2}H^\dagger H + \frac{\lambda_H}{2}(H^\dagger H)^2 + \frac{m_1^2}{2}\phi_1^*\phi_1 + \frac{m_2^2}{2}\phi_2^*\phi_2 + \frac{\lambda_1}{2}(\phi_1^*\phi_1)^2 \\ & + \frac{\lambda_2}{2}(\phi_2^*\phi_2)^2 + \frac{\lambda_{1H}}{2}(\phi_1^*\phi_1)(H^\dagger H) + \frac{\lambda_{2H}}{2}(\phi_2^*\phi_2)(H^\dagger H) \\ & + \frac{\lambda_{12}}{2}(\phi_1^*\phi_1)(\phi_2^*\phi_2) - \eta(\phi_1^2\phi_2^* + \phi_1^{*2}\phi_2).\end{aligned} \tag{6.2.2}$$

If both m_H^2 and m_1^2 are negative but m_2^2 is positive and large, then the vev of ϕ_2, v_2, is only induced by the vev of ϕ_1, v_1, through η and can be made naturally small. Indeed, notice that in the limit $\eta \to 0$ together with $Y_{Ls} \to 0$ and $Y_{Rs} \to 0$, the Lagrangian would be invariant under a separate $U(1)$ transformation of ϕ_1, different from L. Thus, these three parameters are protected by an additional symmetry and very small values for them are natural in the 't Hooft

sense. Parametrising the scalars as $\phi_i = (v_i + \varphi_i)e^{ia_i/v_i}/\sqrt{2}$ and $H = (v_H + h)/\sqrt{2}$ in the unitary gauge, the minimisation conditions read as

$$\begin{aligned} m_H^2 &= -\frac{1}{2}\left(2\lambda_H v_H^2 + \lambda_{1H} v_1^2 + \lambda_{2H} v_2^2\right) \simeq -\frac{\left(2\lambda_H v_H^2 + \lambda_{1H} v_1^2\right)}{2}, \\ m_1^2 &= -\frac{1}{2}\left(2\lambda_1 v_1^2 + \lambda_{1H} v_h^2 + \lambda_{12} v_2^2 - 4\sqrt{2}\eta v_2\right) \simeq -\frac{\left(2\lambda_1 v_1^2 + \lambda_{1H} v_H^2\right)}{2}, \\ m_2^2 &= -\frac{1}{2}\left(2\lambda_2 v_2^2 + \lambda_{12} v_1^2 + \lambda_{2H} v_H^2 - \frac{2\sqrt{2}\eta v_1^2}{v_2}\right) \simeq \frac{\sqrt{2}\eta v_1^2}{v_2}, \end{aligned} \tag{6.2.3}$$

and thus

$$v_2 \simeq \frac{\sqrt{2}\eta v_1^2}{m_2^2}, \tag{6.2.4}$$

where we have assumed $v_2 \ll v_1, v_H$. From Eq. (6.2.4) we can see that indeed v_2 is induced from the vev v_1 and suppressed by η so that $v_2 \to 0$ if $\eta \to 0$ or $m_2 \to \infty$. The scalar mass matrix in the basis $\begin{pmatrix} h & \varphi_1 & \varphi_2 \end{pmatrix}$, in the $v_2 \to 0$ limit reads

$$M^2 \simeq \begin{pmatrix} \lambda_H v_H^2 & \frac{1}{2}\lambda_{1H} v_1 v_H & 0 \\ \frac{1}{2}\lambda_{1H} v_1 v_H & \lambda_1 v_1^2 & -\sqrt{2}\eta v_1 \\ 0 & -\sqrt{2}\eta v_1 & \frac{\eta v_1^2}{\sqrt{2} v_2} \end{pmatrix}, \tag{6.2.5}$$

so that the masses of the physical scalars h, φ_1 and φ_2 are approximately[2]

$$m_h^2 \simeq \lambda_H v_H^2, \quad m_{\varphi_1}^2 \simeq \lambda_1 v_1^2, \quad m_{\varphi_2}^2 \simeq m_2^2/2, \tag{6.2.6}$$

for small mixed quartic couplings. The mixing angles α_{1H} and α_{12} between $h - \varphi_1$ and $\varphi_1 - \varphi_2$ are, respectively,

$$\tan(2\alpha_{1H}) \simeq -\frac{\lambda_{1H} v_1 v_H}{\lambda_1 v_1^2 - \lambda_H v_H^2}, \quad \text{and} \quad \tan(2\alpha_{12}) \simeq 4\frac{v_2}{v_1}. \tag{6.2.7}$$

The physical pseudoscalars are given by

$$\begin{aligned} J &= \frac{1}{\sqrt{v_1^2 + 4v_2^2}}\left(v_1 a_1 + 2v_2 a_2\right), \quad m_J^2 = 0, \\ A &= \frac{1}{\sqrt{v_1^2 + 4v_2^2}}\left(-2v_2 a_1 + v_1 a_2\right), \quad m_A^2 \simeq m_{\varphi_2}^2, \end{aligned} \tag{6.2.8}$$

where J is the Goldstone boson associated to the breaking of L, that is, the Majoron, and therefore massless from the scalar potential. Since L is expected to be broken from gravity effects [285], we will assume that a Majoron mass of the order of the eV scale is induced by them. The mixing angle β between $a_1 - a_2$ is:

$$\tan(2\beta) \simeq 4\frac{v_2}{v_1}. \tag{6.2.9}$$

2 We use the same notation for the mass and flavour CP-even scalar eigenstates for brevity as mixing angles are typically small.

6.2.2 *Neutrino masses*

When all the scalars develop their vevs, v_H, v_1 and v_2 respectively, the neutrino mass matrix takes the inverse Seesaw form:

$$\mathcal{M} = \begin{pmatrix} 0 & 0 & 0 & m_D \\ 0 & \mu_{ss} & \mu_{Ls}^T & \mu_{Rs}^T \\ 0 & \mu_{Ls} & \mu_{LL} & M^T \\ m_D^T & \mu_{Rs} & M & \mu_{RR} \end{pmatrix}, \tag{6.2.10}$$

where we have defined $m_D \equiv v_H Y_\nu/\sqrt{2}$, $\mu_{LL} \equiv v_2 Y_{LL}/\sqrt{2}$, $\mu_{RR} \equiv v_2 Y_{RR}/\sqrt{2}$, $\mu_{Ls} \equiv v_1 Y_{Ls}/\sqrt{2}$ and $\mu_{Rs} \equiv v_1 Y_{Rs}/\sqrt{2}$, arranging the states as $\begin{pmatrix} \nu_L & n_L & N_L & N_R^c \end{pmatrix}$. From now on we will work in the basis where M is diagonal. The approximate expressions for the flavour states in terms of the mass eigenstates are:

$$\begin{aligned} \nu_L &\simeq U\nu_i - \theta^* \left(\mu_{Ls}^* \mu_{ss}^{-1} + M^{-1}\mu_{Rs}\right) \nu_4 + \frac{1}{\sqrt{2}}\theta^* \left(N_+ - iN_-\right), \\ n_L &\simeq \mu_{ss}^{-1}\mu_{Ls}^T \theta^T U\nu_i + \nu_4 + \frac{1}{\sqrt{2}}\mu_{Ls}^\dagger M^{-1}\left(N_+ + iN_-\right) \\ &\quad + \frac{1}{\sqrt{2}}\mu_{Rs}^\dagger M^{-1}\left(N_+ - iN_-\right), \\ N_L &\simeq -\theta^T U\nu_i + \left(\theta^T\theta^* \mu_{Ls}^* \mu_{ss}^{-1} - M^{-1}\mu_{Rs}\right)\nu_4 \\ &\quad + \frac{1}{\sqrt{2}}\left(N_+ - iN_-\right), \\ N_R^c &\simeq -M^{-1}\mu_{Ls}\nu_4 + \frac{1}{\sqrt{2}}\left(N_+ + iN_-\right), \end{aligned} \tag{6.2.11}$$

where ν_i, ν_4, N_+ and N_- are the mass eigenstates with masses

$$\begin{aligned} m_{\nu_i} &\simeq U^T\theta\left(\mu_{LL} - \mu_{Ls}\mu_{ss}^{-1}\mu_{Ls}^T\right)\theta^T U, \quad m_{\nu_4} \simeq \mu_{ss}, \\ m_{N_\pm} &\simeq \sqrt{M^2 + m_D^\dagger m_D} \pm \frac{1}{2}\left(\mu_{LL} + \mu_{RR}\right), \end{aligned} \tag{6.2.12}$$

with $i = 1,2,3$, $\theta \equiv m_D M^{-1}$ characterizing the mixing between the active flavours ν_L and the heavy states $N_\pm$, and U the unitary matrix diagonalising the light neutrino mass matrix after the block diagonalisation. We have assumed that $M \gg m_D \gg \mu$. In particular, we will assume that M is somewhat above the electroweak scale and that it controls the scale of the pseudo-Dirac pairs $N_\pm$. The splitting of the pseudo-Dirac pairs is only through the Majorana masses μ_{LL} and μ_{RR}. We will also assume that μ_{ss} is at the keV scale and is the main contribution to m_{ν_4}, the dark matter candidate mass. For a summary of the approximate ranges of all the model parameters to correctly reproduce neutrino masses and mixings, the DM relic abundace and to improve on the Hubble tension see Table 6.2 where we sumarize our

findings of the following sections. According to these values, all the μ parameters have been treated as a perturbation in the expressions above and the results are to leading order in perturbation theory. Furthermore, we have also approximated the results to leading order in θ to simplify the expressions. Notice that U, the rotation diagonalising the light neutrino mass matrix, m_{ν_i}, corresponds to the PMNS mixing matrix at leading order.

6.3 DARK MATTER

The Majorana fermion singlet n_L, with its $L = 0$ charge assignment, can only mix with the other neutrinos via L-violating, and therefore suppressed, parameters. Furthermore, its allowed interactions with N_L and N_R are via ϕ_1 through the Y_{Ls} and Y_{Rs} parameters respectively. These two parameters, together with η, are all protected by an additional symmetry. Indeed, setting the three of them to zero a new $U(1)$ transformation for ϕ_1, independent from L, becomes a symmetry of the Lagrangian. We will therefore consistently assume small values for these three parameters. As previously discussed, a small value of η guarantees that the induced vev v_2 will be suppressed and thus naturally explain the smallness of neutrino masses. Small values for Y_{Ls} and Y_{Rs} in turn imply that interactions and decays of n_L are very suppressed, making it an ideal DM candidate via freeze-in production. In this way, the same symmetry behind the smallness of neutrino masses also guarantees DM stability in a natural way. In the following we will discuss the production mechanism as well as the main constraints from it and other observations on the parameter space of the model.

6.3.1 *Dark matter production*

The DM candidate in our model is the mass eigenstate ν_4 which is approximately aligned with the fermion singlet n_L with only suppressed mixings with the rest of the interaction eigenstates given the approximate L symmetry, as shown in Eq. (6.2.11). While the active flavour eigenstates ν_L do contain an admixture of the DM candidate ν_4 as given by Eq. (6.2.11), processes that produce ν_L such as decays of the Z and W or of the heavy neutrinos $N_\pm$ via their Yukawa interactions with the Higgs, will not contribute to the production of ν_4 beyond the standard Dodelson-Widrow mechanism [272]. Indeed, the active flavour eigenstates ν_L are already in thermal equilibrium in the early Universe and additional contributions such as these will not modify their abundance. In other words, the thermal masses of the active neutrinos ν_L are very relevant in the early Universe and dominate over the keV-scale mass of ν_4, suppressing the mixing [286]. That is, the interaction eigenstates are approximately the effective mass eigen-

states [287]. Therefore, in this regime, it is more convenient to work in a mixed basis with $N_\pm$ together with $\hat{\nu}_L$ and $\hat{n}_L$: the "incomplete" flavour states ν_L and n_L at energies below $m_{N_\pm}$. In this intermediate basis the original interaction eigenstates read:

$$\begin{aligned}
\nu_L &\simeq \hat{\nu}_L + \frac{\theta^*}{\sqrt{2}}(N_+ - iN_-),\\
n_L &\simeq \hat{n}_L + \frac{1}{\sqrt{2}}\mu_{Ls}^\dagger M^{-1}\left(N_+ + iN_-\right) + \frac{1}{\sqrt{2}}\mu_{Rs}^\dagger M^{-1}\left(N_+ - iN_-\right),\\
N_L &\simeq -\theta^T\hat{\nu}_L - M^{-1}\mu_{Rs}\hat{n}_L + \frac{1}{\sqrt{2}}(N_+ - iN_-),\\
N_R^c &\simeq -M^{-1}\mu_{Ls}\hat{n}_L + \frac{1}{\sqrt{2}}(N_+ + iN_-).
\end{aligned} \tag{6.3.1}$$

Since $\hat{n}_L$ does not share the relevant contributions to the thermal masses with $\hat{\nu}_L$, it is through processes in which $\hat{n}_L$ is produced where contributions to the final DM abundance of ν_4 beyond the Dodelson-Widrow mechanism can be achieved. The main interactions of $\hat{n}_L$ are with the heavy pseudo-Dirac pairs $N_\pm$ and the new scalar particles via the couplings Y_{Ls} and Y_{Rs}. Thus, given the smallness of Y_{Ls} and Y_{Rs}, the main production channel for DM is through freeze-in [288] decays of the heavy neutrinos to a DM state and S, with $S = \varphi_{1(2)}, A, J$ any of the physical scalar degrees of freedom. We find that the total dark matter production rate is

$$\begin{aligned}
\Gamma_{\hat{n}_L} &= \sum_{i=\pm}\Gamma\left(N_i \to \varphi_2 + \hat{n}_L\right) + \Gamma\left(N_i \to A + \hat{n}_L\right)\\
&\quad + \Gamma\left(N_i \to \varphi_1 + \hat{n}_L\right) + \Gamma\left(N_i \to J + \hat{n}_L\right),\\
&= \frac{m_N}{16\pi}\Bigg\{\left(\frac{\mu_{Ls}}{v_1}\right)^2\left(1 + \frac{\mu_{Rs}^2}{\mu_{Ls}^2}\right)\left[c_\beta^2 + c_{12}^2\left(1 - \frac{m_{\varphi_1}^2}{m_N^2}\right)^2\Theta(m_N - m_{\varphi_1})\right]\\
&\quad + \left(\frac{\mu_{LL}\mu_{Rs}}{v_2 M}\right)^2\left(1 + \frac{\mu_{RR}^2\mu_{Ls}^2}{\mu_{LL}^2\mu_{Rs}^2}\right)\Bigg[c_{12}^2\left(1 - \frac{m_{\varphi_2}^2}{m_N^2}\right)^2\Theta(m_N - m_{\varphi_2})\\
&\quad + c_\beta^2\left(1 - \frac{m_A^2}{m_N^2}\right)^2\Theta(m_N - m_A)\Bigg]\Bigg\},
\end{aligned} \tag{6.3.2}$$

where Θ is the Heaviside step function and $c_{12} \equiv \cos\alpha_{12}$ and $c_\beta \equiv \cos\beta$. We have made the approximation $m_{N_+} \sim m_{N_-} \equiv m_N$. If the heavy neutrinos thermalize with the SM plasma, which happens for all the values of θ we will consider, the relic density is given by

$$\Omega_{\nu_4}h^2 \simeq m_{\nu_4}M_{Pl}\sqrt{\frac{5}{\pi}}\frac{405}{8\pi^4 g_\star^{3/2}(m_N)}\frac{\Gamma_{\hat{n}_L}}{m_N^2}\frac{s^0}{\rho_c^0}h^2, \tag{6.3.3}$$

where $M_{Pl} = 1.22 \cdot 10^{19}$ GeV is the Planck mass, s^0 and ρ_c^0 are the present entropy density and critical energy density respectively, h is

the present Hubble constant expressed in units of $100\,\mathrm{km\,s^{-1}Mpc^{-1}}$ and $g_\star(m_N)$ is the number of radiation degrees of freedom during the N_i decays, which we approximate as $g_\star(m_N) = 106.75$ for $m_N \gtrsim 100\,\mathrm{GeV}$. This expression can be simplified to study the analytical scaling of the relic density in two opposing limits of the following ratio

$$r \equiv \frac{\mu_{Rs}}{\mu_{Ls}}. \tag{6.3.4}$$

Nevertheless the full expression of the relic density has been taken into account in the numerical results. Assuming small $r \ll 1$ and that the decay width is dominated by the J and φ_1 final states, the relic abundance scales as

$$\begin{aligned}\Omega_{\nu_4}h^2(r \ll 1) \simeq & 0.13 \left(\frac{m_{\nu_4}}{10\,\mathrm{keV}}\right)^3 \left(\frac{U_{\alpha 4}}{10^{-6}}\right)^2 \left(\frac{10^{-5}}{\theta}\right)^2 \\ & \times \left(\frac{150\,\mathrm{GeV}}{m_N}\right) \left(\frac{200\,\mathrm{GeV}}{v_1}\right)^2,\end{aligned} \tag{6.3.5}$$

where we have neglected the scalar masses with respect to m_N and approximated $c_\beta \sim c_{12} \sim 1$ as well as written μ_{Ls} in terms of $U_{\alpha 4} \sim \theta\mu_{Ls}/m_{\nu_4}$, the mixing between the DM candidate ν_4 and the active neutrinos ν_{L_α} with $\alpha = e, \mu, \tau$ (see Eq. (6.2.11)) for which strong constraints exist from X-ray searches.

In the opposite limit $r \gg 1$ and assuming dominant decays to φ_2 and A, again neglecting their masses with respect to m_N, the relic density scales approximately as

$$\begin{aligned}\Omega_{\nu_4}h^2(r \gg 1) \simeq & 0.11 \left(\frac{r}{10^3}\right)^2 \left(\frac{m_{\nu_4}}{10\,\mathrm{keV}}\right)^3 \left(\frac{m_{\nu_i}}{0.05\,\mathrm{eV}}\right)^2 \left(\frac{U_{\alpha 4}}{10^{-6}}\right)^2 \\ & \times \left(\frac{10^{-3}}{\theta}\right)^6 \left(\frac{120\,\mathrm{GeV}}{m_N}\right)^3 \left(\frac{\mathrm{MeV}}{v_2}\right)^2\end{aligned} \tag{6.3.6}$$

In Fig. 6.1 we show the allowed regions of the parameter space allowed by the X-ray searches and Lyman-α forest constraints on neutrino DM as well as the values of μ_{Rs}/μ_{Ls} for which the correct relic abundance would be obtained for different values of θ. The parameter θ represents the mixing between the active neutrinos and the heaviest mass eigenstates and can be bounded to be $\theta \leq 10^{-2}$ from flavour and electroweak precision tests of the unitarity of the PMNS matrix [155]. As can be seen, for values of θ close to the current upper bound in Fig. 6.1, a sizable hierarchy of about four orders of magnitude between μ_{Rs} and μ_{Ls} would be needed in order to obtain the correct relic abundance through μ_{Rs}. Indeed, the stringent X-ray constraints require sufficiently suppressed active neutrino-DM mixing, which is mainly[3] dominated by μ_{Ls}. Conversely, this hierarchy is

3 Notice that from Eq. (6.2.11) there is also a contribution to $U_{\alpha 4}$ from μ_{Rs}. This contribution is suppressed by the ratio $\sim m_{\nu_4}/m_N$ with respect to the one from μ_{Ls}. Therefore, the dominant contribution is always μ_{Ls} for the parameter space shown in Fig. 6.1 even for the largest values of r depicted.

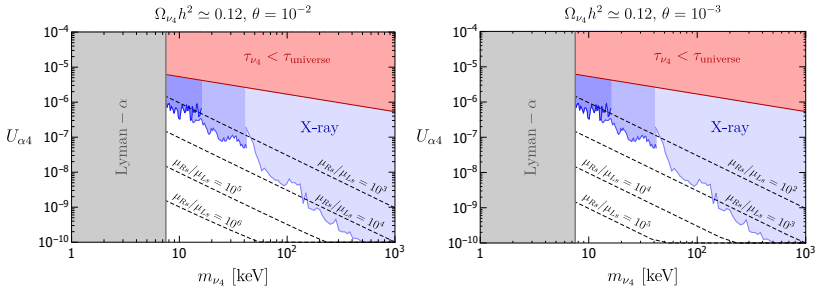

Figure 6.1: Available parameter space allowing to reproduce the correct DM relic abundance for $\theta = 10^{-2}, 10^{-3}$. The y-axis is the mixing angle between the dark matter mass eigenstate and the SM neutrino flavour eigenstates and the x-axis the dark matter mass. Black dashed lines represents the correct relic density for a fixed ratio μ_{Rs}/μ_{Ls}. The three blue shaded regions dubbed "X-ray" represent respectively, from left to right, constraints from XMM-Newton [289], NuSTAR [276] and INTEGRAL [290] on spectral photon lines generated by decaying dark matter. The grey region corresponds to Lyman-α constraints from the matter power spectrum on light free-streaming dark matter particles, estimated from [291]. The red region represents the parameter space for which the dark matter lifetime is shorter than the age of the Universe, estimated using Eq. (6.3.9). In this figure we fixed $m_N = 150$ GeV, $m_{\varphi_2} = m_A = 50$ GeV, $v_1 = 200$ GeV, $m_{\varphi_1} \ll m_N$, $v_2 = 1$ MeV, $\mu_{RR} = 10$ keV.

avoided for smaller values of θ. This choice may be considered more natural, since there is no reason for a significant hierarchy among these parameters from the charge assignments of the fields. However, a lower bound on θ can be extrated from the requirement of perturbative unitarity for the Yukawa coupling Y_{LL} by the relation

$$\theta \simeq 2.5 \cdot 10^{-4} \left(\frac{1}{Y_{LL}}\right)^{1/2} \left(\frac{m_{\nu_i}}{0.05\ \text{eV}}\right)^{1/2} \left(\frac{\text{MeV}}{v_2}\right)^{1/2}, \tag{6.3.7}$$

implying that for $v_2 \lesssim 1$ GeV, θ has to be larger than $\mathcal{O}(10^{-5})$ to ensure perturbativity for Y_{LL}. Moreover, small values of θ would reduce the testability of this region of the parameter space, at least through unitarity constraints of the PMNS matrix or direct searches of the heavy neutrinos at colliders. In this regime, the dominant phenomenology of the model would rather correspond to DM searches via X-rays as well as through cosmology from its impact on the H_0 tension and contributions to ΔN_{eff}.

6.3.2 *Dark matter decay $\nu_4 \to \nu_i + \gamma$*

Sterile-neutrino like dark matter can decay into a neutrino and a photon producing a monochromatic spectral line. The dark matter mixing with active neutrinos, as given by Eq. (6.2.11), is constrained by the International Gamma-Ray Astrophysics Laboratory

(INTEGRAL) [290] by looking for DM decaying in the Milky Way halo, as well as from NuSTAR [276] and XMM-Newton [289]. These constraints correspond to the blue regions in Fig. 6.1.

6.3.3 *Dark Matter lifetime*

Notice that, apart from the usual decay channels to three light neutrinos or a neutrino and an X-ray photon, DM may also decay to a Majoron and a light neutrino. Thus, the associated lifetime of the DM needs to be larger than the age of the Universe. The decay rate is given by

$$\Gamma\left(\nu_4 \to J + \nu_i\right) = \frac{m_{\nu_4}}{16\pi} s_\beta^2 \left(\theta^3 \frac{\mu_{Ls}}{\mu_{ss}} \frac{\mu_{LL}}{v_2}\right)^2 , \tag{6.3.8}$$

which gives

$$\begin{aligned} \frac{\Gamma\left(\nu_4 \to J + \nu_i\right)^{-1}}{\tau_{\text{universe}}} \simeq 28 \left(\frac{v_1}{200\ \text{GeV}}\right)^2 \left(\frac{10\ \text{keV}}{m_{\nu_4}}\right) \\ \times \left(\frac{0.05\ \text{eV}}{m_{\nu_i}}\right)^2 \left(\frac{10^{-6}}{U_{\alpha 4}}\right)^2 . \end{aligned} \tag{6.3.9}$$

The stability condition $\tau_{\nu_4} \equiv \Gamma\left(\nu_4 \to J + \nu_i\right)^{-1} > \tau_{\text{universe}}$ excludes the parameter space corresponding to the red region depicted in Fig. 6.1. Nonetheless, notice that the constraints on the mixing from X-ray searches are always stronger than those from the DM lifetime.

6.3.4 *Constraints from the power spectrum and Lyman-α*

Light dark matter candidates carrying a non-negligible amount of kinetic energy can alter ΛCDM predictions of the matter power spectrum which are probed on the smallest physical scales, i.e. largest Fourier wavenumbers $k \sim (0.1 - 10)h\ \text{Mpc}^{-1}$, by the so-called Lyman-α forest. Constraints from Lyman-α on such DM candidates are typically given in terms of a lower bound for the Warm Dark Matter (WDM) mass [292–298]

$$m_{\text{WDM}} \gtrsim m_{\text{WDM}}^{\text{Ly}-\alpha} = (1.9 - 5.3)\ \text{keV at 95\% C.L.}, \tag{6.3.10}$$

In our scenario the DM density is generated from the decay of non-relativistic heavy neutrinos thermalized with the SM plasma. The effect of the resulting non-thermal phase space distribution on the matter power spectrum has been studied in various works [271, 277, 299–302]. The Lyman-α constraints on our DM candidate can be expressed, following the procedure of [291], as

$$m_{\nu_4} \gtrsim 7.5\ \text{keV} \left(\frac{m_{\text{WDM}}^{\text{Ly}-\alpha}}{3\ \text{keV}}\right)^{4/3} \left(\frac{106.75}{g_{\star s}(m_N)}\right)^{1/3} , \tag{6.3.11}$$

where $g_{\star s}(T)$ is the temperature-dependent effective number of entropy degrees of freedom. This constraint is represented by the grey band in Fig. 6.1 for the reference value $m_{\rm WDM}^{{\rm Ly}-\alpha} = 3$ keV but can be straightforwardly translated to a different value using Eq. (6.3.11).

6.4 THE HUBBLE TENSION

The solution proposed in Refs. [256, 257] to alleviate the present Hubble tension contains two key ingredients. The first is a contribution to $\Delta N_{\rm eff}^{\rm BBN} \sim 0.4$ that should already be present during Big Bang Nucleosynthesis. The second ingredient is an interaction rate between the Majoron and neutrinos that would exceed the Hubble rate between the BBN and CMB epochs. Thus, Majorons will thermalize with neutrinos for temperatures close to the Majoron mass $T \sim m_J$ by decay and inverse decay processes $\bar{\nu}_i \nu_i \leftrightarrow J$. After becoming non-relativistic, Majorons would subsequently decay into neutrinos, resulting in a slight increase of $\Delta N_{\rm eff}$. In addition to this extra late radiation component, Majoron-neutrino interactions cause a damping of the neutrino free streaming by suppressing their anisotropic stress and therefore affect the determination of the Hubble constant from the CMB.

6.4.1 *Majoron contribution to ΔN_{eff}*

Since the scalar φ_1 mixes with the SM Higgs and also couples to the Majoron, the latter will be produced both from interactions with SM fermionic states ψ mediated by virtual φ_1 as well as from φ_1 decays when it is present in the bath through the following couplings, respectively:

$$\mathcal{L}_{\rm eff} \simeq \frac{\lambda_{1H} m_\psi}{2 m_{\varphi_1}^2 m_h^2} \left(\partial_\mu J \partial^\mu J \bar{\psi}\psi\right) - \frac{m_\psi}{v_h} \sin(\alpha_{1H}) \varphi_1 \bar{\psi}\psi. \tag{6.4.1}$$

Such couplings allow to maintain Majorons thermalized with the SM plasma until the freeze-out temperature $T_{\rm FO}$ below which the Majoron population decouples from the thermal bath and behaves as background radiation, potentially leading to a contribution to $\Delta N_{\rm eff}$ that can alleviate the Hubble tension. Both scatterings and (inverse) decays can allow the light scalars to thermalize and are investigated in the following.

- Thermalization via scattering: in order to estimate the freeze-out temperature in this case, one can compare the expansion rate of the Universe to the typical momentum-exchange rate

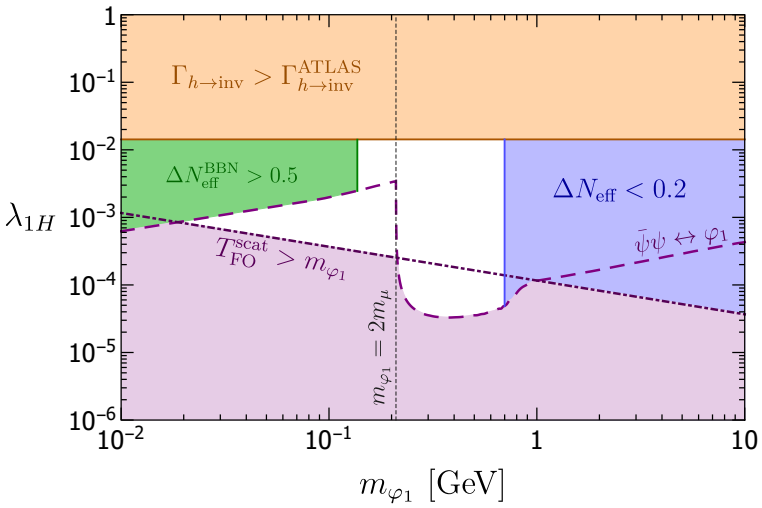

Figure 6.2: Parameter space allowing to alleviate the Hubble tension (white). The blue region corresponds to values than cannot alleviate substantially the Hubble tension, while the green area represents BBN constraints on ΔN_{eff} estimated in Ref. [257]. The orange region is excluded by constraints from ATLAS [303] on Higgs invisible decay as detailed in Sec. 6.4.3. The dashed purple line is determined from the (inverse) decay thermalization criteria of Eq. (6.4.7) and the dash-dotted purple line corresponds to $m_{\varphi_1} < T^{\text{scat}}_{\text{FO}}$ with $T^{\text{scat}}_{\text{FO}}$ obtained from Eq. (6.4.4). The purple region represents the parameter space beyond the range of validity of the analysis described in Sec. 6.4.1 to determine the contribution to ΔN_{eff} and for which a more elaborated estimate should be performed.

induced by the coupling from Eq. (6.4.1). For the process $\bar{\psi}(1) + \psi(2) \to J(3) + J(4)$ such rate can be expressed as

$$\left.\frac{\delta\rho_J}{\delta t}\right|_{\bar{\psi}\psi\to JJ} \equiv \int \prod_{i=1}^{4} \frac{d^3\vec{p}_i}{(2\pi)^3 2E_i} E_1 f_1(\vec{p}_1) f_2(\vec{p}_2) \times |\mathcal{A}_{\bar{\psi}\psi\to JJ}|^2 (2\pi)^4 \delta^4(p_1 + p_2 - p_3 - p_4), \tag{6.4.2}$$

where we follow the notations and conventions from the appendices of Ref. [264]. In the relativistic limit, this quantity can be estimated as

$$\left.\frac{\delta\rho_J}{\delta t}\right|_{\bar{\psi}\psi\to JJ} \simeq \frac{155\pi\zeta(5)\lambda_{1H}^2 m_\psi^2}{448 m_h^4 m_{\varphi_1}^4} T^{11}. \tag{6.4.3}$$

By comparing this quantity to the rate of energy loss induced by the Hubble expansion we can estimate the freeze-out temperature as being

$$T_{\rm FO}^{\rm scat} \simeq 0.067 \text{ GeV} \left(\frac{m_{\varphi_1}}{500 \text{ MeV}}\right)^{4/5} \left(\frac{0.025}{\lambda_{1H}}\right)^{2/5}. \tag{6.4.4}$$

As argued in Ref. [304], such an estimate of the freeze-out temperature is rather reliable given the large temperature dependence of Eq. (6.4.3), which makes the expression derived in Eq. (6.4.4) relatively insensitive to numerical corrections of $\mathcal{O}(1-10)$.

- Thermalization via (inverse) decay: a population of φ_1 could also be produced by inverse decay of SM fermions ψ. Given the fact that $\Gamma_{\varphi_1\to JJ} > \Gamma_{\varphi_1\to\bar{\psi}\psi}$, if the φ_1 production rate induced by inverse decay is sizable enough to ensure φ_1 thermalization with the SM plasma, the Majorons J should thermalize as well. Once the scalars φ_1 become non-relativistic and their abundance is exponentially suppressed, that we estimate to be around $z \equiv m_{\varphi_1}/T \simeq 5$, thermal equilibrium with the SM plasma is lost and the population of J also freezes-out. As the coupling between the scalar φ_1 and ψ is proportional to m_ψ, this process would be relevant for our parameter range mostly when the φ_1 decay channel to muons is open, i.e. for $m_{\varphi_1} > 2m_\mu$. The decay width of φ_1 to a pair of SM fermions is given by

$$\Gamma_{\varphi_1\to\bar{\psi}\psi} = c_\psi \sin^2(\alpha_{1H}) \frac{m_\psi^2}{8\pi v_h^2} m_{\varphi_1} \left(1 - \frac{4m_\psi^2}{m_{\varphi_1}^2}\right)^{3/2}, \tag{6.4.5}$$

where c_ψ is a colour factor. As detailed in [264], the Boltzmann equation relevant for φ_1 production by (inverse) decays can be expressed in term of the yield $Y_{\varphi_1} \equiv n_{\varphi_1}/s$

$$\frac{dY_{\varphi_1}}{dz} = \frac{\Gamma_{\varphi_1\to\bar{\psi}\psi}}{H(z)z} \frac{K_1(z)}{K_2(z)} \left[Y_\varphi^{\rm eq}(z) - Y_\varphi(z)\right], \tag{6.4.6}$$

where $z \equiv m_{\varphi_1}/T$. $Y_\varphi^{\rm eq}(z)$ is the thermal-equilibrium expected value of the yield and $K_{1,2}(z)$ are modified Bessel functions of the second kind. The values of the coupling $\varphi_1 - \psi$ allowing to reach thermal equilibrium at $z = 5$ are given by the condition

$$\Gamma_{\varphi_1 \to \bar{\psi}\psi} \left. \frac{Y_\varphi^{\rm eq}(z)}{H(z)z} \frac{K_1(z)}{K_2(z)} \right|_{z=5} \simeq \left(\frac{\lambda_{1H}}{3\times 10^{-5}}\right)^2 \left(\frac{m_\psi}{m_\mu}\right)^2 \left(\frac{500\,\text{MeV}}{m_{\varphi_1}}\right) \gtrsim 1. \tag{6.4.7}$$

This condition has been checked numerically and yields a rather conservative constraint on the parameter λ_{1H}. For larger couplings than the benchmark point of Eq. (6.4.7), a J population would thermalize with SM fermions and freeze-out at $T_{\rm FO} \simeq m_{\varphi_1}/5$.

In the parameter space for which the condition of Eq. (6.4.7) is satisfied, the (inverse) decay processes are more efficient than scatterings to maintain thermal equilibrium. The resulting contribution to $\Delta N_{\rm eff}$ is [264]

$$\Delta N_{\rm eff} \simeq 0.29 \left(\frac{g_{\star s}(m_\mu)}{g_{\star s}(T_{\rm FO})}\right)^{4/3}, \tag{6.4.8}$$

with $g_{\star s}(m_\mu) \simeq 17.6$. The $\Delta N_{\rm eff}$ range found in [256, 257] that alleviates the Hubble tension is between 0.2 and 0.5, with a preferred value of 0.37. In Fig. 6.2 we depict the values of λ_{1H} and m_{φ_1} that would lead to such a contribution bounded by the blue line corresponding to $\Delta N_{\rm eff} = 0.2$ and the green line corresponding to $\Delta N_{\rm eff} = 0.5$. The white region represents the parameter space that allows to alleviate the Hubble tension. We emphasize that the boundaries of this white region of parameter space might be subject to small corrections given the order of magnitude estimate presented in this section. Nevertheless, a region with $0.2 < \Delta N_{\rm eff} < 0.5$ will be present in that area, since we verified that at least one of the two processes analyzed would allow Majorons to thermalize down to the temperature required. In particular, in Fig. 6.2, in the region between $2m_\mu < m_{\varphi_1} < 700$ MeV the (inverse) decays of φ_1 allow them to thermalize with the SM bath and Majorons as long as λ_{1H} is above the dashed purple line. Hence, the vertical boundaries from the green and blue areas correspond to when we estimate that φ_1 becomes Boltzmann-suppressed and decouples so that also the Majorons freeze-out with $0.2 < \Delta N_{\rm eff} < 0.5$. Conversely, in the white triangle below the dashed purple line, scatterings with SM fermions are able to keep the Majorons in equilibrium instead with a final contribution to $\Delta N_{\rm eff}$ in the same range. In some areas of the parameter space both processes may be relevant simultaneously but such a detailed analysis is beyond the scope of this work and should not lead to sizable deviations from Fig. 6.2.

6.4.2 *Majoron interactions with neutrinos*

The authors of Ref. [257] define an effective width normalized such that for $\Gamma_{\rm eff} \gtrsim 1$ Majorons do thermalize with the active neutrinos as required to alleviate the Hubble tension:

$$\Gamma_{\rm eff} \equiv \left(\frac{\lambda_\nu}{4\times 10^{-14}}\right)^2 \left(\frac{0.1\ {\rm eV}}{m_J}\right), \tag{6.4.9}$$

where λ_ν is the dimensionless Majoron-neutrino coupling:

$$\mathcal{L} \supset \frac{1}{2}\lambda_\nu i J \bar{\nu}_i \gamma_5 \nu_i. \tag{6.4.10}$$

In our setup this parameter corresponds to

$$\lambda_\nu \equiv \sin\beta \frac{m_{\nu_i}}{v_2}, \tag{6.4.11}$$

where we have neglected the contribution from μ_{Ls} to m_{ν_i}. In this approximation

$$\Gamma_{\rm eff} \simeq 52 \left(\frac{m_{\nu_i}}{0.05\ {\rm eV}}\right)^2 \left(\frac{200\ {\rm GeV}}{v_1}\right)^2 \left(\frac{0.3\ {\rm eV}}{m_J}\right). \tag{6.4.12}$$

The best fit for $\Gamma_{\rm eff}$ found in Ref. [257] depends slightly on the number of active neutrinos interacting with the Majoron. Indeed, notice from Eq. (6.4.11) that λ_ν is proportional to the neutrino mass. Thus, if the lightest neutrino is very light or massless, for instance if only two N_R-N_L pairs are considered, its coupling to the Majoron would be negligible. In particular the best fit changes from $\Gamma_{\rm eff} = 67.6$ to $\Gamma_{\rm eff} = 59.9$ when 2 or 3 neutrinos are considered to interact with the Majoron respectively. The dependence of $\Gamma_{\rm eff}$ with $\Delta N_{\rm eff}^{\rm BBN}$ was found to be stronger. Indeed, the best fit $\Gamma_{\rm eff} = 67.6$ corresponding to $\Delta N_{\rm eff}^{\rm BBN} = 0.37$ jumped to $\Gamma_{\rm eff} = 678$ for $\Delta N_{\rm eff}^{\rm BBN} = 0.48$, although this larger contribution to $N_{\rm eff}^{\rm BBN}$ significantly worsened the fit. In all cases the best fit for the Majoron mass was $m_J \sim 0.3$ eV. The preferred values of $\Delta N_{\rm eff}^{\rm BBN} = 0.37$ and $\Gamma_{\rm eff} \sim 60$ can easily be achieved as shown in Fig. 6.2 and Eq. (6.4.12).

6.4.3 *Constraints from Higgs invisible decay*

A coupling between the Higgs and the light scalars J, φ_1 is generated via mixing from the kinetic terms of ϕ_1 and the λ_{1H} term of the scalar potential as

$$\mathcal{L} \supset \sin(\alpha_{1H}) \frac{h}{v_1}\left(\partial_\mu J \partial^\mu J\right) - \frac{\lambda_{1H}}{4} v_H h \varphi_1^2. \tag{6.4.13}$$

Via these couplings, the Higgs can decay invisibly to a Majoron or φ_1 pair with a decay rate

$$\Gamma_{h\to{\rm inv}} = \Gamma_{h\to\varphi_1\varphi_1} + \Gamma_{h\to JJ} \simeq \frac{1}{64\pi}\lambda_{1H}^2 \frac{v_H^2}{m_h}, \tag{6.4.14}$$

where we replaced the mixing angle α_{1H} by its analytical approximation in the limit of small mixing. The invisible branching ratio of the Higgs is constrained to be $\mathcal{B}(h \to \text{inv}) < 0.11\,(0.19)$ from ATLAS [303] (CMS [305]) which translates into

$$\lambda_{1H} < \lambda_{1H}^{\text{ATLAS}} \simeq 0.014. \tag{6.4.15}$$

6.5 SUMMARY OF THE AVAILABLE PARAMETER SPACE

Taking into account all the constraints discussed in the previous sections, we sketch in Tab. 6.2 the ranges for the parameters of the model in which all conditions may be satisfied so that the correct neutrino masses and mixings and dark matter relic density can be recovered together with an improvement of the Hubble tension.

Neutrino masses are controlled by the product $\theta^2\mu_{LL}$. The parameter θ represents the mixing between the active neutrinos and the heavy pseudo-Dirac pairs and is bounded to be $\theta \leq 10^{-2}$ from tests of the PMNS unitarity via precision electroweak and flavour observables [155]. Conversely, if θ is too small, the heavy pseudo-Dirac pairs, which populate the DM abundance via their decays, would not thermalize. This fixes the range for this parameter between roughly 10^{-4} and 10^{-2}. We have shown in Fig. 6.1 that the correct relic abundance can be obtained for $\theta = 10^{-2}, 10^{-3}$, but it can also be recovered for smaller values of θ. The parameter μ_{LL} should then correspond to m_{ν_i}/θ^2, with values in the keV to MeV range. The value of μ_{LL} in turn comes from the breaking of L by two units of the vev of ϕ_2, v_2. Thus, assuming order one Yukawas, v_2 and μ_{LL} will have a similar range as reflected in Tab. 6.2. Finally, v_2 is induced by the vev of ϕ_1, v_1, through the η cubic coupling so that $v_2 \simeq \eta v_1^2/m_{\varphi_2}^2$. The most natural choice for these parameters is to assume that v_1 and m_{φ_2} are close to the electroweak scale, so as to avoid hierarchy problems. Thus, the suppression in v_2 stems from the relative smallness of η, since this parameter is protected by the additional $U(1)$ symmetry which is gained when this parameter together with μ_{Ls} and μ_{Rs} are set to zero.

Regarding the generation and properties of DM, the most stringent constraint is on the parameter μ_{Ls}. Indeed, the mixing of DM with the active neutrinos $U_{\alpha 4} \sim \theta\mu_{Ls}/m_{\nu_4}$ induces its decay to X-rays, for which stringent limits exist as shown in Fig. 6.1. In particular, for $m_{\nu_4} \sim 10$ keV, μ_{Ls} is constrained to be between the eV and keV scales, depending on the value of θ. On the other hand, the DM relic abundance is controlled by μ_{Ls} and μ_{Rs} and a value around 1 keV is required. Thus, as shown in Fig. 6.1, either μ_{Rs} is significantly larger than μ_{Ls}, or $\theta \leq 10^{-4}$. In addition, the DM abundance is induced by the decay of the heavy neutrinos to DM and some scalar degree of freedom. Therefore, the mass of the heavy neutrinos m_N should not be much higher than the TeV scale to avoid further suppressing the

Parameter	m_{ν_4} (keV)	m_N (GeV)	m_{φ_1} (GeV)	m_{φ_2} (GeV)	v_1 (GeV)
Range	$[10, 10^3]$	$[10^2, 10^3]$	$[10^{-1}, 1]$	$[10, 10^3]$	$[1, 10^3]$
Parameter	v_2	η	μ_{ab}	θ	λ_{1H}
Range	keV-MeV	keV-MeV	keV-MeV	$[10^{-4}, 10^{-2}]$	$[10^{-4}, 10^{-2}]$

Table 6.2: Order of magnitude for the allowed range of some relevant parameters allowing to simultaneously explain neutrino masses, the dark matter relic abundance and alleviate the Hubble tension. The subindices for $\mu_{a,b}$ are $a, b = L, R, s$.

DM relic abundance. For large θ, these neutrinos could be searched for at colliders.

Finally, in order to alleviate the Hubble tension two main ingredients are necessary. The first is a sufficient contribution to ΔN_{eff} from the freeze-out of the Majorons. The main parameters controlling this are the mass of φ_1, m_{φ_1} and its coupling to the Higgs λ_{1H}. Indeed, the Majoron is mainly aligned with the angular component of ϕ_1 and it can be kept in thermal equilibrium most efficiently via the mixing of φ_1 with the Higgs. In order to reach $\Delta N_{\text{eff}} \sim 0.4$, the Majoron must decouple roughly with the muons, which can happen for $m_{\varphi_1} < 1$ GeV, as shown in Fig. 6.2. Regarding the coupling, the lack of evidence for an invisible Higgs decay at LHC requires $\lambda_{1H} \lesssim 0.01$. On the other hand, $\lambda_{1H} \geq 10^{-4}$ is necessary to keep the Majorons in thermal equilibrium until sufficiently late times. The second ingredient required to alleviate the Hubble tension is a coupling between the Majoron and the active neutrinos that allows them to thermalize after BBN and a Majoron mass around the eV scale so that it will decay to neutrinos and contribute to ΔN_{eff} at CMB. This decay width depends on the ratio of the neutrino masses over v_1, as well as on the mass of the Majoron itself and the correct value is obtained for $v_1 \sim 100$ GeV for $m_J \sim 1$ eV.

6.6 CONCLUSIONS

Extending the Standard Model particle content with right-handed neutrinos is arguably the simplest extension able to account for the evidence of neutrino masses and mixings. In order to also provide a natural explanation to the smallness of neutrino masses, two options emerge. In the canonical, high-scale type-I Seesaw the ratio between the electroweak scale and the large Majorana mass provides naturally the required suppression. Conversely, in low-scale realizations, such as the linear or inverse Seesaw, the Lepton number L symmetry that protects neutrino masses is instead exploited. If this symmetry is ap-

proximate and only broken by small parameters, these will also naturally suppress the generation of neutrino masses. These low-scale realizations have the twofold advantage of enhancing the relevant phenomenological impact of the model and hence its testability, as well as avoiding a contribution to the Higgs hierarchy problem.

We have explored the possibility that the small breaking of the L symmetry in the inverse Seesaw is dynamical. Its smallness emerges from a Seesaw-like structure in the scalar sector in which the vev of the $L = 2$ scalar responsible for neutrino masses is only indirectly induced by a vev around the electroweak scale, as in the type-II Seesaw. The parameter linking the two is small in a technically natural way since it is protected by an additional symmetry.

This spontaneous breaking of L in turn leads to the existence of a Majoron. We have explored the parameter space and conclude that this Majoron may contribute to the number of relativistic degrees of freedom in the early Universe as well as couple to the active neutrinos with the required values as to significantly alleviate the Hubble tension. This possibility is mainly constrained by the invisible decay of the Higgs, since the Majoron production critically depends on the mixing between the new scalar that breaks the L symmetry and the Higgs. Nevertheless, an order of magnitude smaller mixings than presently allowed by LHC constraints would still allow for a solution to the Hubble tension.

Among the new neutrinos introduced in low-scale Seesaws, two options exist due to the approximate L symmetry. The first are pseudo-Dirac pairs in which the left-handed component has a sizable mixing with the active neutrinos. The second are Majorana sterile neutrinos with couplings suppressed by the L-breaking parameters. For keV-scale masses, these Majorana sterile neutrinos may be sufficiently stable to be good dark matter candidates. While production via mixing through the Dodelson-Widrow mechanism is excluded by X-ray searches, we have shown that the correct relic abundance may be obtained for appropriate values of the model parameters via the freeze-in decays of the heavier pseudo-Dirac pairs to the new scalars and dark matter. These same couplings also control the mixing of the active neutrinos with dark matter as well as with the heavy pseudo-Dirac pairs. The main constraints on these mixings come from searches of the dark matter decays to X-rays and from unitarity tests of the PMNS mixing matrix from precision electroweak and flavour observables respectively. While the combination of these two probes rules out significant parts of the allowed parameter space, the correct relic abundance can still be obtained from the parameter that controls the mixing of dark matter with the right-handed component of the pseudo-Dirac pair. This mixing is more difficult to constrain, since the SM active neutrinos mainly mix to the left-handed component. Two possibilities are then viable. If the mixing between the active

neutrinos and the heavy pseudo-Dirac pairs is sizable, close to their PMNS unitarity constraints, then the parameter that controls the dark matter-right-handed neutrino mixing needs to be significant. This implies a hierarchy of four or five orders of magnitude with respect to the mixing with the left-handed component, which may be considered fine-tuned. Conversely, if the two couplings are similar, the mixing of the heavy neutrinos with the active states needs to be very suppressed, reducing the testability of the model through PMNS unitarity deviations and, eventually, direct production at colliders.

Finally, the heavy pseudo-Dirac pairs could possibly explain the baryon asymmetry of the Universe through the ARS baryogenesis via leptogenesis mechanism [287, 306–316]. While we have assumed that the heavy pseudo-Dirac neutrinos thermalize, the ARS leptogenesis mechanism requires that at least some of them do not reach thermal equilibrium. This could be an option, since we only require one of them to thermalize in order to populate the DM abundance via its decays. Moreover, the correct DM density might also be obtained without thermalization of the heavy pseudo-Dirac pairs. This possibility together with the impact of the additional interactions of the heavy pseudo-Dirac pairs in the context of leptogenesis would be an interesting extension of the present study.

To summarize, we have shown that the SM extension considered with a dynamical breaking of the L symmetry characterizing the inverse Seesaw, is able to account simultaneously for the observed neutrino masses and mixings in a natural way as well as to provide a dark matter candidate with the correct relic abundance and alleviate the present Hubble tension between CMB and supernovae observations. The main constraints on the allowed parameter space come from unitarity tests of the PMNS mixing matrix through precision electroweak and flavour observables, searches for invisible Higgs decays at the LHC and X-ray searches for this decay mode of the sterile neutrino dark matter candidate.

Part III

BARYOGENESIS

7

INTRODUCTION

The origin of the baryon asymmetry (BAU), or in rather philosophical terms, the question of why we are here, is one of the most intriguing open questions in Particle Physics and Cosmology today. It has been inferred comparing observations of primordial element abundances and the CMB with predictions from Big Bang Nucleosynthesis and the CDM model [166] to be

$$Y_B^{obs} \equiv \frac{n_b - n_{\bar{b}}}{s} \simeq (8.59 \pm 0.08) \times 10^{-11}. \tag{7.0.1}$$

The only antimatter we observe is either created on Earth in accelerators or is present as antiprotons in cosmic rays, produced through interactions of protons with the interstellar medium through, for example, the following reaction: $p + p \to 3p + \bar{p}$ [317].

One could argue that there might be big regions of the Universe filled with antimatter and we just happen to live in a domain of matter. However, if this was the case, one would expect annihilation at the boundaries of the matter-antimatter domains, producing a diffuse gamma ray background, which has not been observed, such that on scales larger than about 100 Mpc to 1 Gpc the Universe consists only of matter [318].

Thus, we can conclude that the amount of antimatter in our Universe is negligible with respect to the matter abundance according to all observations. The next step would be to consider how the Universe came to become matter dominated, when in principle from the SM we expect to produce similar amounts of matter and antimatter in the Early Universe. We could attribute this asymmetry to some "initial conditions" with which the Universe was born, but according to the concordance ΛCDM model for Cosmology, in order to solve the "horizon" and "flatness" problems, we need a period of inflation before the radiaton domination era.

The "horizon" problem is the question of why are the CMB temperature fluctuations we observe so uniform, if in principle they were not causally connected at the time of recombination in order for them to be in equilibrium. On the other hand, solving the "flatness" problem would mean understanding why the curvature of the Universe, which could in principle dominate the energy budget of the Universe

today, is so small. These two problems are solved by an initial exponential expansion of the Universe, known as an inflationary period [319]. Now if the Universe started with some initial baryon asymmetry, an inflationary period would wash-out this asymmetry, restoring a matter-symmetric Universe by the end of inflation, and thus a dynamical mechanism to generate the observed matter asymmetry is still required.

7.1 SAKHAROV'S CONDITIONS

In order to dynamically generate any baryon asymmetry three conditions need to be met, the so-called Sakharov's conditions [320, 321]: baryon number (B) violation, C and CP violation, and out of equilibrium conditions [167].

- B violation: indeed in order to produce a baryon asymmetry from a symmetric initial condition, we need interactions which violate baryon number such that more baryons than antibaryons can be produced. Otherwise only initial baryon asymmetric conditions could explain the asymmetry.
- C and CP violation: even if we had B-violating interactions, if the rate for these interactions is the same for particle and antiparticle, meaning C and CP conservation, we would produce the same amount of baryons and antibaryons such as the net baryon number would be zero.
- Out of equilibrium conditions: from CPT invariance, the mass for particle and antiparticle are the same, and in thermal equilibrium any chemical potential related to a non-conserved quantum number vanishes, such that baryons and antibaryons would share the same distribution and thus the number density, $n_b = n_{\bar{b}}$. In other words, if thermal equilibrium holds at temperature T, then the system is stationary and described by $\rho = e^{-\mathcal{H}/T}$ [317] with $\mathcal{H}$ the hamiltonian of the system. The evolution of the baryon number operator $\hat{B}$ is just $\hat{B}(t) = e^{i\mathcal{H}t}\hat{B}(0)e^{-i\mathcal{H}t}$. The mean baryon number for such a system is

$$\left\langle \hat{B}(t) \right\rangle_T = Tr\left[e^{-\mathcal{H}/T} e^{i\mathcal{H}t} \hat{B}(0) e^{i\mathcal{H}t} \right]. \tag{7.1.1}$$

  Using the fact that $\mathcal{H}$ is invariant under $\Theta = \text{CPT}$ while $\hat{B}$ is odd [317], we arrive at

$$\left\langle \hat{B}(t) \right\rangle_T = Tr\left[\Theta^{-1}\Theta e^{-\mathcal{H}/T} \hat{B}(t) \right] = -\left\langle \hat{B}(t) \right\rangle_T, \tag{7.1.2}$$

  such that no net baryon asymmetry can be generated in thermal equilibrium.

Once we know the basic ingredients needed to generate the BAU, the first question we need to answer is if the SM can explain the matter-antimatter asymmetry.

7.2 CAN THE SM GENERATE THE BAU?

In this section we will investigate if the SM of Particle Physics can generate the BAU or if we need BSM physics to explain it. We will revisit each one of the conditions in the context of the SM.

- B violation: baryon and lepton number are accidental symmetries of the SM at the lagrangian level. However, at the quantum level they are broken, such that their divergence is [322, 323][1]

$$\partial_\mu J^\mu_{B(L)} = N_g \frac{g^2}{64\pi^2} \epsilon^{\mu\nu\rho\sigma} W^a_{\mu\nu} W^a_{\rho\sigma}, \tag{7.2.1}$$

  where $W^a_{\mu\nu}$ is a background $SU(2)_L$ field strength tensor and $N_g = 3$ is the number of fermion generations. Notice that the divergence of both currents are anomalous, such that $B + L$ is as well, but the combination $B - L$ is anomaly free. Integrating Eq. (7.2.1) one finds that any process changing baryon or lepton number is related to the change in the Chern-Simmons number by [323]

$$\Delta B = \Delta L = N_g \Delta N_{CS}, \tag{7.2.2}$$

  where N_{CS} is defined as

$$\begin{aligned} N_{CS} &= \int d^3 r K_0(r), \\ K^\mu &= \frac{g^2}{16\pi^2} \epsilon^{\mu\nu\rho\sigma} \left(A^a_\nu \partial_\rho A^a_\sigma + \frac{1}{3} \epsilon_{abc} A^a_\nu A^b_\rho A^c_\sigma \right), \\ \partial_\mu K^\mu &= \frac{1}{N_g} \partial_\mu J^\mu_B(L). \end{aligned} \tag{7.2.3}$$

  The Chern-Simmons number labels the infinite number of degenerate vacuum configurations of the $SU(2)_L$ theory, which are separated by a potential barrier. Baryon and lepton number violation takes place when transitioning from one vacuum to another, either by quantum tunneling or through thermal fluctuations over the barrier at non-zero temperature. This is skectched in Fig. 7.1, where both the quantum tunneling and the thermal fluctuations are depicted by an I and an S, respectively. A transition from one vacuum to a contiguous one produces a change in baryon number of 3 units given that $N_g = 3$.

  At zero temperature, the rate per volume for such transitions is approximately given by [324]

$$\frac{\Gamma}{V} \sim e^{-\frac{8\pi^2}{g^2}} \sim e^{-160}, \tag{7.2.4}$$

  such that this transitions are very suppressed and not expected to happen. However, things are different at finite temperature.

1 In the following we are considering just the $SU(2)_L$ part of the electroweak theory.

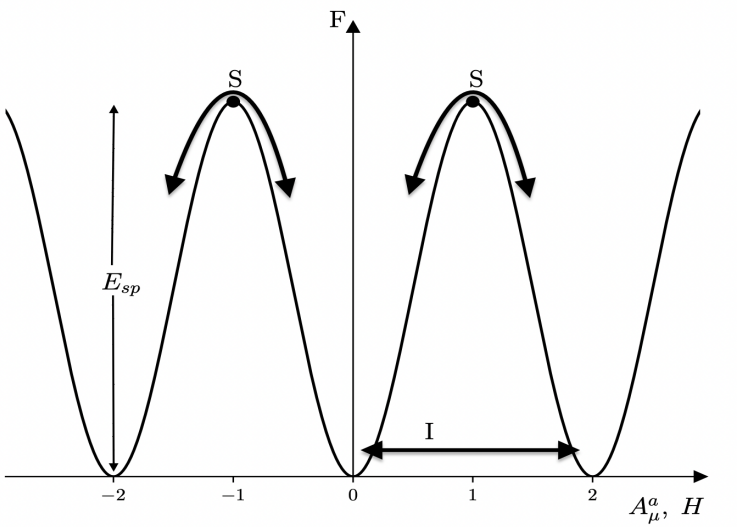

Figure 7.1: Depiction of the barrier separating the different vacua, the instanton tunnelling path, denoted as I, and the sphaleron solution, S, at the top of the barrier. The vertical axes denotes the free energy, F, and the horizontal one the field configurations. The integer numbers correspond to different Chern-Simmons number labelling the vacua.

Indeed, at temperatures below the EW scale the sphaleron solution can be found, which corresponds to classical solutions in field space that sit at the top of the barrier between vacua as depicted in Fig. 7.1. The rate for these transitions is exponentially suppressed as well[2], but for temperatures above the EW scale, $SU(2)_L \times U(1)_Y$ symmetry is restored and the potential barrier between different vacua disappears, thus allowing for transitions from one vacua to another and thus for efficient B and L violation, with a rate given by

$$\Gamma_S \sim 9\kappa\alpha_W^5 T, \tag{7.2.5}$$

where $\kappa \sim 18$ [325] and $\alpha_W = g^2/4\pi$. Thus, comparing to the Hubble rate of expansion, $H \sim T^2/M_{Pl}$, where M_{Pl} is the Planck mass, we see that B-violating interactions are in thermal equilibrium from $T \sim 10^{13}$ GeV down to the EW scale.

- C and CP violation: these are broken in the SM by weak interactions. Indeed, from the CC interaction lagrangian in the quark sector we have

$$\mathcal{L} \supset -\frac{g}{\sqrt{2}} \sum_{\alpha\beta} \bar{u}_\alpha \left(V_{CKM}\right)_{\alpha\beta} \gamma^\mu P_L d_\beta W^+_\mu + h.c., \tag{7.2.6}$$

2 In this case the suppression goes like $\Gamma/V \sim e^{-E_{sp}/T}$, where $E_{sp} \sim 4\pi v/g$ [317].

where V_{CKM} is the CKM quark mixing matrix. Under a C transformation [317], the lagrangian in Eq. (7.2.6) becomes

$$\mathcal{L} \supset -\frac{g}{\sqrt{2}} \sum_{\alpha\beta} \bar{u}_\alpha \left(V_{CKM}\right)_{\alpha\beta} \gamma^\mu P_R d_\beta W_\mu^- + h.c., \tag{7.2.7}$$

such that weak interactions break C (and also P) maximally. Now the lagrangian would be invariant under CP if there were no complex parameters, but V_{CKM} is a 3×3 unitary matrix such that under CP the lagrangian changes to

$$\mathcal{L} \to \mathcal{L}' = -\frac{g}{\sqrt{2}} \sum_{\alpha\beta} \bar{u}_\alpha \left(V_{CKM}^*\right)_{\alpha\beta} \gamma^\mu P_L d_\beta W_\mu^+ + h.c., \tag{7.2.8}$$

and thus there is CP violation as well in quark weak interactions in the SM model.

- Out of equilibrium conditions: the SM contains the Higgs scalar doublet, which gives a mass to the weak gauge bosons and the SM fermions (except neutrinos) when it develops a vev, v_H. However, at temperature significantly larger than the EW scale, the $SU(2)_L \times U(1)_Y$ symmetry is restored. Hence, at some critical temperature, $T = T_c$, there was a phase transition in which the Higgs developed its vev. The order of the phase transition depends on the behaviour of v_H around T_c. If it has a strong discontinuity, then it is a first order phase transition, which would allow to have the out of equilibrium conditions necessary for baryogenesis. In this case, bubbles of true vacuum, v_H, would form and expand in the Early Universe coexisting with regions of symmetric phase. Taking into account quantum corrections for the Higgs potential [317], we can study the behaviour of the phase transition and determine if it is strongly first order.

In principle the SM might satisfy all three Sakharov's conditions, such that we could explain the baryon asymmetry without requiring new Physics. Thus, using the CP violation in the quark sector, $B + L$ violating interactions in the Early Universe and the phase transition in the scalar sector we could generate the BAU. These are the basics of the so-called electroweak baryogenesis (EWBG) mechanism [326, 327].

Once the first order phase transition is triggered, bubbles of true vaccum would nucleate and expand. The bubble wall will separate the symmetric phase, where $B + L$ violating transitions are in thermal equilibrium, from the broken phase, where sphalerons are ineffective. Incoming particles from the symmetric phase will reflect from the bubble wall when interacting with it. If there is CP violation, the reflection rate for particle and antiparticle will be different, thus generating a net baryon asymmetry inside the bubble wall. The opposite asymmetry generated outside, in the symmetric phase, will be erased by sphaleron transitions such that, as the bubble expands

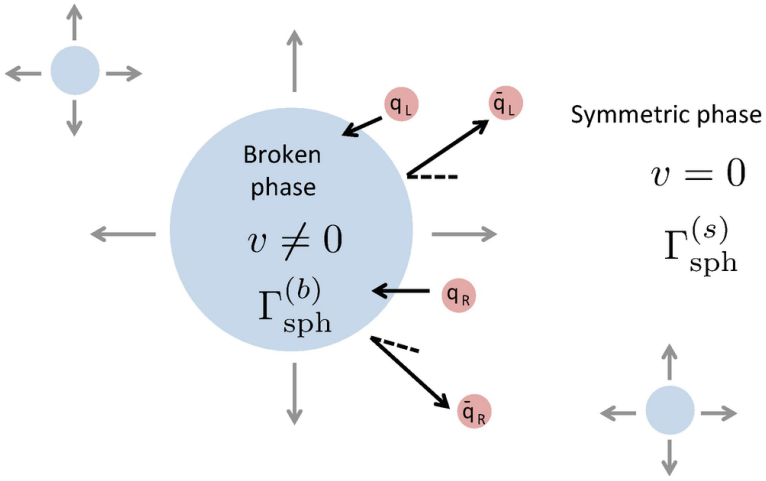

Figure 7.2: Depiction of a bubble of true vacuum expanding in the Early Universe during the first order phase transition taken from Ref. [328]. Quarks and antiquarks interact with the bubble wall with a rate different due to CP violation, generating a net baryon asymmetry inside the bubbles. The opposite asymmetry generated in the symmetric phase will be erased through $B + L$ violating transitions. As the bubbles expand and sphalerons freeze-out inside them, a final non-zero baryon asymmetry will survive until today.

and sphalerons freeze-out inside it, a final non-zero contribution will remain until today. This is schematically depicted in Fig. 7.2 taken from Ref. [328].

Unfortunately, it was shown that there is not enough CP violation in the quark sector, measured by the Jarlskog invariant [329], to generate the BAU [59, 60, 330], and given current measurements of the Higgs mass [331, 332] the phase transition is just a smooth crossover [333]. Thus, we need BSM physics to explain the origin of the matter-antimatter asymmetry of the Universe.

7.3 LEPTOGENESIS

Given that we need new Physics in order to explain the origin of neutrino masses as discussed in Section 3, an interesting question would be if it is possible to generate the BAU taking advantage of the neutrino mass mechanism. Indeed, recalling the lagrangian for the Type-I Seesaw where we included n heavy RH neutrinos

$$\mathcal{L}_{mass} = -\bar{L}_L \tilde{H} Y_\nu N_R - \frac{1}{2}\bar{N}_R^c M N_R + h.c., \tag{7.3.1}$$

where in the Seesaw limit we had $M \gg m_D = v_H Y_\nu / \sqrt{2}$ after SSB, we can check that there are $n(n-1)$ phases in the lagrangian [334] that could violate CP. Thus, we have potentially more relevant sources of CP violation and thus could in principle generate a larger BAU than

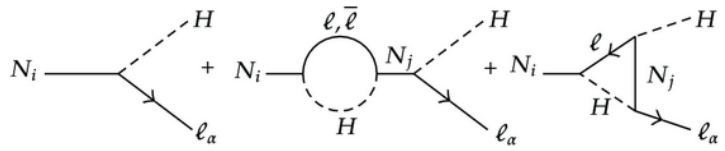

Figure 7.3: Relevant diagrams for the L and CP violating decay of a heavy neutrino, N_i, into a lepton l_α and a higgs doublet component, H. The loop level diagrams are necessary in order for the decay to be CP violating. Taken from Ref. [336].

in the SM. Regarding the out of equilibrium conditions, we can take advantage of the inclusion of some heavy states, the neutrinos with mass $\mathcal{O}(M)$, to fulfill them. Indeed, these states can in principle be in thermal equilibrium in the Early Universe, but at some $T \lesssim M$ the heavy neutrinos become out of equilibrium and their decays into leptons, which can violate CP and also L given their Majorana nature, can generate a lepton asymmetry which in turn can be converted to a baryon one through $B + L$ violating effects. In particular, if M is above the EW scale such that the heavy neutrinos decay before SSB, then the final baryon asymmetry in terms of the lepton asymmetry generated through the N decays is [335]

$$B = -\frac{28}{51} L. \tag{7.3.2}$$

Thus, in principle we could start generating a lepton asymmetry[3] through the decays of the heavy neutrinos in the Early Universe, that would then be converted through $B + L$ violating transitions into a baryon one. This mechanism is known as baryogenesis via leptogenesis, and was first proposed in Ref. [145]. In particular, in order for CP violation to be present, one needs to take into account the interference between the tree and one-loop level decay diagrams for the heavy neutrinos, shown in Fig. 7.3.

Although vanilla leptogenesis through the out of equilibrium decay of very heavy neutrinos can indeed explain the observed BAU, it is very difficult to probe, as these new states cannot be produced in a collider in any near future, and the CP violation necessary for the generation of the BAU cannot be probed in low energy phenomena such as neutrino oscillations or $0\nu2\beta$ decay except in some very particular examples [337–340]. There are, however, some alternatives such as the interesting example of leptogenesis via oscillations [287, 306, 307, 312, 315] in which the new states are never in thermal equilibrium due to rather small Yukawa couplings, that can nonetheless be probed in future experiments for heavy neutrino masses at the $\mathcal{O}(\text{GeV})$ scale [312].

3 Given that $B - L$ is conserved, one actually needs to generate an antilepton asymmetry in order to generate a baryon one, as is also apparent from the minus sign in Eq. (7.3.2).

7.4 ELECTROWEAK BARYOGENESIS AND NEUTRINO MASSES

It is interesting to consider the minimal ingredients we need to add to the SM in order for EWBG to work. As already discussed, the SM lacks enough CP violation in the quark sector and the Higgs itself does not trigger a first order phase transition. An extension of the SM scalar sector could make EWBG [327, 341–344] viable. In particular, new scalars could induce a strong first order phase transition [345–350] at the EW scale and also contribute with new sources of CP violation. In this case, all the interesting physics would be around $\mathcal{O}(100)$ GeV, at the reach of the Large Hadron Collider (LHC) [351–356]. However, new sources of CP violation induce electric dipole moments, which are very tightly constrained [357]. Thus, EWBG models usually rely on some dark sector to avoid them (see for example Refs. [358–360]).

Given that the experimental evidence for neutrino masses from the observation of the neutrino oscillation phenomenon [41, 45, 49, 50, 54, 361] is also at odds with the SM, it represents another main window to new physics. It is therefore interesting to consider whether new sources of CP violation from the neutrino mass mechanism can generate the observed BAU. The lepton number protection present in the inverse or linear variants of the Seesaw mechanism does allow for rather large Yukawa couplings and consequently larger mixing between the new heavy states and the active neutrinos than in the case of the Type-I Seesaw, leading to more interesting phenomenology. Therefore, they also naturally possess all the ingredients for EWBG to work: the large neutrino Yukawa couplings can be a source of the CP violation and an extra singlet scalar can generate the heavy neutrino masses around the EW scale and induce the first order phase transition, while avoiding bounds from electric dipole moments. Variants of this idea, but in the context of a type-I Seesaw without the approximate lepton number symmetry, were studied in Refs. [342, 362, 363].

In the following we will investigate the viability of EWBG in the context of low-scale Seesaw mechanisms in which neutrino masses are generated from a soft breaking of lepton number. The heavy neutrinos will thus be arranged in (pseudo-)Dirac pairs. In particular, we will explore the possibility to have all the new physics at the EW scale. A new scalar singlet, which can be responsible for the required strong first order phase transition, will also induce the Dirac mass of the heavy neutrinos. With these ingredients, a CP asymmetry in the SM neutrinos may be produced through reflections and transmissions with the bubble wall. The imbalance between neutrinos and antineutrinos will then be converted into a baryon asymmetry through $B + L$ violating processes in the unbroken phase. The generated net baryon number then enters the broken phase as the bubbles expand, where

sphalerons are no longer efficient and baryon number is frozen out. This scenario was originally proposed in Ref. [364]. We will revisit its results and reconsider some of the assumptions made in Ref. [364]. In particular, we will study the impact of different wall profiles in the final BAU and also investigate the inclusion of wash-out and flavour effects.

8

ν ELECTROWEAK BARYOGENESIS

8.1 NEUTRINO MASS GENERATION AND CP VIOLATION

In this section we specify the particle content of the model and the parametrization we will adopt. We also discuss the source of CP violation arising from the neutrino mass generation mechanism. The SM is simply extended by three singlet Dirac neutrinos and a scalar singlet:

$$\mathcal{L} = -\bar{L}_L \tilde{H} Y_\nu N_R - \bar{N}_L \phi Y_N N_R + h.c. - V\left(\phi^* \phi, H^\dagger H\right), \qquad (8.1.1)$$

where ϕ is the singlet scalar and H is the Higgs doublet, L_L is the lepton doublet and $N_{R(L)}$ is the right(left)-handed component of the new Dirac neutrinos. Y_ν and Y_N are 3×3 Yukawa matrices. The manifest lepton number symmetry of the Lagrangian will then be broken by either (or both) a Majorana mass for N_L (as in the inverse Seesaw scenarios) or a Yukawa coupling between L_L and N_L^c (as in the linear Seesaw realizations) so as to generate the small neutrino masses. Notice that the symmetry can also be broken by a Majorana mas term for N_R, however the contribution to light neutrino masses arises at the one loop level [365–367]. We will remain agnostic as to the specifics of the lepton-number-violating contribution responsible for the observed neutrino masses, and in what follows, we will neglect these small perturbations on the underlying lepton-number-conserving structure. We only remark that the 3×3 Majorana mass matrix for N_L and the 3×3 Yukawa coupling between L_L and N_L^c contain enough degrees of freedom so as to reproduce the correct pattern of neutrino masses and mixings regardless of the values of Y_ν or Y_N. Thus, no conditions on Y_ν or Y_N can be derived from neutrino oscillation data. The last term in Eq. (8.1.1) refers to the scalar potential, which couples the Higgs doublet to the singlet scalar and can induce the strong first order phase transition [348–350].

After spontaneous symmetry breaking (SSB), we will assume that both the SM Higgs field and the singlet scalar develop a vacuum expectation value (vev), v_H and v_ϕ, respectively, which generate the following Dirac mass terms for the neutrino states:

$$\mathcal{L}_{mass} = -\bar{\nu}_L m_D N_R - \bar{N}_L M_N N_R + h.c., \qquad (8.1.2)$$

where we have defined $m_D \equiv v_H Y_\nu/\sqrt{2}$ and $M_N \equiv v_\phi Y_N$. As discussed above, lepton number conservation ensures that the three heavy neutrinos N_i have Dirac masses while the three light neutrinos ν_i remain massless even for large values of m_D and a low M_N scale[1]. The mixing between the heavy neutrinos and the active states is given by the ratio between the Dirac masses

$$\theta \equiv m_D M_N^{-1}, \tag{8.1.3}$$

and can thus be sizable. There is only one source of CP violation not suppressed by the generally smaller charged lepton Yukawas [334, 364], which is associated to the following basis invariant [329, 368, 369]

$$\delta_{CP} \equiv \text{ImTr}\left[M_N^\dagger M_N m_D^\dagger m_D M_N^\dagger M_N M_N^\dagger M_N m_D^\dagger m_D m_D^\dagger m_D\right]. \tag{8.1.4}$$

In the basis where M_N is real and diagonal with eigenvalues M_i, one finds [364]

$$\begin{aligned}\delta_{CP} = M_1^2 M_2^2 M_3^2 (M_1^2 - M_2^2)(M_2^2 - M_3^2)(M_3^2 - M_1^2) \\ \text{Im}\left[(\theta^\dagger\theta)_{12}(\theta^\dagger\theta)_{23}(\theta^\dagger\theta)_{31}\right].\end{aligned} \tag{8.1.5}$$

Notice that the CP invariant is suppressed by the sixth power of θ, hence the importance of ensuring large mixing and the reason to consider low scale seesaw realizations in this context that decouple its size from the smallness of neutrino masses. Nevertheless, constraints from precision electroweak and flavour observables exist [155, 370–377] on the combination $\theta\theta^\dagger$. Indeed, $\theta\theta^\dagger$ represents the coefficient of the only dimension 6 operator obtained at tree level[2] when integrating out the heavy neutrino degrees of freedom [378]. The $d = 6$ operator physically leads to deviations from unitarity of the PMNS mixing matrix given the non-negligible mixing with the heavy states. These constraints will represent the main limiting factor to the final baryon asymmetry that we will compute in the next sections.

In general, the Dirac mass matrix m_D can be parametrized through a bi-unitary transformation as

$$m_D \equiv U_l m_d V_R^\dagger, \tag{8.1.6}$$

where m_d is a diagonal matrix with positive real entries m_{d_α} and U_l and V_R are 3×3 unitary matrices.

1 Their light masses will instead be tied to the small lepton number breaking parameters of the inverse or linear seesaw that can be safely neglected for the generation of baryon asymmetry.

2 And therefore the least suppressed effective operator in the absence of the Weinberg dimension 5 operator [136], which is only induced by the smaller lepton number-violating parameters.

The physical degrees of freedom of V_R can be parametrized by three mixing angles and one CP violating phase in complete analogy to the CKM matrix. With this parametrization:

$$\begin{aligned}\delta_{CP} = (m_{d_e}^2 - m_{d_\mu}^2)(m_{d_\mu}^2 - m_{d_\tau}^2)(m_{d_\tau}^2 - m_{d_e}^2) \\ (M_1^2 - M_2^2)(M_2^2 - M_3^2)(M_3^2 - M_1^2)J,\end{aligned} \tag{8.1.7}$$

where

$$J = \mathrm{Im}(V_{Ri\alpha} V_{R\beta}^* V_{Rj\alpha}^* V_{Rj\beta}) \tag{8.1.8}$$

is the usual Jarlskog rephasing invariant with $\alpha \neq \beta$ and $i \neq j$. In order to estimate the maximum size of the baryon number asymmetry achievable, in the following sections we will set $J = 1$. This choice fixes the matrix V_R.

From Eq. (8.1.7), a significant hierarchy in the values of m_{d_α} is also desirable so as to maximize δ_{CP}. An advantageous choice is to set one of the three m_{d_α} to zero while the other two differ by a factor $\sqrt{2}$. Their maximum allowed size will be determined by the existing bounds on the product

$$\theta\theta^\dagger = U_l m_d V_R^\dagger M_N^{-2} V_R m_d U_l^\dagger \tag{8.1.9}$$

mentioned above. These constraints are significantly flavour-dependent (see e.g. Ref [155]) and, from Eq. (8.1.9), the flavour structure is controlled by the degrees of freedom in U_l. However, the charged lepton Yukawas imply a stronger suppression as a source of CP violation for baryogenesis compared to that of the neutrinos, so we will neglect them in the rest of this work. Hence, the transformation U_l, which is part of the PMNS lepton mixing matrix, becomes unphysical in this limit and can be absorbed in a field redefinition. Thus, the most meaningful constraint that can be derived from $\theta\theta^\dagger$ on m_{d_α} is through $Tr[\theta\theta^\dagger] \leq 0.007$ [155] at 2σ, since this quantity does not depend on U_l.

For the sake of definiteness, we will set $U_l = I$ and choose $m_{d_e} = m_{d_\tau}/\sqrt{2}$ and $m_{d_\mu} = 0$. This choice for m_{d_α} implies that the neutrino Yukawa couplings to the second and third heavy states have the same magnitude. Additionally, it makes the coupling to the muon to vanish, for which the bounds on $\theta\theta^\dagger$ are the most stringent [155, 376, 377]. Therefore, the matrix m_D now depends on a single parameter, m_{d_τ}. Note, however, that rotations of this particular choice with other values of U_l would be completely equivalent. In other words, all the "flavour" indices in this work will not necessarily correspond to the electron, muon or tau flavours, since their masses have been neglected.

In the following sections we will present results as a function of the remaining free parameters of the model. Namely, the three diagonal entries of M_N (M_i) which correspond to leading order with the

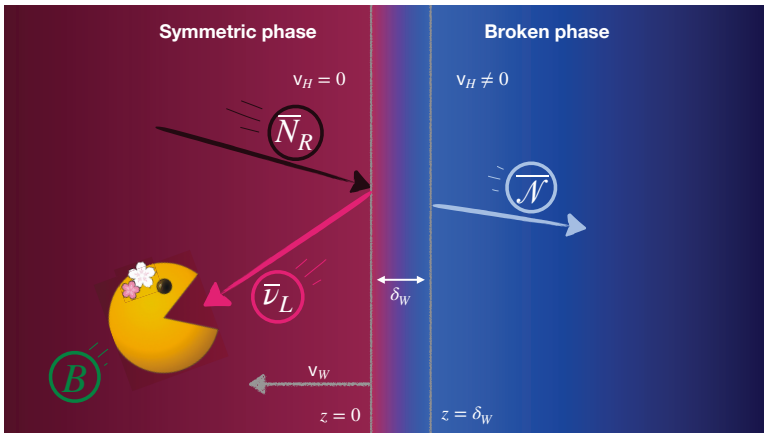

Figure 8.1: Sketch of the reflection of $\bar{N}_R$ off a bubble whose wall width is δ_W to $\bar{\nu}_L$ and its subsequent conversion to baryons through shpaleron processes. If there is CP violation, the reflected ν_L will be different to the $\bar{\nu}_L$ and thus a baryon asymmetry can be generated.

physical masses of the three heavy Dirac neutrinos, as well as m_{d_τ}, respecting the constraints on $Tr[\theta\theta^\dagger]$ through Eq. (8.1.9) for the different values of M_i considered.

8.2 GENERATION OF A CP ASYMMETRY

In the presence of the new scalar singlet, a strong first order phase transition is possible [348–350]. Depending on the parameters of the scalar sector and its couplings to fermions, bubbles of a given width δ_W will start nucleating at the temperature T_c and expand at a velocity v_W. Neutrinos travelling from the unbroken phase towards the bubble wall will be reflected by the wall as depicted in Fig. 8.1. In the presence of CP violation, the reflection rate for neutrinos and antineutrinos will be different, generating an asymmetry in ν_L, which will subsequently be converted to a baryon asymmetry through sphaleron transitions. In the following we will assume that the phase transition is sufficiently strong. Consequently, the sphaleron rate will be suppressed inside the bubbles, such that any baryon asymmetry generated in the symmetric phase will be preserved after entering the regions of true vacuum.

We will devote the rest of this section to describe the generation of the CP asymmetry through reflections and transmissions of neutrinos in the bubble wall. We assume that the bubbles are sufficiently large such that their surface can be described as a plane and gravitational effects can be neglected [379]. We closely follow the method developed in Refs. [344, 380] to solve the Dirac equation for the different neutrino species. An asymmetry may be induced through the dependence of their mass matrix on the direction perpendicular to the wall,

z. The z-dependence of the mass matrix arises solely from the change in the value of the scalar vevs from the unbroken to the broken phase. Performing a boost to the wall rest frame, only the dependence in the spatial dimension z is relevant. The formal solution to the Dirac equation can be written as [380]

$$\mathcal{N} = e^{-iEt} \begin{pmatrix} L(z) \\ R(z) \end{pmatrix} \otimes \chi_s, \tag{8.2.1}$$

where E is the energy of the state and we have separated the chirality states ($L \equiv \begin{pmatrix} \nu_L & N_L \end{pmatrix}^T$ and $R \equiv N_R$) and the spin state χ_s. Spin is conserved upon reflection or transmission, such that $\sigma_3 \chi_s = s\chi_s$. Using this ansatz we find that the chirality states satisfy

$$(is\partial_z + \mathcal{Q}(z)) \begin{pmatrix} L(z) \\ R(z) \end{pmatrix} = 0, \quad \mathcal{Q}(z) \equiv \begin{pmatrix} E & -\mathcal{M}(z) \\ \mathcal{M}(z)^\dagger & -E \end{pmatrix}, \tag{8.2.2}$$

where $\mathcal{M}(z) \equiv \begin{pmatrix} m_D(z) & M_N(z) \end{pmatrix}^T$ and we generally denote with E diagonal submatrices of the appropriate dimension with the energy of the corresponding states. The formal solution to Eq. (8.2.2) at a position z can be expressed as

$$\begin{pmatrix} L(z) \\ R(z) \end{pmatrix} = \mathcal{P} \left(e^{\frac{i}{s} \int_0^z \mathcal{Q}(z')dz'} \right) \begin{pmatrix} L(0) \\ R(0) \end{pmatrix}, \tag{8.2.3}$$

where $\mathcal{P}$ denotes the z-ordered product and $z = 0$ is the position where the bubble wall starts in the unbroken phase. Given that the mass matrix only varies within the bubble wall, but is constant inside or outside the bubble, we can simplify the previous expression to

$$\begin{pmatrix} L(z) \\ R(z) \end{pmatrix} = e^{\frac{i}{s}\mathcal{Q}_0(z-\delta_W)} \mathcal{P} \left(e^{\frac{i}{s} \int_0^{\delta_W} \mathcal{Q}(z')dz'} \right) \begin{pmatrix} L(0) \\ R(0) \end{pmatrix}, \tag{8.2.4}$$

with the constant matrix

$$\mathcal{Q}_0 \equiv \begin{pmatrix} E & -\mathcal{M}_0 \\ \mathcal{M}_0^\dagger & -E \end{pmatrix}, \tag{8.2.5}$$

where $\mathcal{M}_0 = \mathcal{M}(z > \delta_W)$ is the mass matrix in the broken phase.

The reflection coefficient from an incident right-handed neutrino, N_R, to a left-handed one, ν_L (N_L), can be simply obtained by imposing a suitable boundary condition. Namely, that at $z = \delta_W$ all states travel towards the inside of the bubble (see Fig. 8.1). The matrix $\mathcal{Q}_0$ needs to be diagonalized to find the basis of propagating states inside the bubble so as to set this boundary condition. This can be done through the following series of transformations:

$$\begin{pmatrix} \mathcal{U}_L^\dagger & 0 \\ 0 & \mathcal{V}_R^\dagger \end{pmatrix} \begin{pmatrix} E & -\mathcal{M}_0 \\ \mathcal{M}_0^\dagger & -E \end{pmatrix} \begin{pmatrix} \mathcal{U}_L & 0 \\ 0 & \mathcal{V}_R \end{pmatrix} = \begin{pmatrix} E & -\mathcal{M}_d \\ \mathcal{M}_d^T & -E \end{pmatrix}, \tag{8.2.6}$$

where $\mathcal{U}_L$ ($\mathcal{V}_R$) is a unitary matrix which diagonalizes $\mathcal{M}_0\mathcal{M}_0^\dagger$ ($\mathcal{M}_0^\dagger\mathcal{M}_0$) such that $\mathcal{M}_d = \begin{pmatrix} 0 & M_d \end{pmatrix}^T$ and M_d is the diagonal 3×3 matrix with the heavy Dirac neutrino mass eigenvalues. Finally, we can do a second transformation $\mathcal{W}$ to rotate $\mathcal{Q}_0$ to its diagonal form

$$\mathcal{W}^{-1}\begin{pmatrix} E & 0 & 0 \\ 0 & E & -M_d \\ 0 & M_d & -E \end{pmatrix}\mathcal{W} = \begin{pmatrix} E & 0 & 0 \\ 0 & \sqrt{E^2-M_d^2} & 0 \\ 0 & 0 & -\sqrt{E^2-M_d^2} \end{pmatrix}, \tag{8.2.7}$$

with

$$\mathcal{W} \equiv \begin{pmatrix} 1 & 0 & 0 \\ 0 & \cosh\Theta & \sinh\Theta \\ 0 & \sinh\Theta & \cosh\Theta \end{pmatrix}, \quad \tanh 2\Theta = E^{-1}M_d. \tag{8.2.8}$$

Performing these rotations, we can now impose the boundary condition at $z = \delta_W$ and obtain the reflection coefficient, $\mathcal{R}^u$, as $L(0) = \mathcal{R}^u R(0)$. The results for antiparticles ($\overline{\mathcal{R}}^u$) are found by replacing $\mathcal{M} \to \mathcal{M}^*$ and $\mathcal{U}_L$ ($\mathcal{V}_R$) $\to \mathcal{U}_L^*$ ($\mathcal{V}_R^*$). Following a similar procedure and setting the appropriate boundary condition[3], we can also calculate the transmission coefficient from a state inside the bubble to a left-handed neutrino in the unbroken phase, $\mathcal{T}^b$. Note that the superscript on the reflection and transmission coefficients denotes the position of the initial state in those processes, either the unbroken phase ("u") or the broken phase ("b").

Now we can calculate the CP asymmetry generated by reflections or transmissions induced in the SM neutrino sector as

$$\begin{aligned} \Delta\mathcal{R}^u(N_{Ri} \to \nu_{L\alpha}) &\equiv |\mathcal{R}^u_{\alpha i}|^2 - |\overline{\mathcal{R}}^u_{\alpha i}|^2, \\ \Delta\mathcal{T}^b(\mathcal{N}_i \to \nu_{L\alpha}) &\equiv |\mathcal{T}^b_{\alpha i}|^2 - |\overline{\mathcal{T}}^b_{\alpha i}|^2, \end{aligned} \tag{8.2.9}$$

where $\mathcal{N}_i \equiv \begin{pmatrix} \nu_i & N_i \end{pmatrix}^T$ is a propagation eigenstate (either massless, ν_i, or massive, N_i) inside the bubble which travels from the broken to the unbroken phase. As an example, the CP asymmetries both for reflection and transmission to ν_L are presented in Fig. 8.2 for a benchmark point. Notice that the reflection from N_R to ν_L is possible for any energy (see left panel), while the transmission from massive states to ν_L is only possible when the energy is larger than its mass (see right panel). Moreover, as the mass threshold is overcome, the reflection and transmission from massless states are suppressed.

Following Ref. [381], performing an expansion of the z-ordered product in Eq. (8.2.4), it can be shown that the reflection asymmetry for a particular $\nu_{L\alpha}$ to first non-trivial order goes like

$$\sum_i \Delta\mathcal{R}^u\left(N_{Ri} \to \nu_{L\alpha}\right) \sim \int_z \sum_{i,j,\beta} f(z) m^2_{d_\alpha} \mathrm{Im}(V_{Ri\alpha}V^*_{Ri\beta}V^*_{Rj\alpha}V_{Rj\beta}), \tag{8.2.10}$$

3 Namely, that at $z = 0$ there are no states propagating towards the broken phase.

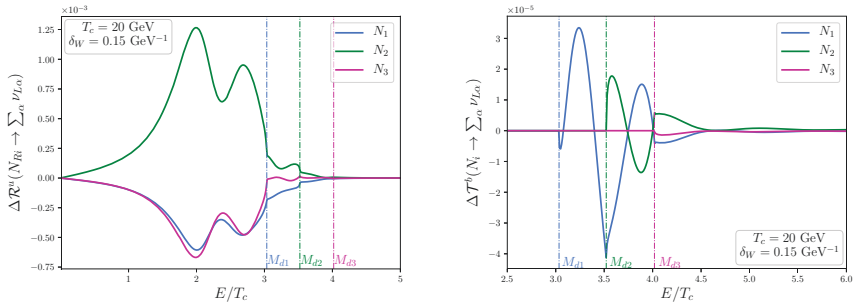

Figure 8.2: CP asymmetries from the reflection of states from the unbroken phase off the bubble wall (left panel) and transmission of states from the broken to the symmetric phase (right panel). Here we have used the FLOR profile defined in Eq. (8.2.12). M_1, M_2 and M_3 are set to 60, 70 and 80 GeV respectively while m_D has been fixed as discussed at the end of Section 8.1. The energy dependence has been normalized to T_c, here chosen to be 20 GeV, but it has no actual impact on the computation of the transmission and reflection coefficients. The heavy-active mixing has been set to $Tr[\theta\theta^\dagger] = 0.045$.

where m_{d_α} are the eigenvalues of m_D in the broken phase, f is a function of the masses which depends on the position z and the last term is the Jarlskog rephasing invariant defined in Eq. (8.1.8). When summing over all final neutrino states $\nu_{L\alpha}$, the expected Glashow–Iliopoulos–Maiani (GIM) suppression with the differences of the squared masses is found.

Although our main interest is the asymmetry generated in ν_L as they are charged under $SU(2)_L$ and therefore source sphaleron processes, asymmetries in N_L and N_R are also generated through this mechanism and they may play a relevant role in the BAU generation as we will discuss in the next sections.

8.2.1 *Vacuum expectation value profiles*

The dependence of the mass matrix $\mathcal{M}(z)$ on the position z comes solely from the change of the scalar vevs along the bubble wall. It is important to note from Eq. (8.2.4) that the Higgs vev, $v_H(z)$, and the one from the singlet scalar, $v_\phi(z)$, need to have a different spatial dependence in order for the particle and antiparticle rates to be different. Otherwise, one could rotate $\mathcal{Q}(z)$ everywhere to the basis where it is diagonal, finding $\overline{\mathcal{R}}^u = (\mathcal{R}^u)^*$, such that $\Delta\mathcal{R}^u = 0$, and the same applies to the transmission coefficients. In particular, the authors in Ref. [364] made the following choice

$$\frac{v_H(z)}{v_H} = \begin{cases} 0, & z \leq 0 \\ \frac{z}{\delta_W}, & 0 < z \leq \delta_W \\ 1, & z > \delta_W \end{cases}, \qquad \frac{v_\phi(z)}{v_\phi} = \mathcal{H}(z), \tag{8.2.11}$$

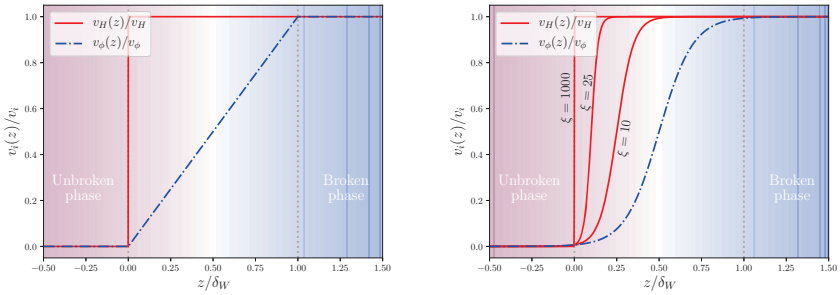

Figure 8.3: Profile for the vev of the scalars in the bubble wall. The left panel shows the FLOR profile from Eq. (8.2.12) while the right panel corresponds to the second set of profiles from Eq. (8.2.13) with smooth and continuous functions for different values of ξ.

where $\mathcal{H}(z)$ is the Heaviside step function. We refer to this choice as the Hernández-Rius (HR) profile. In Eq. (8.2.11) $v_H \sim 246$ GeV and v_ϕ are the vevs for the Higgs and singlet scalar in the broken phase, respectively. In the following we will explore v_ϕ in the range between 2 and 10 TeV. Thus, barring a strong hierarchy among the scalar potential quartic couplings whose study is beyond the scope of this work, we expect the mixing between the higgs and the scalar singlet to be below 10%, in agreement with present LHC constraints [305]. It is important to notice that different wall profiles will result in different values of the heavy-active mixing θ inside the bubble wall and translate to very different sizes for the CP invariant given in Eq. (8.1.5) along the bubble wall. In fact, even though the relative size between $v_H(z)$ and $v_\phi(z)$ changes within the bubble wall, the HR profile is rather conservative and tends to produce a small CP asymmetry because the mixing θ in the wall is always smaller than that at the broken phase where strong constrains apply [155].

We have thus gone beyond Ref. [364] and studied two particular sets of profiles, which are depicted in Fig. 8.3. The first one follows Ref. [364], but assigning the profiles to the opposite scalars so as to have larger mixing θ inside the wall with respect to the broken phase, namely

$$\frac{v_H(z)}{v_H} = \mathcal{H}(z), \quad \frac{v_\phi(z)}{v_\phi} = \begin{cases} 0, & z \leq 0 \\ \frac{z}{\delta_W}, & 0 < z \leq \delta_W \\ 1, & z > \delta_W \end{cases} . \tag{8.2.12}$$

We dub this choice as the "Fernández-López-Ota-Rosauro" (FLOR) profile and we will investigate it in detail in the following sections. The second profile we have studied is a smoothed variant of the FLOR

profile, parametrizing the dependence on z with hyperbolic tangents:

$$\begin{aligned} \frac{v_H(z)}{v_H} &= \frac{1}{2}\left[1+\tanh\left(\xi\frac{z-(5/\xi)\,\delta_W/2}{\delta_W}\right)\right], \\ \frac{v_\phi(z)}{v_\phi} &= \frac{1}{2}\left[1+\tanh\left(5\frac{z-\delta_W/2}{\delta_W}\right)\right]. \end{aligned} \tag{8.2.13}$$

We have checked that the particular realization for the profiles from Eq. (8.2.13), although slightly reducing the final BAU, gives very similar results to the FLOR profile. We will study the dependence of the generated BAU on the ξ parameter, controlling the steepness of the profile for the Higgs vev, at the end of Section 8.4 and leave an in-depth study of the scalar potential and the vev profiles for future work.

8.3 DIFFUSION EQUATIONS

The subsequent evolution of the CP asymmetry generated by the interactions with the bubble walls and its eventual conversion into a baryon number asymmetry will be governed by the diffusion equations of the different particle species. In principle, all particle species and possible interactions between them should be taken into account, but there are some approximations that can help to simplify the description and make the problem more tractable while providing a good estimation of the baryon asymmetry generated. A fully detailed study of the diffusion equations is beyond the scope of this work, and thus we limit our discussion to two simplified cases which nonetheless contain the relevant physical ingredients, closely following the analysis of Ref. [382].

The first case we study contains the most minimal set of diffusion equations, where we only follow the total baryon and lepton number densities, neglecting all possible wash-out effects and tracking the conversion from lepton to baryon number via the weak sphaleron processes that provide the necessary baryon number violation. We will refer to this as the vanilla scenario, which was studied in Ref. [364] for the HR profile.

In the second case, we introduce the effect of partial wash-out of the asymmetry generated in the different flavours as a further refinement. In particular, we include the wash-out from the Yukawa interaction between SM and RH neutrinos, which, for some regions of parameter space, may dominate over the sphaleron rate [382]. In this case, we will need to follow the asymmetries in the different neutrino species separately, which can prevent the strong cancellation which appears in the total CP asymmetry when summing over all flavour contributions. This cancellation among the different flavour contributions originates from the GIM mechanism, as outlined in Eq. (8.2.10). It is depicted both for the reflection and transmission coefficients in an ex-

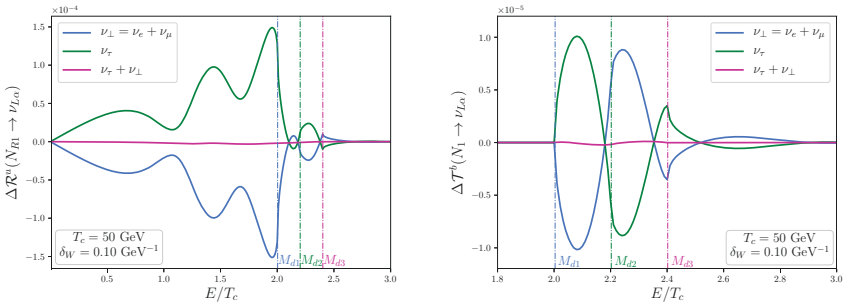

Figure 8.4: CP asymmetries in the reflection and transmission of N_{R1} (left panel) and N_1 (right panel), respectively, into the τ-flavour neutrino or the combination of $e + \mu$ flavours. In magenta we have the sum of the two asymmetries, which tend to cancel each other. Here we have used the FLOR profile defined in Eq. (8.2.12). M_1, M_2 and M_3 are set to 100, 110 and 120 GeV respectively while m_D has been fixed as discussed at the end of Section 8.1. The heavy-active mixing has been set to $Tr[\theta\theta^\dagger] = 0.007$ [155]. The energy dependence has been normalized to T_c, here chosen to be 50 GeV, but it has no actual impact on the computation of the transmission and reflection coefficients.

ample shown in Fig. 8.4, where we plot separately the CP asymmetry stored in ν_τ and $\nu_\perp \equiv \nu_e + \nu_\mu$ as well as the total asymmetry. As can be seen from the figure, the total asymmetry is strongly suppressed as a consequence of the cancellation between the two contributions with the different flavours, which could be prevented through the flavour-dependent wash-out effect. We will refer to this case as the flavoured scenario.

8.3.1 *Vanilla scenario*

The minimal set of the diffusion equations we consider is [364]

$$\begin{aligned} &D_B\partial_z^2 n_B - v_W\partial_z n_B - 3\Gamma_S\mathcal{H}(-z)n_B - \Gamma_S\mathcal{H}(-z)n_L = 0, \\ &D_L\partial_z^2 n_L - v_W\partial_z n_L - \Gamma_S\mathcal{H}(-z)n_L - 3\Gamma_S\mathcal{H}(-z)n_B = \xi_L j_\nu \partial_z\delta(z), \end{aligned} \tag{8.3.1}$$

where we only follow the evolution of total baryon (n_B) and lepton number (n_L) asymmetries and their conversion through weak sphaleron processes. In Eq. (8.3.1), $D_{B(L)}$ is the diffusion constant for baryons (leptons) which we estimate following Ref. [382], v_W is the wall velocity, $\Gamma_S = 9\kappa\alpha_W^5 T$ is the sphaleron rate with $\kappa \simeq 18$ [325] and α_W the weak coupling constant and we have neglected the bubble width. The CP current generated through reflections and transmissions of neutrinos, j_ν, can be computed from the coefficients derived in the previous sections convoluted with the corresponding distribution functions for each species:

$$j_\nu = \frac{1}{\gamma}\sum_{i,\alpha}\int\frac{d^3p}{(2\pi)^3}\Big\{\Delta\mathcal{T}^b(\mathcal{N}_i\to\nu_{L\alpha})\frac{|p^b_{zi}|}{E^b_i}f^b_i(p^b_i) \\ \Delta\mathcal{R}^u(N_{Ri}\to\nu_{L\alpha})\frac{|p^u_{zi}|}{E^u_i}f^u_i(p^u_i)\Big\}, \tag{8.3.2}$$

where $p^b_{zi}\in(-\infty,0]$ and $p^u_{zi}\in[0,\infty)$ are the momentum perpendicular to the bubble wall for transmissions and reflections, respectively. The gamma factor $\gamma\equiv 1/\sqrt{1-v_W^2}$ comes from boosting to the wall rest frame where $\Delta\mathcal{T}^b$ and $\Delta\mathcal{R}^u$ are computed. The energy of the particle i in the broken phase is defined as $E^b_i\equiv\sqrt{p_T^2+(p^b_{zi})^2+m_i^2}$ with p_T the transverse momentum and m_i the physical mass of the particle, while the energy in the unbroken phase is given by $E^u_i=\sqrt{p_T^2+(p^u_{zi})^2}$, since all the particles are massless. The distribution function $f_i^{b(u)}$ for an initial state with index i in the broken (unbroken) phase is the Fermi-Dirac distribution boosted to the wall rest frame:

$$f^b_i(p^b_i)=\frac{1}{1+e^{\frac{\gamma}{T}(E^b_i-v_W p^b_{zi})}},\quad f^u_i(p^u_i)=\frac{1}{1+e^{\frac{\gamma}{T}(E^u_i-v_W p^u_{zi})}}. \tag{8.3.3}$$

Finally, ξ_L parametrizes the persistence length of the current in the vicinity of the wall and is estimated in Ref. [382] as $\xi_L\sim 6D_Lv_i$, where v_i is the mean velocity of the reflected and transmitted particles. In the following, we will conservatively estimate the generated BAU assuming $\xi_L\sim D_L$, although our survey over the points of interest in the parameter space shows that $v_i\sim 0.6-0.8$ and we do not obtain any values below 0.4.

In order to solve Eq. (8.3.1), a set of boundary conditions needs to be imposed. In particular, the asymmetry in the number densities should vanish far from the wall when $z\to-\infty$ and become constant as $z\to\infty$ inside the broken phase. Additionally, by integrating once and twice the diffusion equations given in Eq. (8.3.1), we find the following continuity equations along the bubble wall:

$$D_i\partial_z n_i - v_W n_i\big|^+_- = 0,\ \text{for } i=B,L, \tag{8.3.4}$$

and

$$D_B n_B\big|^+_- = 0,\quad D_L n_L\big|^+_- = \xi_L j_\nu, \tag{8.3.5}$$

respectively. This means that the lepton number density presents a discontinuity between $z=0^-$ and $z=0^+$ due to the injected CP

asymmetry in the SM neutrinos. The solutions of the diffusion equations Eq. (8.3.1) can be expressed as

$$n_B = \begin{cases} B_1 e^{k_1 z} + B_2 e^{k_2 z}, & z < 0 \\ B, & z > 0 \end{cases}, \qquad n_L = \begin{cases} L_1 e^{k_1 z} + L_2 e^{k_2 z}, & z < 0 \\ L, & z > 0 \end{cases}, \tag{8.3.6}$$

where $k_i > 0$ are the solutions to the following cubic equation:

$$D_B D_L k^3 - v_W (D_B + D_L) k^2 + \left[v_w^2 - \Gamma_S (3 D_L + D_B) \right] k + 4 v_W \Gamma_S = 0. \tag{8.3.7}$$

The constants $B_{1,2}$, $L_{1,2}$, B, and L are determined using Eq. (8.3.1), (8.3.4), and (8.3.5). B corresponds to the baryon number asymmetry in the broken phase, which we find to be

$$B = \frac{\Gamma_S v_W \xi_L j_\nu}{D_L^2 k_1 k_2 (D_B k_1 + D_B k_2 - v_W)}, \tag{8.3.8}$$

where we observe, as expected, that the baryon number is proportional to the injected lepton asymmetry and that the proportionality constant depends on the sphaleron rate, the expansion velocity of the bubble wall, and the diffusion of particles in the symmetric phase. The final asymmetry, Y_B, will be given by

$$Y_B = \frac{B}{s(T_c)}, \tag{8.3.9}$$

where $s(T_c)$ is the entropy density at the temperature T_c. A solution to the diffusion equations can be found in Fig. 8.5 for a benchmark parameter point. In Fig. 8.5 we can see how a baryon asymmetry n_B is slowly generated approaching the bubble wall ($z \to 0$) and is then frozen out at a given value inside the bubble ($z \to \infty$) where sphalerons are no longer effective.

8.3.2 *Flavoured scenario*

A potentially relevant effect not considered in Eq. (8.3.1) are the (flavour-dependent) wash-out processes. The most important contribution from the SM charged leptons would be that of the tau Yukawa coupling to the Higgs boson. Nonetheless, the rate of this interaction is still smaller than the sphaleron rate [382]:

$$\frac{\Gamma_\tau}{T} \sim 0.28 \alpha_W Y_\tau^2 \ll \frac{\Gamma_S}{T} = 9 \kappa \alpha_W^5, \tag{8.3.10}$$

where $Y_\tau \sim 0.01$ is the SM tau Yukawa coupling. Thus, we will neglect these contributions.

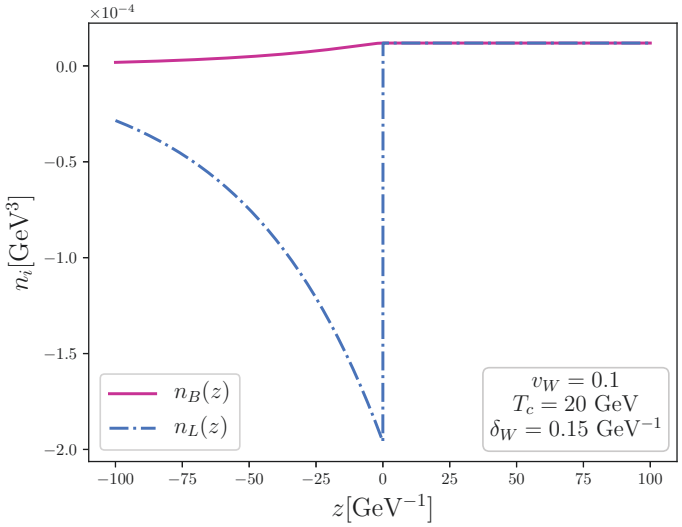

Figure 8.5: Evolution of lepton and baryon number asymmetries as they transition from the symmetric phase ($z \to -\infty$) to the broken phase ($z \to \infty$). The masses of the heavy neutrinos in this case are $M_1 = 60$ GeV, $M_2 = 70$ GeV and $M_3 = 80$ GeV while m_D has been fixed as discussed at the end of Section 8.1. The heavy-active mixing has been set to $Tr[\theta\theta^\dagger] = 0.045$. The final BAU found for this particular point is $Y_B \sim Y_B^{obs}/3$.

However, the neutrino Yukawa couplings may also mediate wash-out processes and are naturally sizable in the low-scale Seesaw scenarios assumed in this work. In particular, the SM neutrino flavour eigenstates may annihilate with the massless N_{Ri} in the symmetric phase to third generation quarks via an s-channel Higgs exchange, washing out the CP asymmetry stored in $\nu_{L\alpha}$. The rate for these interactions is given by [382]

$$\frac{\Gamma_{N_{Ri}\nu_{L\alpha}}}{T} \sim \frac{1}{128\pi}\left(Y_t^2 + Y_b^2\right)|(Y_\nu)_{\alpha i}|^2 \sim 0.0024|\theta_{\alpha i}|^2\frac{2M_i^2}{v_H^2}, \qquad (8.3.11)$$

where $Y_t(Y_b)$ is the top (bottom) Yukawa coupling, and we have replaced the neutrino Yukawa coupling with the heavy-active neutrino mixing $\theta_{\alpha i}$ defined in Eq. (8.1.3) and the Dirac mass M_i of a heavy neutrino N_{Ri}. From Eq. (8.3.11) and given the present bounds on the mixing [155] at 2σ, it is possible to have $\Gamma_{N_{Ri}\nu_{L\alpha}} > \Gamma_S$ for heavy Dirac neutrinos with masses $M_i \gtrsim 200$ GeV. Therefore, the possible wash-out between $\nu_{L\alpha} \leftrightarrow N_{Ri}$ can, in principle, play an important role in the parameter regions with large M_N. Furthermore, a sizable CP invariant from Eq. (8.1.5) requires some hierarchy in the mixing θ, making it thus necessary to consider the different flavours with different wash-out rates. Taking the wash-out effect due to Y_ν into

account, the extended set of flavour-dependent diffusion equations we consider is the following

$$
\begin{aligned}
D_B\partial_z^2 n_B - v_W\partial_z n_B - 3\Gamma_S\mathcal{H}(-z)n_B - \Gamma_S\mathcal{H}(-z)\left(n_{\nu_e}+n_{\nu_\tau}\right) = 0,\\
D_L\partial_z^2 n_{\nu_e} - v_W\partial_z n_{\nu_e} - 3\Gamma_S\mathcal{H}(-z)n_B - \Gamma_S\mathcal{H}(-z)\left(n_{\nu_e}+n_{\nu_\tau}\right)\\
-\Gamma_{N_1\nu_e}\left(\frac{1}{2}n_{\nu_e}-n_{N_1}\right) - \Gamma_{N_2\nu_e}\left(\frac{1}{2}n_{\nu_e}-n_{N_2}\right) = \xi_L j_{\nu_e}\partial_z\delta(z),\\
D_L\partial_z^2 n_{\nu_\tau} - v_w\partial_z n_{\nu_\tau} - 3\Gamma_S\mathcal{H}(-z)n_B - \Gamma_S\mathcal{H}(-z)\left(n_{\nu_e}+n_{\nu_\tau}\right)\\
-\Gamma_{N_1\nu_\tau}\left(\frac{1}{2}n_{\nu_\tau}-n_{N_1}\right) - \Gamma_{N_2\nu_\tau}\left(\frac{1}{2}n_{\nu_\tau}-n_{N_2}\right) = \xi_L j_{\nu_\tau}\partial_z\delta(z),\\
D_{R_1}\partial_z^2 n_{N_1} - v_W\partial_z n_{N_1} + \Gamma_{N_1\nu_e}\left(\frac{1}{2}n_{\nu_e}-n_{N_1}\right)\\
+\Gamma_{N_1\nu_\tau}\left(\frac{1}{2}n_{\nu_\tau}-n_{N_1}\right) = \xi_{R_1} j_{N_1}\partial_z\delta(z),\\
D_{R_2}\partial_z^2 n_{N_2} - v_W\partial_z n_{N_2} + \Gamma_{N_2\nu_e}\left(\frac{1}{2}n_{\nu_e}-n_{N_2}\right)\\
+\Gamma_{N_2\nu_\tau}\left(\frac{1}{2}n_{\nu_\tau}-n_{N_2}\right) = \xi_{R_2} j_{N_2}\partial_z\delta(z),
\end{aligned}
\tag{8.3.12}
$$

where the current j_{ν_α} of the CP asymmetry in $\nu_{L\alpha}$ is defined as Eq. (8.3.2) but without taking the sum over the flavour index α.

There are also source terms for the N_R, j_{Ni}, arising from reflections and transmissions, that can be computed similarly to the ones for ν_L and may also become relevant since they are linked to the active neutrino CP asymmetry through the potentially sizable Yukawa interactions of Eq. (8.3.11). We estimate the diffusion constants for the RH neutrinos as

$$
D_{R_i}^{-1} \sim max\left\{Y_\nu^4, Y_N^4\right\}(4\pi)^{-2}T \tag{8.3.13}
$$

following Ref. [362]. Therefore, if the Yukawa coupling between the heavy neutrinos and the singlet scalar Y_N dominates the diffusion constants[4], $D_{R_{2(3)}} \sim D_{R_1} M_{N1}^4/M_{N2(3)}^4$. Thus, the smallest diffusion constant is the one of the heaviest neutrino N_{R3}, while the N_{R3} Yukawa couplings to the SM flavour eigenstates are equal in size to those of N_{R2} (see discussion after Eq. (8.1.8)). Therefore, the impact of the evolution of N_{R3} in the flavour eigenstates will be smaller than that of N_{R2} and is expected, in any case, to be between the results of the following two simplified cases. In the first case we simply neglect its influence altogether, while in the second scenario we overestimate it by assuming that the diffusion constant for N_{R3} is the same as for N_{R2}. Both limiting cases are conveniently described by the reduced set of Eqs. (8.3.12). In particular, when N_{R3} is assumed to have the same diffusion coefficient as N_{R2} it is only necessary to replace $j_{N_2} \to j_{N_2} + j_{N_3}$ in the source term and $(1/2n_{\nu_\alpha} - n_{N_2}) \to (n_{\nu_\alpha} - n_{N_2})$

4 This happens in the parameter space of interest as long as $Y_N \gtrsim 0.04$ for the lightest heavy neutrino N_{R1}.

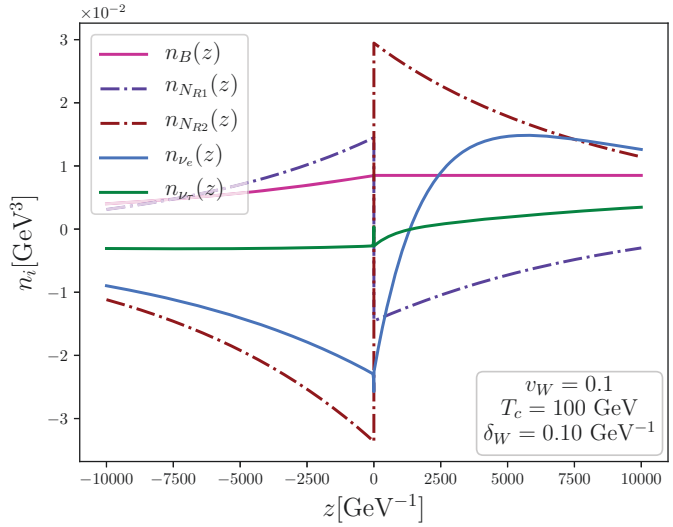

Figure 8.6: Evolution of the number densities for baryons and ν_e and ν_τ from the symmetric phase ($z \to -\infty$) to the broken phase ($z \to \infty$) in the flavoured scenario. The masses of the heavy neutrinos in this particular case are $M_1 = 80$ GeV, $M_2 = 90$ GeV and $M_3 = 160$ GeV while m_D has been fixed as discussed at the end of Section 8.1. The heavy-active mixing has been set to $Tr[\theta\theta^\dagger] = 0.007$ [155]. The final BAU found for this particular point is $Y_B \sim 2 \times Y_B^{obs}$.

in the wash-out terms. An additional equation following the ν_μ density has not been considered since, as outlined in the discussion after Eq. (8.1.8), we chose $m_d = diag(m_{d_\tau}/\sqrt{2}, 0, m_{d_\tau})$, and hence no asymmetry is generated in ν_μ. Notice that the neutrino flavours in Eqs. (8.3.12) are only labels and do not necessarily correspond to the actual electron, μ or τ flavours as discussed at the end of Section 8.1.

In Fig. 8.6 we show the solution of the diffusion equations for the different particle densities for a benchmark parameter point. As expected, even though the injected asymmetries for the different neutrino flavours tend to cancel due to the GIM mechanism, the different wash-out rates from interactions with the RH singlet neutrinos partially prevent the cancellation and thus a larger asymmetry than in the vanilla case may be generated.

8.4 RESULTS

In this section, we parametrize the mass matrix so as to maximize the invariant from Eq. (8.1.7) as discussed at the end of Section 8.1, leaving only one free parameter, m_{d_τ}, which can be constrained through the bounds on heavy neutrino mixing [155]. In Fig. 8.7 we present contours of constant baryon yield, Y_B, generated in the vanilla scenario as a function of the mass of the lightest singlet

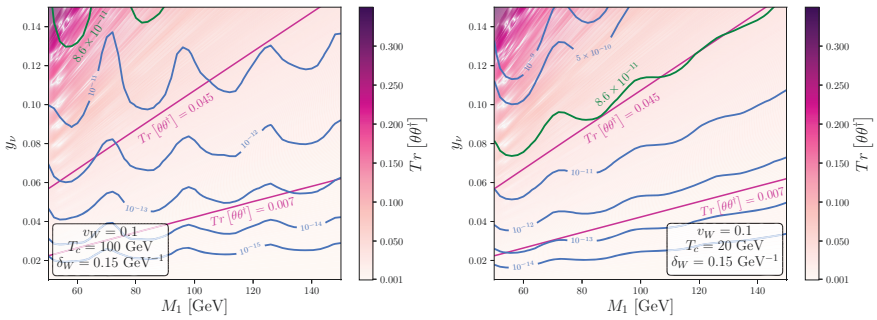

Figure 8.7: Resulting baryon asymmetry as a function of the Yukawa coupling y_ν and the smallest heavy neutrino mass M_1 in the vanilla case for two different temperatures of the phase transition, $T_c = 100$ GeV (left panel) and $T_c = 20$ GeV (right panel). The masses of the other two heavy neutrinos are $M_2 = M_1 + 10$ GeV and $M_3 = M_2 + 10$ GeV while m_D has been fixed as discussed at the end of Section 8.1. Along the green line the observed BAU is reproduced. The value of $Tr\left[\theta\theta^\dagger\right]$ is represented by the color bar legend, while the current bound for this quantity is represented with the two magenta lines for $Tr\left[\theta\theta^\dagger\right] = 0.007$ [155] and $Tr\left[\theta\theta^\dagger\right] = 0.045$ taking into account or not the invisible width of the Z, respectively.

neutrino M_1 and the Yukawa coupling $y_\nu \equiv \sqrt{2} m_{d_\tau}/v_H$, using the FLOR profile. The other two heavy neutrino masses have been fixed to $M_2 = M_1 + 10$ GeV and $M_3 = M_2 + 10$ GeV. We show our results for two cases with different temperatures T_c. The colour shading indicates the value of the neutrino mixing $Tr[\theta\theta^\dagger]$, while the magenta lines correspond to the 2σ bounds from electroweak precision and flavour observables including (not including) the invisible decay of the Z boson [155]: $Tr[\theta\theta^\dagger] = 0.007$ ($Tr[\theta\theta^\dagger] = 0.045$).

As expected, larger y_ν and lighter M_N translate into larger heavy-active mixing, enhancing the final CP asymmetry and consequently the final Y_B. Given the strong constraints from precision electroweak and flavour observables imposing $Tr[\theta\theta^\dagger] \leq 0.007$, in both cases the final BAU falls short by two or three orders of magnitude. Thus, even though the FLOR profile maximizes neutrino mixing along the wall width, the bounds on this mixing today are too stringent to generate the observed baryon asymmetry. Therefore, we conclude that it is not possible to explain the matter-antimatter asymmetry within the vanilla scenario unless the constraints on the heavy-active neutrino mixing in the broken phase can somehow be evaded.

A possibility in this direction would be that the singlet heavy neutrinos couple to some other dark species, making their decays invisible. Moreover, for heavy neutrino masses below the mass of the Z boson, M_Z, the bounds on the mixing would be relaxed to $Tr[\theta\theta^\dagger] \sim 0.045$ since one of the most stringent constraints, the one stemming from the invisible width of the Z, would also be avoided.

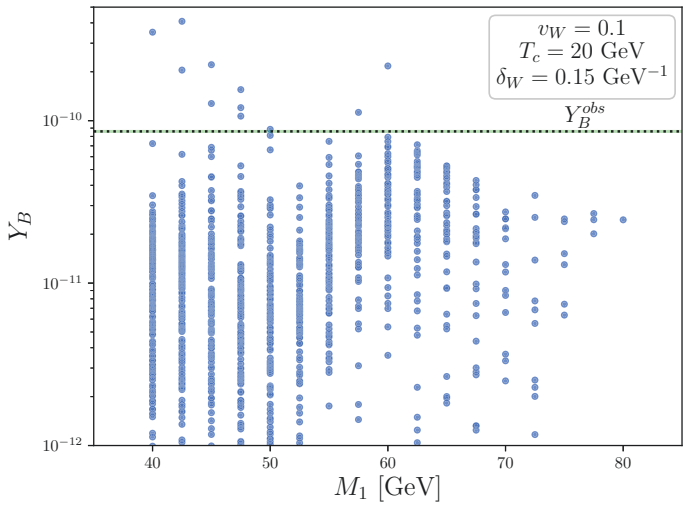

Figure 8.8: Generated baryon asymmetry if the invisible decay of the Z boson does not apply to the bounds on neutrino mixing. In this case the singlet neutrinos need to be lighter than the Z, favoring lower temperatures for the phase transition. The different mass ranges are $M_1 \in [40\text{ GeV}, M_Z]$, $M_2 \in [M_1 + 2.5\text{ GeV}, M_Z]$ and $M_3 \in [M_2 + 2.5\text{ GeV}, M_Z]$, scanned in steps of 2.5 GeV, while m_D has been fixed as discussed at the end of Section 8.1. The heavy-active mixing has been set to $Tr[\theta\theta^\dagger] = 0.045$.

In this case, for low temperatures of the phase transition such as $T_c = 20$ GeV, it is indeed possible to generate the observed asymmetry, as can be seen in the right panel of Fig. 8.7. This is further confirmed in Fig. 8.8, where we scan over the three heavy neutrino masses assuming $M_i < M_Z$. As can be observed in the figure, the BAU can be explained in some small regions of parameter space for $T_c = 20$ GeV. Finally, to highlight the effect of the vev profile assumed, we scanned over the same parameter space for the HR profile of Ref. [364]. We find that the BAU generated is typically suppressed by about $2 - 3$ orders of magnitude with respect to the one obtained with the FLOR profile.

In Fig. 8.9 we present our results on the final BAU generated in the flavoured scenario where we include the wash-out effect due to the interaction between ν_L and N_R. We show contours of Y_B as a function of M_1 and y_ν while the colour gradation indicates the value of $Tr[\theta\theta^\dagger]$. The bound on the mixing at 2σ from electroweak precision and flavour observables is shown as a magenta contour [155]. As expected, in contrast to the results for the vanilla scenario shown in Fig. 8.7, introducing the flavour effects prevents the GIM cancellation found when summing over different species, and thus the baryon asymmetry can potentially be explained within present bounds. Moreover, for the regions of parameter space with some hierarchy in the

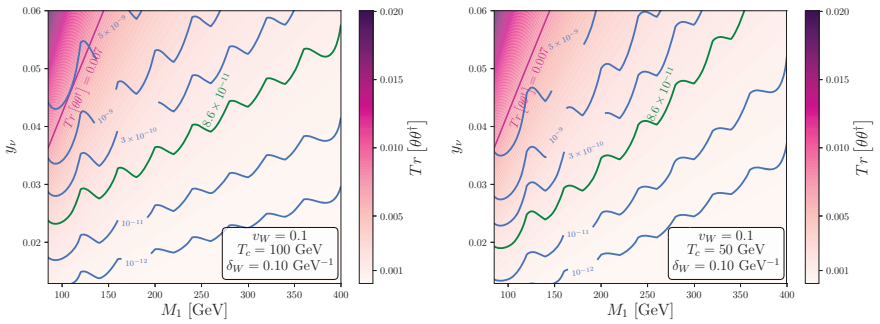

Figure 8.9: Resulting baryon asymmetry as a function of the Yukawa coupling y_ν and the smallest heavy neutrino mass M_1 in the flavoured scenario for $T_c = 100$ GeV (left panel) and $T_c = 50$ GeV (right panel). The masses of the other two heavy neutrinos are $M_2 = M_1 + 10$ GeV and $M_3 = M_2 + 10$ GeV. Along the green line the observed BAU is reproduced. The value of $Tr\left[\theta\theta^\dagger\right]$ is represented by the color bar legend, while the bound for this quantity is represented with the magenta line for $Tr\left[\theta\theta^\dagger\right] = 0.007$ [155].

RH neutrino spectrum and hence in their diffusion constants, the corresponding GIM cancellation in the RH sector asymmetry is also prevented. This asymmetry can also be converted into a SM neutrino asymmetry and then to a baryon one through the Yukawa and sphaleron processes, respectively. Thus, flavour effects enhance the final baryon asymmetry in a two-fold way, and a baryon asymmetry significantly larger than that in the vanilla scenario is obtained, as shown in Fig. 8.9 (to be compared with Fig. 8.7).

Indeed, in Fig. 8.10 in which the three heavy neutrino masses are scanned over a large range of values, we find that most sample points can reproduce or exceed the observed BAU. The main contribution to the BAU actually stems from the injection of the particle asymmetry in the N_R sector. Since its diffusion coefficients are much larger because of its weaker interactions, they may more efficiently induce asymmetries in the other species. In general, the asymmetry becomes larger for larger T_c because particles in the broken phase suffer from Boltzmann suppression, thus explaining why for $T_c = 50$ GeV the asymmetry does not increase for larger M_1 while it does for $T_c = 100$ GeV. As mentioned at the end of Section 8.3, we have also analyzed the case in which N_{R3} is taken into account with its diffusion constant taken to be equal to that of N_{R2}, which is an overestimation of its importance. This is depicted by the magenta dots in Fig. 8.10, for which the generated BAU is reduced with respect to the blue dots in which the role of N_{R3} was neglected. Indeed, the asymmetries generated in the N_R, analogously to the ones generated for ν_L, tend to cancel each other through the GIM mechanism when a sum over all possible states is performed. The actual contribution of N_{R3} with its corresponding diffusion constant would yield a result lying between the two limits corresponding to the magenta and blue points. Finally,

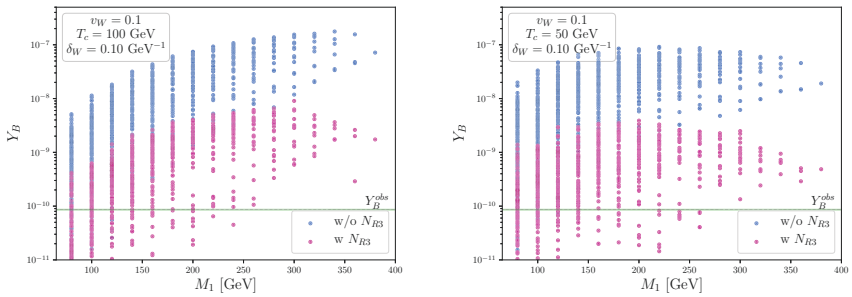

Figure 8.10: Final BAU generated in the flavoured scenario for different masses of the singlet neutrinos and two temperatures for the phase transition, $T_c = 100$ GeV (left panel) and $T_c = 50$ GeV (right panel). The mass ranges are $M_1 \in [80, 400]$ GeV, $M_2 \in [M1 + 10, 400]$ GeV and $M_3 \in [M2 + 10, 400]$ GeV, scanned in steps of 20 GeV, while m_D has been fixed as discussed at the end of Section 8.1. For the blue dots the contribution of N_{R3} has been neglected as in Eq. (8.3.12), while the magenta points overestimate its importance, as described at the end of Section 8.3.2. The heavy-active mixing has been set to $Tr[\theta\theta^\dagger] = 0.007$ [155].

we have estimated the impact of some effects we did not incorporate in our analysis, such as the inclusion of possible decoherence within the bubble wall or of thermal masses, and conclude that, for the parameters studied here, they can induce $\mathcal{O}(1)$ corrections that would not modify our conclusions.

It is interesting to point out that, even though Fig. 8.10 shows that, within the approximations performed, the present constraints allow for a generation of a BAU up to 2 orders of magnitude larger than the observed one, we choose the neutrino Yukawa couplings so as to maximize the relevant CP invariant throughout this study. Moreover, the final BAU scales with three powers of $\theta\theta^\dagger$, as can be seen in Eq. (8.1.5). Thus, improving our present constraints on $\theta\theta^\dagger$ by about a factor 5 could potentially allow to probe the whole parameter space for the setup and make it testable at the LHC and future collider experiments [156–158, 383–387].

Finally, we show in Fig. 8.11 the final BAU for a benchmark point with $M_1 = 80$ GeV, $M_2 = 90$ GeV, and $M_3 = 100$ GeV, using the profiles from Eq. (8.2.13) as a function of the ξ parameter controlling the steepness of the Higgs vev within the wall. As can be noted, when using the kink profiles a slightly larger baryon asymmetry is generated with respect to the one obtained using the FLOR profile (blue star) when ξ is large. However, as ξ becomes smaller and the z-dependence of both profiles is more similar, the generated BAU starts shrinking until it becomes zero when $v_H(z)/v_H \to v_\phi(z)/v_\phi$, as expected.

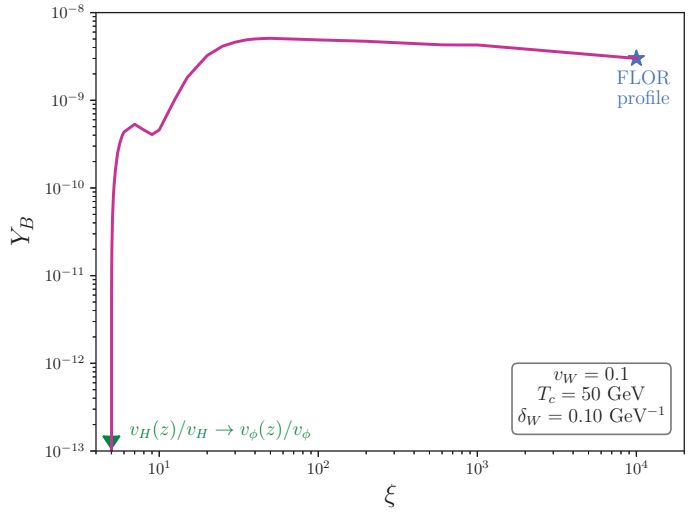

Figure 8.11: Generated Y_B as a function of ξ as defined in Eq. (8.2.13) for a benchmark point. The blue star corresponds to the asymmetry generated using the FLOR profile, while the green triangle points towards the limiting case in which both vev profiles have the same shape where no asymmetry is generated. The masses of the heavy neutrinos in this particular case are $M_1 = 80$ GeV, $M_2 = 90$ GeV and $M_3 = 100$ GeV while m_D has been fixed as discussed at the end of Section 8.1. The heavy-active mixing has been set to $Tr[\theta\theta^\dagger] = 0.007$ [155].

8.5 CONCLUSIONS

The origin of the matter-antimatter asymmetry in the Universe is still an open question in particle physics and cosmology. Several interesting possibilities have been proposed and developed in the literature to explain this unbalance. Among them, leptogenesis and electroweak baryogenesis are particularly compelling.

Leptogenesis models have the appeal of connecting the generation of the baryon asymmetry with the mechanisms explaining neutrino masses, thus linking two experimental indications of new physics. However, there are only few examples where these scenarios can be probed at present or near future facilities, rendering the mechanism essentially untestable in most cases. Conversely, electroweak baryogenesis scenarios aim to explain the asymmetry through physics around the electroweak scale, which possibly relate to the Higgs hierarchy problem, making them much more testable, to the extent that measurements of electric dipole moments rule out many options. To avoid such constraints, it is typically necessary to include a dark sector with new sources of CP violation which generate the observed BAU while evading the tight EDM bounds.

In this work we have studied the possibility that the mechanism responsible for neutrino masses also helps in the production of the BAU within the context of electroweak baryogenesis. Indeed, low scale realizations of the Seesaw mechanism such as the inverse or linear realizations, not only naturally explain the origin of tiny neutrino masses through an approximate lepton number symmetry, but are also testable since they allow for new heavy neutrinos at the electroweak scale with a sizeable mixing with their active partners. It is therefore tantalizing to explore the role of these new states and sources of CP violation at the electroweak scale in electroweak baryogenesis, particularly because the neutrino sector naturally avoids the problematic EDM constraints.

This idea was first studied in Ref. [364], which was the starting point of our analysis that we expanded in several aspects, such as the impact of the vev profiles and the inclusion of flavour-dependent wash-out effects. In particular, we notice that the vev profiles studied in Ref. [364] are rather conservative and tend to lead to a smaller BAU since the heavy-active neutrino mixing in the bubble wall is strictly smaller than its value in the broken phase, for which stringent constraints from flavour and electroweak precision observables apply. Indeed, the CP-invariant is proportional to the sixth power of this mixing and thus this choice critically impacts the final BAU asymmetry that may be obtained. In fact, upon solving the same set of diffusion equations described in Ref. [364] where only the sphaleron process is included, we find that, even assuming the most suitable choices of the vev profiles, the observed BAU cannot be explained in this

"vanilla" scenario due to the tight bounds on heavy-active neutrino mixing [155]. However, if the singlet neutrinos were lighter than the Z boson and decayed invisibly to a dark sector, some of these bounds would be sufficiently relaxed to allow the generation of the observed BAU in some small regions of the parameter space.

Next, we studied in detail the effect of including the interactions between the right-handed and SM neutrinos mediated by their Yukawa couplings in the final BAU. We find a very significant enhancement with respect to the vanilla scenario. Indeed, the GIM cancellation that takes place when adding the asymmetries from the different neutrino flavours is prevented by the different wash-out rates that each of them would have from their Yukawa interactions. Moreover, the asymmetries induced in the right-handed neutrino sector diffuse much farther from the bubble wall, given their weaker interactions, and can be transferred to the SM neutrinos and to baryons via the Yukawa and sphaleron processes, respectively. Thus, we find it is indeed possible to explain the observed BAU in agreement with current bounds on neutrino mixing when these effects are considered.

In this framework, the explanation of the observed BAU does require the extra neutrinos predicted by the low-scale Seesaw realizations to have masses around 100 GeV and sizable mixing with the active neutrinos. This mechanism is thus potentially testable with collider searches and we leave a detailed exploration of the full parameter space as well as its detection prospects for future investigation. Another interesting open avenue of investigation is a detailed study of the scalar potential and the parameters characterizing the phase transition so as to ensure that suitable vev profiles are achievable.

To summarize, we have studied two scenarios where the baryon asymmetry is generated from the CP violation stemming from the neutrino Yukawa couplings in a low-scale Seesaw mechanism. In the simplest case, neglecting the flavour-dependent Yukawa rates, we find it is not possible to explain the observed BAU unless present bounds on heavy-active neutrino mixing can be avoided. For instance, if the singlet neutrinos decay invisibly and are lighter than the Z boson the constraints are sufficiently relaxed to achieve the observed BAU in a small window of the parameter space. More interestingly, when the flavour-dependent wash-out rates are included, the observed BAU can be successfully explained within present constraints. In any event, the required mixing is always large and these scenarios could be testable by future collider searches.

PERSPECTIVA Y CONCLUSIONES

El descubrimiento de las oscilaciones de neutrinos abrió la puerta a explorar nueva física (NF) en experimentos de laboratorio, ya que la existencia de este fenómeno claramente apunta hacia la existencia de física más allá del Modelo Estándar (BSM) dada la necesidad de explicar masas de neutrinos. Después de más de dos décadas de esfuerzos experimentales, la imagen resultante para la matriz de mezcla leptónica está casi completa y es muy diferente de su contraparte en los quarks, por tanto aumentando el misterio del puzle de sabor en el Modelo Estándar (ME).

Sin embargo, aun hay ciertos parametros que continuúan teniendo que ser medidos en el sector de los neutrinos, como la fase de violación CP o el ángulo de mezcla "atmosférico", su octante o cuánto se desvía de mezcla máxima, junto con el orden de masas. En la primera parte de esta tesis hemos estudiado las capacidades de un experimento de oscilaciones de neutrinos para medir con precisión la violación de CP en el sector leptónico en combinación con los datos de neutrinos atmosféricos para ayudar también en la determinación de el orden de las masas de los neutrinos y el ángulo de mezcla atmosférico, por tanto ayudando potencialmente a esclarecer el puzle del sabor. Efectivamente, actuales y futuros experimentso de oscilaciones están alcanzando la precisión suficiente para discriminar entre distintos modelos de sabor atacando el puzle del sabor en el sector leptónico.

Dada la necesidad de explicar las masas de los neutrinos ligeros, nos hemos centrado a continuación en las sinergias entre la NF responsable de ellas y otros problemas abiertos del ME. Por un lado, tenemos evidencias robustas a favor de la existencia de materia oscura (MO), pero nos sigue faltando una señal en nuestros experimentos de detección directa e indirecta. Dada la naturaleza elusiva de los neutrinos, hemos investigado la posibilidad de que la MO estuviera interaccionando principalmente con ellos, de manera que pudieran escapar de nuestras búsquedas. Si este fuera el caso, entonces futuros experimentos como DUNE o Hyper-Kamiokande serían no solo potentes máquinas para estudiar oscilaciones, sino que también nuestra mejor esperanza para encontrar MO a través de su aniquilación en neutrinos en regiones con alta densidad de MO, como el halo de la Vía Láctea, o al menos constreñir estos escenarios.

Por otro lado, podría ser el caso que el mecanismo de masas de neutrinos en sí mismo fuera directamente responsable de la MO del Universo, a través de un neutrino de orden $\mathcal{O}(\text{keV})$ que constituya la MO que observamos. Esto se desarrolla de manera natural en esce-

narios "Seesaw" de baja escala, y se estudió en particular el caso del "inverse Seesa" con una ruptura dinámica de número leptónico. Esto además puede ayudar a aliviar la creciente tensión entre medidas de la constante de Hubble a través de supernovas y su inferencia de medidas del fondo cósmico de microondas (CMB) en el contexto del modelo ΛCDM. Las mejores pruebas de tal escenario sería a través de sus huellas astrofísicas del decaimiento de la MO, que se puede estudiar a través de búsquedas de rayos X, y sus huellas cosmológicas en el número efectivo de grados de libertad relativistas. Algunos estados más pesados, responsables de las masas de los neutrinos y de la población de MO a través de sus decaimientos, pueden ser testados de forma efectiva a través de pruebas de la unitariedad de la matriz de mezcla leptónica usando observables de sabor y de precisión electrodébil.

Finalmente estudiamos la posibilidad de generar la asimetría bariónica del Universo (ABU) en el contexto de escenarios "Seesaw" de baja escala también, que se pueden testar en colisionadores ya que los nuevos estados están alrededor de la escala electrodébil (ED) y tienen couplings de Yukawa relativamente grandes. Si hay otro escalar generando las masas de los neutrinos pesados y desencadenando la transición de fase de primer orden, entonces la ABU puede efectivamente ser explicada a través de este mecanismo de masas de neutrinos, y estaría al alcance de los experimentos actuales y futuros. O bien estos nuevos estados, tanto el escalar singlete como los neutrinos pesados, se encuentran en el futuro, o se ponen restricciones más fuertes en la mezcla entre neutrinos activos y pesados, de tal manera que este escenario estaría eventualmente descartado. Esto contrasta con los escenarios estándar de leptogenesis, en los que aunque se explica facilmente la ABU, hay pocas esperanzas de testar tales mecanismos en un futuro cercano.

Considerándolo tood, hemos encontrado y explorad nuevas posibles conexiones entre el origen de las masas de los neutrinos y otros misterios fundamentales del ME. En particular, los neutrinos podrían estar relacionados con el origen de la materia en el Universo, tanto oscura como bariónica. Además, dado que son piezas fundamentales en el puzle del sabor, descubrir el mecanismo de masas particular en el futuro sería un gran paso en el camino a entender la enigmática estructura de sabor del ME. Desvelar la teoría de neuva física subyacente al ME y explicar sus numerosos problemas abiertos sigue siendo la principal meta de los esfuerzos en investigación en física de partículas. Hemos mostrado que el sector de los neutrinos, con su evidencia establecida a favor de nueva física, puede ser la ventana a través de la cual otros enigmas están conectados y la nueva teoría es descubierta. Es por tanto muy prometedor proseguir esta seductora línea de investigación en el futuro.

SUMMARY AND OUTLOOK

The discovery of neutrino oscillations opened the window to probe new Physics (NP) at laboratory experiments, as the existence of such a phenomenon clearly points towards beyond the Standard Model (BSM) Physics due to the necessity to explain neutrino masses. After more than two decades of experimental efforts, the resulting picture for the lepton mixing matrix is almost complete and very different from its quark counterpart, thus increasing the mystery of the flavour puzzle in the Standard Model (SM).

Nonetheless, there are still some parameters that remain to be measured in the neutrino sector, such as the Dirac CP violating phase or the "atmospheric" mixing angle, its octant or how far it deviates from maximal mixing, together with the mass ordering. In the first part of this thesis we studied the capabilities of a neutrino oscillation experiment to precisely probe the CP violation in the lepton sector in combination with atmospheric neutrino data to also help in the determination of the neutrino mass ordering and the atmospheric mixing angle, thus potentially helping to disentangle the flavour puzzle. Indeed, present and future oscillation experiments are reaching enough precision to discriminate between some flavour models tackling the flavour puzzle in the lepton sector.

Given the necessity to explain light neutrino masses, we focused next on the possible synergies between the NP responsible for them and other open problems of the SM. On the one hand, we have outstanding evidence for the existence of dark matter (DM), but we still lack a positive signal in our direct and indirect detection experiments. Given the elusive nature of neutrinos, we investigated the possibility that DM was primarily interacting with them, in such a way that they could elude our searches. If this was the case, then future neutrino detectors such as DUNE or Hyper-Kamiokande would not only be powerful machines to study oscillations, but also our best hope to find the DM through its annihilation into neutrinos in high DM density regions, such as the Milky Way halo, or at least constrain these scenarios.

On the other hand, it could very well be the case that the neutrino mass mechanism itself is directly responsible for the DM of the Universe, through an $\mathcal{O}(\text{keV})$ scale neutrino that comprises the DM we observe. This is naturally realised in the context of low-scale Seesaw scenarios, and we studied it in the particular case of the inverse Seesaw with a dynamical breaking of lepton number. This in turn can help alleviate the growing tension between late time measurements of the Hubble rate and its inference from cosmic microwave background

(CMB) measurements in the context of the ΛCDM model. The best probes for such a scenario would be through its astrophysical imprints from DM decay, that can be studied through X ray searches, and its cosmological imprints on the effective number of relativistic degrees of freedom. Some heavier states, responsible for neutrino masses and the population of the DM through their decays, can also be effectively probed through tests of the unitarity of the lepton mixing matrix via precision electroweak and flavour observables.

Finally we studied the possibility to generate the baryon asymmetry of the Universe (BAU) within the context of low-scale Seesaw scenarios as well, which can be probed in colliders as the new states live at the electroweak (EW) scale and have relatively large Yukawa couplings. If there is another scalar generating heavy neutrino masses and triggering the first order phase transition, then the BAU can indeed be explained through this neutrino mass mechanism, and in reach for present and future experiments. Indeed, either these new states, both the singlet scalar and the heavy neutrinos, are found in the future, or tighter constraints can be put on the active-heavy neutrino mixing, such that this scenario would eventually be ruled out. This is in contrast to vanilla leptogenesis scenarios, in which although the BAU can be easily explained, there is little hope to probing such a mechanism in the near future.

All in all, we have found and explored new possible links between the origin of neutrino masses and other fundamental mysteries of the SM. In particular, neutrinos could be intimately related to the origin of matter in the Universe, both dark and baryonic. Moreover, given that they are fundamental pieces of the flavour puzzle, discovering the particular neutrino mass mechanism in the future could be a stepping stone in the way to understanding the enigmatic flavour structure of the SM. Unveiling the new Physics theory underlying the SM and explaining its numerous open problems remains the main goal of the research efforts in Particle Physics. We have shown that the neutrino sector, with its established evidence for new physics, can be the window through which other enigmas are connected and the new theory is revealed. It is therefore very promising to further pursue this tantalizing line of research in the future.

BIBLIOGRAPHY

[1] S. L. Glashow. «Partial Symmetries of Weak Interactions.» In: *Nucl. Phys.* 22 (1961), pp. 579–588. DOI: 10.1016/0029-5582(61)90469-2.

[2] Steven Weinberg. «A Model of Leptons.» In: *Phys. Rev. Lett.* 19 (1967), pp. 1264–1266. DOI: 10.1103/PhysRevLett.19.1264.

[3] Abdus Salam. «Weak and Electromagnetic Interactions.» In: *Conf. Proc. C* 680519 (1968), pp. 367–377. DOI: 10.1142/9789812795915_0034.

[4] Steven Weinberg. «Nonabelian Gauge Theories of the Strong Interactions.» In: *Phys. Rev. Lett.* 31 (1973), pp. 494–497. DOI: 10.1103/PhysRevLett.31.494.

[5] David J. Gross and Frank Wilczek. «Ultraviolet Behavior of Nonabelian Gauge Theories.» In: *Phys. Rev. Lett.* 30 (1973). Ed. by J. C. Taylor, pp. 1343–1346. DOI: 10.1103/PhysRevLett.30.1343.

[6] H. Fritzsch, Murray Gell-Mann, and H. Leutwyler. «Advantages of the Color Octet Gluon Picture.» In: *Phys. Lett. B* 47 (1973), pp. 365–368. DOI: 10.1016/0370-2693(73)90625-4.

[7] H. David Politzer. «Reliable Perturbative Results for Strong Interactions?» In: *Phys. Rev. Lett.* 30 (1973). Ed. by J. C. Taylor, pp. 1346–1349. DOI: 10.1103/PhysRevLett.30.1346.

[8] F. Englert and R. Brout. «Broken Symmetry and the Mass of Gauge Vector Mesons.» In: *Phys. Rev. Lett.* 13 (1964). Ed. by J. C. Taylor, pp. 321–323. DOI: 10.1103/PhysRevLett.13.321.

[9] Peter W. Higgs. «Broken Symmetries and the Masses of Gauge Bosons.» In: *Phys. Rev. Lett.* 13 (1964). Ed. by J. C. Taylor, pp. 508–509. DOI: 10.1103/PhysRevLett.13.508.

[10] Peter W. Higgs. «Spontaneous Symmetry Breakdown without Massless Bosons.» In: *Phys. Rev.* 145 (1966), pp. 1156–1163. DOI: 10.1103/PhysRev.145.1156.

[11] B. Pontecorvo. «Mesonium and anti-mesonium.» In: *Sov.Phys.JETP* 6 (1957), p. 429.

[12] B. Pontecorvo. «Inverse beta processes and nonconservation of lepton charge.» In: *Sov.Phys.JETP* 7 (1958), pp. 172–173.

[13] Z. Maki, M. Nakagawa, Y. Ohnuki, and S. Sakata. «A unified model for elementary particles.» In: *Prog.Theor.Phys.* 23 (1960), pp. 1174–1180. DOI: 10.1143/PTP.23.1174.

[14] Ziro Maki, Masami Nakagawa, and Shoichi Sakata. «Remarks on the unified model of elementary particles.» In: *Prog.Theor.Phys.* 28 (1962), pp. 870–880. DOI: 10.1143/PTP.28.870.

[15] B. Pontecorvo. «Neutrino Experiments and the Problem of Conservation of Leptonic Charge.» In: *Sov.Phys.JETP* 26 (1968), pp. 984–988.

[16] M. Aker et al. «First direct neutrino-mass measurement with sub-eV sensitivity.» In: (May 2021). arXiv: 2105.08533 [hep-ex].

[17] J. Schechter and J. W. F. Valle. «Neutrinoless Double beta Decay in SU(2) x U(1) Theories.» In: *Phys. Rev. D* 25 (1982), p. 2951. DOI: 10.1103/PhysRevD.25.2951.

[18] Jose F. Nieves. «Dirac and Pseudodirac Neutrinos and Neutrinoless Double Beta Decay.» In: *Phys. Lett. B* 147 (1984), pp. 375–379. DOI: 10.1016/0370-2693(84)90136-9.

[19] Eiichi Takasugi. «Can the Neutrinoless Double Beta Decay Take Place in the Case of Dirac Neutrinos?» In: *Phys. Lett. B* 149 (1984), pp. 372–376. DOI: 10.1016/0370-2693(84)90426-X.

[20] Boris Kayser. «IMPLICATIONS OF DOUBLE BETA DECAY FOR NEUTRINO MASS.» In: *23rd International Conference on High-Energy Physics*. July 1986.

[21] S. T. Petcov. «MASSIVE NEUTRINOS AND NEUTRINO MIXING.» In: *6th Moriond Workshop: Massive Neutrinos in Particle Physics and Astrophysics*. 1986.

[22] Simon Peter Rosen. «Double beta decay.» In: *The Benjamin Franklin Symposium in Celebration of the Discovery of the Neutrino*. Sept. 1992. arXiv: hep-ph/9210202.

[23] A. Gando et al. «Search for Majorana Neutrinos Near the Inverted Mass Hierarchy Region with KamLAND-Zen.» In: *Phys. Rev. Lett.* 117 (8 2016), p. 082503. DOI: 10.1103/PhysRevLett.117.082503. URL: https://link.aps.org/doi/10.1103/PhysRevLett.117.082503.

[24] Particle Data Group et al. «Review of Particle Physics.» In: *Progress of Theoretical and Experimental Physics* 2020.8 (Aug. 2020). 083C01. ISSN: 2050-3911. DOI: 10.1093/ptep/ptaa104. eprint: https://academic.oup.com/ptep/article-pdf/2020/8/083C01/34673740/rpp2020-vol2-2015-2092_18.pdf. URL: https://doi.org/10.1093/ptep/ptaa104.

[25] C. Alduino et al. «First Results from CUORE: A Search for Lepton Number Violation via $0\nu\beta\beta$ Decay of ^{130}Te.» In: *Phys. Rev. Lett.* 120 (13 2018), p. 132501. DOI: 10.1103/PhysRevLett.120.132501. URL: https://link.aps.org/doi/10.1103/PhysRevLett.120.132501.

[26] M. Agostini et al. «Improved Limit on Neutrinoless Double-β Decay of ^{76}Ge from GERDA Phase II.» In: *Phys. Rev. Lett.* 120 (13 2018), p. 132503. DOI: 10.1103/PhysRevLett.120.132503. URL: https://link.aps.org/doi/10.1103/PhysRevLett.120.132503.

[27] Michelle J. Dolinski, Alan W. P. Poon, and Werner Rodejohann. «Neutrinoless Double-Beta Decay: Status and Prospects.» In: *Ann. Rev. Nucl. Part. Sci.* 69 (2019), pp. 219–251. DOI: 10.1146/annurev-nucl-101918-023407. arXiv: 1902.04097 [nucl-ex].

[28] Julien Lesgourgues, Gianpiero Mangano, Gennaro Miele, and Sergio Pastor. *Neutrino Cosmology*. Cambridge University Press, 2013. DOI: 10.1017/CBO9781139012874.

[29] Shouvik Roy Choudhury and Sandhya Choubey. «Updated Bounds on Sum of Neutrino Masses in Various Cosmological Scenarios.» In: *JCAP* 09 (2018), p. 017. DOI: 10.1088/1475-7516/2018/09/017. arXiv: 1806.10832 [astro-ph.CO].

[30] R. Adam et al. «Planck 2015 results. I. Overview of products and scientific results.» In: *Astron. Astrophys.* 594 (2016), A1. DOI: 10.1051/0004-6361/201527101. arXiv: 1502.01582 [astro-ph.CO].

[31] Shadab Alam et al. «The clustering of galaxies in the completed SDSS-III Baryon Oscillation Spectroscopic Survey: cosmological analysis of the DR12 galaxy sample.» In: *Mon. Not. Roy. Astron. Soc.* 470.3 (2017), pp. 2617–2652. DOI: 10.1093/mnras/stx721. arXiv: 1607.03155 [astro-ph.CO].

[32] Ashley J. Ross, Lado Samushia, Cullan Howlett, Will J. Percival, Angela Burden, and Marc Manera. «The clustering of the SDSS DR7 main Galaxy sample – I. A 4 per cent distance measure at $z = 0.15$.» In: *Mon. Not. Roy. Astron. Soc.* 449.1 (2015), pp. 835–847. DOI: 10.1093/mnras/stv154. arXiv: 1409.3242 [astro-ph.CO].

[33] Florian Beutler, Chris Blake, Matthew Colless, D. Heath Jones, Lister Staveley-Smith, Lachlan Campbell, Quentin Parker, Will Saunders, and Fred Watson. «The 6dF Galaxy Survey: baryon acoustic oscillations and the local Hubble constant.» In: 416.4 (Oct. 2011), pp. 3017–3032. DOI: 10.1111/j.1365-2966.2011.19250.x. arXiv: 1106.3366 [astro-ph.CO].

[34] Raymond Davis Jr., Don S. Harmer, and Kenneth C. Hoffman. «Search for neutrinos from the sun.» In: *Phys. Rev. Lett.* 20 (1968), pp. 1205–1209. DOI: 10.1103/PhysRevLett.20.1205.

[35] B. T. Cleveland, Timothy Daily, Raymond Davis Jr., James R. Distel, Kenneth Lande, C. K. Lee, Paul S. Wildenhain, and Jack Ullman. «Measurement of the solar electron neutrino flux with the Homestake chlorine detector.» In: *Astrophys. J.* 496 (1998), pp. 505–526. DOI: 10.1086/305343.

[36] K. Lande et al. «The Homestake solar neutrino program.» In: *Nucl. Phys. B Proc. Suppl.* 77 (1999). Ed. by Y. Suzuki and Y. Totsuka, pp. 13–19. DOI: 10.1016/S0920-5632(99)00383-7.

[37] A. I. Abazov et al. «Search for neutrinos from sun using the reaction Ga-71 (electron-neutrino e-) Ge-71.» In: *Phys. Rev. Lett.* 67 (1991), pp. 3332–3335. DOI: 10.1103/PhysRevLett.67.3332.

[38] W. Hampel et al. «GALLEX solar neutrino observations: results for GALLEX IV.» In: *Physics Letters B* 447.1 (1999), pp. 127–133. ISSN: 0370-2693. DOI: https://doi.org/10.1016/S0370-2693(98)01579-2. URL: https://www.sciencedirect.com/science/article/pii/S0370269398015792.

[39] T.A Kirsten. «Progress in GNO.» In: *Nuclear Physics B - Proceedings Supplements* 118 (2003). Proceedings of the XXth International Conference on Neutrino Physics and Astrophysics, pp. 33–38. ISSN: 0920-5632. DOI: https://doi.org/10.1016/S0920-5632(03)01301-X. URL: https://www.sciencedirect.com/science/article/pii/S092056320301301X.

[40] Y. Fukuda et al. «The Super-Kamiokande detector.» In: *Nucl. Instrum. Meth.* A501 (2003), pp. 418–462. DOI: 10.1016/S0168-9002(03)00425-X.

[41] Q.R. Ahmad et al. «Measurement of the rate of $\nu_e + d \rightarrow p + p + e^-$ interactions produced by ^8B solar neutrinos at the Sudbury Neutrino Observatory.» In: *Phys. Rev. Lett.* 87 (2001), p. 071301. DOI: 10.1103/PhysRevLett.87.071301. arXiv: nucl-ex/0106015.

[42] Q. R. Ahmad et al. «Direct evidence for neutrino flavor transformation from neutral current interactions in the Sudbury Neutrino Observatory.» In: *Phys. Rev. Lett.* 89 (2002), p. 011301. DOI: 10.1103/PhysRevLett.89.011301. arXiv: nucl-ex/0204008.

[43] Q. R. Ahmad et al. «Measurement of day and night neutrino energy spectra at SNO and constraints on neutrino mixing parameters.» In: *Phys. Rev. Lett.* 89 (2002), p. 011302. DOI: 10.1103/PhysRevLett.89.011302. arXiv: nucl-ex/0204009.

[44] S. N. Ahmed et al. «Measurement of the total active B-8 solar neutrino flux at the Sudbury Neutrino Observatory with enhanced neutral current sensitivity.» In: *Phys. Rev. Lett.* 92 (2004), p. 181301. DOI: 10.1103/PhysRevLett.92.181301. arXiv: nucl-ex/0309004.

[45] Y. Fukuda et al. «Evidence for oscillation of atmospheric neutrinos.» In: *Phys. Rev. Lett.* 81 (1998), pp. 1562–1567. DOI: 10.1103/PhysRevLett.81.1562. arXiv: hep-ex/9807003 [hep-ex].

[46] T. Araki et al. «Measurement of neutrino oscillation with KamLAND: Evidence of spectral distortion.» In: *Phys. Rev. Lett.* 94 (2005), p. 081801. DOI: 10.1103/PhysRevLett.94.081801. arXiv: hep-ex/0406035.

[47] D. G. Michael et al. «Observation of muon neutrino disappearance with the MINOS detectors and the NuMI neutrino beam.» In: *Phys. Rev. Lett.* 97 (2006), p. 191801. DOI: 10.1103/PhysRevLett.97.191801. arXiv: hep-ex/0607088.

[48] M. H. Ahn et al. «Indications of neutrino oscillation in a 250 km long baseline experiment.» In: *Phys. Rev. Lett.* 90 (2003), p. 041801. DOI: 10.1103/PhysRevLett.90.041801. arXiv: hep-ex/0212007.

[49] Y. Abe et al. «Indication of Reactor $\bar{\nu}_e$ Disappearance in the Double Chooz Experiment.» In: *Phys. Rev. Lett.* 108 (2012), p. 131801. DOI: 10.1103/PhysRevLett.108.131801. arXiv: 1112.6353 [hep-ex].

[50] J.K. Ahn et al. «Observation of Reactor Electron Antineutrino Disappearance in the RENO Experiment.» In: *Phys. Rev. Lett.* 108 (2012), p. 191802. DOI: 10.1103/PhysRevLett.108.191802. arXiv: 1204.0626 [hep-ex].

[51] Elizabeth Worcester. «Observation of electron antineutrino disappearance by the Daya Bay Reactor Neutrino Experiment.» In: *Meeting of the APS Division of Particles and Fields*. Sept. 2013. arXiv: 1309.7991 [hep-ex].

[52] S. P. Mikheyev and A. Yu. Smirnov. «Resonance Amplification of Oscillations in Matter and Spectroscopy of Solar Neutrinos.» In: *Sov. J. Nucl. Phys.* 42 (1985), pp. 913–917.

[53] L. Wolfenstein. «Neutrino Oscillations in Matter.» In: *Phys. Rev.* D17 (1978). [,294(1977)], pp. 2369–2374. DOI: 10.1103/PhysRevD.17.2369.

[54] F.P. An et al. «Observation of electron-antineutrino disappearance at Daya Bay.» In: *Phys. Rev. Lett.* 108 (2012), p. 171803. DOI: 10.1103/PhysRevLett.108.171803. arXiv: 1203.1669 [hep-ex].

[55] Y. Abe et al. «Reactor electron antineutrino disappearance in the Double Chooz experiment.» In: *Phys.Rev.* D86 (2012), p. 052008. DOI: 10.1103/PhysRevD.86.052008. arXiv: 1207.6632 [hep-ex].

[56] P. Adamson et al. «Improved search for muon-neutrino to electron-neutrino oscillations in MINOS.» In: *Phys.Rev.Lett.* 107 (2011), p. 181802. DOI: 10.1103/PhysRevLett.107.181802. arXiv: 1108.0015 [hep-ex].

[57] K. Abe et al. «Indication of Electron Neutrino Appearance from an Accelerator-produced Off-axis Muon Neutrino Beam.» In: *Phys.Rev.Lett.* 107 (2011), p. 041801. DOI: 10.1103/PhysRevLett.107.041801. arXiv: 1106.2822 [hep-ex].

[58] Ivan Esteban, M. C. Gonzalez-Garcia, Michele Maltoni, Thomas Schwetz, and Albert Zhou. «The fate of hints: updated global analysis of three-flavor neutrino oscillations.» In: *JHEP* 09 (2020), p. 178. DOI: 10.1007/JHEP09(2020)178. arXiv: 2007.14792 [hep-ph].

[59] M. B. Gavela, P. Hernandez, J. Orloff, and O. Pene. «Standard model CP violation and baryon asymmetry.» In: *Mod. Phys. Lett.* A9 (1994), pp. 795–810. DOI: 10.1142/S0217732394000629. arXiv: hep-ph/9312215 [hep-ph].

[60] M. B. Gavela, P. Hernandez, J. Orloff, O. Pene, and C. Quimbay. «Standard model CP violation and baryon asymmetry. Part 2: Finite temperature.» In: *Nucl. Phys.* B430 (1994), pp. 382–426. DOI: 10.1016/0550-3213(94)00410-2. arXiv: hep-ph/9406289 [hep-ph].

[61] K. Abe et al. «Combined Analysis of Neutrino and Antineutrino Oscillations at T2K.» In: *Phys. Rev. Lett.* 118.15 (2017), p. 151801. DOI: 10.1103/PhysRevLett.118.151801. arXiv: 1701.00432 [hep-ex].

[62] K. Abe et al. «Constraint on the Matter-Antimatter Symmetry-Violating Phase in Neutrino Oscillations.» In: (2019). arXiv: 1910.03887 [hep-ex].

[63] M. A. Acero et al. «First Measurement of Neutrino Oscillation Parameters using Neutrinos and Antineutrinos by NOvA.» In: (2019). arXiv: 1906.04907 [hep-ex].

[64] K. Abe et al. «Physics potential of a long-baseline neutrino oscillation experiment using a J-PARC neutrino beam and Hyper-Kamiokande.» In: *PTEP* 2015 (2015), p. 053C02. DOI: 10.1093/ptep/ptv061. arXiv: 1502.05199 [hep-ex].

[65] R. Acciarri et al. «Long-Baseline Neutrino Facility (LBNF) and Deep Underground Neutrino Experiment (DUNE).» In: (2015). arXiv: 1512.06148 [physics.ins-det].

[66] E. Baussan et al. «A very intense neutrino super beam experiment for leptonic CP violation discovery based on the European spallation source linac.» In: *Nucl. Phys.* B885 (2014), pp. 127–149. DOI: 10.1016/j.nuclphysb.2014.05.016. arXiv: 1309.7022 [hep-ex].

[67] A. de Bellefon et al. «MEMPHYS: A Large scale water Cerenkov detector at Frejus.» In: (2006). arXiv: hep-ex/0607026 [hep-ex].

[68] L. Agostino, M. Buizza-Avanzini, M. Dracos, D. Duchesneau, M. Marafini, M. Mezzetto, L. Mosca, T. Patzak, A. Tonazzo, and N. Vassilopoulos. «Study of the performance of a large scale water-Cherenkov detector (MEMPHYS).» In: *JCAP* 1301 (2013), p. 024. DOI: 10.1088/1475-7516/2013/01/024. arXiv: 1206.6665 [hep-ex].

[69] Sanjib Kumar Agarwalla, Sandhya Choubey, and Suprabh Prakash. «Probing Neutrino Oscillation Parameters using High Power Superbeam from ESS.» In: *JHEP* 12 (2014), p. 020. DOI: 10.1007/JHEP12(2014)020. arXiv: 1406.2219 [hep-ph].

[70] Kaustav Chakraborty, K. N. Deepthi, and Srubabati Goswami. «Spotlighting the sensitivities of Hyper-Kamiokande, DUNE and ESSνSB.» In: *Nucl. Phys. B* 937 (2018), pp. 303–332. DOI: 10.1016/j.nuclphysb.2018.10.013. arXiv: 1711.11107 [hep-ph].

[71] Kaustav Chakraborty, Srubabati Goswami, Chandan Gupta, and Tarak Thakore. «Enhancing the hierarchy and octant sensitivity of ESSνSB in conjunction with T2K, NOνA and ICAL@INO.» In: *JHEP* 05 (2019), p. 137. DOI: 10.1007/JHEP05(2019)137. arXiv: 1902.02963 [hep-ph].

[72] Ivan Esteban, M. C. Gonzalez-Garcia, Alvaro Hernandez-Cabezudo, Michele Maltoni, and Thomas Schwetz. «Global analysis of three-flavour neutrino oscillations: synergies and tensions in the determination of θ_{23}, δ_{CP}, and the mass ordering.» In: *JHEP* 01 (2019), p. 106. DOI: 10.1007/JHEP01(2019)106. arXiv: 1811.05487 [hep-ph].

[73] D. Adey et al. «Measurement of the Electron Antineutrino Oscillation with 1958 Days of Operation at Daya Bay.» In: *Phys. Rev. Lett.* 121.24 (2018), p. 241805. DOI: 10.1103/PhysRevLett.121.241805. arXiv: 1809.02261 [hep-ex].

[74] G. Bak et al. «Measurement of Reactor Antineutrino Oscillation Amplitude and Frequency at RENO.» In: *Phys. Rev. Lett.* 121.20 (2018), p. 201801. DOI: 10.1103/PhysRevLett.121.201801. arXiv: 1806.00248 [hep-ex].

[75] A. Cervera, A. Donini, M. B. Gavela, J. J. Gomez Cadenas, P. Hernandez, Olga Mena, and S. Rigolin. «Golden measurements at a neutrino factory.» In: *Nucl. Phys.* B579 (2000). [Erratum: Nucl. Phys.B593,731(2001)], pp. 17–55. DOI: 10.1016/S0550-3213(00)00606-4, 10.1016/S0550-3213(00)00221-2. arXiv: hep-ph/0002108 [hep-ph].

[76] Pilar Coloma and Enrique Fernandez-Martinez. «Optimization of neutrino oscillation facilities for large θ_{13}.» In: *JHEP* 04 (2012), p. 089. DOI: 10.1007/JHEP04(2012)089. arXiv: 1110.4583 [hep-ph].

[77] Gian Luigi Fogli and E. Lisi. «Tests of three flavor mixing in long baseline neutrino oscillation experiments.» In: *Phys. Rev.* D54 (1996), pp. 3667–3670. DOI: 10.1103/PhysRevD.54.3667. arXiv: hep-ph/9604415 [hep-ph].

[78] Monojit Ghosh and Tommy Ohlsson. «A comparative study between ESSnuSB and T2HK in determining the leptonic CP phase.» In: (2019). arXiv: 1906.05779 [hep-ph].

[79] Hisakazu Minakata and Hiroshi Nunokawa. «Exploring neutrino mixing with low-energy superbeams.» In: *JHEP* 10 (2001), p. 001. DOI: 10.1088/1126-6708/2001/10/001. arXiv: hep-ph/0108085 [hep-ph].

[80] Patrick Huber, Michele Maltoni, and Thomas Schwetz. «Resolving parameter degeneracies in long-baseline experiments by atmospheric neutrino data.» In: *Phys. Rev.* D71 (2005), p. 053006. DOI: 10.1103/PhysRevD.71.053006. arXiv: hep-ph/0501037 [hep-ph].

[81] Jean-Eric Campagne, M. Maltoni, M. Mezzetto, and T. Schwetz. «Physics potential of the CERN-MEMPHYS neutrino oscillation project.» In: *JHEP* 04 (2007), p. 003. DOI: 10.1088/1126-6708/2007/04/003. arXiv: hep-ph/0603172 [hep-ph].

[82] J. Burguet-Castell, M. B. Gavela, J. J. Gomez-Cadenas, P. Hernandez, and Olga Mena. «On the Measurement of leptonic CP violation.» In: *Nucl. Phys.* B608 (2001), pp. 301–318. DOI: 10.1016/S0550-3213(01)00248-6. arXiv: hep-ph/0103258 [hep-ph].

[83] V. Barger, D. Marfatia, and K. Whisnant. «Breaking eight fold degeneracies in neutrino CP violation, mixing, and mass hierarchy.» In: *Phys. Rev.* D65 (2002), p. 073023. DOI: 10.1103/PhysRevD.65.073023. arXiv: hep-ph/0112119 [hep-ph].

[84] Hisakazu Minakata and Stephen J. Parke. «Correlated, precision measurements of θ_{23} and δ using only the electron neutrino appearance experiments.» In: *Phys. Rev.* D87.11 (2013), p. 113005. DOI: 10.1103/PhysRevD.87.113005. arXiv: 1303.6178 [hep-ph].

[85] Pilar Coloma, Hisakazu Minakata, and Stephen J. Parke. «Interplay between appearance and disappearance channels for precision measurements of θ_{23} and δ.» In: *Phys. Rev.* D90 (2014), p. 093003. DOI: 10.1103/PhysRevD.90.093003. arXiv: 1406.2551 [hep-ph].

[86] Monojit Ghosh, Pomita Ghoshal, Srubabati Goswami, Newton Nath, and Sushant K. Raut. «New look at the degeneracies in the neutrino oscillation parameters, and their resolution by T2K, NOνA and ICAL.» In: *Phys. Rev.* D93.1 (2016),

p. 013013. DOI: 10.1103/PhysRevD.93.013013. arXiv: 1504.06283 [hep-ph].

[87] Pilar Coloma, Patrick Huber, Joachim Kopp, and Walter Winter. «Systematic uncertainties in long-baseline neutrino oscillations for large θ_{13}.» In: *Phys. Rev.* D87.3 (2013), p. 033004. DOI: 10.1103/PhysRevD.87.033004. arXiv: 1209.5973 [hep-ph].

[88] Soumya C, K. N. Deepthi, and R. Mohanta. «A comprehensive study of the discovery potential of NOvA, T2K and T2HK experiments.» In: *Adv. High Energy Phys.* 2016 (2016), p. 9139402. DOI: 10.1155/2016/9139402. arXiv: 1408.6071 [hep-ph].

[89] Monojit Ghosh, Srubabati Goswami, and Sushant K. Raut. «Maximizing the DUNE early physics output with current experiments.» In: *Eur. Phys. J.* C76.3 (2016), p. 114. DOI: 10.1140/epjc/s10052-016-3962-7. arXiv: 1412.1744 [hep-ph].

[90] K. Abe et al. «A Long Baseline Neutrino Oscillation Experiment Using J-PARC Neutrino Beam and Hyper-Kamiokande.» In: 2014. arXiv: 1412.4673 [physics.ins-det].

[91] Monojit Ghosh and Osamu Yasuda. «Effect of systematics in the T2HK, T2HKK, and DUNE experiments.» In: *Phys. Rev.* D96.1 (2017), p. 013001. DOI: 10.1103/PhysRevD.96.013001. arXiv: 1702.06482 [hep-ph].

[92] K. Abe et al. «Hyper-Kamiokande Design Report.» In: (2018). arXiv: 1805.04163 [physics.ins-det].

[93] C. Adams et al. «The Long-Baseline Neutrino Experiment: Exploring Fundamental Symmetries of the Universe.» In: *Snowmass 2013: Workshop on Energy Frontier Seattle, USA, June 30-July 3, 2013*. 2013. arXiv: 1307.7335 [hep-ex]. URL: http://lss.fnal.gov/archive/2014/pub/fermilab-pub-14-022.pdf.

[94] Vernon Barger, Atri Bhattacharya, Animesh Chatterjee, Raj Gandhi, Danny Marfatia, and Mehedi Masud. «Configuring the Long-Baseline Neutrino Experiment.» In: *Phys. Rev.* D89.1 (2014), p. 011302. DOI: 10.1103/PhysRevD.89.011302. arXiv: 1307.2519 [hep-ph].

[95] Monojit Ghosh, Pomita Ghoshal, Srubabati Goswami, and Sushant K. Raut. «Synergies between neutrino oscillation experiments: an 'adequate' configuration for LBNO.» In: *JHEP* 03 (2014), p. 094. DOI: 10.1007/JHEP03(2014)094. arXiv: 1308.5979 [hep-ph].

[96] S. K. Agarwalla et al. «The mass-hierarchy and CP-violation discovery reach of the LBNO long-baseline neutrino experiment.» In: *JHEP* 05 (2014), p. 094. DOI: 10.1007/JHEP05(2014)094. arXiv: 1312.6520 [hep-ph].

[97] Vernon Barger, Atri Bhattacharya, Animesh Chatterjee, Raj Gandhi, Danny Marfatia, and Mehedi Masud. «Optimal configurations of the Deep Underground Neutrino Experiment.» In: *Int. J. Mod. Phys.* A31.07 (2016), p. 1650020. DOI: 10.1142/S0217751X16500202. arXiv: 1405.1054 [hep-ph].

[98] Kalpana Bora, Debajyoti Dutta, and Pomita Ghoshal. «Determining the octant of θ_{23} at LBNE in conjunction with reactor experiments.» In: *Mod. Phys. Lett.* A30.14 (2015), p. 1550066. DOI: 10.1142/S0217732315500662. arXiv: 1405.7482 [hep-ph].

[99] Newton Nath, Monojit Ghosh, and Srubabati Goswami. «The physics of antineutrinos in DUNE and determination of octant and δ_{CP}.» In: *Nucl. Phys.* B913 (2016), pp. 381–404. DOI: 10.1016/j.nuclphysb.2016.09.017. arXiv: 1511.07496 [hep-ph].

[100] Valentina De Romeri, Enrique Fernandez-Martinez, and Michel Sorel. «Neutrino oscillations at DUNE with improved energy reconstruction.» In: *JHEP* 09 (2016), p. 030. DOI: 10.1007/JHEP09(2016)030. arXiv: 1607.00293 [hep-ph].

[101] B. Abi et al. «The DUNE Far Detector Interim Design Report Volume 1: Physics, Technology and Strategies.» In: (2018). arXiv: 1807.10334 [physics.ins-det].

[102] André De Gouvêa, Kevin J. Kelly, G. V. Stenico, and Pedro Pasquini. «Physics with Beam Tau-Neutrino Appearance at DUNE.» In: *Phys. Rev. D* 100.1 (2019), p. 016004. DOI: 10.1103/PhysRevD.100.016004. arXiv: 1904.07265 [hep-ph].

[103] Anish Ghoshal, Alessio Giarnetti, and Davide Meloni. «On the role of the $\nu_?$ appearance in DUNE in constraining standard neutrino physics and beyond.» In: *JHEP* 12 (2019), p. 126. DOI: 10.1007/JHEP12(2019)126. arXiv: 1906.06212 [hep-ph].

[104] Davide Meloni. «On the systematic uncertainties in DUNE and their role in New Physics studies.» In: *JHEP* 08 (2018), p. 028. DOI: 10.1007/JHEP08(2018)028. arXiv: 1805.01747 [hep-ph].

[105] Shinya Fukasawa, Monojit Ghosh, and Osamu Yasuda. «Complementarity Between Hyperkamiokande and DUNE in Determining Neutrino Oscillation Parameters.» In: *Nucl. Phys.* B918 (2017), pp. 337–357. DOI: 10.1016/j.nuclphysb.2017.02.008. arXiv: 1607.03758 [hep-ph].

[106] Peter Ballett, Stephen F. King, Silvia Pascoli, Nick W. Prouse, and TseChun Wang. «Sensitivities and synergies of DUNE and T2HK.» In: *Phys. Rev.* D96.3 (2017), p. 033003. DOI: 10.1103/PhysRevD.96.033003. arXiv: 1612.07275 [hep-ph].

[107] Jun Cao et al. «Muon-decay medium-baseline neutrino beam facility.» In: *Phys. Rev. ST Accel. Beams* 17 (2014), p. 090101. DOI: 10.1103/PhysRevSTAB.17.090101. arXiv: 1401.8125 [physics.acc-ph].

[108] Mattias Blennow, Pilar Coloma, and Enrique FernÃ¡ndez-Martinez. «The MOMENT to search for CP violation.» In: *JHEP* 03 (2016), p. 197. DOI: 10.1007/JHEP03(2016)197. arXiv: 1511.02859 [hep-ph].

[109] Pouya Bakhti and Yasaman Farzan. «CP-Violation and Non-Standard Interactions at the MOMENT.» In: *JHEP* 07 (2016), p. 109. DOI: 10.1007/JHEP07(2016)109. arXiv: 1602.07099 [hep-ph].

[110] Jian Tang, Sampsa Vihonen, and Tse-Chun Wang. «Precision measurements on δ_{CP} in MOMENT.» In: *JHEP* 12 (2019), p. 130. DOI: 10.1007/JHEP12(2019)130. arXiv: 1909.01548 [hep-ph].

[111] Masaki Ishitsuka, Takaaki Kajita, Hisakazu Minakata, and Hiroshi Nunokawa. «Resolving neutrino mass hierarchy and CP degeneracy by two identical detectors with different baselines.» In: *Phys. Rev.* D72 (2005), p. 033003. DOI: 10.1103/PhysRevD.72.033003. arXiv: hep-ph/0504026 [hep-ph].

[112] Kaoru Hagiwara, Naotoshi Okamura, and Ken-ichi Senda. «Solving the neutrino parameter degeneracy by measuring the T2K off-axis beam in Korea.» In: *Phys. Lett.* B637 (2006). [Erratum: Phys. Lett.B641,491(2006)], pp. 266–273. DOI: 10.1016/j.physletb.2006.09.003,10.1016/j.physletb.2006.04.041. arXiv: hep-ph/0504061 [hep-ph].

[113] Kaoru Hagiwara, Naotoshi Okamura, and Ken-ichi Senda. «Physics potential of T2KK: An Extension of the T2K neutrino oscillation experiment with a far detector in Korea.» In: *Phys. Rev.* D76 (2007), p. 093002. DOI: 10.1103/PhysRevD.76.093002. arXiv: hep-ph/0607255 [hep-ph].

[114] Takaaki Kajita, Hisakazu Minakata, Shoei Nakayama, and Hiroshi Nunokawa. «Resolving eight-fold neutrino parameter degeneracy by two identical detectors with different baselines.» In: *Phys. Rev.* D75 (2007), p. 013006. DOI: 10.1103/PhysRevD.75.013006. arXiv: hep-ph/0609286 [hep-ph].

[115] Kaoru Hagiwara and Naotoshi Okamura. «Solving the degeneracy of the lepton-flavor mixing angle theta(ATM) by the T2KK two detector neutrino oscillation experiment.» In: *JHEP* 01 (2008), p. 022. DOI: 10.1088/1126-6708/2008/01/022. arXiv: hep-ph/0611058 [hep-ph].

[116] Kaoru Hagiwara and Naotoshi Okamura. «Re-evaluation of the T2KK physics potential with simulations including backgrounds.» In: *JHEP* 07 (2009), p. 031. DOI: 10.1088/1126-6708/2009/07/031. arXiv: 0901.1517 [hep-ph].

[117] Kaoru Hagiwara, Naotoshi Okamura, and Ken-ichi Senda. «The earth matter effects in neutrino oscillation experiments from Tokai to Kamioka and Korea.» In: *JHEP* 09 (2011), p. 082. DOI: 10.1007/JHEP09(2011)082. arXiv: 1107.5857 [hep-ph].

[118] Kaoru Hagiwara, Takayuki Kiwanami, Naotoshi Okamura, and Ken-ichi Senda. «Physics potential of neutrino oscillation experiment with a far detector in Oki Island along the T2K baseline.» In: *JHEP* 06 (2013), p. 036. DOI: 10.1007/JHEP06(2013)036. arXiv: 1209.2763 [hep-ph].

[119] Kaoru Hagiwara, Pyungwon Ko, Naotoshi Okamura, and Yoshitaro Takaesu. «Revisiting T2KK and T2KO physics potential and $\nu_\mu - \bar{\nu}_\mu$ beam ratio.» In: *Eur. Phys. J. C* 77.3 (2017), p. 138. DOI: 10.1140/epjc/s10052-017-4684-1. arXiv: 1605.02368 [hep-ph].

[120] K. Abe et al. «Physics potentials with the second Hyper-Kamiokande detector in Korea.» In: *PTEP* 2018.6 (2018), p. 063C01. DOI: 10.1093/ptep/pty044. arXiv: 1611.06118 [hep-ex].

[121] Sushant K. Raut. «Matter effects at the T2HK and T2HKK experiments.» In: *Phys. Rev.* D96.7 (2017), p. 075029. DOI: 10.1103/PhysRevD.96.075029. arXiv: 1703.07136 [hep-ph].

[122] M. Freund, M. Lindner, S. T. Petcov, and A. Romanino. «Testing matter effects in very long baseline neutrino oscillation experiments.» In: *Nucl. Phys.* B578 (2000), pp. 27–57. DOI: 10.1016/S0550-3213(00)00179-6. arXiv: hep-ph/9912457 [hep-ph].

[123] Evgeny K. Akhmedov, Robert Johansson, Manfred Lindner, Tommy Ohlsson, and Thomas Schwetz. «Series expansions for three flavor neutrino oscillation probabilities in matter.» In: *JHEP* 04 (2004), p. 078. DOI: 10.1088/1126-6708/2004/04/078. arXiv: hep-ph/0402175 [hep-ph].

[124] Hisakazu Minakata and Stephen J Parke. «Simple and Compact Expressions for Neutrino Oscillation Probabilities in Matter.» In: *JHEP* 01 (2016), p. 180. DOI: 10.1007/JHEP01(2016)180. arXiv: 1505.01826 [hep-ph].

[125] José Bernabeuu and Alejandro Segarra. «Signatures of the genuine and matter-induced components of the CP violation asymmetry in neutrino oscillations.» In: *JHEP* 11 (2018), p. 063. DOI: 10.1007/JHEP11(2018)063. arXiv: 1807.11879 [hep-ph].

[126] Pilar Coloma, Andrea Donini, Enrique Fernandez-Martinez, and Pilar Hernandez. «Precision on leptonic mixing parameters at future neutrino oscillation experiments.» In: *JHEP* 06 (2012), p. 073. DOI: 10.1007/JHEP06(2012)073. arXiv: 1203.5651 [hep-ph].

[127] E. Kh. Akhmedov, Soebur Razzaque, and A. Yu. Smirnov. «Mass hierarchy, 2-3 mixing and CP-phase with Huge Atmospheric Neutrino Detectors.» In: *JHEP* 02 (2013). [Erratum: JHEP07,026(2013)], p. 082. DOI: 10.1007/JHEP02(2013)082,10.1007/JHEP07(2013)026. arXiv: 1205.7071 [hep-ph].

[128] Patrick Huber, M. Lindner, and W. Winter. «Simulation of long-baseline neutrino oscillation experiments with GLoBES (General Long Baseline Experiment Simulator).» In: *Comput. Phys. Commun.* 167 (2005), p. 195. DOI: 10.1016/j.cpc.2005.01.003. arXiv: hep-ph/0407333 [hep-ph].

[129] Patrick Huber, Joachim Kopp, Manfred Lindner, Mark Rolinec, and Walter Winter. «New features in the simulation of neutrino oscillation experiments with GLoBES 3.0: General Long Baseline Experiment Simulator.» In: *Comput. Phys. Commun.* 177 (2007), pp. 432–438. DOI: 10.1016/j.cpc.2007.05.004. arXiv: hep-ph/0701187 [hep-ph].

[130] Mattias Blennow, Pilar Coloma, and Enrique Fernandez-Martinez. «Searching for sterile neutrinos at the ESSνSB.» In: *JHEP* 12 (2014), p. 120. DOI: 10.1007/JHEP12(2014)120. arXiv: 1407.1317 [hep-ph].

[131] Costas Andreopoulos, Christopher Barry, Steve Dytman, Hugh Gallagher, Tomasz Golan, Robert Hatcher, Gabriel Perdue, and Julia Yarba. «The GENIE Neutrino Monte Carlo Generator: Physics and User Manual.» In: (2015). arXiv: 1510.05494 [hep-ph].

[132] Morihiro Honda, T. Kajita, K. Kasahara, and S. Midorikawa. «A New calculation of the atmospheric neutrino flux in a 3-dimensional scheme.» In: *Phys. Rev.* D70 (2004), p. 043008. DOI: 10.1103/PhysRevD.70.043008. arXiv: astro-ph/0404457 [astro-ph].

[133] Y. Ashie et al. «A Measurement of atmospheric neutrino oscillation parameters by SUPER-KAMIOKANDE I.» In: *Phys. Rev.* D71 (2005), p. 112005. DOI: 10.1103/PhysRevD.71.112005. arXiv: hep-ex/0501064 [hep-ex].

[134] S. S. Wilks. «The Large-Sample Distribution of the Likelihood Ratio for Testing Composite Hypotheses.» In: *Annals Math. Statist.* 9.1 (1938), pp. 60–62. DOI: 10.1214/aoms/1177732360.

[135] Mattias Blennow, Pilar Coloma, and Enrique Fernandez-Martinez. «Reassessing the sensitivity to leptonic CP violation.» In: *JHEP* 03 (2015), p. 005. DOI: 10.1007/JHEP03(2015)005. arXiv: 1407.3274 [hep-ph].

[136] Steven Weinberg. «Baryon and Lepton Nonconserving Processes.» In: *Phys. Rev. Lett.* 43 (1979), pp. 1566–1570. DOI: 10.1103/PhysRevLett.43.1566.

[137] Martin B. Krauss, Toshihiko Ota, Werner Porod, and Walter Winter. «Neutrino mass from higher than d=5 effective operators in SUSY, and its test at the LHC.» In: *Phys. Rev. D* 84 (2011), p. 115023. DOI: 10.1103/PhysRevD.84.115023. arXiv: 1109.4636 [hep-ph].

[138] Peter Minkowski. «$\mu \to e\gamma$ at a Rate of One Out of 10^9 Muon Decays?» In: *Phys. Lett.* 67B (1977), pp. 421–428. DOI: 10.1016/0370-2693(77)90435-X.

[139] Rabindra N. Mohapatra and Goran Senjanovic. «Neutrino Mass and Spontaneous Parity Nonconservation.» In: *Phys. Rev. Lett.* 44 (1980). [,231(1979)], p. 912. DOI: 10.1103/PhysRevLett.44.912.

[140] Tsutomu Yanagida. «Horizontal gauge symmetry and masses of neutrinos.» In: *Conf. Proc.* C7902131 (1979), pp. 95–99.

[141] Murray Gell-Mann, Pierre Ramond, and Richard Slansky. «Complex Spinors and Unified Theories.» In: *Conf. Proc.* C790927 (1979), pp. 315–321. arXiv: 1306.4669 [hep-th].

[142] M. Magg and C. Wetterich. «Neutrino Mass Problem and Gauge Hierarchy.» In: *Phys. Lett. B* 94 (1980), pp. 61–64. DOI: 10.1016/0370-2693(80)90825-4.

[143] J. Schechter and J. W. F. Valle. «Neutrino Masses in SU(2) x U(1) Theories.» In: *Phys. Rev. D* 22 (1980), p. 2227. DOI: 10.1103/PhysRevD.22.2227.

[144] C. Wetterich. «Neutrino Masses and the Scale of B-L Violation.» In: *Nucl. Phys. B* 187 (1981), pp. 343–375. DOI: 10.1016/0550-3213(81)90279-0.

[145] M. Fukugita and T. Yanagida. «Baryogenesis Without Grand Unification.» In: *Phys. Lett.* B174 (1986), pp. 45–47. DOI: 10.1016/0370-2693(86)91126-3.

[146] Francesco Vissani. «Do experiments suggest a hierarchy problem?» In: *Phys. Rev. D* 57 (1998), pp. 7027–7030. DOI: 10.1103/PhysRevD.57.7027. arXiv: hep-ph/9709409.

[147] J.A. Casas, J.R. Espinosa, and I. Hidalgo. «Implications for new physics from fine-tuning arguments. 1. Application to SUSY and seesaw cases.» In: *JHEP* 11 (2004), p. 057. DOI: 10.1088/1126-6708/2004/11/057. arXiv: hep-ph/0410298.

[148] R. N. Mohapatra. «Mechanism for Understanding Small Neutrino Mass in Superstring Theories.» In: *Phys. Rev. Lett.* 56 (1986), pp. 561–563. DOI: 10.1103/PhysRevLett.56.561.

[149] R. N. Mohapatra and J. W. F. Valle. «Neutrino Mass and Baryon Number Nonconservation in Superstring Models.» In: *Phys. Rev.* D34 (1986). [,235(1986)], p. 1642. DOI: 10.1103/PhysRevD.34.1642.

[150] J. Bernabeu, A. Santamaria, J. Vidal, A. Mendez, and J. W. F. Valle. «Lepton Flavor Nonconservation at High-Energies in a Superstring Inspired Standard Model.» In: *Phys. Lett.* B187 (1987), pp. 303–308. DOI: 10.1016/0370-2693(87)91100-2.

[151] Michal Malinsky, J. C. Romao, and J. W. F. Valle. «Novel supersymmetric SO(10) seesaw mechanism.» In: *Phys. Rev. Lett.* 95 (2005), p. 161801. DOI: 10.1103/PhysRevLett.95.161801. arXiv: hep-ph/0506296 [hep-ph].

[152] G. C. Branco, W. Grimus, and L. Lavoura. «THE SEESAW MECHANISM IN THE PRESENCE OF A CONSERVED LEPTON NUMBER.» In: *Nucl. Phys.* B312 (1989), p. 492. DOI: 10.1016/0550-3213(89)90304-0.

[153] Jörn Kersten and Alexei Yu. Smirnov. «Right-Handed Neutrinos at CERN LHC and the Mechanism of Neutrino Mass Generation.» In: *Phys. Rev.* D76 (2007), p. 073005. DOI: 10.1103/PhysRevD.76.073005. arXiv: 0705.3221 [hep-ph].

[154] A. Abada, C. Biggio, F. Bonnet, M. B. Gavela, and T. Hambye. «Low energy effects of neutrino masses.» In: *JHEP* 12 (2007), p. 061. DOI: 10.1088/1126-6708/2007/12/061. arXiv: 0707.4058 [hep-ph].

[155] Enrique Fernandez-Martinez, Josu Hernandez-Garcia, and Jacobo Lopez-Pavon. «Global constraints on heavy neutrino mixing.» In: *JHEP* 08 (2016), p. 033. DOI: 10.1007/JHEP08(2016)033. arXiv: 1605.08774 [hep-ph].

[156] F. del Aguila and J.A. Aguilar-Saavedra. «Distinguishing seesaw models at LHC with multi-lepton signals.» In: *Nucl. Phys. B* 813 (2009), pp. 22–90. DOI: 10.1016/j.nuclphysb.2008.12.029. arXiv: 0808.2468 [hep-ph].

[157] Anupama Atre, Tao Han, Silvia Pascoli, and Bin Zhang. «The Search for Heavy Majorana Neutrinos.» In: *JHEP* 05 (2009), p. 030. DOI: 10.1088/1126-6708/2009/05/030. arXiv: 0901.3589 [hep-ph].

[158] Stefan Antusch and Oliver Fischer. «Testing sterile neutrino extensions of the Standard Model at future lepton colliders.» In: *JHEP* 05 (2015), p. 053. DOI: 10.1007/JHEP05(2015)053. arXiv: 1502.05915 [hep-ph].

[159] F. Zwicky. «Die Rotverschiebung von extragalaktischen Nebeln.» In: *Helv. Phys. Acta* 6 (1933), pp. 110–127. DOI: 10.1007/s10714-008-0707-4.

[160] Vera C. Rubin and W. Kent Ford Jr. «Rotation of the Andromeda Nebula from a Spectroscopic Survey of Emission Regions.» In: *Astrophys. J.* 159 (1970), pp. 379–403. DOI: 10.1086/150317.

[161] K. C. Freeman. «On the disks of spiral and SO Galaxies.» In: *Astrophys. J.* 160 (1970), p. 811. DOI: 10.1086/150474.

[162] K. G. Begeman, A. H. Broeils, and R. H. Sanders. «Extended rotation curves of spiral galaxies: Dark haloes and modified dynamics.» In: *Mon. Not. Roy. Astron. Soc.* 249 (1991), p. 523.

[163] Maxim Markevitch, A. H. Gonzalez, D. Clowe, A. Vikhlinin, L. David, W. Forman, C. Jones, S. Murray, and W. Tucker. «Direct constraints on the dark matter self-interaction cross-section from the merging galaxy cluster 1E0657-56.» In: *Astrophys. J.* 606 (2004), pp. 819–824. DOI: 10.1086/383178. arXiv: astro-ph/0309303.

[164] Douglas Clowe, Marusa Bradac, Anthony H. Gonzalez, Maxim Markevitch, Scott W. Randall, Christine Jones, and Dennis Zaritsky. «A direct empirical proof of the existence of dark matter.» In: *Astrophys. J. Lett.* 648 (2006), pp. L109–L113. DOI: 10.1086/508162. arXiv: astro-ph/0608407.

[165] G. Hinshaw et al. «Nine-Year Wilkinson Microwave Anisotropy Probe (WMAP) Observations: Cosmological Parameter Results.» In: *Astrophys. J. Suppl.* 208 (2013), p. 19. DOI: 10.1088/0067-0049/208/2/19. arXiv: 1212.5226 [astro-ph.CO].

[166] N. Aghanim et al. «Planck 2018 results. VI. Cosmological parameters.» In: (2018). arXiv: 1807.06209 [astro-ph.CO].

[167] Edward W. Kolb and Michael S. Turner. *The Early Universe*. Vol. 69. 1990. ISBN: 978-0-201-62674-2.

[168] E. Aprile et al. «Excess electronic recoil events in XENON1T.» In: *Phys. Rev. D* 102.7 (2020), p. 072004. DOI: 10.1103/PhysRevD.102.072004. arXiv: 2006.09721 [hep-ex].

[169] Marco Battaglieri et al. «US Cosmic Visions: New Ideas in Dark Matter 2017: Community Report.» In: (2017). arXiv: 1707.04591 [hep-ph].

[170] Dan Hooper. «TASI Lectures on Indirect Searches For Dark Matter.» In: *PoS* TASI2018 (2019), p. 010. arXiv: 1812.02029 [hep-ph].

[171] Julio F. Navarro, Carlos S. Frenk, and Simon D. M. White. «The Structure of cold dark matter halos.» In: *Astrophys. J.* 462 (1996), pp. 563–575. DOI: 10.1086/177173. arXiv: astro-ph/9508025.

[172] A. Albert et al. «Searching for Dark Matter Annihilation in Recently Discovered Milky Way Satellites with Fermi-LAT.» In: *Astrophys. J.* 834.2 (2017), p. 110. DOI: 10.3847/1538-4357/834/2/110. arXiv: 1611.03184 [astro-ph.HE].

[173] Antonio Boveia and Caterina Doglioni. «Dark Matter Searches at Colliders.» In: *Ann. Rev. Nucl. Part. Sci.* 68 (2018), pp. 429–459. DOI: 10.1146/annurev-nucl-101917-021008. arXiv: 1810.12238 [hep-ex].

[174] C. Boehm, Pierre Fayet, and R. Schaeffer. «Constraining dark matter candidates from structure formation.» In: *Phys. Lett.* B518 (2001), pp. 8–14. DOI: 10.1016/S0370-2693(01)01060-7. arXiv: astro-ph/0012504 [astro-ph].

[175] Celine Boehm and Richard Schaeffer. «Constraints on dark matter interactions from structure formation: Damping lengths.» In: *Astron. Astrophys.* 438 (2005), pp. 419–442. DOI: 10.1051/0004-6361:20042238. arXiv: astro-ph/0410591 [astro-ph].

[176] Gianpiero Mangano, Alessandro Melchiorri, Paolo Serra, Asantha Cooray, and Marc Kamionkowski. «Cosmological bounds on dark matter-neutrino interactions.» In: *Phys. Rev.* D74 (2006), p. 043517. DOI: 10.1103/PhysRevD.74.043517. arXiv: astro-ph/0606190 [astro-ph].

[177] Edmund Bertschinger. «The Effects of Cold Dark Matter Decoupling and Pair Annihilation on Cosmological Perturbations.» In: *Phys. Rev.* D74 (2006), p. 063509. DOI: 10.1103/PhysRevD.74.063509. arXiv: astro-ph/0607319 [astro-ph].

[178] Paolo Serra, Federico Zalamea, Asantha Cooray, Gianpiero Mangano, and Alessandro Melchiorri. «Constraints on neutrino – dark matter interactions from cosmic microwave background and large scale structure data.» In: *Phys. Rev.* D81 (2010), p. 043507. DOI: 10.1103/PhysRevD.81.043507. arXiv: 0911.4411 [astro-ph.CO].

[179] Laura G. van den Aarssen, Torsten Bringmann, and Christoph Pfrommer. «Is dark matter with long-range interactions a solution to all small-scale problems of Λ CDM cosmology?» In: *Phys. Rev. Lett.* 109 (2012), p. 231301. DOI: 10.1103/PhysRevLett.109.231301. arXiv: 1205.5809 [astro-ph.CO].

[180] Torsten Bringmann, Jasper Hasenkamp, and Jörn Kersten. «Tight bonds between sterile neutrinos and dark matter.» In: *JCAP* 07 (2014), p. 042. DOI: 10.1088/1475-7516/2014/07/042. arXiv: 1312.4947 [hep-ph].

[181] Ryan J. Wilkinson, Celine Boehm, and Julien Lesgourgues. «Constraining Dark Matter-Neutrino Interactions using the CMB and Large-Scale Structure.» In: *JCAP* 1405 (2014), p. 011. DOI: 10.1088/1475-7516/2014/05/011. arXiv: 1401.7597 [astro-ph.CO].

[182] C. Boehm, J. A. Schewtschenko, R. J. Wilkinson, C. M. Baugh, and S. Pascoli. «Using the Milky Way satellites to study interactions between cold dark matter and radiation.» In: *Mon. Not. Roy. Astron. Soc.* 445 (2014), pp. L31–L35. DOI: 10.1093/mnrasl/slu115. arXiv: 1404.7012 [astro-ph.CO].

[183] J. A. Schewtschenko, R. J. Wilkinson, C. M. Baugh, C. Bœhm, and S. Pascoli. «Dark matter–-radiation interactions: the impact on dark matter haloes.» In: *Mon. Not. Roy. Astron. Soc.* 449.4 (2015), pp. 3587–3596. DOI: 10.1093/mnras/stv431. arXiv: 1412.4905 [astro-ph.CO].

[184] Francis-Yan Cyr-Racine, Kris Sigurdson, Jesus Zavala, Torsten Bringmann, Mark Vogelsberger, and Christoph Pfrommer. «ETHOS—-an effective theory of structure formation: From dark particle physics to the matter distribution of the Universe.» In: *Phys. Rev. D* 93.12 (2016), p. 123527. DOI: 10.1103/PhysRevD.93.123527. arXiv: 1512.05344 [astro-ph.CO].

[185] Mark Vogelsberger, Jesus Zavala, Francis-Yan Cyr-Racine, Christoph Pfrommer, Torsten Bringmann, and Kris Sigurdson. «ETHOS—-an effective theory of structure formation: dark matter physics as a possible explanation of the small-scale CDM problems.» In: *Mon. Not. Roy. Astron. Soc.* 460.2 (2016), pp. 1399–1416. DOI: 10.1093/mnras/stw1076. arXiv: 1512.05349 [astro-ph.CO].

[186] Ottavia Balducci, Stefan Hofmann, and Alexis Kassiteridis. «Cosmological Singlet Diagnostics of Neutrinophilic Dark Matter.» In: *Phys. Rev.* D98.2 (2018), p. 023003. DOI: 10.1103/PhysRevD.98.023003. arXiv: 1710.09846 [hep-ph].

[187] Andrés Olivares-Del Campo, Céline Bœhm, Sergio Palomares-Ruiz, and Silvia Pascoli. «Dark matter-neutrino interactions through the lens of their cosmological implications.» In: *Phys. Rev. D* 97.7 (2018), p. 075039. DOI: 10.1103/PhysRevD.97.075039. arXiv: 1711.05283 [hep-ph].

[188] John F. Beacom, Nicole F. Bell, and Gregory D. Mack. «General Upper Bound on the Dark Matter Total Annihilation Cross Section.» In: *Phys. Rev. Lett.* 99 (2007), p. 231301. DOI: 10.1103/PhysRevLett.99.231301. arXiv: astro-ph/0608090 [astro-ph].

[189] Sergio Palomares-Ruiz and Silvia Pascoli. «Testing MeV dark matter with neutrino detectors.» In: *Phys. Rev.* D77 (2008), p. 025025. DOI: 10.1103/PhysRevD.77.025025. arXiv: 0710.5420 [astro-ph].

[190] Manfred Lindner, Alexander Merle, and Viviana Niro. «Enhancing Dark Matter Annihilation into Neutrinos.» In: *Phys. Rev.* D82 (2010), p. 123529. DOI: 10.1103/PhysRevD.82.123529. arXiv: 1005.3116 [hep-ph].

[191] Chaimae El Aisati, Camilo Garcia-Cely, Thomas Hambye, and Laurent Vanderheyden. «Prospects for discovering a neutrino line induced by dark matter annihilation.» In: *JCAP* 1710.10 (2017), p. 021. DOI: 10.1088/1475-7516/2017/10/021. arXiv: 1706.06600 [hep-ph].

[192] Yasaman Farzan and Sergio Palomares-Ruiz. «Dips in the Diffuse Supernova Neutrino Background.» In: *JCAP* 1406 (2014), p. 014. DOI: 10.1088/1475-7516/2014/06/014. arXiv: 1401.7019 [hep-ph].

[193] Tarso Franarin, Malcolm Fairbairn, and Jonathan H. Davis. «JUNO Sensitivity to Resonant Absorption of Galactic Supernova Neutrinos by Dark Matter.» In: (2018). arXiv: 1806.05015 [hep-ph].

[194] Carlos A. Argüelles, Ali Kheirandish, and Aaron C. Vincent. «Imaging Galactic Dark Matter with High-Energy Cosmic Neutrinos.» In: *Phys. Rev. Lett.* 119.20 (2017), p. 201801. DOI: 10.1103/PhysRevLett.119.201801. arXiv: 1703.00451 [hep-ph].

[195] Sujata Pandey, Siddhartha Karmakar, and Subhendu Rakshit. «Interactions of Astrophysical Neutrinos with Dark Matter: A model building perspective.» In: *JHEP* 01 (2019), p. 095. DOI: 10.1007/JHEP01(2019)095. arXiv: 1810.04203 [hep-ph].

[196] Siddhartha Karmakar, Sujata Pandey, and Subhendu Rakshit. «Are We Looking at Neutrino Absorption Spectra at IceCube?» In: (2018). arXiv: 1810.04192 [hep-ph].

[197] Bob Holdom. «Two U(1)'s and Epsilon Charge Shifts.» In: *Phys. Lett.* 166B (1986), pp. 196–198. DOI: 10.1016/0370-2693(86)91377-8.

[198] Brian Patt and Frank Wilczek. «Higgs-field portal into hidden sectors.» In: (2006). arXiv: hep-ph/0605188 [hep-ph].

[199] Adam Falkowski, Jose Juknevich, and Jessie Shelton. «Dark Matter Through the Neutrino Portal.» In: (2009). arXiv: 0908.1790 [hep-ph].

[200] Vannia Gonzalez Macias and Jose Wudka. «Effective theories for Dark Matter interactions and the neutrino portal paradigm.» In: *JHEP* 07 (2015), p. 161. DOI: 10.1007/JHEP07(2015)161. arXiv: 1506.03825 [hep-ph].

[201] Gianfranco Bertone, ed. *Particle Dark Matter: Observations, Models and Searches*. Cambridge: Cambridge Univ. Press, 2010. ISBN: 9781107653924. URL: http://www.cambridge.org/uk/catalogue/catalogue.asp?isbn=9780521763684.

[202] Adam Falkowski, Joshua T. Ruderman, and Tomer Volansky. «Asymmetric Dark Matter from Leptogenesis.» In: *JHEP* 05 (2011), p. 106. DOI: 10.1007/JHEP05(2011)106. arXiv: 1101.4936 [hep-ph].

[203] Bridget Bertoni, Seyda Ipek, David McKeen, and Ann E. Nelson. «Constraints and consequences of reducing small scale structure via large dark matter-neutrino interactions.» In: *JHEP* 04 (2015), p. 170. DOI: 10.1007/JHEP04(2015)170. arXiv: 1412.3113 [hep-ph].

[204] Vannia González-Macías, José I. Illana, and José Wudka. «A realistic model for Dark Matter interactions in the neutrino portal paradigm.» In: *JHEP* 05 (2016), p. 171. DOI: 10.1007/JHEP05(2016)171. arXiv: 1601.05051 [hep-ph].

[205] Brian Batell, Tao Han, David McKeen, and Barmak Shams Es Haghi. «Thermal Dark Matter Through the Dirac Neutrino Portal.» In: *Phys. Rev.* D97.7 (2018), p. 075016. DOI: 10.1103/PhysRevD.97.075016. arXiv: 1709.07001 [hep-ph].

[206] John F. Cherry, Alexander Friedland, and Ian M. Shoemaker. «Neutrino Portal Dark Matter: From Dwarf Galaxies to IceCube.» In: (2014). arXiv: 1411.1071 [hep-ph].

[207] G Alimonti et al. «Science and technology of BOREXINO: A Real time detector for low-energy solar neutrinos.» In: *Astropart. Phys.* 16 (2002), pp. 205–234. DOI: 10.1016/S0927-6505(01)00110-4. arXiv: hep-ex/0012030 [hep-ex].

[208] Hasan Yuksel, Shunsaku Horiuchi, John F. Beacom, and Shin'ichiro Ando. «Neutrino Constraints on the Dark Matter Total Annihilation Cross Section.» In: *Phys. Rev.* D76 (2007), p. 123506. DOI: 10.1103/PhysRevD.76.123506. arXiv: 0707.0196 [astro-ph].

[209] Katarzyna Frankiewicz. «Searching for Dark Matter Annihilation into Neutrinos with Super-Kamiokande.» In: *Proceedings, Meeting of the APS Division of Particles and Fields (DPF 2015): Ann Arbor, Michigan, USA, 4-8 Aug 2015*. 2015. arXiv: 1510.07999 [hep-ex]. URL: https://inspirehep.net/record/1401009/files/arXiv:1510.07999.pdf.

[210] Andres Olivares-Del Campo, Sergio Palomares-Ruiz, and Silvia Pascoli. «Implications of a Dark Matter-Neutrino Coupling at Hyper-Kamiokande.» In: *53rd Rencontres de Moriond on Electroweak Interactions and Unified Theories (Moriond EW 2018) La Thuile, Italy, March 10-17, 2018*. 2018. arXiv: 1805.09830 [hep-ph].

[211] Niki Klop and Shin'ichiro Ando. «Constraints on MeV dark matter using neutrino detectors and their implication for the 21-cm results.» In: *Phys. Rev.* D98.10 (2018), p. 103004. DOI: 10.1103/PhysRevD.98.103004. arXiv: 1809.00671 [hep-ph].

[212] G. Bellini et al. «Study of solar and other unknown anti-neutrino fluxes with Borexino at LNGS.» In: *Phys. Lett.* B696 (2011), pp. 191–196. DOI: 10.1016/j.physletb.2010.12.030. arXiv: 1010.0029 [hep-ex].

[213] Christoph Berger et al. «The Frejus Nucleon Decay Detector.» In: *Nucl. Instrum. Meth.* A262 (1987), p. 463. DOI: 10.1016/0168-9002(87)90890-4.

[214] Francis Halzen et al. «The AMANDA neutrino telescope.» In: *Nucl. Phys. Proc. Suppl.* 77 (1999). [,474(1998)], pp. 474–485. DOI: 10.1016/S0920-5632(99)00469-7. arXiv: hep-ex/9809025 [hep-ex].

[215] Gerard Jungman, Marc Kamionkowski, and Kim Griest. «Supersymmetric dark matter.» In: *Phys. Rept.* 267 (1996), pp. 195–373. DOI: 10.1016/0370-1573(95)00058-5. arXiv: hep-ph/9506380 [hep-ph].

[216] J. Aalbers et al. «DARWIN: towards the ultimate dark matter detector.» In: *JCAP* 1611 (2016), p. 017. DOI: 10.1088/1475-7516/2016/11/017. arXiv: 1606.07001 [astro-ph.IM].

[217] David McKeen and Nirmal Raj. «Monochromatic dark neutrinos and boosted dark matter in noble liquid direct detection.» In: (2018). arXiv: 1812.05102 [hep-ph].

[218] K. Choi et al. «Search for neutrinos from annihilation of captured low-mass dark matter particles in the Sun by Super-Kamiokande.» In: *Phys. Rev. Lett.* 114.14 (2015), p. 141301. DOI: 10.1103/PhysRevLett.114.141301. arXiv: 1503.04858 [hep-ex].

[219] M. G. Aartsen et al. «Search for annihilating dark matter in the Sun with 3 years of IceCube data.» In: *Eur. Phys. J.* C77.3 (2017), p. 146. DOI: 10.1140/epjc/s10052-017-4689-9. arXiv: 1612.05949 [astro-ph.HE].

[220] M. L. Ahnen et al. «Limits to dark matter annihilation cross-section from a combined analysis of MAGIC and Fermi-LAT observations of dwarf satellite galaxies.» In: *JCAP* 1602.02 (2016), p. 039. DOI: 10.1088/1475-7516/2016/02/039. arXiv: 1601.06590 [astro-ph.HE].

[221] Tracy R. Slatyer. «Indirect dark matter signatures in the cosmic dark ages. I. Generalizing the bound on s-wave dark matter annihilation from Planck results.» In: *Phys. Rev.* D93.2 (2016), p. 023527. DOI: 10.1103/PhysRevD.93.023527. arXiv: 1506.03811 [hep-ph].

[222] E. Aprile et al. «Dark Matter Search Results from a One Ton-Year Exposure of XENON1T.» In: *Phys. Rev. Lett.* 121.11 (2018), p. 111302. DOI: 10.1103/PhysRevLett.121.111302. arXiv: 1805.12562 [astro-ph.CO].

[223] Rouven Essig, Tomer Volansky, and Tien-Tien Yu. «New Constraints and Prospects for sub-GeV Dark Matter Scattering off Electrons in Xenon.» In: *Phys. Rev.* D96.4 (2017), p. 043017. DOI: 10.1103/PhysRevD.96.043017. arXiv: 1703.00910 [hep-ph].

[224] Rouven Essig, Mukul Sholapurkar, and Tien-Tien Yu. «Solar Neutrinos as a Signal and Background in Direct-Detection Experiments Searching for Sub-GeV Dark Matter With Electron Recoils.» In: *Phys. Rev.* D97.9 (2018), p. 095029. DOI: 10.1103/PhysRevD.97.095029. arXiv: 1801.10159 [hep-ph].

[225] Matthew J. Dolan, Felix Kahlhoefer, and Christopher McCabe. «Directly detecting sub-GeV dark matter with electrons from nuclear scattering.» In: *Phys. Rev. Lett.* 121.10 (2018), p. 101801. DOI: 10.1103/PhysRevLett.121.101801. arXiv: 1711.09906 [hep-ph].

[226] Pasquale Dario Serpico and Georg G. Raffelt. «MeV-mass dark matter and primordial nucleosynthesis.» In: *Phys. Rev.* D70 (2004), p. 043526. DOI: 10.1103/PhysRevD.70.043526. arXiv: astro-ph/0403417 [astro-ph].

[227] Fabio Iocco, Gianpiero Mangano, Gennaro Miele, Ofelia Pisanti, and Pasquale D. Serpico. «Primordial Nucleosynthesis: from precision cosmology to fundamental physics.» In: *Phys. Rept.* 472 (2009), pp. 1–76. DOI: 10.1016/j.physrep.2009.02.002. arXiv: 0809.0631 [astro-ph].

[228] Céline Boehm, Matthew J. Dolan, and Christopher McCabe. «A Lower Bound on the Mass of Cold Thermal Dark Matter from Planck.» In: *JCAP* 1308 (2013), p. 041. DOI: 10.1088/1475-7516/2013/08/041. arXiv: 1303.6270 [hep-ph].

[229] Kenneth M. Nollett and Gary Steigman. «BBN And The CMB Constrain Neutrino Coupled Light WIMPs.» In: *Phys. Rev.* D91.8 (2015), p. 083505. DOI: 10.1103/PhysRevD.91.083505. arXiv: 1411.6005 [astro-ph.CO].

[230] Miguel Escudero. «Neutrino decoupling beyond the Standard Model: CMB constraints on the Dark Matter mass with a fast and precise N_{eff} evaluation.» In: *JCAP* 1902 (2019), p. 007. DOI: 10.1088/1475-7516/2019/02/007. arXiv: 1812.05605 [hep-ph].

[231] Miguel Escudero, Laura Lopez-Honorez, Olga Mena, Sergio Palomares-Ruiz, and Pablo Villanueva-Domingo. «A fresh look into the interacting dark matter scenario.» In: *JCAP* 1806.06 (2018), p. 007. DOI: 10.1088/1475-7516/2018/06/007. arXiv: 1803.08427 [astro-ph.CO].

[232] G. Belanger, F. Boudjema, A. Pukhov, and A. Semenov. «MicrOMEGAs: A Program for calculating the relic density in the MSSM.» In: *Comput. Phys. Commun.* 149 (2002), pp. 103–120. DOI: 10.1016/S0010-4655(02)00596-9. arXiv: hep-ph/0112278 [hep-ph].

[233] Enrico Bertuzzo, Cristian J. Caniu Barros, and Giovanni Grilli di Cortona. «MeV Dark Matter: Model Independent Bounds.» In: *JHEP* 09 (2017), p. 116. DOI: 10.1007/JHEP09(2017)116. arXiv: 1707.00725 [hep-ph].

[234] Maxim Pospelov, Adam Ritz, and Mikhail B. Voloshin. «Secluded WIMP Dark Matter.» In: *Phys. Lett.* B662 (2008), pp. 53–61. DOI: 10.1016/j.physletb.2008.02.052. arXiv: 0711.4866 [hep-ph].

[235] Miguel Escudero, Nuria Rius, and Verónica Sanz. «Sterile neutrino portal to Dark Matter I: The $U(1)_{B-L}$ case.» In: *JHEP* 02 (2017), p. 045. DOI: 10.1007/JHEP02(2017)045. arXiv: 1606.01258 [hep-ph].

[236] Miguel Escudero, Nuria Rius, and Verónica Sanz. «Sterile Neutrino portal to Dark Matter II: Exact Dark symmetry.» In: *Eur. Phys. J.* C77.6 (2017), p. 397. DOI: 10.1140/epjc/s10052-017-4963-x. arXiv: 1607.02373 [hep-ph].

[237] Miguel G. Folgado, Germán A. Gómez-Vargas, Nuria Rius, and Roberto Ruiz De Austri. «Probing the sterile neutrino portal to Dark Matter with γ rays.» In: *JCAP* 1808.08 (2018), p. 002. DOI: 10.1088/1475-7516/2018/08/002. arXiv: 1803.08934 [hep-ph].

[238] Priyotosh Bandyopadhyay, Eung Jin Chun, Rusa Mandal, and Farinaldo S. Queiroz. «Scrutinizing Right-Handed Neutrino Portal Dark Matter With Yukawa Effect.» In: *Phys. Lett.* B788 (2019), pp. 530–534. DOI: 10.1016/j.physletb.2018.12.003. arXiv: 1807.05122 [hep-ph].

[239] Joshua Ellis. «TikZ-Feynman: Feynman diagrams with TikZ.» In: *Comput. Phys. Commun.* 210 (2017), pp. 103–123. DOI: 10.1016/j.cpc.2016.08.019. arXiv: 1601.05437 [hep-ph].

[240] Neil D. Christensen and Claude Duhr. «FeynRules - Feynman rules made easy.» In: *Comput. Phys. Commun.* 180 (2009), pp. 1614–1641. DOI: 10.1016/j.cpc.2009.02.018. arXiv: 0806.4194 [hep-ph].

[241] Adam Alloul, Neil D. Christensen, Céline Degrande, Claude Duhr, and Benjamin Fuks. «FeynRules 2.0 - A complete toolbox for tree-level phenomenology.» In: *Comput. Phys. Commun.* 185 (2014), pp. 2250–2300. DOI: 10.1016/j.cpc.2014.04.012. arXiv: 1310.1921 [hep-ph].

[242] Thomas Hahn. «Generating Feynman diagrams and amplitudes with FeynArts 3.» In: *Comput. Phys. Commun.* 140 (2001), pp. 418–431. DOI: 10.1016/S0010-4655(01)00290-9. arXiv: hep-ph/0012260 [hep-ph].

[243] T. Hahn and M. Perez-Victoria. «Automatized one loop calculations in four-dimensions and D-dimensions.» In: *Comput. Phys. Commun.* 118 (1999), pp. 153–165. DOI: 10.1016/S0010-4655(98)00173-8. arXiv: hep-ph/9807565 [hep-ph].

[244] Paul W. Angel, Yi Cai, Nicholas L. Rodd, Michael A. Schmidt, and Raymond R. Volkas. «Testable two-loop radiative neutrino mass model based on an $LLQd^cQd^c$ effective operator.» In: *JHEP* 10 (2013), p. 118. DOI: 10.1007/JHEP10(2013)118. arXiv: 1308.0463 [hep-ph].

[245] Juan Herrero-Garcia, Emiliano Molinaro, and Michael A. Schmidt. «Dark matter direct detection of a fermionic singlet at one loop.» In: *Eur. Phys. J.* C78.6 (2018), p. 471. DOI: 10.1140/epjc/s10052-018-5935-5. arXiv: 1803.05660 [hep-ph].

[246] Claudia Hagedorn, Juan Herrero-García, Emiliano Molinaro, and Michael A. Schmidt. «Phenomenology of the Generalised Scotogenic Model with Fermionic Dark Matter.» In: *JHEP* 11 (2018), p. 103. DOI: 10.1007/JHEP11(2018)103. arXiv: 1804.04117 [hep-ph].

[247] K. S. Babu, Christopher F. Kolda, and John March-Russell. «Implications of generalized Z - Z-prime mixing.» In: *Phys. Rev.* D57 (1998), pp. 6788–6792. DOI: 10.1103/PhysRevD.57.6788. arXiv: hep-ph/9710441 [hep-ph].

[248] Roni Harnik, Joachim Kopp, and Pedro A. N. Machado. «Exploring nu Signals in Dark Matter Detectors.» In: *JCAP* 1207 (2012), p. 026. DOI: 10.1088/1475-7516/2012/07/026. arXiv: 1202.6073 [hep-ph].

[249] Martin Bauer, Patrick Foldenauer, and Joerg Jaeckel. «Hunting All the Hidden Photons.» In: *JHEP* 07 (2018), p. 094. DOI: 10.1007/JHEP07(2018)094. arXiv: 1803.05466 [hep-ph].

[250] J. P. Lees et al. «Search for Invisible Decays of a Dark Photon Produced in e^+e^- Collisions at BaBar.» In: *Phys. Rev. Lett.* 119.13 (2017), p. 131804. DOI: 10.1103/PhysRevLett.119.131804. arXiv: 1702.03327 [hep-ex].

[251] Anson Hook, Eder Izaguirre, and Jay G. Wacker. «Model Independent Bounds on Kinetic Mixing.» In: *Adv. High Energy Phys.* 2011 (2011), p. 859762. DOI: 10.1155/2011/859762. arXiv: 1006.0973 [hep-ph].

[252] L. Verde, T. Treu, and A. G. Riess. «Tensions between the Early and the Late Universe.» In: *Nature Astron.* 3 (July 2019), p. 891. DOI: 10.1038/s41550-019-0902-0. arXiv: 1907.10625 [astro-ph.CO].

[253] Kenneth C. Wong et al. «HoLiCOW – XIII. A 2.4 per cent measurement of Ho from lensed quasars: 5.3σ tension between early- and late-Universe probes.» In: *Mon. Not. Roy. Astron. Soc.* 498.1 (2020), pp. 1420–1439. DOI: 10.1093/mnras/stz3094. arXiv: 1907.04869 [astro-ph.CO].

[254] Adam G. Riess, Stefano Casertano, Wenlong Yuan, Lucas M. Macri, and Dan Scolnic. «Large Magellanic Cloud Cepheid Standards Provide a 1% Foundation for the Determination of the Hubble Constant and Stronger Evidence for Physics beyond ΛCDM.» In: *Astrophys. J.* 876.1 (2019), p. 85. DOI: 10.3847/1538-4357/ab1422. arXiv: 1903.07603 [astro-ph.CO].

[255] Eleonora Di Valentino, Olga Mena, Supriya Pan, Luca Visinelli, Weiqiang Yang, Alessandro Melchiorri, David F. Mota, Adam G. Riess, and Joseph Silk. «In the Realm of the Hubble tension – a Review of Solutions.» In: (Mar. 2021). arXiv: 2103.01183 [astro-ph.CO].

[256] Miguel Escudero and Samuel J. Witte. «A CMB search for the neutrino mass mechanism and its relation to the Hubble tension.» In: *Eur. Phys. J. C* 80.4 (2020), p. 294. DOI: 10.1140/epjc/s10052-020-7854-5. arXiv: 1909.04044 [astro-ph.CO].

[257] Miguel Escudero and Samuel J. Witte. «The Hubble Tension as a Hint of Leptogenesis and Neutrino Mass Generation.» In: (Mar. 2021). arXiv: 2103.03249 [hep-ph].

[258] Federica Bazzocchi. «Minimal Dynamical Inverse See Saw.» In: *Phys. Rev. D* 83 (2011), p. 093009. DOI: 10.1103/PhysRevD.83.093009. arXiv: 1011.6299 [hep-ph].

[259] A. G. Dias, C. A. de S. Pires, and P. S. Rodrigues da Silva. «How the Inverse See-Saw Mechanism Can Reveal Itself Natural, Canonical and Independent of the Right-Handed Neutrino Mass.» In: *Phys. Rev. D* 84 (2011), p. 053011. DOI: 10.1103/PhysRevD.84.053011. arXiv: 1107.0739 [hep-ph].

[260] Valentina De Romeri, Enrique Fernandez-Martinez, Julia Gehrlein, Pedro A. N. Machado, and Viviana Niro. «Dark Matter and the elusive Z' in a dynamical Inverse Seesaw scenario.» In: *JHEP* 10 (2017), p. 169. DOI: 10.1007/JHEP10(2017)169. arXiv: 1707.08606 [hep-ph].

[261] Enrico Bertuzzo, Sudip Jana, Pedro A. N. Machado, and Renata Zukanovich Funchal. «Neutrino Masses and Mixings Dynamically Generated by a Light Dark Sector.» In: *Phys. Lett. B* 791 (2019), pp. 210–214. DOI: 10.1016/j.physletb.2019.02.023. arXiv: 1808.02500 [hep-ph].

[262] Peter Ballett, Matheus Hostert, and Silvia Pascoli. «Neutrino Masses from a Dark Neutrino Sector below the Electroweak Scale.» In: *Phys. Rev. D* 99.9 (2019), p. 091701. DOI: 10.1103/PhysRevD.99.091701. arXiv: 1903.07590 [hep-ph].

[263] Peter Ballett, Matheus Hostert, and Silvia Pascoli. «Dark Neutrinos and a Three Portal Connection to the Standard Model.» In: *Phys. Rev. D* 101.11 (2020), p. 115025. DOI: 10.1103/PhysRevD.101.115025. arXiv: 1903.07589 [hep-ph].

[264] Julia Gehrlein and Mathias Pierre. «A testable hidden-sector model for Dark Matter and neutrino masses.» In: *JHEP* 02 (2020), p. 068. DOI: 10.1007/JHEP02(2020)068. arXiv: 1912.06661 [hep-ph].

[265] Sanjoy Mandal, Rahul Srivastava, and José W. F. Valle. «Electroweak symmetry breaking in the inverse seesaw mechanism.» In: *JHEP* 03 (2021), p. 212. DOI: 10.1007/JHEP03(2021)212. arXiv: 2009.10116 [hep-ph].

[266] Sanjoy Mandal, Jorge C. Romão, Rahul Srivastava, and José W. F. Valle. «Dynamical inverse seesaw mechanism as a simple benchmark for electroweak breaking and Higgs boson studies.» In: (Mar. 2021). arXiv: 2103.02670 [hep-ph].

[267] Xinyi Zhang and Shun Zhou. «Inverse Seesaw Model with a Modular S_4 Symmetry: Lepton Flavor Mixing and Warm Dark Matter.» In: (June 2021). arXiv: 2106.03433 [hep-ph].

[268] Arindam Das, Srubabati Goswami, Vishnudath K. N., and Tanmay Kumar Poddar. «Freeze-in sterile neutrino dark matter in a class of U(1)′ models with inverse seesaw.» In: (Apr. 2021). arXiv: 2104.13986 [hep-ph].

[269] Asmaa Abada, Giorgio Arcadi, and Michele Lucente. «Dark Matter in the minimal Inverse Seesaw mechanism.» In: *JCAP* 10 (2014), p. 001. DOI: 10.1088/1475-7516/2014/10/001. arXiv: 1406.6556 [hep-ph].

[270] Asmaa Abada and Michele Lucente. «Looking for the minimal inverse seesaw realisation.» In: *Nucl. Phys. B* 885 (2014), pp. 651–678. DOI: 10.1016/j.nuclphysb.2014.06.003. arXiv: 1401.1507 [hep-ph].

[271] Sami Boulebnane, Julian Heeck, Anne Nguyen, and Daniele Teresi. «Cold light dark matter in extended seesaw models.» In: *JCAP* 04 (2018), p. 006. DOI: 10.1088/1475-7516/2018/04/006. arXiv: 1709.07283 [hep-ph].

[272] Scott Dodelson and Lawrence M. Widrow. «Sterile-neutrinos as dark matter.» In: *Phys. Rev. Lett.* 72 (1994), pp. 17–20. DOI: 10.1103/PhysRevLett.72.17. arXiv: hep-ph/9303287.

[273] Xiang-Dong Shi and George M. Fuller. «A New dark matter candidate: Nonthermal sterile neutrinos.» In: *Phys. Rev. Lett.* 82 (1999), pp. 2832–2835. DOI: 10.1103/PhysRevLett.82.2832. arXiv: astro-ph/9810076.

[274] J. Ghiglieri and M. Laine. «Sterile neutrino dark matter via GeV-scale leptogenesis?» In: *JHEP* 07 (2019), p. 078. DOI: 10.1007/JHEP07(2019)078. arXiv: 1905.08814 [hep-ph].

[275] J. Ghiglieri and M. Laine. «Sterile neutrino dark matter via coinciding resonances.» In: *JCAP* 07 (2020), p. 012. DOI: 10.1088/1475-7516/2020/07/012. arXiv: 2004.10766 [hep-ph].

[276] Brandon M. Roach, Kenny C. Y. Ng, Kerstin Perez, John F. Beacom, Shunsaku Horiuchi, Roman Krivonos, and Daniel R. Wik. «NuSTAR Tests of Sterile-Neutrino Dark Matter: New Galactic Bulge Observations and Combined Impact.» In: *Phys. Rev. D* 101.10 (2020), p. 103011. DOI: 10.1103/PhysRevD.101.103011. arXiv: 1908.09037 [astro-ph.HE].

[277] Kalliopi Petraki and Alexander Kusenko. «Dark-matter sterile neutrinos in models with a gauge singlet in the Higgs sector.» In: *Phys. Rev. D* 77 (2008), p. 065014. DOI: 10.1103/PhysRevD.77.065014. arXiv: 0711.4646 [hep-ph].

[278] Alexander Merle, Viviana Niro, and Daniel Schmidt. «New Production Mechanism for keV Sterile Neutrino Dark Matter by Decays of Frozen-In Scalars.» In: *JCAP* 03 (2014), p. 028. DOI: 10.1088/1475-7516/2014/03/028. arXiv: 1306.3996 [hep-ph].

[279] Marco Drewes and Jin U Kang. «Sterile neutrino Dark Matter production from scalar decay in a thermal bath.» In: *JHEP* 05 (2016), p. 051. DOI: 10.1007/JHEP05(2016)051. arXiv: 1510.05646 [hep-ph].

[280] M. Drewes et al. «A White Paper on keV Sterile Neutrino Dark Matter.» In: *JCAP* 01 (2017), p. 025. DOI: 10.1088/1475-7516/2017/01/025. arXiv: 1602.04816 [hep-ph].

[281] Valentina De Romeri, Dimitrios Karamitros, Oleg Lebedev, and Takashi Toma. «Neutrino dark matter and the Higgs portal: improved freeze-in analysis.» In: *JHEP* 10 (2020), p. 137. DOI: 10.1007/JHEP10(2020)137. arXiv: 2003.12606 [hep-ph].

[282] K. Moffat, S. Pascoli, and C. Weiland. «Equivalence between massless neutrinos and lepton number conservation in fermionic singlet extensions of the Standard Model.» In: (Dec. 2017). arXiv: 1712.07611 [hep-ph].

[283] George Lazarides, Q. Shafi, and C. Wetterich. «Proton Lifetime and Fermion Masses in an SO(10) Model.» In: *Nucl. Phys. B* 181 (1981), pp. 287–300. DOI: 10.1016/0550-3213(81)90354-0.

[284] Rabindra N. Mohapatra and Goran Senjanovic. «Neutrino Masses and Mixings in Gauge Models with Spontaneous Parity Violation.» In: *Phys. Rev. D* 23 (1981), p. 165. DOI: 10.1103/PhysRevD.23.165.

[285] Evgeny K. Akhmedov, Z. G. Berezhiani, R. N. Mohapatra, and G. Senjanovic. «Planck scale effects on the majoron.» In: *Phys. Lett. B* 299 (1993), pp. 90–93. DOI: 10.1016/0370-2693(93)90887-N. arXiv: hep-ph/9209285.

[286] Louis Lello, Daniel Boyanovsky, and Robert D. Pisarski. «Production of heavy sterile neutrinos from vector boson decay at electroweak temperatures.» In: *Phys. Rev. D* 95.4 (2017), p. 043524. DOI: 10.1103/PhysRevD.95.043524. arXiv: 1609.07647 [hep-ph].

[287] Asmaa Abada, Giorgio Arcadi, Valerie Domcke, Marco Drewes, Juraj Klaric, and Michele Lucente. «Low-scale leptogenesis with three heavy neutrinos.» In: *JHEP* 01 (2019), p. 164. DOI: 10.1007/JHEP01(2019)164. arXiv: 1810.12463 [hep-ph].

[288] Lawrence J. Hall, Karsten Jedamzik, John March-Russell, and Stephen M. West. «Freeze-In Production of FIMP Dark Matter.» In: *JHEP* 03 (2010), p. 080. DOI: 10.1007/JHEP03(2010)080. arXiv: 0911.1120 [hep-ph].

[289] Joshua W. Foster, Marius Kongsore, Christopher Dessert, Yujin Park, Nicholas L. Rodd, Kyle Cranmer, and Benjamin R. Safdi. «A deep search for decaying dark matter with XMM-Newton blank-sky observations.» In: (Feb. 2021). arXiv: 2102.02207 [astro-ph.CO].

[290] Alexey Boyarsky, Denys Malyshev, Andrey Neronov, and Oleg Ruchayskiy. «Constraining DM properties with SPI.» In: *Mon. Not. Roy. Astron. Soc.* 387 (2008), p. 1345. DOI: 10.1111/j.1365-2966.2008.13003.x. arXiv: 0710.4922 [astro-ph].

[291] Guillermo Ballesteros, Marcos A.G. Garcia, and Mathias Pierre. «How warm are non-thermal relics? Lyman-α bounds on out-of-equilibrium dark matter.» In: (Nov. 2020). arXiv: 2011.13458 [hep-ph].

[292] Vijay K. Narayanan, David N. Spergel, Romeel Dave, and Chung-Pei Ma. «Constraints on the mass of warm dark matter particles and the shape of the linear power spectrum from the Lyα forest.» In: *Astrophys. J. Lett.* 543 (2000), pp. L103–L106. DOI: 10.1086/317269. arXiv: astro-ph/0005095.

[293] Matteo Viel, Julien Lesgourgues, Martin G. Haehnelt, Sabino Matarrese, and Antonio Riotto. «Constraining warm dark matter candidates including sterile neutrinos and light gravitinos with WMAP and the Lyman-alpha forest.» In: *Phys. Rev. D* 71 (2005), p. 063534. DOI: 10.1103/PhysRevD.71.063534. arXiv: astro-ph/0501562.

[294] Matteo Viel, George D. Becker, James S. Bolton, and Martin G. Haehnelt. «Warm dark matter as a solution to the small scale crisis: New constraints from high redshift Lyman-α forest data.» In: *Phys. Rev. D* 88 (2013), p. 043502. DOI: 10.1103/PhysRevD.88.043502. arXiv: 1306.2314 [astro-ph.CO].

[295] Julien Baur, Nathalie Palanque-Delabrouille, Christophe Yèche, Christophe Magneville, and Matteo Viel. «Lyman-alpha Forests cool Warm Dark Matter.» In: *JCAP* 08 (2016), p. 012. DOI: 10.1088/1475-7516/2016/08/012. arXiv: 1512.01981 [astro-ph.CO].

[296] Vid Iršič et al. «New Constraints on the free-streaming of warm dark matter from intermediate and small scale Lyman-α forest data.» In: *Phys. Rev. D* 96.2 (2017), p. 023522. DOI: 10.1103/PhysRevD.96.023522. arXiv: 1702.01764 [astro-ph.CO].

[297] Nathalie Palanque-Delabrouille, Christophe Yèche, Nils Schöneberg, Julien Lesgourgues, Michael Walther, Solène Chabanier, and Eric Armengaud. «Hints, neutrino bounds and WDM constraints from SDSS DR14 Lyman-α and Planck full-survey data.» In: *JCAP* 04 (2020), p. 038. DOI: 10.1088/1475-7516/2020/04/038. arXiv: 1911.09073 [astro-ph.CO].

[298] A. Garzilli, O. Ruchayskiy, A. Magalich, and A. Boyarsky. «How warm is too warm? Towards robust Lyman-α forest bounds on warm dark matter.» In: (Dec. 2019). arXiv: 1912.09397 [astro-ph.CO].

[299] Kyu Jung Bae, Ayuki Kamada, Seng Pei Liew, and Keisuke Yanagi. «Light axinos from freeze-in: production processes, phase space distributions, and Ly-α forest constraints.» In: *JCAP* 01 (2018), p. 054. DOI: 10.1088/1475-7516/2018/01/054. arXiv: 1707.06418 [hep-ph].

[300] Ayuki Kamada and Keisuke Yanagi. «Constraining FIMP from the structure formation of the Universe: analytic mapping from m_{WDM}.» In: *JCAP* 11 (2019), p. 029. DOI: 10.1088/1475-7516/2019/11/029. arXiv: 1907.04558 [hep-ph].

[301] Julian Heeck and Daniele Teresi. «Cold keV dark matter from decays and scatterings.» In: *Phys. Rev. D* 96.3 (2017), p. 035018. DOI: 10.1103/PhysRevD.96.035018. arXiv: 1706.09909 [hep-ph].

[302] Francesco D'Eramo and Alessandro Lenoci. «Lower Mass Bounds on FIMPs.» In: (Dec. 2020). arXiv: 2012.01446 [hep-ph].

[303] «Combination of searches for invisible Higgs boson decays with the ATLAS experiment.» In: (Oct. 2020).

[304] Steven Weinberg. «Goldstone Bosons as Fractional Cosmic Neutrinos.» In: *Phys. Rev. Lett.* 110.24 (2013), p. 241301. DOI: 10.1103/PhysRevLett.110.241301. arXiv: 1305.1971 [astro-ph.CO].

[305] Albert M Sirunyan et al. «Search for invisible decays of a Higgs boson produced through vector boson fusion in proton-proton collisions at $\sqrt{s} = 13$ TeV.» In: *Phys. Lett. B* 793 (2019), pp. 520–551. DOI: 10.1016/j.physletb.2019.04.025. arXiv: 1809.05937 [hep-ex].

[306] Evgeny K. Akhmedov, V. A. Rubakov, and A. Yu. Smirnov. «Baryogenesis via neutrino oscillations.» In: *Phys. Rev. Lett.* 81 (1998), pp. 1359–1362. DOI: 10.1103/PhysRevLett.81.1359. arXiv: hep-ph/9803255 [hep-ph].

[307] Takehiko Asaka and Mikhail Shaposhnikov. «The nuMSM, dark matter and baryon asymmetry of the universe.» In: *Phys. Lett.* B620 (2005), pp. 17–26. DOI: 10.1016/j.physletb.2005.06.020. arXiv: hep-ph/0505013 [hep-ph].

[308] Mikhail Shaposhnikov. «The nuMSM, leptonic asymmetries, and properties of singlet fermions.» In: *JHEP* 08 (2008), p. 008. DOI: 10.1088/1126-6708/2008/08/008. arXiv: 0804.4542 [hep-ph].

[309] Laurent Canetti and Mikhail Shaposhnikov. «Baryon Asymmetry of the Universe in the NuMSM.» In: *JCAP* 09 (2010), p. 001. DOI: 10.1088/1475-7516/2010/09/001. arXiv: 1006.0133 [hep-ph].

[310] Asmaa Abada, Giorgio Arcadi, Valerie Domcke, and Michele Lucente. «Lepton number violation as a key to low-scale leptogenesis.» In: *JCAP* 11 (2015), p. 041. DOI: 10.1088/1475-7516/2015/11/041. arXiv: 1507.06215 [hep-ph].

[311] P. Hernández, M. Kekic, J. López-Pavón, J. Racker, and N. Rius. «Leptogenesis in GeV scale seesaw models.» In: *JHEP* 10 (2015), p. 067. DOI: 10.1007/JHEP10(2015)067. arXiv: 1508.03676 [hep-ph].

[312] P. Hernández, M. Kekic, J. López-Pavón, J. Racker, and J. Salvado. «Testable Baryogenesis in Seesaw Models.» In: *JHEP* 08 (2016), p. 157. DOI: 10.1007/JHEP08(2016)157. arXiv: 1606.06719 [hep-ph].

[313] M. Drewes, B. Garbrecht, P. Hernandez, M. Kekic, J. Lopez-Pavon, J. Racker, N. Rius, J. Salvado, and D. Teresi. «ARS Leptogenesis.» In: *Int. J. Mod. Phys. A* 33.05n06 (2018), p. 1842002. DOI: 10.1142/S0217751X18420022. arXiv: 1711.02862 [hep-ph].

[314] Asmaa Abada, Giorgio Arcadi, Valerie Domcke, and Michele Lucente. «Neutrino masses, leptogenesis and dark matter from small lepton number violation?» In: *JCAP* 12 (2017), p. 024. DOI: 10.1088/1475-7516/2017/12/024. arXiv: 1709.00415 [hep-ph].

[315] E.J. Chun et al. «Probing Leptogenesis.» In: *Int. J. Mod. Phys. A* 33.05n06 (2018), p. 1842005. DOI: 10.1142/S0217751X18420058. arXiv: 1711.02865 [hep-ph].

[316] Andrea Caputo, Pilar Hernandez, and Nuria Rius. «Leptogenesis from oscillations and dark matter.» In: *Eur. Phys. J. C* 79.7 (2019), p. 574. DOI: 10.1140/epjc/s10052-019-7083-y. arXiv: 1807.03309 [hep-ph].

[317] Werner Bernreuther. «CP violation and baryogenesis.» In: *Lect. Notes Phys.* 591 (2002), pp. 237–293. arXiv: hep-ph/0205279.

[318] Andrew G. Cohen, A. De Rujula, and S. L. Glashow. «A Matter - antimatter universe?» In: *Astrophys. J.* 495 (1998), pp. 539–549. DOI: 10.1086/305328. arXiv: astro-ph/9707087.

[319] Alan H. Guth. «Inflationary universe: A possible solution to the horizon and flatness problems.» In: *Phys. Rev. D* 23 (2 1981), pp. 347–356. DOI: 10.1103/PhysRevD.23.347. URL: https://link.aps.org/doi/10.1103/PhysRevD.23.347.

[320] A. D. Sakharov. «Violation of CP Invariance, C asymmetry, and baryon asymmetry of the universe.» In: *Pisma Zh. Eksp. Teor. Fiz.* 5 (1967). [JETP Lett.5,24(1967); Sov. Phys. Usp.34,no.5,392(1991); Usp. Fiz. Nauk161,no.5,61(1991)], pp. 32–35. DOI: 10.1070/PU1991v034n05ABEH002497.

[321] D. Toussaint, S. B. Treiman, Frank Wilczek, and A. Zee. «Matter-antimatter accounting, thermodynamics, and black-hole radiation.» In: *Phys. Rev. D* 19 (4 1979), pp. 1036–1045. DOI: 10.1103/PhysRevD.19.1036. URL: https://link.aps.org/doi/10.1103/PhysRevD.19.1036.

[322] G. 't Hooft. «Symmetry Breaking through Bell-Jackiw Anomalies.» In: *Phys. Rev. Lett.* 37 (1 1976), pp. 8–11. DOI: 10.1103/PhysRevLett.37.8. URL: https://link.aps.org/doi/10.1103/PhysRevLett.37.8.

[323] Dmitri Diakonov, Maxim V. Polyakov, Peter Sieber, Jorg Schaldach, and Klaus Goeke. «Sphaleron transitions in the minimal standard model and the upper bound for the Higgs mass.» In: *Phys. Rev. D* 53 (1996), pp. 3366–3391. DOI: 10.1103/PhysRevD.53.3366. arXiv: hep-ph/9502245.

[324] James M. Cline. «TASI Lectures on Early Universe Cosmology: Inflation, Baryogenesis and Dark Matter.» In: *PoS* TASI2018 (2019), p. 001. arXiv: 1807.08749 [hep-ph].

[325] Michela D'Onofrio, Kari Rummukainen, and Anders Tranberg. «Sphaleron Rate in the Minimal Standard Model.» In: *Phys. Rev. Lett.* 113.14 (2014), p. 141602. DOI: 10.1103/PhysRevLett.113.141602. arXiv: 1404.3565 [hep-ph].

[326] V. A. Kuzmin, V. A. Rubakov, and M. E. Shaposhnikov. «On the Anomalous Electroweak Baryon Number Nonconservation in the Early Universe.» In: *Phys. Lett.* 155B (1985), p. 36. DOI: 10.1016/0370-2693(85)91028-7.

[327] M. E. Shaposhnikov. «Baryon Asymmetry of the Universe in Standard Electroweak Theory.» In: *Nucl. Phys.* B287 (1987), pp. 757–775. DOI: 10.1016/0550-3213(87)90127-1.

[328] Kaori Fuyuto. «Electroweak Baryogenesis.» In: *Electroweak Baryogenesis and Its Phenomenology*. Singapore: Springer Singapore, 2018, pp. 9–33. ISBN: 978-981-13-1008-9. DOI: 10.1007/978-981-13-1008-9_2. URL: https://doi.org/10.1007/978-981-13-1008-9_2.

[329] C. Jarlskog. «Commutator of the Quark Mass Matrices in the Standard Electroweak Model and a Measure of Maximal CP Violation.» In: *Phys. Rev. Lett.* 55 (1985), p. 1039. DOI: 10.1103/PhysRevLett.55.1039.

[330] M. B. Gavela, M. Lozano, J. Orloff, and O. Pene. «Standard model CP violation and baryon asymmetry. Part 1: Zero temperature.» In: *Nucl. Phys.* B430 (1994), pp. 345–381. DOI: 10.1016/0550-3213(94)00409-9. arXiv: hep-ph/9406288 [hep-ph].

[331] Georges Aad et al. «Observation of a new particle in the search for the Standard Model Higgs boson with the ATLAS detector at the LHC.» In: *Phys. Lett.* B716 (2012), pp. 1–29. DOI: 10.1016/j.physletb.2012.08.020. arXiv: 1207.7214 [hep-ex].

[332] Serguei Chatrchyan et al. «Observation of a New Boson at a Mass of 125 GeV with the CMS Experiment at the LHC.» In: *Phys. Lett. B* 716 (2012), pp. 30–61. DOI: 10.1016/j.physletb.2012.08.021. arXiv: 1207.7235 [hep-ex].

[333] Giuseppe Degrassi, Stefano Di Vita, Joan Elias-Miro, Jose R. Espinosa, Gian F. Giudice, Gino Isidori, and Alessandro Strumia. «Higgs mass and vacuum stability in the Standard Model at NNLO.» In: *JHEP* 08 (2012), p. 098. DOI: 10.1007/JHEP08(2012)098. arXiv: 1205.6497 [hep-ph].

[334] Arcadi Santamaria. «Masses, mixings, Yukawa couplings and their symmetries.» In: *Phys. Lett.* B305 (1993), pp. 90–97. DOI: 10.1016/0370-2693(93)91110-9. arXiv: hep-ph/9302301 [hep-ph].

[335] Jeffrey A. Harvey and Michael S. Turner. «Cosmological baryon and lepton number in the presence of electroweak fermion number violation.» In: *Phys. Rev.* D42 (1990), pp. 3344–3349. DOI: 10.1103/PhysRevD.42.3344.

[336] Chee Sheng Fong, Enrico Nardi, and Antonio Riotto. «Leptogenesis in the Universe.» In: *Adv. High Energy Phys.* 2012 (2012), p. 158303. DOI: 10.1155/2012/158303. arXiv: 1301.3062 [hep-ph].

[337] S. Pascoli, S. T. Petcov, and Antonio Riotto. «Leptogenesis and Low Energy CP Violation in Neutrino Physics.» In: *Nucl. Phys.* B774 (2007), pp. 1–52. DOI: 10.1016/j.nuclphysb.2007.02.019. arXiv: hep-ph/0611338 [hep-ph].

[338] K. Moffat, S. Pascoli, S. T. Petcov, and J. Turner. «Leptogenesis from Low Energy *CP* Violation.» In: *JHEP* 03 (2019), p. 034. DOI: 10.1007/JHEP03(2019)034. arXiv: 1809.08251 [hep-ph].

[339] Vincenzo Cirigliano, Gino Isidori, and Valentina Porretti. «CP violation and Leptogenesis in models with Minimal Lepton Flavour Violation.» In: *Nucl. Phys.* B763 (2007), pp. 228–246. DOI: 10.1016/j.nuclphysb.2006.11.015. arXiv: hep-ph/0607068 [hep-ph].

[340] L. Merlo and S. Rosauro-Alcaraz. «Predictive Leptogenesis from Minimal Lepton Flavour Violation.» In: *JHEP* 07 (2018), p. 036. DOI: 10.1007/JHEP07(2018)036. arXiv: 1801.03937 [hep-ph].

[341] Andrew G. Cohen and David B. Kaplan. «Thermodynamic Generation of the Baryon Asymmetry.» In: *Phys. Lett.* B199 (1987), pp. 251–258. DOI: 10.1016/0370-2693(87)91369-4.

[342] Andrew G. Cohen, David B. Kaplan, and Ann E. Nelson. «Baryogenesis at the weak phase transition.» In: *Nucl. Phys.* B349 (1991), pp. 727–742. DOI: 10.1016/0550-3213(91)90395-E.

[343] Andrew G. Cohen, David B. Kaplan, and Ann E. Nelson. «WEAK SCALE BARYOGENESIS.» In: *Phys. Lett.* B245 (1990), pp. 561–564. DOI: 10.1016/0370-2693(90)90690-8.

[344] A. E. Nelson, D. B. Kaplan, and Andrew G. Cohen. «Why there is something rather than nothing: Matter from weak interactions.» In: *Nucl. Phys.* B373 (1992), pp. 453–478. DOI: 10.1016/0550-3213(92)90440-M.

[345] Michael Dine, Patrick Huet, Robert L. Singleton Jr, and Leonard Susskind. «Creating the baryon asymmetry at the electroweak phase transition.» In: *Phys. Lett.* B257 (1991), pp. 351–356. DOI: 10.1016/0370-2693(91)91905-B.

[346] Michael Dine, Patrick Huet, and Robert L. Singleton Jr. «Baryogenesis at the electroweak scale.» In: *Nucl. Phys.* B375 (1992), pp. 625–648. DOI: 10.1016/0550-3213(92)90113-P.

[347] Greg W. Anderson and Lawrence J. Hall. «The Electroweak phase transition and baryogenesis.» In: *Phys. Rev.* D45 (1992), pp. 2685–2698. DOI: 10.1103/PhysRevD.45.2685.

[348] J. R. Espinosa and M. Quiros. «The Electroweak phase transition with a singlet.» In: *Phys. Lett.* B305 (1993), pp. 98–105. DOI: 10.1016/0370-2693(93)91111-Y. arXiv: hep-ph/9301285 [hep-ph].

[349] Jose R. Espinosa, Thomas Konstandin, and Francesco Riva. «Strong Electroweak Phase Transitions in the Standard Model with a Singlet.» In: *Nucl. Phys.* B854 (2012), pp. 592–630. DOI: 10.1016/j.nuclphysb.2011.09.010. arXiv: 1107.5441 [hep-ph].

[350] A. Tofighi, O. N. Ghodsi, and M. Saeedhoseini. «Phase transition in multi-scalar-singlet extensions of the Standard Model.» In: *Phys. Lett.* B748 (2015), pp. 208–211. DOI: 10.1016/j.physletb.2015.07.009. arXiv: 1510.00791 [hep-ph].

[351] Stefano Profumo, Michael J. Ramsey-Musolf, and Gabe Shaughnessy. «Singlet Higgs phenomenology and the electroweak phase transition.» In: *JHEP* 08 (2007), p. 010. DOI: 10.1088/1126-6708/2007/08/010. arXiv: 0705.2425 [hep-ph].

[352] Jose M. No and Michael Ramsey-Musolf. «Probing the Higgs Portal at the LHC Through Resonant di-Higgs Production.» In: *Phys. Rev.* D89.9 (2014), p. 095031. DOI: 10.1103/PhysRevD.89.095031. arXiv: 1310.6035 [hep-ph].

[353] Stefano Profumo, Michael J. Ramsey-Musolf, Carroll L. Wainwright, and Peter Winslow. «Singlet-catalyzed electroweak phase transitions and precision Higgs boson studies.» In: *Phys. Rev.* D91.3 (2015), p. 035018. DOI: 10.1103/PhysRevD.91.035018. arXiv: 1407.5342 [hep-ph].

[354] Jonathan Kozaczuk, Stefano Profumo, Laurel Stephenson Haskins, and Carroll L. Wainwright. «Cosmological Phase Transitions and their Properties in the NMSSM.» In: *JHEP* 01 (2015), p. 144. DOI: 10.1007/JHEP01(2015)144. arXiv: 1407.4134 [hep-ph].

[355] G. C. Dorsch, S. J. Huber, K. Mimasu, and J. M. No. «The Higgs Vacuum Uplifted: Revisiting the Electroweak Phase Transition with a Second Higgs Doublet.» In: *JHEP* 12 (2017), p. 086. DOI: 10.1007/JHEP12(2017)086. arXiv: 1705.09186 [hep-ph].

[356] T. Huang, J. M. No, L. Pernié, M. Ramsey-Musolf, A. Safonov, M. Spannowsky, and P. Winslow. «Resonant di-Higgs boson production in the $b\bar{b}WW$ channel: Probing the electroweak phase transition at the LHC.» In: *Phys. Rev.* D96.3 (2017), p. 035007. DOI: 10.1103/PhysRevD.96.035007. arXiv: 1701.04442 [hep-ph].

[357] V. Andreev et al. «Improved limit on the electric dipole moment of the electron.» In: *Nature* 562 (Oct. 2018), pp. 355–360. DOI: 10.1038/s41586-018-0599-8.

[358] Eleanor Hall, Thomas Konstandin, Robert McGehee, Hitoshi Murayama, and Géraldine Servant. «Baryogenesis From a Dark First-Order Phase Transition.» In: *JHEP* 04 (2020), p. 042. DOI: 10.1007/JHEP04(2020)042. arXiv: 1910.08068 [hep-ph].

[359] Marcela Carena, Mariano Quirós, and Yue Zhang. «Electroweak Baryogenesis from Dark-Sector CP Violation.» In: *Phys. Rev. Lett.* 122.20 (2019), p. 201802. DOI: 10.1103/PhysRevLett.122.201802. arXiv: 1811.09719 [hep-ph].

[360] Huai-Ke Guo, Ying-Ying Li, Tao Liu, Michael Ramsey-Musolf, and Jing Shu. «Lepton-Flavored Electroweak Baryogenesis.» In: *Phys. Rev.* D96.11 (2017), p. 115034. DOI: 10.1103/PhysRevD.96.115034. arXiv: 1609.09849 [hep-ph].

[361] K. Eguchi et al. «First results from KamLAND: Evidence for reactor anti-neutrino disappearance.» In: *Phys. Rev. Lett.* 90 (2003), p. 021802. DOI: 10.1103/PhysRevLett.90.021802. arXiv: hep-ex/0212021.

[362] Andrew J. Long, Andrea Tesi, and Lian-Tao Wang. «Baryogenesis at a Lepton-Number-Breaking Phase Transition.» In: *JHEP* 10 (2017), p. 095. DOI: 10.1007/JHEP10(2017)095. arXiv: 1703.04902 [hep-ph].

[363] Lawrence J. Hall, Hitoshi Murayama, and Gilad Perez. «Electroweak baryogenesis from late neutrino masses.» In: *Phys. Rev. Lett.* 95 (2005), p. 111301. DOI: 10.1103/PhysRevLett.95.111301. arXiv: hep-ph/0504248 [hep-ph].

[364] P. Hernandez and N. Rius. «Neutral heavy leptons and electroweak baryogenesis.» In: *Nucl. Phys.* B495 (1997), pp. 57–80. DOI: 10.1016/S0550-3213(97)00193-4. arXiv: hep-ph/9611227 [hep-ph].

[365] Apostolos Pilaftsis. «Radiatively induced neutrino masses and large Higgs neutrino couplings in the standard model with Majorana fields.» In: *Z. Phys. C* 55 (1992), pp. 275–282. DOI: 10.1007/BF01482590. arXiv: hep-ph/9901206.

[366] Walter Grimus and Luis Lavoura. «One-loop corrections to the seesaw mechanism in the multi-Higgs-doublet standard model.» In: *Phys. Lett. B* 546 (2002), pp. 86–95. DOI: 10.1016/S0370-2693(02)02672-2. arXiv: hep-ph/0207229.

[367] J. Lopez-Pavon, S. Pascoli, and Chan-fai Wong. «Can heavy neutrinos dominate neutrinoless double beta decay?» In: *Phys. Rev. D* 87.9 (2013), p. 093007. DOI: 10.1103/PhysRevD.87.093007. arXiv: 1209.5342 [hep-ph].

[368] Elizabeth Ellen Jenkins and Aneesh V. Manohar. «Rephasing Invariants of Quark and Lepton Mixing Matrices.» In: *Nucl. Phys.* B792 (2008), pp. 187–205. DOI: 10.1016/j.nuclphysb.2007.09.031. arXiv: 0706.4313 [hep-ph].

[369] Elizabeth Ellen Jenkins and Aneesh V. Manohar. «Algebraic Structure of Lepton and Quark Flavor Invariants and CP Violation.» In: *JHEP* 10 (2009), p. 094. DOI: 10.1088/1126-6708/2009/10/094. arXiv: 0907.4763 [hep-ph].

[370] Robert E. Shrock. «General Theory of Weak Leptonic and Semileptonic Decays. 1. Leptonic Pseudoscalar Meson Decays, with Associated Tests For, and Bounds on, Neutrino Masses and Lepton Mixing.» In: *Phys. Rev.* D24 (1981), p. 1232. DOI: 10.1103/PhysRevD.24.1232.

[371] Robert E. Shrock. «General Theory of Weak Processes Involving Neutrinos. 2. Pure Leptonic Decays.» In: *Phys. Rev.* D24 (1981), p. 1275. DOI: 10.1103/PhysRevD.24.1275.

[372] Paul Langacker and David London. «Mixing Between Ordinary and Exotic Fermions.» In: *Phys.Rev.* D38 (1988), p. 886. DOI: 10.1103/PhysRevD.38.886.

[373] D. Tommasini, G. Barenboim, J. Bernabeu, and C. Jarlskog. «Nondecoupling of heavy neutrinos and lepton flavor violation.» In: *Nucl. Phys. B* 444 (1995), pp. 451–467. DOI: 10.1016/0550-3213(95)00201-3. arXiv: hep-ph/9503228.

[374] S. Antusch, C. Biggio, E. Fernandez-Martinez, M.B. Gavela, and J. Lopez-Pavon. «Unitarity of the Leptonic Mixing Matrix.» In: *JHEP* 10 (2006), p. 084. DOI: 10.1088/1126-6708/2006/10/084. arXiv: hep-ph/0607020.

[375] Stefan Antusch, Jochen P. Baumann, and Enrique Fernandez-Martinez. «Non-Standard Neutrino Interactions with Matter from Physics Beyond the Standard Model.» In: *Nucl. Phys. B* 810 (2009), pp. 369–388. DOI: 10.1016/j.nuclphysb.2008.11.018. arXiv: 0807.1003 [hep-ph].

[376] Stefan Antusch and Oliver Fischer. «Non-unitarity of the leptonic mixing matrix: Present bounds and future sensitivities.» In: *JHEP* 10 (2014), p. 094. DOI: 10.1007/JHEP10(2014)094. arXiv: 1407.6607 [hep-ph].

[377] Antonio M. Coutinho, Andreas Crivellin, and Claudio Andrea Manzari. «Global Fit to Modified Neutrino Couplings and the Cabibbo-Angle Anomaly.» In: (2019). arXiv: 1912.08823 [hep-ph].

[378] A. Broncano, M.B. Gavela, and Elizabeth Ellen Jenkins. «The Effective Lagrangian for the seesaw model of neutrino mass and leptogenesis.» In: *Phys. Lett. B* 552 (2003). [Erratum: Phys.Lett.B 636, 332 (2006)], pp. 177–184. DOI: 10.1016/S0370-2693(02)03130-1. arXiv: hep-ph/0210271.

[379] Sidney R. Coleman and Frank De Luccia. «Gravitational Effects on and of Vacuum Decay.» In: *Phys. Rev.* D21 (1980), p. 3305. DOI: 10.1103/PhysRevD.21.3305.

[380] James M. Cline, Michael Joyce, and Kimmo Kainulainen. «Supersymmetric electroweak baryogenesis.» In: *JHEP* 07 (2000), p. 018. DOI: 10.1088/1126-6708/2000/07/018. arXiv: hep-ph/0006119 [hep-ph].

[381] Patrick Huet and Ann E. Nelson. «Electroweak baryogenesis in supersymmetric models.» In: *Phys. Rev.* D53 (1996), pp. 4578–4597. DOI: 10.1103/PhysRevD.53.4578. arXiv: hep-ph/9506477 [hep-ph].

[382] Michael Joyce, Tomislav Prokopec, and Neil Turok. «Nonlocal electroweak baryogenesis. Part 1: Thin wall regime.» In: *Phys. Rev.* D53 (1996), pp. 2930–2957. DOI: 10.1103/PhysRevD.53.2930. arXiv: hep-ph/9410281 [hep-ph].

[383] Frank F. Deppisch, P.S. Bhupal Dev, and Apostolos Pilaftsis. «Neutrinos and Collider Physics.» In: *New J. Phys.* 17.7 (2015), p. 075019. DOI: 10.1088/1367-2630/17/7/075019. arXiv: 1502.06541 [hep-ph].

[384] Stefan Antusch, Eros Cazzato, and Oliver Fischer. «Sterile neutrino searches at future e^-e^+, pp, and e^-p colliders.» In: *Int. J. Mod. Phys. A* 32.14 (2017), p. 1750078. DOI: 10.1142/S0217751X17500786. arXiv: 1612.02728 [hep-ph].

[385] Yi Cai, Tao Han, Tong Li, and Richard Ruiz. «Lepton Number Violation: Seesaw Models and Their Collider Tests.» In: *Front. in Phys.* 6 (2018), p. 40. DOI: 10.3389/fphy.2018.00040. arXiv: 1711.02180 [hep-ph].

[386] P.S. Bhupal Dev and Yongchao Zhang. «Displaced vertex signatures of doubly charged scalars in the type-II seesaw and its left-right extensions.» In: *JHEP* 10 (2018), p. 199. DOI: 10.1007/JHEP10(2018)199. arXiv: 1808.00943 [hep-ph].

[387] Silvia Pascoli, Richard Ruiz, and Cedric Weiland. «Heavy neutrinos with dynamic jet vetoes: multilepton searches at $\sqrt{s} =$ 14 , 27, and 100 TeV.» In: *JHEP* 06 (2019), p. 049. DOI: 10.1007/JHEP06(2019)049. arXiv: 1812.08750 [hep-ph].